to my Family, where Life begins and Love never ends,

to my Father, on the other side of the street.
Life may separate us, but Love will continue…

Table of Contents

Index of Figures

Abstract

Composites materials are continuously evolving and their use for the repair and retrofit of civil structures has become a common practice among the engineering community. Fabric Reinforced Cementitious Matrix (FRCM) and Steel Reinforced Grout (SRG) systems represent a new repair methodology for structural strengthening and rehabilitation, including historical restoration; they are becoming a viable alternative to FRP, whenever the project conditions do not allow the use of organic polymer based composites.

FRCM is described by the American Concrete Institute (ACI) committee 549 as a composite material consisting of a sequence of one or more layers of cement-based matrix reinforced with dry fibers in the form of open single or multiple meshes that, when adhered to concrete or masonry structural members, forms a FRCM system.

FRCM and SRG are usually constituted by dry fabrics and it is proved that the bond at the matrix-fibers interface is not optimal, since only the external filaments are in contact with the matrix and able to transfer the load, while the inner filaments slip due to the low friction between the fibers.

To this end, an experimental program was undertaken to investigate the mechanical behavior in order to determine the material properties needed for design and to evaluate its performance in environmental conditions.

Two new fabric meshes impregnated by means of two several matrices were selected for this research. The fabric meshes are steel textiles constituted by cords of Ultra High Tensile Strength Steel (UHTSS) micro-wires with different mass density, namely *G6* (600 g/m^2) and *G12* (1200 g/m^2); while the matrices are a cement-based mortar, *GLT*, and a lime-based mortar, *GCF*.

This work aims to advance the state of cement-based composite materials testing methodology with a goal towards standardization and it is presented through two parts, which in turn divided in four chapter.

First Part reports the following chapters:

1. An introductory chapter, which gives a brief overview of composites, focusing on the classification of brittle matrix composites in order to provide a contextual field within which FRCM and SRG are differentiated.

2. Second chapter provides to frame cement-based composite materials in an evolutionary context as reinforcement system. In fact, Fiber Reinforced Cementitious Matrix (FRCM) composites are an alternative to Fiber Reinforced Polymer (FRP) composites and they have gained some interest in the last decade. In particular, the need of effective, versatile and cost efficient strengthening methods has encouraged producers to develop and sell steel textiles for structural rehabilitation purposes, in other words Steel Reinforced Grout (SRG) systems.
3. Given the increased interest in the utilization of cement-based composite systems for structural retrofitting applications, their specifications need to be necessary. In third chapter, the development of acceptance criteria for masonry and concrete strengthening using Fabric-Reinforced Cementitious Matrix (FRCM) and Steel Reinforced Grout (SRG) composite systems has been discussed.
4. Experimental program, which investigates the tensile test method used to characterize FRCM material properties, specifically the load transfer gripping mechanism, namely clevis type grips and clamping grips.

Second Part presents the results of characterization experiments performed on SRG systems. In particular, tensile, interlaminar shear, bond and compressive tests were performed on specimens in control condition. Two types of steel fabrics, *G6* and *G12*, and two types of mortars, *GLT* and *GCF*, have been used to produce a total of four SRG systems, namely *GLT-G6, GLT-G12, GCF-G6* and *GCF-G12*. The purpose of second part is to evaluate the performance of SRGs and so to understand their mechanical behavior and the effectiveness and compatibility with concrete and masonry substrates. In addition, the preliminary considerations obtained from this thesis can be considered as first step toward the development of proper design formulae for characterization of SRG systems. Therefore, the following chapters show:

1. *Compressive tests*. Two types of mortar were chosen among those present on the market, specifically designed for structural reinforcement, namely cement based mortar (*GLT*) and hydraulic lime based mortar (*GCF*). Then, they were

casted in cubical molds of 50 mm side length according to standard requirements. After a curing time of three, seven, fourteen and twenty-eight days, they were tested with the help of a hydraulic type universal test frame. Finally, the maximum load carried by the sample during the test was recorded and the type of fracture pattern was noted. The primary mode of failure was compression of the cube resulting to be a cone like structure as desired. Based on the experimental tests presented, both the cement-based mortar, *GLT*, and the hydraulic lime-based mortar, *GCF*, meets the requirements of AC434.

2. *Tensile tests.* Rectangular coupons with nominal size 510 x 51 x 10 mm were made in a flat glass mold by applying a first layer of cementitious mortar (5 mm), the fiber mesh and a second layer of cementitious mortar (5 mm). After a curing time of 28 days in humidity chamber, tests were performed using a screw driven universal test frame. Uniaxial tensile load was applied to all specimens by means of clevis grip setup. Load was applied under displacement control at a rate of 0.25 mm/minute and recorded by the load cell integrated in the testing machine. Axial deformation was measured using two extensometers with a 100 mm and 50 mm gauge length, placed mid-length of the specimen. The results of tests for each tested coupons are presented as tensile strength versus strain curves. Then, based on experimental results, maximum force, ultimate strength and strain, and cracked elastic modulus have been calculated. Finally, failure mode has been described for each tested specimens. Failure mode is not been equal for all specimens. In most cases, the collapse is due to the splitting of the matrix around the fiber cords with consequent slippage of fibers. However, the detachment of the tab from the coupon and the enlargement of cracks, which caused breakage of the specimen into several pieces, occurred as well.
3. *Interlaminar shear tests*. This test is a three-point bending test on short beam, where a transverse shear is induced in specimens with low support to specimen thickness ratios. This test method determines the apparent interlaminar shear strength of high-modulus fiber-reinforced composite materials. Specimens were machined from 330 x 508 mm panels with a diamond blade saw later a curing of 28 days in humidity chamber. Short beams were characterized by two

layers of fiber mesh embedded in two layers of 4 mm cementitious mortar. The fibers were also divided by another thin layer di mortar. A total of five tests per product under control ambient conditions were carried out. Finally, the peak load recorded during test, the ultimate strength computed as per standard requirement and the failure mode were reported. The systems packaged with *G6* steel fabrics have presented a collapse due to the matrix cracking in the tension side, while in the case of the systems packaged with *G12* steel fabrics, the primary mode of failure was interlaminar shear. Indeed, it has been observed the development of two cracks at fiber-matrix interface that propagated from the center of the specimen to the edge. The reason is because the *G12* fabric has mass density higher than that of *G6* textile and did not permit the complete penetration in the matrix. Therefore, the bond at fiber-matrix interface was not efficient.

4. *Pull-off tests.* In order to investigate the bond at the SRG reinforcement-substrate interface, 28 pull-off tests were carried out on several types of substrate, namely concrete blocks, clay bricks and cementitious masonry units. The reinforcement were applied onto the substrate, previously cleaned, for a minimum of 63 mm thick. Later 28 days of curing time, hexagonal cuts, perpendicular to the substrate of the specimen, were performed in order to circumscribe the disk used for testing according to standard requirements. Then, the steel disks were attached by epoxy to the reinforcement surface as a means to pull-off the circular area. Uniaxial tensile load was applied perpendicular to the test surface using a pull-off test machine. Tensile loading device was connected to the steel disk using a coupling fixture. Tensile load was applied to the steel disk until failure occurred. Finally, the ultimate load recorded during test, the ultimate strength computed as per standard requirement and the failure mode were reported. Main collapse mode of SRG composite is failure at reinforcement-matrix interface, so the density of fabric is an important parameter. In fact, the lower is the mass density and the higher is the bond strength. The reason is that the matrix can penetrate more easily between the bundles and so the bond increases.

Chapter 1
Introduction

1.1. The Use of Composite Materials for Civil Applications

Civil infrastructure facilities deteriorate due to aging, overuse, misuse, exposure to aggressive environments, and lack of maintenance. Throughout the world, conservation, maintenance, and upgrading the structural performance of existing structures is of fundamental, cultural, economic, and human safety importance. Rehabilitation, rather than demolition and reconstruction, is a feasible economic alternative. Moreover, extending the design life of infrastructure is a necessary sustainable decision, in particular when intervention involves infrastructure with historical significance, where many national regulations may prevent demolition.

Structural retrofit involves upgrading or changing a structure to implement changes in its use, design needs, or regulatory requirements; while rehabilitation involves making structural repairs to damaged or weakened elements in order to bring them up to required safety standards. Material systems and methods for structural retrofit and rehabilitation include the installation of Fiber Reinforced Polymer (FRP) composite systems, steel plate bonding, section enlargement, installation of near surface mounted bars, and external post-tensioning. Typical structural elements to strengthen are beams, slabs, columns, and walls.

The use of FRP systems has become a common technique for strengthening reinforced concrete (RC) elements. Since then, numerous research studies have been conducted in order to analyze, study and comprehend the properties of these materials and their optimal uses. Despite all of their advantages, the FRP strengthening technique has some limitations including:

- Poor behavior of epoxy resins at temperatures above the glass transition temperature;
- Long term durability uncertainty;
- Inability to apply FRP on wet surfaces or at low temperatures;
- Lack of vapor permeability, which may cause damage to the concrete structures;

- Concern that the use of epoxy resins could be a toxic hazard to the installer.

An alternative solution is the replacement of organic with inorganic binders, i.e., use a composite made with a cement-based matrix, instead of an organic polymer matrix. One such solution is the development of Fabric Reinforced Cementitious Matrix composites (FRCM) that consist of a fabric in a cementitious matrix. The inorganic matrix (cementitious mortar) in FRCM does not fully penetrate and impregnate the fiber strands in the fabric. This is a significant factor affecting the mechanical behavior and performance of the FRCM composite and must be understood.

The use of composite materials for civil applications dates back to ancient times, when different materials were mixed together to obtain a new material with high performances. In fact, Egyptian and Mesopotamian builders used a mixture of mud and straw to create strong and durable buildings. In the modern era, concrete is the most common artificial composite material consisting of loose stones (aggregate) held with a cement-based matrix. However, concrete is a very strong material, but cannot bear tensile loading. Therefore, steel bars are often added to it in order to create a reinforced concrete that is able to endure to tensile stresses.

1.2. Definition of Composite Material

Nowadays, the definition of "*composite materials*" is universally acknowledged as a system, constituted by two or more material phases conveniently arranged, which provides mechanical performance and properties better than those of the constituent materials. One of the phases is dispersed and stronger, called *reinforcement*, another phase is continuous and weaker, called *matrix*. Classification of composites depends on the nature of the matrix and the reinforcement type can be particulates, short distributed fibers, and continuous fibers.

Based on the type of matrix, a general subdivision of the composites is showed as follows:

- **PMC** (*Polymer Matrix Composite*): thermoplastic (such as nylon) or thermoset (such as epoxy resins);
- **MMC** (*Metallic Matrix Composite*): aluminum, titanium and their alloys;

- **BMC** (*Brittle Matrix Composite*) divided into:
  - *Ceramic Matrix Composites*;
  - *Cementitious Matrix Composites;*
  - *Not-Cementitious Matrix Composites*, lime based mortar or geo-polymer matrix.

This overview is limited to polymer and brittle matrix composites only, in order to frame the context from within which FRCM composites are studied and can be better understood.

The mechanical behavior of fiber-reinforced composites is governed by a complex relationship between the material properties of the constituent materials, their volume fraction, the bond interface between them, and their orientation with respect to the load applied. For example, FRP, that is a polymer matrix composite, has a very strong interfacial bond with a fiber reinforcement strain limit lower than the strain limit for the epoxy matrix, ($\varepsilon_f < \varepsilon_m$). In this case, the longitudinal (fiber parallel to direction of load) and transverse (fiber perpendicular to direction of load) elastic moduli, E_{long} and E_{tran}, respectively, can be estimated using the rule of mixtures model (Daniel & Ishai 1994), that states that each constituent material contributes to the composite properties in a manner proportional to their volume fraction.

Known the elastic modulus and volume fraction of the fiber, E_f and V_f, and the elastic modulus and volume fraction of the matrix, E_m and V_m, it can calculate:

$$E_{long} = E_f \cdot V_f + E_m \cdot V_m \tag{1}$$

$$E_{tran} = \frac{E_f \cdot E_m}{E_f \cdot V_m + E_m \cdot V_f} \tag{2}$$

Eq. 1 is used for estimation of the longitudinal modulus, where the fiber and matrix are assumed under same state of strain, and the composite will theoretically fail when the strain limit of the fibers is reached.

Eq. 2 is used for estimation of the transverse modulus where the fiber and matrix are assumed to be under same state of stress. Initially, the matrix and fibers deform elastically. Eventually, the matrix yields and deforms plastically but the fibers continue to stretch elastically (Callister & Rethwisch 2012). These relationships give rise to the nearly linear elastic characteristic stress-strain curve shown in Figure 1.1.

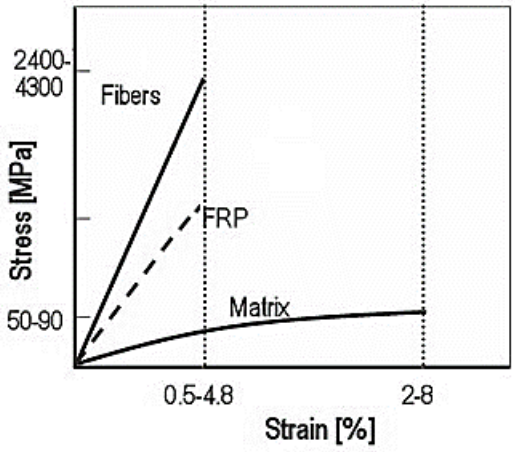

Figure 1.1 - Characteristic mechanical behavior of organic polymer matrix composites [Callister & Rethwisch 2012]

Figure 1.2 shows a comparison of the idealized mechanical behavior of carbon FRP (C-FRP) and glass FRP (G-FRP) composites, and steel to show that while PMCs have superior strength, once they reach their ultimate capacity, the fail exhibiting no yielding.

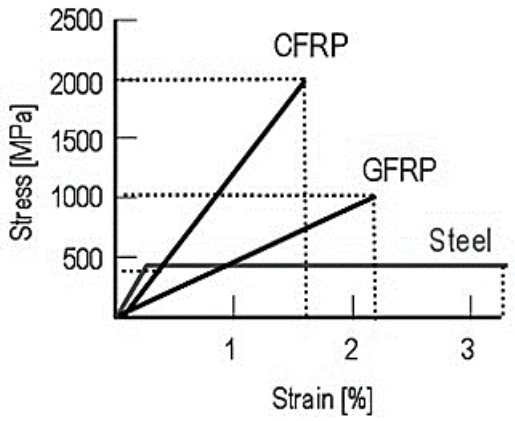

Figure 1.2 - Comparison of behavior between carbon (CFRP) and glass (GFRP) composites, and steel [Callister & Rethwisch 2012]

1.3. Brittle-Matrix Composites: TRC and FRCM

In brittle matrix composites (BMC), the matrix is either a ceramic or a cement-based material such as grout, mortar, or concrete that are typically porous and have a relative high compressive strength, but low tensile strength. The behavior of BMC is very different from polymer or metal composites and the rule of mixtures model usually cannot be applied because, for some BMCs, the interfacial bond between fiber and matrix is weaker and more complex or because the strain limit of the matrix is much lower than that of the fibers ($\varepsilon_m << \varepsilon_f$). In those cases, the matrix starts to crack at its strain limit and instead, fibers debonding and slipping are the mechanisms that mitigate cracks localization. This is a desirable behavior as it leads to pseudo-ductility. Fibers in brittle matrices hinder the cracking (Callister & Rethwisch 2012) and allow the redistribution of stress, leading to improve both tensile capacity and toughness. An additional benefit is reduction in crack size. Referring to Figure 1.3, BMCs behave linear-elastically up to the tensile strength of the matrix. Then, as the stress increases, multiple cracks develop in the matrix and the stress is redistributed through the fibers, allowing the composite material to sustain additional strain. At this point, either strain-softening or strain-hardening behavior will develop depending on the amount of fibers and the quality of the interfacial bond.

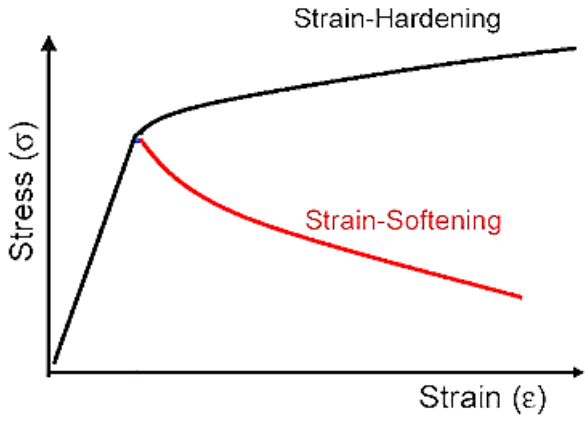

Figure 1.3 - Graphic representation of brittle composite behavior [Callister & Rethwisch 2012]

In strain softening, the load resistance will decrease with continued strain, while in strain hardening, it will increase and multiple cracking will develop.

Composites materials are often classified based on the type of used matrix and on the geometry and arrangement of the fiber reinforcement. A brief overview of the general classification used for BMCs is:

- **BMC** (*Brittle Matrix Composite*):
  - ***Cementitious Matrix Composites***:
    - Short dispersed fibers:
      - FRC, GRC, SFRC
      - HPFRC, UHPFRC, SHCC
      - ECC
    - Continuous fibers:
      - Ferrocement
      - TRC, TRM, MBC
      - FRCM, FRFRCM
  - ***Ceramic Matrix Composites****;*

Composites made from ceramic matrices are in a different category in respect to cementitious matrix composites, because they are generally not used in the construction field, even if they share similar mechanical enhancement properties as Fiber Reinforced Concrete (FRC).

1.3.1. Cementitious Matrix Reinforced with Short Dispersed Fibers

Cementitious composites made with short dispersed fibers can be used in bulk or as thin elements. In the US, they are included in the domain of **ACI Technical Committee 544 - Fiber Reinforced Concrete** whose scope is to develop and report information on concrete reinforced with short, discontinuous, randomly dispersed fibers.

1.3.1.1. Fiber Reinforced Concrete/Cement (FRC)

Fiber Reinforced Concrete/Cement (FRC) is concrete or cementitious material reinforced with short and dispersed fibers that range in length to a maximum of 75

mm. ACI544 (2002) defines FRC as concrete made primarily of hydraulic cements, aggregates, and discrete reinforcing fibers. Fibers suitable for reinforcing concrete have been produced from steel, glass, and organic polymers (synthetic fibers). The matrix can be concrete, mortar or cement paste.

FRC has been classified by fiber content and mechanical behavior, likely because the first influences the latter. To this end, by fiber content (Mehta & Monteiro 2006), the following is considered:

- *Low volume fraction* (< 1 %). The fibers are used mainly to reduce shrinkage cracking. These fibers are used in slabs and pavements that have large exposed surface leading to high shrinkage crack. Dispersed fibers offer various advantages over steel bars and wire-mesh to reduce shrinkage cracks such as:
    1) Fibers are uniformly distributed in three-dimensions making an efficient load distribution;
    2) Fibers are less sensitive to corrosion than the reinforcing steel bars;
    3) Fibers can reduce the labor cost of placing the bars and wire-mesh.
- *Moderate volume fraction* (between 1 and 2 %). The presence of fibers at this volume fraction increases the modulus of rupture, fracture toughness and impact resistance. These composites are used in construction methods such as shotcrete and in structures that require energy absorption capability, improved capacity against delamination, spalling and fatigue.
- *High volume fraction* (greater than 2 %). The fibers used at this level lead to strain hardening of the composite that can be used to enhance the performance of structural elements.

Naaman & Reinhardt (2006) proposed a FRC classification based on the stress-strain response of the material loaded in tension. Strain hardening FRC is called **High Performance Fiber Reinforced Cement Composites (HPFRCC)**, **Ultra High Performance Fiber Reinforced Cement (UHPFRC)**, and also **Strain Hardening Cement Based Composites (SHCC)**.

Other terms commonly used for FRC materials based on fiber material used are **Steel Fiber Reinforced Concrete** or **Cement (SFRC** or **SFRCC)**, **Glass Fiber Reinforced Concrete** or **Cement (GRC** or **GFRC)** and **Multi-Scale Fiber-**

Reinforced Concrete (MSFRC) that consists of a combination of different size fibers.

1.3.1.2. Engineered Cementitious Composite (ECC)

Engineered Cementitious Composite (ECC) is similar in composition to FRC, but has higher toughness in the form of pseudo-ductility. ECC contains water, cement, sand, fiber, and some common chemical additives. Coarse aggregates are not used as they tend to adversely affect the unique ductile behavior of the composite. A typical composition employs water/cement ratio and sand/cement ratio of 0.5 or lower. Unlike some high performance FRC, ECC does not utilize large amounts of fiber. In general, 2 % or less by volume of discontinuous fiber is adequate, even though the composite is designed for structural applications (Li & Kanda 1998). Applications of ECC range from structural reinforced concrete, precast concrete, and rehabilitation of structural components in both seismic and non-seismic regions (Li 2003).

1.3.2. Cementitious Matrix Reinforced with Continuous Fibers

Cementitious matrices reinforced with continuous fibers in the form of meshes, textiles, or fabrics with an open grid arrangement fall in the category of thin reinforced cementitious products and have also been called cement based laminates. In the US, they are included in the domain of **ACI Technical Committee 549 - Thin Reinforced Cementitious Products and Ferrocement**.

Two types of brittle-matrix composites reinforced with continuous fibers can be distinguished: *Textile Reinforced Concrete* (**TRC**) and *Fiber Reinforced Cementitious Matrix* (**FRCM**).

1.3.2.1. Textile Reinforced Concrete (TRC)

TRC is a composite material made of open-meshed textile structures and a fine-grained concrete. The technical textiles are mainly made of alkali resistant (AR)-glass and sometimes of other materials as carbon or aramid. They are placed in the main stress direction of the composite and leads to a high performance compared to randomly distributed short fibers in the already known glass fiber reinforced

concrete (GFRC). In addition, TRC is cost competitive material if used as thin cement composite products.

TRC can be considered as an evolution of the most ancient *ferrocement*, a composite material invented and patented around the forties by Pier Luigi Nervi. Ferrocement consists in a mortar or plaster reinforced by a series of metal meshes layers of small diameter held together by a limited number of steel rods such as rebars. Committee 549 of the American Concrete Institute (ACI) provided the following definition: *"Ferrocement is a type of thin-wall reinforced concrete commonly constructed of hydraulic-cement mortar reinforced with closely spaced layers of continuous and relatively small-size wire mesh. The mesh may be made of metallic or other suitable materials".*

The mechanical behavior consists of a first linear stage until cracks start to form in the matrix, followed by a decrease in elastic modulus where cracks enlarge, until the steel yielding phase prior to failure (Fig. 1.4).

Its strength and lightness, combined with the possibility to be molded into complex shapes, made it ideal for such applications as hulls for boats, shell roofs and water tanks (Fig. 1.5).

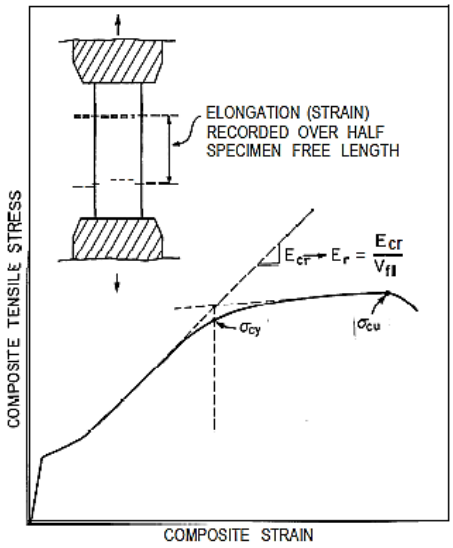

Figure 1.4 - Typical stress-strain curve for ferrocement in tension [ACI 549-1999]

Figure 1.5 - Ferrocement boat hull built by Nervi, 1972

An interesting definition of TRC is given by A. E. Naaman [1]:

"Textile reinforced concrete is a type of reinforced concrete commonly constructed of hydraulic-cement matrix reinforced with several layers of closely spaced continuous 2D textiles, or one or several layers of 3D textiles (Fig. 1.6). At least one textile layer should be placed near each of the two extreme surfaces of the resulting structure. The textiles may be made of polymer, synthetic, metallic, organic or other suitable materials. The fineness of the cementitious matrix and its composition should be compatible with the textile armature system. It is meant to encapsulate. The matrix may contain discontinuous fibers or microfibers of appropriate dimensions."

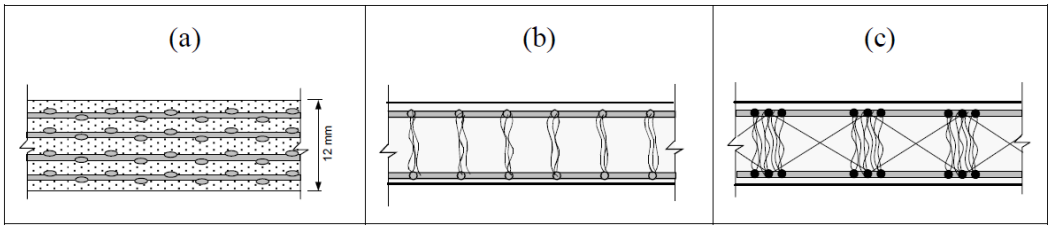

Figure 1.6 - Typical sections of thin textile reinforce concrete (TRC) product with: a) several layers of 2D textile reinforcements, or b,c) one layer of 3D textiles [Naaman, 2010]

Another term commonly used for this composite is **Textile Reinforced Mortar (TRM)**.

1.3.2.2. Fiber Reinforced Cementitious Matrix (FRCM)

Fiber Reinforced Cementitious Matrix (FRCM) is a composite system specifically designed for the repair and rehabilitation of concrete and masonry structures. It is an alternative to the existing repair technology such as steel plate bonding, welded steel meshes, section enlargement, external post-tensioning and FRP.

However, FRCM systems have recently emerged as a suitable method for strengthening concrete and masonry structures. It is a composite material consisting of one or more layers of cement-based matrix reinforced with fibers fabric. The cement-based matrixes are typically made of combinations of Portland cement, silica fume, and fly ash as the binder. The use of inorganic matrix allows overcoming some issues, typical of FRPs, such as limited temperatures and fire resistance, lack of vapor permeability and impossibility of application on damp surfaces. On the other hand, FRCM composites also have some drawbacks, as for instance a lower level of adhesion between the fabric and the matrix and a brittle behavior of the matrix itself (Table 1.1). Inorganic matrices may provide higher compatibility with the substrate, in particular in the case of ancient masonry construction (clay bricks, tuff, stone blocks). In addition, they offer better quality in terms of reversibility of the intervention and advantages in term of cost and time of installation, especially on irregular surfaces. The main difference between FRP and FRCM systems is the matrix used to bond the fibers. In fact, the fibers are embedded and fully impregnated within an organic matrix (epoxy resin) in the case of FRP, while the inorganic mortar is used for FRCM and is not able to fully penetrate between the fibers.

FRCM has also known as **Fabric-Reinforced Fiber Reinforced Cementitious Mortar (FRFRCM)**, because the mortar matrix used can itself be reinforced with short dispersed fibers. However, this term is not common. When the mortar used is mineral-based matrix, FRCM composites can also be denominated as **Mineral Based Composites (MBC)**.

Table 1.1 - FRCM and FRP: advantages and drawbacks

FRCM (Fiber Reinforced Cementitious Matrix)		**FRP (Fiber Reinforced Polymer)**	
Advantages	**Drawbacks**	**Advantages**	**Drawbacks**
Good compatibility with the concrete or masonry substrate in terms of chemical, physical and mechanical properties	The inorganic matrix is brittle and so it cracks under tensile loads	Lightweight and ease of application	Not applicable and durable in moist environment
Ease of installation as traditional plastering or trowel trades can be used	Bond at the matrix-fibers interface not so strong as in FRP systems	High stiffness and tensile strength	Health hazards for applicators
Breathability of the system, that allows air and moisture transport through the matrix	Its mechanical characterization and full-exploitation needs further studies	Resistance to corrosion and chemical attacks	Low vapor permeability
Good performance at elevated temperatures in addition to partial fire resistance		It can be tailored to give the required mechanical properties in various directions	High temperature and fire resistance (it needs thermal insulation)
Efficient in aggressive environment such as alkaline, water vapor and sea water environments			Difficult to recycle
Reversibility, essential for the conservation of historic structures			Irreversibility of the intervention

1.3.2.2.1. Constituent Materials: Matrices and Fabrics

The principal components of FRCM are the cementitious matrix and the structural reinforcement fabric. The former is typically a grout system based on Portland cement and a low dosage of dry polymers at less than 5 percent by weight of cement. In the case of historical structures, not-cementitious mortars, such as limed-based mortars may be used as binders.

The mechanical effectiveness of FRCM systems is strongly influenced by:

a) Capacity of the cementitious matrix to impregnate the fiber strands [2], [3], [4], [5];
b) Effective bond properties at interface fiber/matrix [6], [7], [8], [9], [10], [11], [12], [13], [14], [15];
c) Adherence of the cementitious matrix on concrete or masonry substrate [16], [17].

Fibers can be *natural*, produced by plants and geological processes; *chemical*, when the chemical composition, structure and properties are significantly modified during the manufacturing process; *ceramic* and *metallic*. Fibers used as reinforcement in civil applications are usually synthetic fibers, coming entirely from synthetic materials such as petrochemicals. The properties, the amount and the arrangement of the fibers have a great influence on the characteristics of the composite.

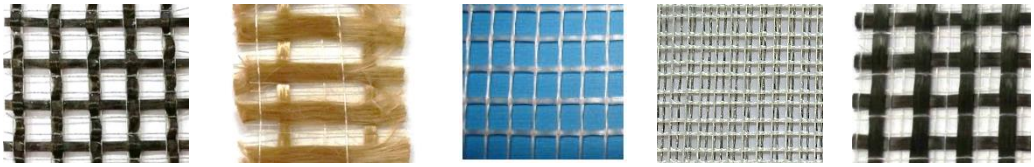

a) b) c) d) e)

Figure 1.7 - Typical fabrics used as reinforcement in FRCM applications: a) carbon, b) PBO, c) glass, d) steel, e) basalt

To ensure the durability of the composite material, fibers have to withstand the alkaline environment of the matrix without losing their properties. Fibers must also meet guarantee small relaxation under permanent load, good and constant adhesion between reinforcement and substrate, low cost and easy processing by textile machinery.

The mechanical properties of the most common fibers used in FRCM applications are shown in Table 1.2.

Table 1.2 - Properties of the most common fibers used as reinforcement

Material	Modulus of Elasticity (GPa)	Tensile Strength (MPa)	Elongation at break (%)	Density (g/cm^3)
Glass E	72-80	3000	4.8	2.55
Glass S	84-88	4500	5.4	2.47
Aramid	130	3600	3.6	1.40
Carbon HM	390 - 760	2400 - 3400	0.5 - 0.8	1.85
Carbon HT	240 - 280	4100 - 5100	1.6 – 1.7	1.75
Basalt	89	3000 - 4840	3.15	2.70
PBO	270	5800	2.15	1.56
Steel	190 - 210	340 - 600	20 - 30	7.86

The fabrics used in FRCM systems made by yarns woven in the two principal directions (primary direction, *PD*, and secondary, *SD*). The typical spacing of the yarns is less than 25 mm, and the total coverage area of the fiber mesh is less than 2/3 of total area. Besides, the geometry of the fabric plays an important role in determining the behavior of FRCM systems. Fabric architecture can enhance [18] or reduce [19] the FRCM performances. Cohen demonstrated that the warp and weft of yarns provides mechanical anchoring of the reinforcement such improving the overall composite performance. Richter shown that the transverse yarns strongly decrease the elastic modulus of the composite.

The properties of the yarns are strongly influenced by the size of the filaments. The size has a great influence on the quality of the adhesion between the filaments and it influences the load bearing performance. Furthermore, yarns can be coated with various types of polymers in order to enhance the mechanical behavior when coupled with inorganic matrices. The final purpose is to exploit better the high mechanical capability of the elementary fibers.

1.3.2.2.1.1. Fabrics

1.3.2.2.1.1.1. Glass Fibers

Glass fibers (Fig. 1.8) derive from an industrial fusion process of calcium oxide, silicon, magnesium, aluminum and boron that together form the *tank*. The oxides, melted at 1500 °C, are blended and abruptly cooled up to a temperature of 1200 °C. Thus melted glass obtained pass through special holes made on the bottom of platinum spinneret. The filaments are grouped together to form a braid or fiber

consisting of 204 filaments with an average diameter of about 10 μm and covered with a binder. Glass fibers are also available in the form of thin sheets, called *mats*, that can be made of both continuous long fibers and short fibers (25-50 mm) casually arranged in the plane and held together by a chemical binder.

Figure 1.8 - Glass fibers [Mapei website]

The commercially available glass fibers are: E-glass and Alkali-Resistant (AR). The former contain large amounts of boric acid and aluminate, the latter contain a small amount of zirconium oxide that is used to prevent corrosion from attacks due to the presence of alkali on cementitious materials. In general, they are all sensitive to water. Depending on the proportions of the raw materials used, products with different mechanical characteristics and performance are obtained. Seven different types of glass fibers can be found on the market (Table 1.3 - 1.4).

Table 1.3 - Glass fibers

Material	Density (kg/m^3)	Elastic Modulus (GPa)	Tensile Strength (MPa)	Elongation at break (%)
Glass fibers E	2550	70	3500	3.8
Glass fibers S	2500	90	4700	5.5

Table 1.4 - Use of the glass fibers

Use of fibers	Type of glass
High mechanical resistance	R, S
Acid corrosion resistant	A, C, R
Multi-purpose	E
High dielectric characteristics	D

The most common types of fibers are "*E"* and "*S"*; Type E is less valuable and has modest mechanical characteristics than type *S*. Glass fibers have a Young's

modulus lower than that of carbon and aramid fibers. They offer relatively low abrasion resistance and therefore require particular attentions during placement. This type of fiber has a pronounced viscous sliding attitude and a modest fatigue resistance. In order to not be exposed to the action of the alkali, that are present in the concrete (K^+ and Na^+), treatment of the glass fibers is necessary. In fact, these ions can react with amorphous silica (SiO_2 is the main constituent of the glass) generating a gelatinous form of hydrated alkaline silicates and it causes the degradation of glass fibers and relative decrease in mechanical performance. The solution to this problem is to ensure adhesion between fibers and matrix during placement.

Glass fibers need to be conform to the technical specifications UNI 8746, UNI 9409 and UNI EN 15422.

1.3.2.2.1.1.2. Carbon Fibers

Carbon fibers (Fig. 1.9) are made of petroleum or charcoal and nitrile in polymethylmethacrylate (PAN). They are an imperfect graphite crystal aggregate. They may have corrosion problems in direct contact with steel, because they are good conductors of electricity. The industrial process involves particular polymers called *precursors* and takes place at high temperatures. The result is the polymethylmethacrylate (PAN) commonly used in the textile and construction products field.

Figure 1.9 - Carbon fibers [Ruredil website]

The transformation process of PAN in carbon is composed into three phases:

- Phase 1: Stabilization. At this step, the fibers are subjected to heat treatment in air at 200 °C - 240 °C for 24 hours. Thus, the molecular structure undergoes a preferential orientation in the direction of the applied load;
- Phase 2: Carbonization. At this stage, PAN fibers are treated at 1500 °C in inert atmosphere. This treatment removes most chemical elements different from carbon;
- Phase 3: Grafting. At this step, temperature is very high, 3000 °C in inert atmosphere, so that the crystal structure of the fibers can develop completely, closing to that of the graphite.

Two types of carbon fibers can be identified: *PASSO* fibers and *PAN* fibers. The PASSO fibers have a lower quality of 20 % than that of the PAN fibers, but both are characterized by:

- *HT fibers* (HT = high stress), with high strength, but low elastic modulus;
- *HM fibers* (HM = high modulus), with low strength, but high elastic modulus.

In the field of constructions, high elastic modulus fibers and high strength fibers are preferred (Table 1.5).

Table 1.5 - Carbon fibers

Material	Density (kg/m^3)	Elastic Modulus (GPa)	Tensile Strength (MPa)	Elongation at break (%)
High strength Carbon	1800	230	5000	2.0
High modulus Carbon	1850	400	3000	0.9
Most High modulus Carbon	2100	700	1500	0.3

Carbon fibers are usually used for the production of high performance composites. They exhibit a brittle behavior, characterized by a modest absorption of energy, although the stress at break are high and, conversely, less sensitive (compared to glass fibers and aramid) to phenomena of viscous sliding (creep) and of fatigue, being characterized by a modest decrease in long-term resistance. In general, carbon fibers show excellent resistance to alkali, fresh water and seawater, but they are

much expensive. For FRCM applications, they need to be conform to ISO 13002 and UNI EN 13002-2.

1.3.2.2.1.1.3. Aramid Fibers

The aramid fibers (Fig. 1.10) are organic fibers and are characterized by high mechanical performances. The term "*aramid*" refers to ARomatic poly-AMIDEs. The first aramid fibers were developed and patented by DuPont™ researchers in 1971 and were named Kevlar®. The polymer is synthesized in strongly acidic solution, at high temperature and high speed, and then cooled and dried fast. Thus, the fibers are wrapped on a bobbin in order to orient themselves and to increase the mechanical characteristics. The different chemical structure allows obtaining products with different mechanical performance (Table 1.6).

Table 1.6 - Aramid fibers

Material	Density (kg/m^3)	Elastic Modulus (GPa)	Tensile Strength (MPa)	Elongation at break (%)
Kevlar® 29	1440	70	36000	3.6
Kevlar® 39	1450	140	3600	1.9
Kevlar® 149	1470	160	3200	1.5

In addition to the aramid fibers KEVLAR, there are three other types: TWARON, TECHNORA and SVM.

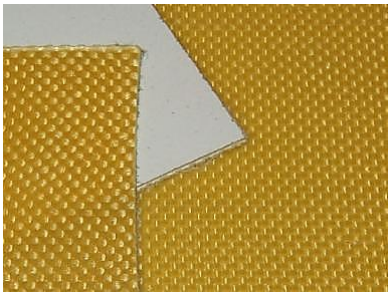

Figure 1.10 - Aramid fibers [DuPont website]

Aramid fibers have an elastic modulus higher than that of glass fibers and is about 1/3 of the carbon fibers modulus. The tensile strength is higher than that of glass fibers and lower than that of carbon fibers as well. For these reasons, their use is

not competitive in the civil engineering field. However, their advantage is the rupture combined with the formation of micro-fibrils, a phenomenon that allows a great dissipation of fracture energy, offering to Kevlar a great impact resistance and making it ideal for production of various products, such as anti-hurricane booths or bulletproof vests.

1.3.2.2.1.1.4. PBO Fibers

Polyparaphenylenebenzobisoxazole (PBO) is a synthetic polymer and is the strongest and stiffest material used to repair and strengthen concrete and masonry structures in externally bonded composite systems. Experimental studies showed that the PBO-FRCM systems present a better bonding and a better stress transfer mechanism between matrix and filaments in respect to the carbon or glass fibers. The PBO textile has a geometry such to ease the penetration of the mortar in the mesh and a high friction level between the filaments due to the physical and chemical properties of the material. It has good fire and UV resistance, excellent stability and a very low absorption in humid environment (0.6 %). Despite these characteristics, it is a soft and lightweight fiber, very malleable but highly expensive. The mechanical properties of the fibers in PBO shown in Table 1.7. It needs to be conform to UNI EN 13003-1-2-3.

Figure 1.11 - PBO fibers [Ruredil website]

Table 1.7 – PBO fibers

Material	Density (kg/m^3)	Elastic Modulus (GPa)	Tensile Strength (MPa)	Elongation at break (%)
PBO	1560	270	5800	2.15

1.3.2.2.1.1.5. Basalt Fibers

Basalt fibers made of fine basalt filaments. They are similar to carbon and glass fibers, but they have better physic and mechanical properties than glass fiber and they are cheaper than carbon fibers. In the last decade, basalt has emerged as a suitable alternative in the fiber reinforcement, because they are naturally resistant to ultraviolet (UV) and high-energy electromagnetic radiation, they maintain their properties in cold temperatures, and provides better acid resistance. Moreover, basalt fibers are extremely resistant to high temperatures. Some studies showed that the basalt fibers kept about 90 % of the normal temperature strength after exposure at 600 °C for 2 hours. The mechanical properties of the fibers in basalt shown in Table 1.8. For these advantages, the applicability of the basalt fibers as structural strengthening material is highly expected.

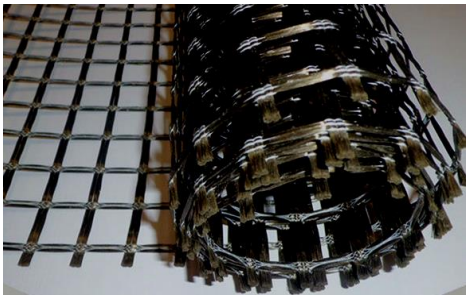

Figure 1.12 - Basalt fibers [Kerakoll website]

Table 1.8 - Basalt fibers

Material	Density (kg/m^3)	Elastic Modulus (GPa)	Tensile Strength (MPa)	Elongation at break (%)
Basalt	2700	89	4840	3.15

1.3.2.2.1.1.6. Steel Fibers

The need of effective, versatile and cost efficient strengthening methods has encouraged producers to develop and sell steel-based reinforcements for structural rehabilitation purposes as the seismic retrofitting of masonry walls [20] and vaults [21] and for the flexural strengthening of reinforced concrete beams [22]. They offer particularly good mechanical performance thanks to the high tensile strength

of the textile and the effective cord-to-mortar interlocking [23], at relatively low costs. Based on information provided by the suppliers, steel textiles are constituted by cords of Ultra High Tensile Strength Steel (UHTSS) micro wires. The steel cords available today in the market have tensile strength of 2800-3200 N/mm^2 and Young's modulus of 180-210 kN/mm^2. Depending on the spacing between the cords, the surface mass density ranges widely from 600 g/m^2 to 3300 g/m^2 corresponding to maximum loads per unit width varying from 230 kN/m to 1300 kN/m. Given their small diameter (0.1-0.5 mm), the wires are either coated (with zinc or brass) or made of stainless steel, to provide protection against corrosion.

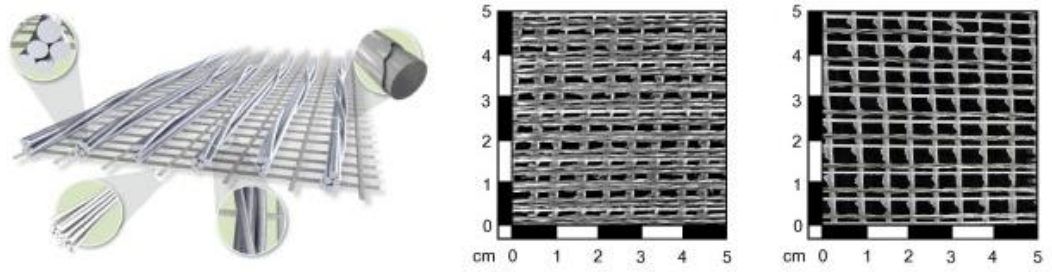

Figure 1.13 - Steel fibers [Kerakoll website]

Chapter 2
Evolution of reinforcement systems: from FRP to FRCM and SRG

2.1. Introduction

None of the homogeneous traditional materials has the ideal combination of properties for structural applications (Table 2.1). This consideration has led to the development of materials that combine two or more homogeneous materials and allow taking advantage of the best properties of each materials in synergistic way.

Table 2.1 – Behavior of homogeneous traditional materials

Properties	**Metals**	**Ceramics**		**Polymers**
		in mass	**in fibers**	
Tensile Strength	Good	Mediocre	Excellent	Mediocre
Stiffness	Excellent	Mediocre	Excellent	Mediocre
Toughness	Good	Mediocre	Mediocre	Good
Impact Resistance	Good	Mediocre	Mediocre	Good
Fatigue Limit	Good	Mediocre	Good	Good
Creep	Mediocre	Mediocre	Excellent	Mediocre
Hardness	Good	Good	Good	Mediocre
Density	Mediocre	Good	Good	Excellent
Dimensional stability	Good	Mediocre	Good	Mediocre
Thermal stability	Mediocre	Good	Excellent	Mediocre
Hygroscopic characteristics	Excellent	Mediocre	Good	Mediocre
Environmental resistance	Mediocre	Mediocre	Mediocre	Good
Exploitation	Good	Good	Good	Mediocre
Corrosion resistance	Mediocre	Mediocre	Mediocre	Excellent

The eighties were characterized by the development of the first industrial composite materials, namely special mortars made with the addition of short polymeric fibers (carbon and polyvinyl alcohol) for the structural refurbishment of concrete and masonry elements.

In the 1990s, innovation is continued in the industrial flooring sector with the replacement of welded wire mesh and metal fibers with a new generation of synthetic structural fibers based on modified polymers. This technology had both operational and functional advantages, as well as considerably increasing the durability of the structures in aggressive environments.

With the new millennium, we are present at the introduction of the composite materials with long fibers that use an inorganic matrix as adhesive, overcoming all the limits of epoxy resins in terms of effectiveness, applicability and durability.
These materials, compared to traditional FRPs, are eco-sustainable due to negligible impact on the environment and health of operators; in fact, epoxy resins contain harmful substances to humans and pollutants to the environment.
Today, another step forward is the possibility to use new generation structural fibers, with different nets and several ecological matrices, for the reinforcement of all types of structures.

2.2. The Reasons of Structural Reinforcements

During the service life of the building, it can happen that the carrying capacity of the structure is not able to carry out the static and dynamic functions provided by the project anymore or produced from variations in use. The reasons could be:

- Degradation of the materials of the building, that can cause both the decrease in the resistance section and the deterioration of the mechanical properties of the structure;
- Variation in the use of a building, that could cause an unexpected overload in the structural members;
- Unpredictable events such as failures in the foundations, strong impacts, fires and earthquakes, that can cause localized or extensive damage to the whole construction.

If static loads create problems on the directly concerned individual structural elements, dynamic loads, such as earthquakes, also test the connections between them, such as the beam-pillar joints in reinforced concrete structures and the connections between walls, slabs and vaults in masonry structures (Fig. 2.1).

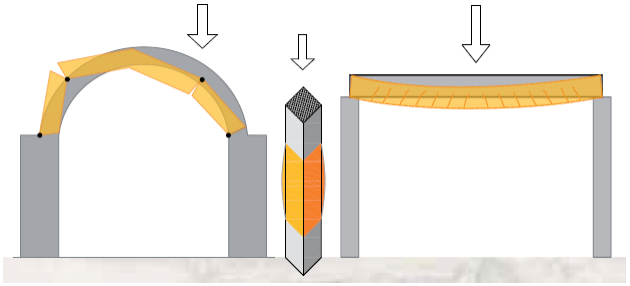

Figure 2.1 - Connections between the structural elements [Ruredil book]

2.3. Evolution in Reinforcement Systems

Traditional reinforcements consist in the replacing or reintegrating the degraded materials used in the structures (blocks, mortars, concrete, bars) with the scope to rebuild the original section and continuity, possibly increasing the sections to ensure greater carrying capacity and safety.

In ancient times, wood and iron elements such as chains, tie rods and reinforcement ring were included into the masonry in order to improve the structural performance or to withstand the forces action that damage the structural scheme. Instead, in recent times, the confinement on reinforced concrete pillars, as well as steel slabs attached at intrados and base glued with epoxy resins are used.

These types of operations are difficult to perform and strongly invasive for static and aesthetics of constructions. In addition, they also exhibit a poor durability to maintain the effectiveness of reinforcement through time. In fact, used materials (resins or epoxy-based mortars) are characterized by mechanical performance that are higher than those of the reinforced structure. This cause greater mechanical stress in the weakest material that will achieve the collapse easier, defeating the reinforcement.

Structural reinforcements are composite materials made up of the union of high mechanical performance long fibers and a matrix, used as adhesive that allows the transfer of stresses from the structure to the fibers. The fibers used for structural reinforcement have high elastic modulus and high tensile strength, such as carbon, aramid and PBO (polyparafenylbenzobisoxazole). Originally, they were developed for aeronautical and aerospace applications. However, only in the last twenty years, with the reduction of interventions in these areas, the surplus of these materials has promoted a decrease in prices so that it can be used in other fields, such as

construction, where they have been used as anti-seismic coatings on reinforced concrete and masonry structures.

For the exceptional mechanical properties of structural fibers, this technology allows to use a reinforcement characterized by practicality, reduced invasiveness, speed of application and low cost if compared with the traditional techniques.

Their lightness is well suited for use on particularly weak structures, without increasing the loads of the structure and respecting the architectural character of the building and the functionality of the structural elements.

Finally, the ease of installation and the great ability to adapt to all the structural elements have decreed the success of this material even in the construction field.

2.4. Composite Materials Advantages

Composite materials allow gaining the following advantages:

- Increase of carrying capacity;
- Reduction of deformations;
- Limitation of cracked states;
- Prevention of failure mechanisms;
- Increase of duttility.

There are many fields of application, among which:

- The longitudinal application of deflected structural elements at the intrados (such as beams or joists) is associated with that of a U-shaped transverse bracket that is used to reinforce the area where shear stress is maximum.
- The reinforcement ring of compressed elements or bended elements through axial compression, such as pillars in reinforced concrete and masonry structures or stone columns.
- The application of the reinforcement on panels bearing the shear stress and vault in masonry.

2.5. Fiber Reinforced Polymer (FRP)

FRP composite are heterogeneous materials, because of the presence of different components, and anisotropic, and show a linear elastic behavior until failure, then contrarily to steel ductility, isotropy and plasticity do not exist (Fig. 2.2). The anisotropic nature leads with different strength material in compression and in tension and consequently with different elastic modulus values. Indeed, in case of orthogonal stress to the fiber direction, the material strength and stiffness are significantly reduced. Otherwise, in case of stress along the fiber direction, strength and stiffness reach their maximum value. This peculiar characteristic does not represent an issue, but it should be considered during the design [24], because the reinforcement needs to develop its maximum strength in the right directions.

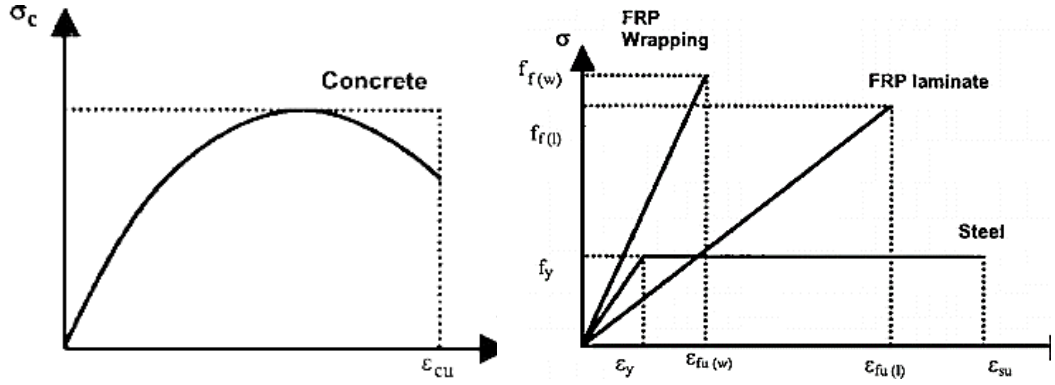

Figure 2.2 - Idealized stress-strain curves for construction materials [Karbhari, 2007]

Fiber reinforced materials are characterized by different constituents, namely reinforcement material, matrix, additives and other components present in small quantities such as fillers and pigments. Fiber is the reinforcement material and it can be made of organic materials such as carbon, inorganic such as glass or polymeric materials such as aramid, but this last case is quite rare. The reinforcing fraction in FRP composites varies from 25 to 70% depending on the manufacturing process chosen and it is higher than the reinforcement content in reinforced concrete, which accounts only 5% [24].

The matrix made of a polymeric or epoxy resin is a continuous embedment [25], [26], [27], [28]. It locks the reinforcement and, at the same time, it transfers the external load to the fibers [29]. Additionally matrix covers the reinforcement

protecting it against environmental effects. The interface is the contact area between the reinforcement and the matrix and it needs to be considered carefully because the variation of the interfacial interaction may affect the performance of the composite FRP system.

The constitutive relations of a fiber reinforced composite material, fiber and matrix show that the composite material has lower strength than fiber, but the same value of strain failure, because once this strain value is overcome, the stress transfer from the matrix to the fiber cannot occur (Fig. 2.3). Then, the compatibility of chosen fiber-resin system is significantly important. Indeed, when the composite is loaded in tension, the resin should be able to reach at least the same level of fiber deformation.

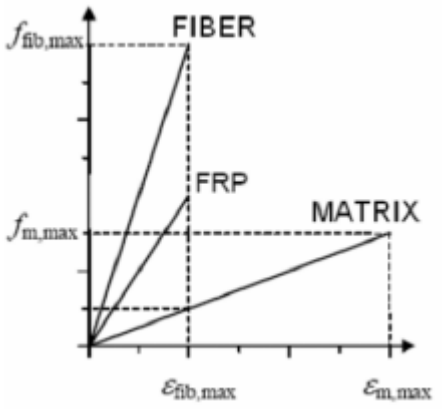

Figure 2.3 - Qualitative comparison of constituent's stress-strain relations [Mela, 2013]

2.5.1. Applications of FRP in Civil Structures

Adopted materials and application techniques differentiate Externally Bonded Fiber Reinforced Polymer Reinforcement systems (**FRP EBR**) in two groups:

- *Precured systems*: manufactured flat laminates made by pultrusion and glued to the structural element with adhesive;
- *Systems impregnated in situ*: dry sheets impregnated in situ with resin or partially pre-impregnated. The system curing occurs in place and the resin represents the adhesive between fiber and structural element.

2.5.1.1. Precured Systems

Pultrusion is a technology used for many composite materials. In the production process, fibers are withdraw from reels and directed to resin bath, where their impregnation occurs. After the composite enters in a heated mold, where it is consolidated under pressure. When the resulted material exits from the mold, the matrix solidifies and the composite can be cut with a circular saw. These laminates are completely polymerized, then they are rigid and they can be applied in flat surfaces or with a curvature smaller than 3 m. Special shaped versions can be applied in corners and nodes.

Their peculiar characteristics are:

- Uniform and controlled resin;
- Lower weight;
- 10 – 20 % better performance than wet lay-up.

The advantages are:

- No adherence problems between matrix and fiber;
- Uniform material;
- Perfect fiber arrangement;
- Low sensitivity to the procedure adopted in the canter.

2.5.1.2. Systems Impregnated in situ

The fiber arrangement divides this system in two categories, *unidirectional* and *bidirectional*. The choice depends on the type of structure and on the type of solicitation. Unidirectional tissues are exploited when structural elements are subjected to mono-axial traction or flexure. Generally, these tissues are used when the isostatics of traction are know in advance. The installation is performed arranging fibers along the direction of the maximum traction stresses. Otherwise elements subjected to shear, torsion or solicitation with different directions are more efficiently reinforced with bidirectional tissues, an alternative and effective solution can be the application of many unidirectional tissues arranged along different directions. Tissues for structural reinforcement are generally provided in rolls. They are dry, then not impregnated with resin or pre-impregnated with resin partially

polymerized. They are glued on the substrate with or without the use of additive resins. The first operation is the preparation of the resin, generally the use of epoxy bi-components is preferable in which the mix of pre-polymer and hardening occurs. After the resin is spread uniformly along the concrete surface and, when the FRP external reinforcement is applied, the resin should present low viscosity to allow the complete impregnation of fibers before hardening. When FRP is positioned, fibers alignment and the elimination of air inside need to be insured [30].

2.5.2. FRP Composite Materials in Structural Reinforcement

In the last thirty years, FRP composite materials have experienced a wide diffusion in the construction sector thanks to its great effectiveness in retrofitting and repairing structural elements. The large variety of geometries and mechanical properties makes this technology exploitable for a very wide range of reinforcing interventions such as:

- Bandage of elements under compression or under combined compressive and bending stress, as columns, to increase their compressive strength, ductility and resistance against seismic actions;
- Rapping of cylindrical elements subjected to hydrostatic pressure such as pipes and silos;
- Plating of nodes beam-column in seismic zone to improve ductility and the capacity to dissipate energy;
- Bending and shear reinforcement of beams, floors and ceilings;
- Reinforcement of masonry structures.

This technique allows increasing the strength and reduces breakings and deformations. The great advantage provided by the exploitation of composite materials for reinforcing structural elements is the performance improvement in short time, without the interruption of the building use, and long-term protection. The exploitation of FRP has allowed the recovery of degraded and damaged structures, structural and seismic adjustment and securing of buildings in emergency situations. The reinforcement should be arranged to develop its

maximum strength where recovery is needed and the choice to exploit unidirectional or bidirectional tissues is up to the designer.

2.5.3. American Guideline ACI 440

The American Concrete Institute (ACI), founded in 1904, has the aim to share the knowledge about design of concrete structures in order to develop building codes and to enhance existing ones. ACI Document 440.2R-08 (2008) called "*Guide for the Design and Construction of Externally Bonded FRP Systems for Strengthening Concrete Structures*" in section 9.4 called "*Design material properties*" provides values for environmental reduction factors with respect to the specific FRP system chosen and with respect to the exposure condition. Specifically, depending on the exposure condition: interior, exterior or aggressive environments, a specific reduction factor is assigned to each fiber type (carbon, glass or aramid) and is shown in Table 2.2.

Table 2.2 - Environmental Reduction Coefficients in ACI 440

Exposure condition	**Fiber type**	**Environmental reduction factor C_E**
Interior exposure	Carbon Glass Aramid	0.95 0.75 0.85
Exterior exposure (bridges, piers, and unenclosed parking garage)	Carbon Glass Aramid	0.85 0.65 0.75
Aggressive environment (chemical plants and wastewater treatment plants)	Carbon Glass Aramid	0.85 0.50 0.70

Particularly, the reduction factor of interior exposure will be close equal to the unity when the environment is the most benign. On the contrary, the exposure to aggressive environments leads to lower environmental reduction factors.

The ACI 440.2R-08 (2008) guideline provides then specific values for reduction factors by considering the environmental effect, that otherwise would not be considered in the design procedure, while the manufacturing procedure is not taken into account.

The environmental factors showed in Table 2.2 are based on the long-term exposure and they are used in the Step 1 of design procedure involving the computation of FRP material properties such as composite strength and strain at break (Eq. 2.1, Eq. 2.2):

$$f_{fu} = C_E \cdot f^*_{fu} \tag{2.1}$$

$$\varepsilon_{fu} = C_E \cdot \varepsilon^*_{fu} \tag{2.2}$$

where

f_{fu} is the design ultimate strength;

ε_{fu} is the design ultimate strain;

f^*_{fu} is the characteristic design strength;

ε^*_{fu} is the characteristic design strain.

Specifically, characteristic tensile strength and strain value are evaluated as follows:

$$f^*_{fu} = \overline{f_{fu}} - 3\sigma \tag{2.3}$$

$$\varepsilon^*_{fu} = \overline{\varepsilon_{fu}} - 3\sigma \tag{2.4}$$

where

$\overline{f_{fu}}$ is the mean ultimate strength;

$\overline{\varepsilon_{fu}}$ is the mean ultimate strain;

σ is the standard deviation.

The subtraction of 3σ from the mean ultimate strength value makes the characteristic strength representative of the strength found in 99.86 % of all sample in a population and it corresponds to a percentile equal to 0.14 [31].

The ACI 440.2R-08 (2008) assumes that the elastic modulus does not change before and after the conditioning of the specimens, because it is not affected by environmental conditions and it can be approximated with the mean of all elastic moduli of the specimens. Since FRP materials are characterized by linear elastic behavior until failure, the modulus of elasticity is calculated by means of Hooke's law (Eq. 2.5), namely it is equal to the ratio between the ultimate tensile strength and the rupture strain, and they are reduced by means of the same environmental factor:

$$E_f = \frac{f_{fu}}{\varepsilon_{fu}} \tag{2.5}$$

2.5.4. Italian Government Guidelines for Identification, Qualification and Acceptance Control

The Superior Council of Public Works approved the *Guidelines For The Use Of Fiber Reinforced Polymer Matrix Composite (FRP)* for the structural consolidation of existing constructions in July 2016. The guideline "*Linea Guida per la identificazione, la qualificazione ed il controllo di accettazione di compositi fibrorinforzati a matrice polimerica (FRP) da utilizzarsi per il consolidamento strutturale di costruzioni esistenti*" has been approved by Decree of the President of the Superior Council of Public Works n. 220 of July 09, 2015. It has been approved with favourable opinion n.115/2013 of 19 February 2015 by the First Section of the Superior Council of Public Works.

Pursuant to Article 2 of the Approval Decree, until 8 July 2016, with regard to the use of fiber reinforced polymer matrix composite (FRP) for the structural consolidation of existing constructions, it was possible to continue to refer to point 8.6 of the Technical Standards for Construction according with the Ministry Decree of 14 January 2008.

2.5.4.1. Scope of the Guidelines

The Technical Standards for Buildings in force, approved by Ministry Decree of January 14 2008 (hereinafter NTC 2008) stipulate, in Section 11.1, that all materials and construction products, when employed for structural use, must be identifiable, possessing specific qualification for expected use and also be subject to control in the acceptance step by the Work Manager.

For this purpose, the aforementioned Decree provides that the materials and construction products for structural use, when not marked CE pursuant to Regulation (EU) n. 305/2011 or not endorsed by the European Technical Assessment, must be in possession of a Technical Suitability Certificate (hereinafter CIT) issued by the Central Technical Service (hereinafter STC), on the basis of guidelines approved by the Superior Council of Public Works.

Particular attention is paid to the rules on the use of not-traditional materials, including Fiber Reinforced Polymer matrix composite (FRP). Thermoplastic polymer matrices are excluded from this Guideline.

The structural use of these materials in the context of existing building consolidation interventions, and is currently dealt with in point 8.6 of the NTC 2008.

This Guideline provides procedures for the identification, qualification and acceptance of FRP reinforcement systems. Therefore, it replaces the procedures for the identification, qualification and acceptance contained in the “Linee guida per la Progettazione, l'Esecuzione ed il Collaudo di Interventi di Rinforzo di strutture di c.a., c.a.p. e murarie mediante FRP” approved on July 24 2009 by the General Assembly of the Superior Council of Public Works and published by the STC.

For the technical characteristics of the used materials such as yarns, fabrics and matrices, it might refer to the documents in Chapter 12 of the NTC 2008 and, in particular, to the above Guidelines “*Linee guida per la Progettazione, l'Esecuzione ed il Collaudo di Interventi di Rinforzo di strutture di c.a., c.a.p. e murarie mediante FRP* ”.

2.5.5. The Limits of Traditional Composite Systems: FRP Systems are not reliable

The limits of Fiber Reinforced Polymer (FRP) systems, in which fibers are bonded with a polymer matrix, are due to the presence of epoxy resins. These are unreliable for reinforcement purposes, because they are not durable for certain thermo-hygrometric operating conditions. In fact, the poor durability of the resin causes the decrease of adhesion of the FRP to the support and the inability to transfer the stress from the structure to the composite material.

The characteristics of the resins depend on the environmental conditions, namely:

- **Poor resistance at medium temperatures**: organic resins undergo progressive changes from 30 °C with the gradual loss of adhesion from the support;
- **None fire resistance:** organic resins burn and release toxic fumes;
- **Loss of efficacy with high environmental humidity:** even when the curing of the matrix has already occurred, the resin exhibits a significant loss of adhesion from the support if the relative humidity of the air remains high during the use of the structure (80-90 %);
- **Limited application depending on ambient temperature:** hardening of the epoxy resin is only between +10 °C and +30 °C;
- **Inability of application at high humidity conditions:** polymerization of the organic resin is prevented with surface humidity above 6 % and U.R. over 85%;
- **None vapor permeability:** application of the system can cause surface condensation on the opposite side of the reinforced wall, that provokes surface degradation phenomena;
- **Brittle behavior of the reinforced structure at the breaking load:** the high stiffness of the organic matrix, compared with that of the support, causes a reduced elongation under load that provokes the sudden detachment of the reinforcement;
- **Irreversibility of reinforcement application:** the adhesion of organic resins, that impregnate the substrate deeply, prevents the complete removal of the matrix from the structure.

2.6. The New Frontier of the Reinforcement: FRCM Composite Materials

FRCM (*Fiber Reinforced Cementitious Matrix*) structural reinforcement systems are made of a high performance fiber and a stabilized inorganic matrix, used with the adhesive function, thus to replace the epoxy resins of traditional FRP systems. Therefore, there is the introduction of a worldwide innovation in the field of structural reinforcements that is the development of several FRCM reinforcement systems used for the reinforcement and seismic adaptation of the new and existing structures.

Different types of fibers are used in reinforcement systems that have high performance mechanical properties in order to absorb the stresses generated by overloads and exceptional events such as earthquakes.

Inorganic matrices, different for each specific reinforcement system, ensure effective adhesion both to the structural fibers of the mesh and to the substrate, guaranteeing high reliability of the structural reinforcement.

Composite reinforcements use structural fibers with different textures (bidirectional and unidirectional) to ensure maximum versatility of use in different loading situations: column undergone to combined compressive and bending stress, shear strength of panels, bending of beams and slabs, directional variability of seismic actions.

2.6.1. Innovation of Inorganic Matrix

Using an inorganic matrix to apply structural reinforcement means overcoming all limits regarding the safety, reliability and durability of the mechanical performance of FRP systems, because the stabilized matrix is more compatible with the substrate. FRCM reinforcement systems guarantee:

- **Applicability on damp substrates:** the binder used is hydraulic type and therefore is not affected by the presence of moisture;
- **Fire resistance:** the matrix exhibits the same reaction of the support when it is in direct contact with fire, namely it is not combustible, has low emission of fume and does not release heated particles;

- **Good resistance at high temperatures:** inorganic binders keep unaltered their mechanical and adhesion characteristics to the support from +5 °C to + 550 °C;
- **High resistance to freezing and thawing cycles;**
- **Water vapor permeability:** the matrix avoids the condensation phenomena that can damage the masonry;
- **No toxicity:** the matrix is not a harmful product for the health of the operator or for the environment, so it can be applied without the use of special protections and can be disposed of without special precautions;
- **Ease of application:** the matrix must be mixed only with water and does not require the use of specialized teams for applying;
- **High reliability of the reinforcement system even after reaching the breaking load:** ductile post-cracking behavior avoids the detachment of the FRCM system from the reinforced structure;
- **Durability even at high environmental humidity:** the inorganic matrix does not change its adhesion characteristics to the support;
- **Workability in a wide range of temperatures:** there are not significant differences in workability, curing and hardening time between + 5 °C and + 40 °C;
- **Reversibility of the system:** the adhesion mechanism of the inorganic matrix allows removing the reinforcement.

2.7. Behavior of FRCM and FRP Reinforcement Systems at High Temperatures

In order to understand the behavior of FRCM and FRP reinforcement systems at high temperatures, flexural strength has been taken in consideration. The reason is that compressive strength of concrete is much more sensitive to the degradation that occurs in the concrete due to heat.

The decay of the mechanical performance of the concrete begins at 130 °C as shown in the Figure 2.4. It can also be noted that structural reinforcement by composite materials maintains the increase in flexural strength with respect to unreinforced concrete when the test temperature increases. In fact, FRCM reinforcement systems

maintain their effectiveness up to 550 °C. Even at 550 °C, the advantage increases (+ 173 %) compared to ambiental temperature (+ 121.5 %) because the reinforcement is able to completely oppose the decoesion phenomenon between inerts and cement paste, which causes the loss of strength in un-reinforced concrete.

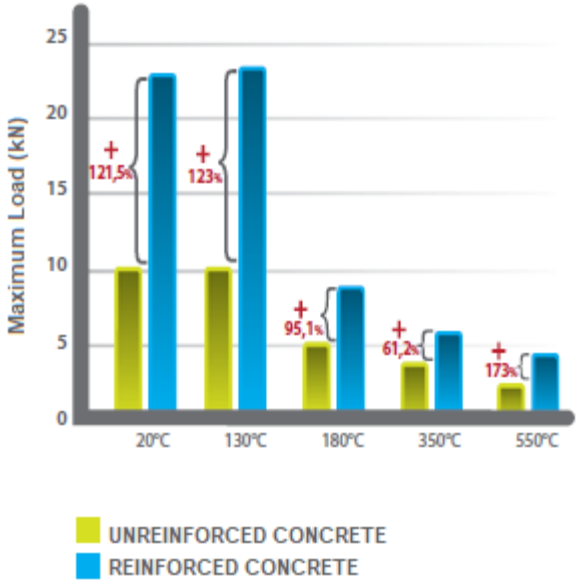

Figure 2.4 - Change of flexural strength based on temperature [Ruredil book]

2.8. Post-cracking Ductility and Fire Resistance

FRCM reinforcement systems modify the brittle failure behavior characteristic of FRP reinforced masonry structures, in favor of greater deformation capacity of the single element and an overall increase of reinforcement effectiveness on the entire structure.

Structural reinforcement of masonry is more effective and reliable when it exhibits a ductile behavior after reaching the maximum load. This property coincides with the measurement of the area under the load-displacement curve detected during a bending test. So, the greater the area, the greater the capacity of the system to disperse energy.

The FRCM systems provide excellent performance, since the deformations of the matrix under load are similar to those of the supports, ensuring adhesion of reinforcement even after the peak load.

All FRP systems are classified as “Type E” because they use an organic adhesive that contributes to the generation and propagation of the fire and therefore they need to adequate fire protection.

According the European regulations in force UNI EN 13501-1, the classes of fire reaction are as follows:

Table 2.3 - Classification of reaction to fire according to UNI EN 13501-1

CLASSIFICATION OF REACTION TO FIRE		
A1 –A2	No Flammability	Absence of flash
B	No Flammability	Absence of flash
C	Low Flammability	Absence of flash-over
D	Normal Flammability	Risk of flash-over
E	Poor reaction to fire properties	Risk of flash-over
F	No reaction to fire properties	Risk of flash-over

2.9. The Properties of Reinforcement Systems for Seismic Adaptation of Structures

The structural reinforcement is aimed to upgrade the structure in the seismic zone. Composite materials are particularly suitable for this purpose thanks to their strength, lightness and ease of application. The seismic adaptation strategy is to avoid all the mechanisms in and out plan that can cause the collapse of the single bearing element, as well as improving the overall bearing capacity of the structure. This requirement is obtained increasing the ductility of the plastic hinges in the reinforced concrete structures and ensuring a box-like behavior of the structures in masonry to make them more resistant to horizontal forces, avoiding the orthogonal thrusts to the panels and connecting the perpendicular bearing elements (Fig. 2.5).

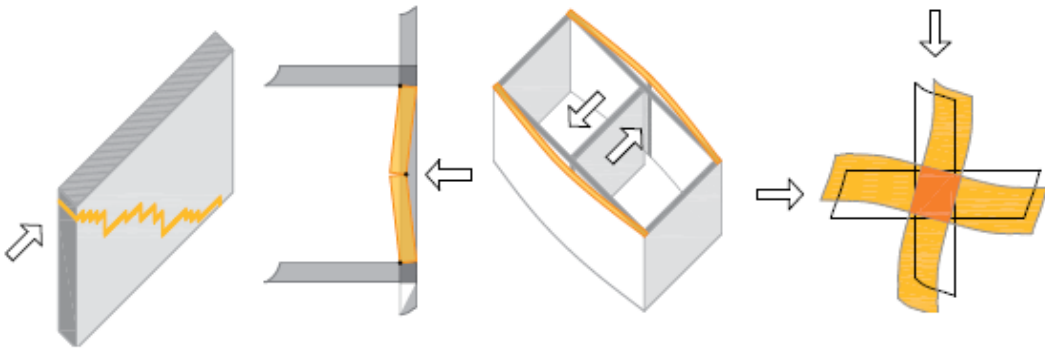

Figure 2.5 - Collapse mechanisms [Ruredil book]

For the effectiveness and reliability of the seismic adaptation, the deformation capacity of the single reinforced element and the reinforcement adhesion to the structure, even after the first cracking in the support, are important. FRCM reinforcements guarantee these features.

2.10. Durability Based on Humidity and Ambient Temperature

FRCM systems maintain performance independently of humidity and serviceability temperature, unlike the FRPs that only guarantee them under standard thermo-hygrometric conditions (20 °C and 50 % H.R.), as shown in Figures 2.6 - 2.7.

From the experimental experiences, it turns out that the presence of moisture on the surface of the FRP reinforced structures causes a change in the type of failure. In fact, it becomes from cohesive, namely in the support, to adhesive, that is to the support-reinforcement interface. In Figures 2.7 - 2.8, it can be noted that prolonged exposure to moisture determines a progressive deterioration of shear and flexural mechanical strength. It becomes ever faster at increasing of the temperature in the 23 ÷ 40 °C range.

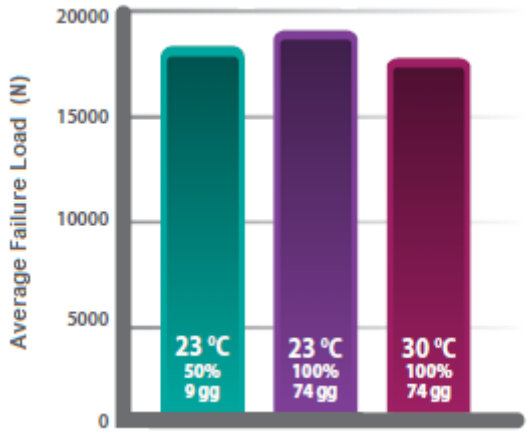

Figure 2.6 - Flexural strength of FRCM based on temperature, relative humidity and days of exposure [Ruredil book]

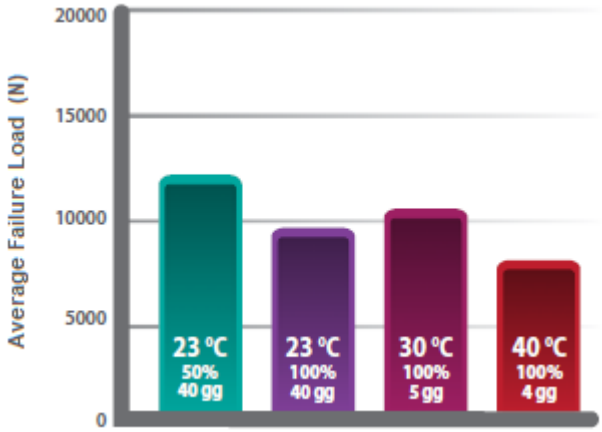

Figure 2.7 - Flexural strength of FRP based on temperature, relative humidity and days of exposure [Ruredil book]

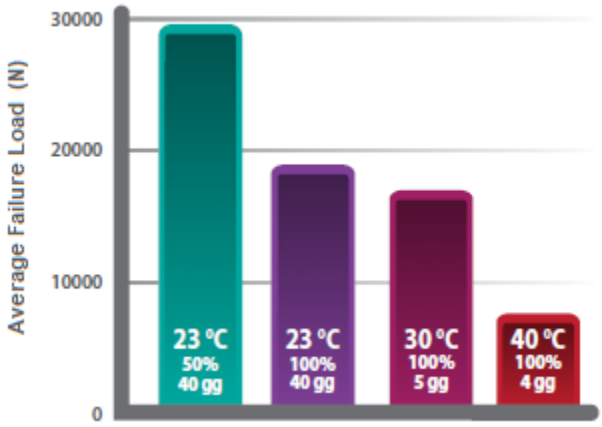

Figure 2.8 – Shear strength of FRP based on temperature, relative humidity and days of exposure [Ruredil book]

The ACI 440.2R-08 standard highlights that the epoxy resins become from rigid to viscous at 30 °C, provoking the degradation of adhesive and therefore mechanical properties of FRP systems.

In addition, it establishes that the effective reinforcement serviceability temperature is obtained decreasing of 15 °C the glass transition temperature of the resin (T_g). For example, if T_g is 50 °C, the maximum serviceability temperature that guarantees the effectiveness of the FRP reinforcement is 35 °C.

2.11. A New Tool in the Repair Toolbox: Steel Reinforced Grout

SRG is the latest development on repair techniques. It is another tool among the concrete and masonry strengthening methods that complements existing FRCM and FRP. SRG has emerged as promising and cost-effective technology for the external strengthening of RC structures. It consists of a reinforcement fabric made of ultra-high-strength steel cords embedded in a cementitious grout and externally bonded to the substrate.

2.11.1. SRG Composite Systems

Composite systems have been increasingly used in the last two decades for repair and strengthening reinforced concrete and masonry structures. They consist of high strength textiles externally bonded to the surface of the structural elements and, thanks to their high strength-to-weight ratio, provide a significant improvement of the structural capacity with minimum mass increase. Nevertheless, drawbacks related to brittle failure, long-term durability, sensitivity to impacts, and high cost have limited their widespread use. After the diffusion of Fiber Reinforced Polymers (FRPs), mortar-based composites have been recently developed, which make use of high performance textiles (continuum dry fibers arranged in the form of open mesh or fabric) externally bonded with either cement or lime mortars. These systems are known as either TRMs (Textile Reinforced Mortars) or FRCMs (Fiber Reinforced Cementitious Matrices). Despite their adhesion, strength may be lower than FRPs in certain cases, they offer important advantages in terms of fire resistance, vapour permeability, removability, and ease, time and cost of

installation, thanks to the use of inorganic matrices in place of resins [32], [33], [34].

Numerous textile materials can be used, including carbon [35], [36], glass [37], [38], steel [39], [40], [41], basalt [42], PBO [43], [44], [45], and natural fibers [46], [47]. Amongst all these possibilities, steel-based reinforcements offer particularly good mechanical performance thanks to the high tensile strength of the textile and the effective cord-to-mortar interlocking [48], [49], at relatively low costs.

Steel textiles are constituted by cords of Ultra High Tensile Strength Steel (UHTSS) micro wires and have been initially developed for the reinforcement of automobile tyres. The first application in civil engineering was proposed for the flexural strengthening of reinforced concrete beams [50], [51], [52] taking the name of Steel Reinforced Grout (SRG). Then, SRG has been used in other research studies on reinforced concrete beams [53], [54], [55], [56], [57] masonry arches [58], [59], and walls [60], [61]. The need of effective, versatile and cost efficient strengthening methods has encouraged producers to develop and sell steel textiles for structural rehabilitation purposes, such that SRG has already been used in the field for the seismic retrofitting of masonry walls [62], [63], [64] and vaults [65], [66].

Despite the scientific and industrial research carried out so date, and the existing applications realized, there are still important issues which need to be further investigated, such as the influence of textile layout, mortar strength and substrate properties on the SRG-to-masonry bond performance and the durability of the steel textiles.

2.11.2. Properties of the SRG Composite Systems

The SRGs consist of small strands of thin Ultra-High Strength Steel (UHSS) cords, that are continuous and braided to form strands, which are then assembled into a “fabric” and impregnated by means of a cement-based matrix (Fig 2.9). The cords are either coated (with zinc or brass) or made of stainless steel, to provide protection against corrosion, and are fixed to a fiberglass micromesh to facilitate installation, which can be installed using a mineral mortar or a natural hydraulic lime mortar according to project and building site requirements. The structural strengthening sheet is thus extremely easy to handle and shape, and combines excellent

mechanical and installation properties with high durability thanks to coating of the individual cords. Coating steel fiber sheets guarantee unique structural and mechanical properties, much higher than traditional carbon-glass-aramid fiber sheets, making them particularly effective in the various structural strengthening and seismic upgrade or compliance retrofit solutions, as well as the creation of suitable connection systems.

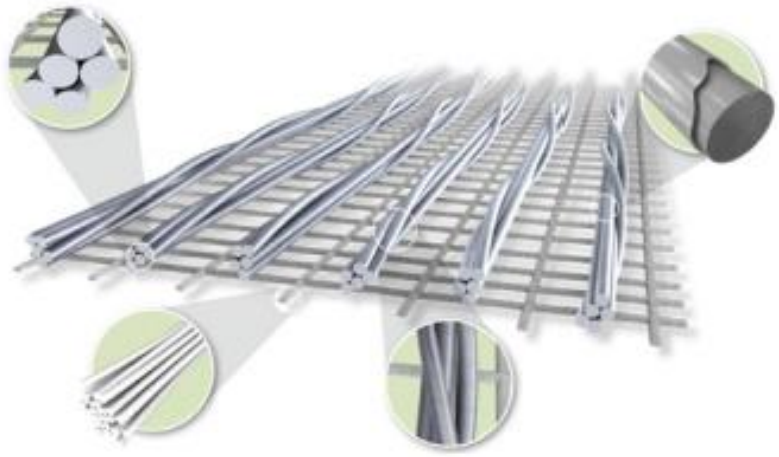

Figure 2.9 - Ultra-High Strength Steel textile [Kerakoll catalogue]

2.11.3. Physical-geometric Characteristics

Physical-geometric factors able to influence the mechanical response of the composite are the filament resistance class, the wire diameter, the type of strand, and the density of the fabric. The novelty of these composites lies in the used steel, that is an evolution of a perlitic or hypereutectic steel (with carbon content between 0.8 % and 0.96 %) subjected to a process that can be summarized in a first wire drawing process, followed by tempering treatment, brass or zinc plating, fine wire drawing and cutting. The achievement of such high resistance classes (between 2400 and 4000 MPa) with very small diameters, suitable for use in composite materials, leads to a loss of ductility of the yarn. It implicates, consequently, the risk of brittle failure by delamination and a lesser elongation at break if compared with larger diameter wires.

Single wires have diameters between 0.20 - 0.48 mm; therefore, the strand has a variable size between 0.89 and 1.02 mm (hence less than one tenth of the minimum

diameter of a pre-stressing strand). The reduced dimensions of steel filaments are functional to produce flexible laminates with small thickness (between 1.19 mm and 1.32 mm), and are essential to achieve high resistances sufficiently to allow their use for the structural purpose.

The type of strand depends by the requirement to ensure a suitable mechanical adhesion between the matrix and the reinforcement element. In fact, it is desirable to make a composite in which the reinforcement breaks before it slides into the matrix. In this regard, the use of single small diameter wires would involve insufficient resistance to the interface with the matrix. Therefore, strands, obtained by twisted wires, are used (Fig. 2.10). These wires have a corrugated surface to guarantee an adequate adhesion.

Another import factor that influence the performance of the reinforcement is the density of the fabric, namely the number of strands per width unit (Fig. 2.10). This parameter affects both the mechanical response of the composite in terms of mechanical strength, stiffness, etc., and the choice of matrices with different viscosity values.

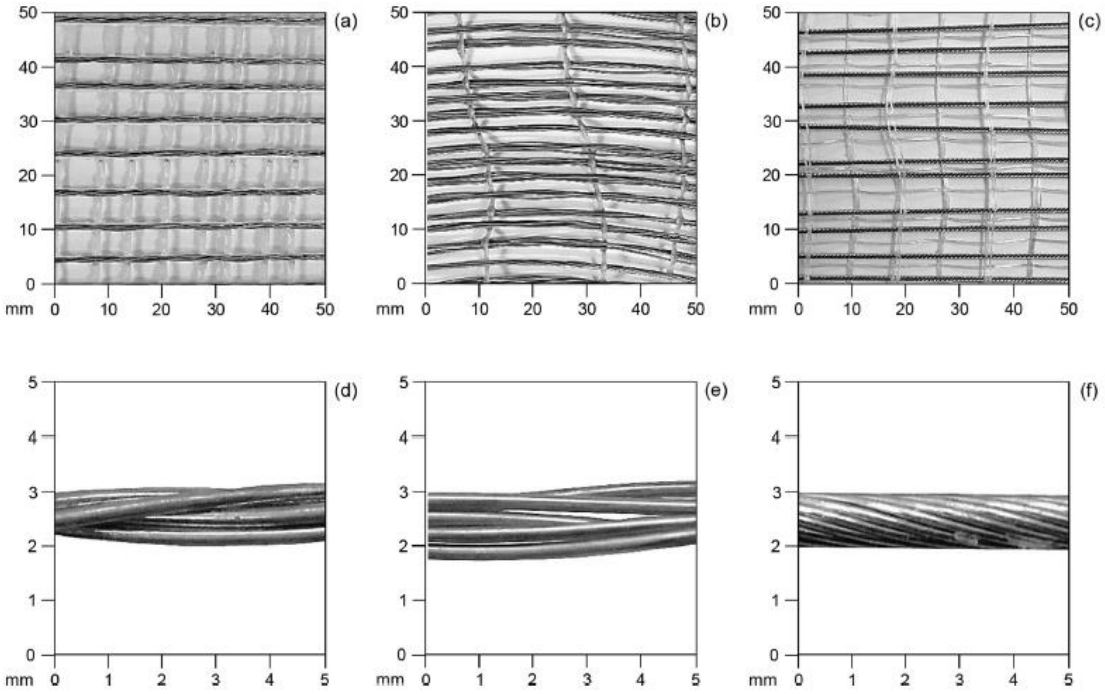

Figure 2.10 - Textiles (a, b, c) and detail of cord/rope (d, e, f) of steel types G (galvanized steel cords, a, d), S (stainless steel cords, b, e), and R (stainless steel ropes, c, f) [De Santis et al, 2017]

2.11.3.1. Mechanical Characteristics

Use of Ultra-High Strength Steel fibers (Table 2.4) increases the ductility of the reinforced elements. It is higher than that of conventional reinforcements in composite, thus favoring the applications in the case of seismic problems. Another important element is shear strength of steel that simplifies the connection and anchoring issues. Low and medium density fabrics allow employing cement based mortars. This implicates benefit in cost, fire resistance and operational simplicity, which are typical limit of the use of traditional composite materials.

Table 2.4 -Properties of steel textiles

Textile	Label	c (cords/mm)	Δ (mm)	γ (kg/m^2)	t (mm)
Galvanized steel cords	G	0.157	6.35	670	0.084
Stainless steel cords	S	0.315	3.18	1500	0.188
Stainless steel ropes	R	0.200	5.00	1057	0.138

In fact, the mechanical behavior of resins passes from fragile and hard to plastic and malleable at temperature upper than 60 °C and 80 °C, undergoing a decay resulting in loss of load transfer capacity to reinforcement. Instead, cement based mortars are able to retain crystallization water and hence to reach much higher temperatures before recording a degradation of the mechanical properties of the material.

Chapter 3
Characterization testing of FRCM and SRG

3.1. Introduction

Even if FRCM are now widely used for repair and strengthening existing structures and fundamental information has been recently provided by research studies on tensile response, durability, and bond performance on both masonry and concrete substrates, there is still a lack of standard codes that provide producers, designers and contractors recommendations for testing, design, installation, and control.

At present, mortar-based systems are however made available in the European market, used in current design practice, and installed without having undergone a standardized mechanical characterization, such that the actual reliability of the strengthening work remains uncertain and hardly verifiable [67].

The first document regarding the use of FRCM was released by the International Code Council Evaluation Services (ICC-ES) and approved in 2003, entitled *"Acceptance Criteria for Cement-Based Matrix Fabric Composite Systems for Reinforced and Unreinforced Masonry"* followed by the *"Acceptance Criteria for Masonry and Concrete Strengthening Using Fabric-Reinforced Cementitious Matrix (FRCM) and Steel Reinforced Grout (SRG) Composite Systems"* (AC434) issued by ICC-ES in 2016. The reason for the development of these criteria is to provide guidelines for the evaluation of alternative strengthening methods for masonry and concrete structural elements, where the codes do not provide requirements for testing and determination of structural capacity, reliability and serviceability of these products.

For manufacturers, AC434 establishes the guidelines for tests and calculations in order to receive a product Evaluation Report from ICC-ES. Once obtained, the "evaluated" FRCM system is recognized as an approved repair method by any building official.

Another document titled "*Guide to Design and Construction of Externally Bonded Fabric-Reinforced Cementitious Matrix (FRCM) Systems for Repair and Strengthening Concrete and Masonry Structures*" has been released by ACI

Committee 549 in December 2013 (ACI549.4R-13). This document is harmonized with the revised version of AC434 and provides the needed tools for material selection, design and installation.

In July 2002, *RILEM* (International Union of Laboratories and Experts in Construction Materials, Systems and Structures) formed the Technical Committee 201-Textile Reinforced Concrete that published a state of the art report (RILEM TC 201-TR 2006). This report includes information on applications of textile reinforced concrete and strengthening systems for unreinforced masonry. In addition, the Italian department "Consiglio Nazionale delle Ricerche" (CNR) is developing a new document in order to provide guidelines and information in compliance with the European standards.

Test procedures need to be defined in details and reported in guidelines or recommendations. A relevant work has been done in this direction by the RILEM Technical Committee (232-TDT), in cooperation with ACI549, and it is a direct follow-up of the successful Committee TC 201-TRC.

Anyway, standard procedures should provide the fundamental mechanical parameters for the structural design and for both product qualification and material assurance purposes, combining simplicity and reliability. The purpose of qualification testing is to establish requirements for recognition of Fabric Reinforced Cementitious Matrix (FRCM) and Steel Reinforced Grout (SRG) composite systems, used for the strengthening of masonry and concrete structures. The reason is to provide acceptance criteria for the evaluation of FRCM and SRG material properties, force and deformation limit states, including failure modes of the composite material and each structural system to support a rational analysis and design procedure. The specimens shall be prepared to verify the range of the FRCM and SRG composite material configurations such as layers, thickness, components, bonding agents, etc. Tests shall simulate the anticipated range of loading conditions, load levels, deflections, ductility and performance under environmental exposures and exposure to fire conditions. According to AC434, evaluation of test results shall be made based on the average values obtained from a minimum of five specimens for each condition. The term "*condition*" refers to placement of the fabric, environment conditioning and test type. In particular, it is important to understand

the physical and mechanical properties of composite materials under different conditioning such as ambient, freezing and thawing, aging with water, saltwater and alkali, and fuel resistance. However, for experimental study of this thesis, just ambient conditionings have been taken in consideration.

Table 3.1 offers a summary of the minimum material tests required for each FRCM and SRG material system.

Table 3.1 - Summary of material tests required for each FRCM/SRG system

Part a: Physical and Mechanical Properties of FRCM/SRG Composite Material

Fabric	Conditioning	Test Type	Hours	Number of replicates
Continuous	Ambient	Direct tension	N/A	20
	Freeze/thaw		N/A	5
	Ambient	Inter. shear	N/A	5
	Freeze/thaw		N/A	5
				Total 35
Continuous	Ambient	Direct tension	1,000	5
	Water			5
	Saltwater			5
	Alkali			5
	Ambient		3,000	5
	Water			5
	Saltwater			5
	Alkali			5
	Ambient	Inter. shear	1,000	5
	Water			5
	Saltwater			5
	Alkali			5
	Ambient		3,000	5
	Water			5
	Saltwater			5
	Alkali			5
				Total 80
Continuous	Ambient	Direct tension	N/A	5
	Fuel		N/A	5
				Total 10
Lap	Ambient	Direct tension	N/A	10
	Water	Direct tension	1000 and 3000	5 each case Total 30
	Saltwater			
	Alkali			
				Total 40
Continuous	Ambient	Bond	Before aging	5
	Ambient		1,000	5
	Water			5

	Saltwater			5
	Alkali			5
	Ambient		3,000	5
	Water			5
	Saltwater			5
	Alkali			5
				Total **45**

Part b: Properties of Matrix

Fabric	Conditioning	Test Type	Hours	Number of replicates
None	N/A	Compression	N/A	5 specimen at 7 days and 5 specimens at 28 days
		Dry shrinkage	N/A	5
		Void content	N/A	5
			Total	**20**

3.2. Physical and Mechanical Properties of FRCM and SRG Composite Material

Modeling and design are the main scope of engineering in the development of new products and processes. An important aspect of design is the use of parameters to describe the behavior of material that consist in mechanical properties derived from mechanical testing**.**

In order to provide a better understanding of physical and mechanical behavior of FRCM and SRG composite material, tensile tests, interlaminar shear tests and bond testing have to be carried out and their respective strength calculated. Obviously, compressive strength of mortar matrix should also be investigated to have a complete overview of composite behavior.

Material characterization tests according to the AC434 are shown below. In several cases, the ASTMs are also cited. The *American Society for Testing and Materials* (ASTM) is a world-renowned leader in the development of international standards. In fact, ASTM standards are used around the world to improve product quality, increase security, facilitate market access and trade, and build consumer confidence.

3.2.1. Mortar Matrix Compressive Strength

Mortar used in FRCM and SRG composites shall comply with ASTM C387/C387M for cement or polymer modified cement-based mortars, or ASTM C141/141M for hydraulic lime-based mortars. The compressive strength of the mortars is the average of the results of a minimum of five specimens for each mortar type and is representative of the mortar strength used in structural tests.

The five cubic specimens shall be cast by hand tamping the mortar in three layers in cube molds. Cube size shall be 50 mm and compressive nominal strength shall be determined at ages of 3, 7, 14 and 28 days of curing in humidity chamber. Uniaxial compression load shall be applied to the cube specimens using a hydraulic universal test frame. Load shall be applied to the cube faces that are in contact with the mold surfaces per standard requirements.

3.2.2. Composite Continuous Tensile Strength

Tensile testing shall be conducted on nominal rectangular coupons cut from FRCM and SRG panels, laid up in apposite mold, to determine the tensile strength and strain along with modulus of elasticity. The test procedures shall comply with the "*Tensile Testing of Fabric-Reinforced Cementitious Matrix (FRCM) and Steel Reinforced Grout (SRG) Composite Specimens*" included in Annex A. Tests shall be conducted for both primary and secondary grid directions, if different and required in the structural application. A total of ten specimens is tested for each FRCM and SRG configurations under control condition after 28 days of curing time in humidity chamber.

3.2.3. Composite Lap Tensile Strength

In the case of strengthening with FRCM and SRG composite materials of structural masonry or concrete members, such as columns, laps are necessary for the grid reinforcement. To determine the relative tensile strength at the grid overlap area, lap tensile strength testing shall be calculated by lap tensile test. The laps should be staggered from the laps in the nearby layer for a minimum distance equivalent to the tab length.

3.2.4. Composite Interlaminar Shear Strength

General procedures of ASTM D2344 shall be followed to determine interlaminar shear strength on FRCM or SRG panels. The scope of this standard test method is to determine the short-beam strength of high-modulus fiber-reinforced composite materials. It is important for quality control and process specification purposes. In fact, interlaminar shear strength could be used for comparative testing of composite materials, providing that failures occur consistently in the same mode, namely they are normally dominated by resin and interlaminar properties.

3.2.5. Composite Bond Strength

The effectiveness of an FRCM or SRG external reinforcement strongly depends on the bond between the strengthening material and the substrate and on the substrate mechanical properties. For this reason, mechanical properties of the single constituent materials are not sufficient to design an appropriate structural reinforcement and further tests should be performed for a complete characterization of the system. The bond test determines the bond strength to the substrate or the tensile strength of either the overlay or substrate, whichever is weaker. It may also be used to evaluate the adhesive strength of bonding agents. When the test is performed on the surface of a material applied to the substrate, the measured strength is controlled by the failure mechanism requiring the least stress. Thus, it is not possible to know beforehand which strength will be measured by the test. For this reason, the failure mode has to be reported for each individual test result, and tests results will be averaged only if the same failure mode occurs.

The bond between FRCM/SRG and substrate has different peculiarities with respect to FRP. In fact, FRP systems failure usually takes place within the substrate or at the interface *FRP-substrate*, while materials debonding mechanisms at the interface *fabric-matrix* are observed in the case of FRCM [68]. The two main tests to determine the bonding properties of FRCM/SRG composite on concrete or masonry substrate are the single (or double) *shear test* and the *pull-off test*.

3.3. Mechanical Testing of FRCM and SRG Composite Material

3.3.1. Composite Tensile Test

A thin flat coupon of material having a near-constant rectangular cross section is mounted in the grips of a mechanical testing screw driven machine and loaded with monotonically increasing load in tension while recording load and displacement. The ultimate strength of the material can be determined from a maximum load carried before failure. The coupon elongation is monitored with extensometer of four inch to determine the nominal stress-strain response of the material, and from that the cracking stress and strain, transition point, ultimate tensile strength and strain, tensile modulus of elasticity before and after cracking of cement-based matrix.

Particular attention shall be paid to material and specimen preparation, gripping, and test system alignment. The reason is that poor material fabrication practices, lack of control in alignment of fiber grid, and damage induced by improper cutting and machining the coupons are known causes of high material data scatter. Specimen gripping problems can also cause a high percentage of grip-influenced failures and therefore more scatter in data. Then, every effort shall be made to eliminate excess bending due to system misalignment and out-of-tolerance conditions caused by poor specimen preparation.

The testing machine shall be in conformance with Practices ASTM E4. The testing machine has both an essentially stationary head and a movable head. The screw driven mechanism shall be such to imparting to the movable head a controlled velocity with respect to the stationary head. The accuracy of instruments used for measuring dimensions of the test specimens shall be able for reading to within 1 percent of the sample dimensions. Each head of the testing machine shall carry one clevis-type grip for holding the test specimen in coincident with the longitudinal axis of the specimen and transfer the load from the testing machine to the specimen. It is desirable to use clevis-type grips, because they allow rotation in two perpendicular planes in order to minimize bending stresses in the coupon.

An initial minimal tension, less than 5 percent of the anticipated failure load, shall be applied to straighten potential bow in the specimen. The load is applied under displacement control with a standard rate of 0.01 mm/min (0.2 in/min).

No clamping force (i.e. pressure exerted on the tabs) should be applied to the specimen during testing. An illustration depicting the gripping mechanism with typical specimen dimensions is shown in Figure 3.1. An extensometer, satisfying Practice ASTM E83, Class B-1 requirements, can be used for elongation measurement. A gage length of 100 mm (4 inches) shall be used, because the coupon undergoes cracking in the early stages of loading, so the gage length has to be adequate to at least include within itself one transverse crack. The displacement transducer shall be attached to the specimen symmetrically about the mid-span, mid-width location. The bearing points of the extensometer on the coupon have not to be disturbed by cracking, else the extensometer moved and so the specimen should be unloaded. Possible discontinuity in elongation reading can be removed in data reduction process by matching the stop and restart point or similar means. This will likely result in a near bilinear response curve (Fig. 3.3) with an initial branch for un-cracked specimen, a secondary branch for cracked specimen, and possibly a curved transition segment in between.

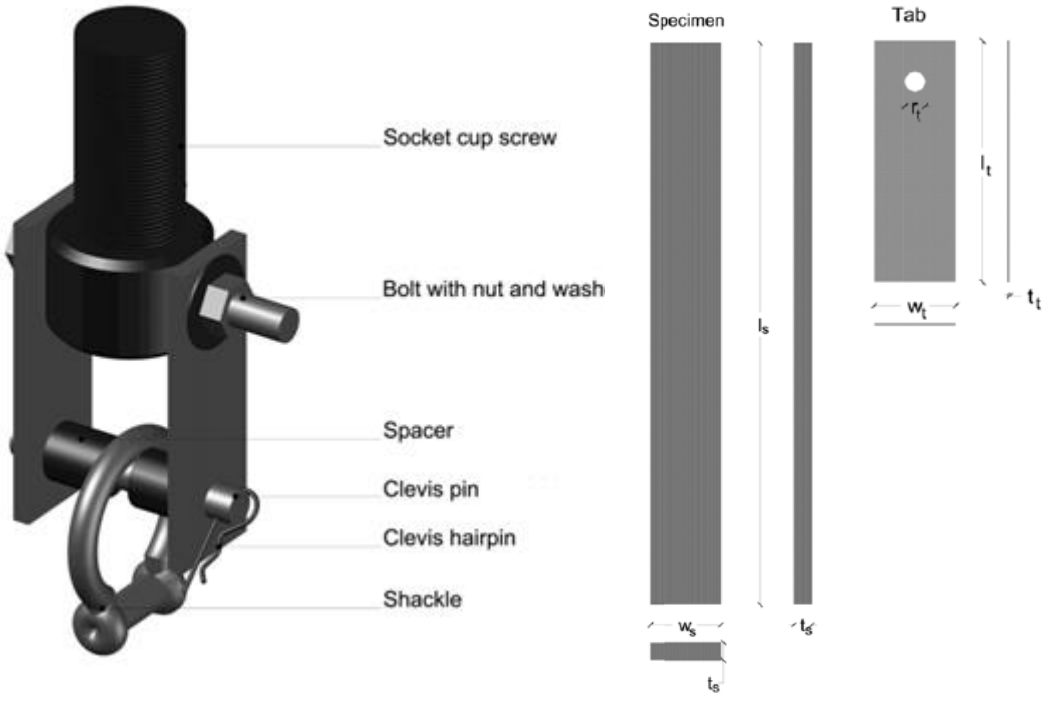

Figure 3.1 - Gripping mechanism and typical specimen dimensions [AC434]

Control of fiber grid alignment is critical in lay-up procedure. Effective cutting tools and methods need to used, and precautions shall be taken to avoid notches, undercuts, uneven surfaces or delaminations. Specimens shall be labeled properly to be distinct from each other and traceable to the raw material and curing age.

The thickness of rectangular coupons depends on number of layers and thickness of matrix for each layer. The width of the coupon shall be adequate to include a minimum number of strands and shall be not less than four times the thickness of the specimen. The length of the coupon shall be such to include gripping distance, plus twice the width plus gage length.

Steel tabs (e.g. steel, aluminum) are recommended to avoid damage to the specimen by the clevis-type grips. The tabs can be glued to the specimen ends (two at each end, one at each face) with adhesive epoxy, as shown in Figure 3.2. The tabs shall have the same width of the coupon in order to distribute uniformly the gripping force to the overall width of the coupons.

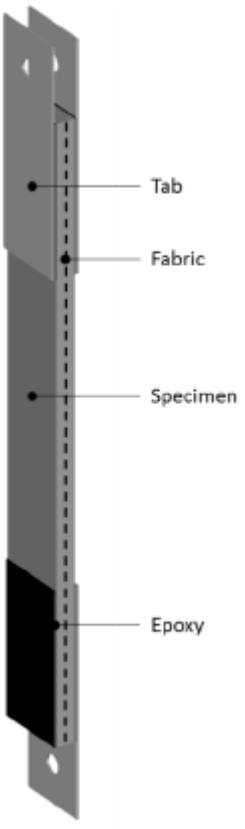

Figure 3.2 – Attaching of tabs by epoxy resin [Arboleda, 2014]

The tab length depends on the maximum expected tensile load, glue and tab bond strength to the matrix, and development length of the fiber strands within matrix. So a minimum of 101 mm (4 in) tab length is recommended. It should be noted that the tensile specimen must have sufficient fabric area to achieve 50 percent strength over transition point, so that the $0.6f_{fu}$ and $0.9f_{fu}$ will be in the correct part of the curve.

After conditioning and before testing, coupon type and geometry and environmental conditioning test parameters, as temperature and relative humidity, are specified. The overall cross-sectional area of the specimen is calculated as follows:

$$A = w \cdot t \tag{3.1}$$

where w is the nominal width and t is the nominal thickness of the coupon.

The width and thickness are measured at three locations along the specimen and averaged. For computation of FRCM and SRG mechanical properties, the area of grid reinforcement by unit width, A_f measured mm^2/mm (in^2/in), as reported by the manufacturer, is used.

3.3.2. Expected Tensile Stress-Strain Curve

The expected tensile stress, f_f, versus tensile strain, ε_f, curve of an FRCM and SRG coupon specimen is shown in Figure 3.3.

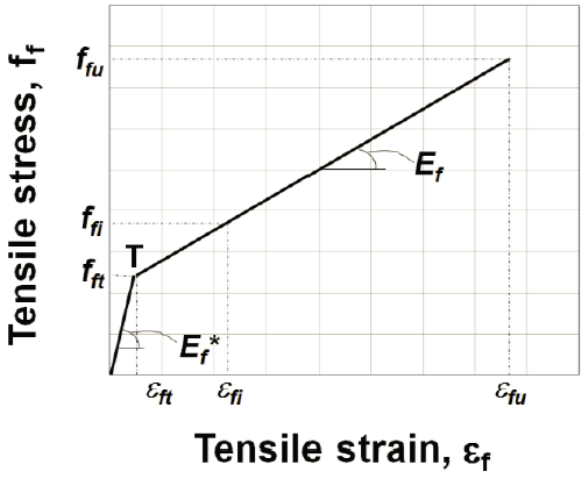

Figure 3.3 - The expected tensile stress-strain curve of an FRCM/SRG coupon specimen [AC434]

where

E_f is tensile modulus of elasticity of the cracked specimen, MPa (psi);

E_f* is tensile modulus of elasticity of the un-cracked specimen, MPa (psi);

f_{fi} is tensile stress at i^{th} data point, MPa (psi);

f_{fu} is ultimate tensile strength, MPa (psi);

f_{ft} is tensile stress corresponding to the transition point, MPa (psi);

ε_{fi} is tensile strain at i^{th} data point, mm/mm (in/in);

ε_{fu} is ultimate tensile strain, mm/mm (in/in);

ε_{ft} is tensile strain corresponding to the transition point, mm/mm (in/in);

T is transition point.

The ultimate tensile strength is calculated using the following equations:

$$f_{fu} = \frac{P_{max}}{A'_f \cdot w} \tag{3.2}$$

where

P_{max} is maximum load before failure, N (lbf);

$A'_f \cdot w$ is obtained as the product of the area of each strand A_{fi} and n, where n is the number of strands effectively present in the width of the coupon.

Tensile stress and strain, at a specific data point, are calculated using the following equations:

$$f_{fi} = \frac{P_i}{A_f \cdot w} \tag{3.3}$$

$$\varepsilon_{fi} = \frac{\delta_i}{L_g} \tag{3.4}$$

where:

P_i is load at i^{th} data point, N (lbf);

A_f is area of grid reinforcement by unit width, mm^2/mm (in^2/in);

W_s is nominal width of the specimen, mm (in);

δi is extensometer displacement at i^{th} data point, mm (in);

L_g is extensometer gage length, mm (in).

On the linear segment of the initial branch of the response bilinear curve corresponding to un-cracked behavior of the specimen, two points connecting the results in a line that closely follows the trend and slope of the response curve at that region are selected. The tensile modulus of elasticity of the un-cracked specimen is calculated using:

$$E_f^* = \frac{\Delta f}{\Delta \varepsilon} \tag{3.5}$$

where:

Δf is the difference in tensile stress between two selected points, MPa (psi);

$\Delta\varepsilon$ is the difference in tensile strain between two selected points, mm/mm (in/in).

On the segment of the response curve corresponding to cracked behavior after the transition, two points are selected on the experimental curve at a stress level equal to $0.90f_{fu}$ and $0.60f_{fu}$. The slope of the line that connects these two points represents the tensile modulus of elasticity of the cracked specimen:

$$E_f = \frac{\Delta f}{\Delta \varepsilon} = \frac{(0{,}90 \cdot f_{fu} - 0{,}60 \cdot f_{fu})}{\varepsilon_{f\_0.90f_{fu}} - \varepsilon_{f\_0.60f_{fu}}} \tag{3.6}$$

3.3.3. Composite Lap Tensile Test

Curing, specimen preparation, tab preparation and properties, tab installation and grip conditions shall follow those described in the tensile strength testing in Annex A. The general test procedures shall be used with exposures listed in Table 3.1. Forty specimens shall be cut from larger FRCM/SRG material panels. The panel consist of only one layer of FRCM or SRG material, consisting in two-piece with an overlap length in the middle. The lap length may vary, but a minimum 101 mm

(4 inches) lap length is recommended. The coupons shall be cut having the same dimensions as described in the tensile strength testing process in Annex A, such that the overlap length is positioned at mid-length (Fig. 3.4).

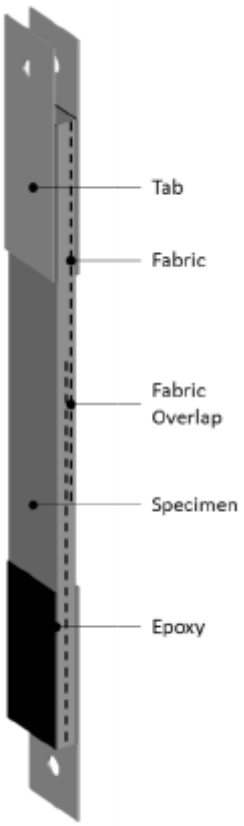

Figure 3.4 – Coupon with overlap length for composite Lap Tensile Test [Arboleda, 2014]

3.3.4. Composite Interlaminar Shear Test

A total of five specimens is performed for each FRCM or SRG configuration. The specimen is a short beam with length equal to thickness × 6 and width equal to thickness × 2. The beam is strengthened from a laminate up to 6.00 mm (0.25 in) thick and is loaded in three-point bending, as shown in Figure 3.5.

Alignment and center of the specimen shall be such that its longitudinal axis is perpendicular to the loading nose and side supports. The loading nose should be located equidistant between the side supports. Both the loading nose and side supports should overhang the specimen width by at least 2 mm (0.08 in) at each side, while the specimen end should overhang the side support centers by at least

the specimen thickness. The speed of testing shall be set at a rate of crosshead movement of 1.0 mm (0.05 in)/min.

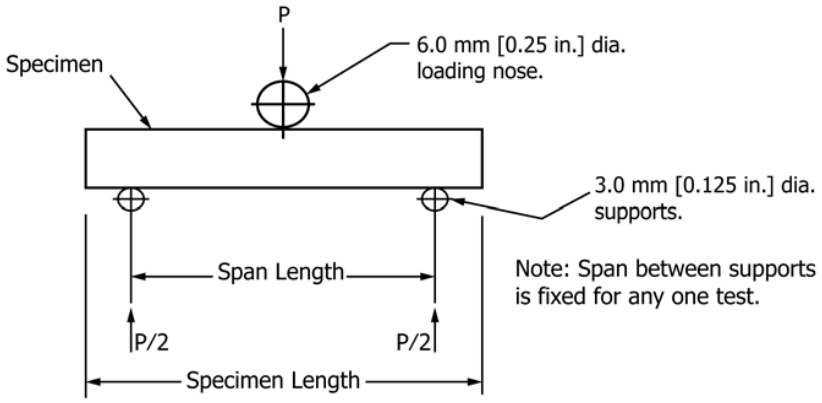

Figure 3.5 - Horizontal shear load diagram (Flat Laminate) [ASTM D2344]

The load is applied until either of the following occurred:

1. A load drop-off of 30 %;
2. Two-piece specimen failure;
3. The head travel exceeds the specimen nominal thickness.

This test method provides load versus crosshead displacement data as well as failure mode. Typical failure modes, that can be identified visually, are shown in Figure 3.6. However, these may be preceded by less obvious, local damage modes such as trans-ply cracking, namely horizontal cracking between two layer of FRCM or SRG reinforcement.

Known the maxim load observed during the test and the geometry of specimen, the short-beam strength is calculated as:

$$f_{sbs} = \frac{P_{max}}{b \cdot h} \tag{3.7}$$

where

f_{sbs} is short-beam strength, MPa (psi);

P_{max} is maximum load observed during the test, N (lbf);

b is measured specimen width, mm (in.);

h is measured specimen thickness, mm (in.).

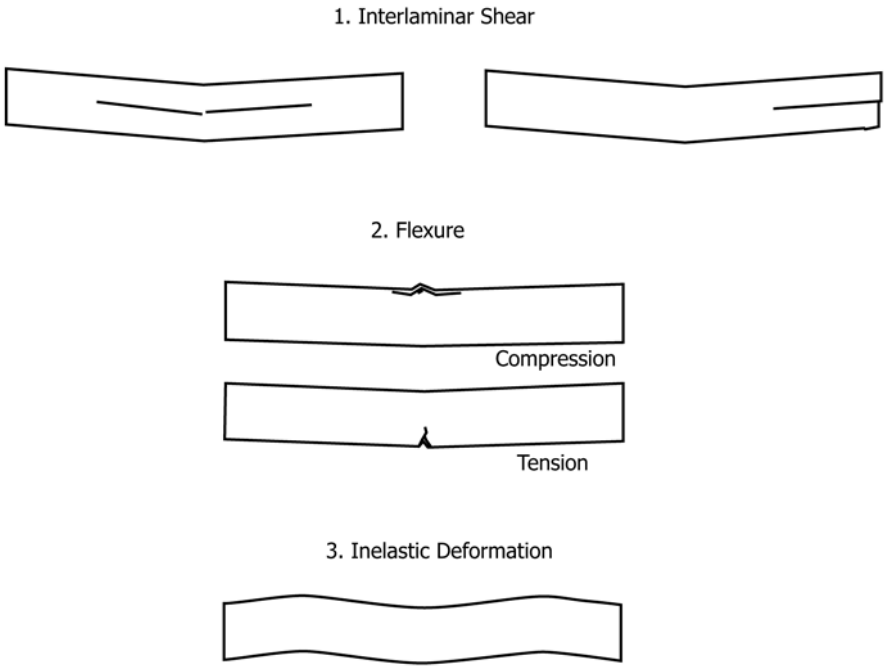

Figure 3.6 - Typical failure modes in the Short Beam Test [ASTM D2344]

3.3.5. Composite Bond Test

3.3.5.1. Lap Shear Test

In order to investigate the adherence behavior of FRCM or SRG reinforcement systems on masonry or concrete substrate, single (or double) lap shear test can be performed. The reinforcement applied on the face of the support (or on the two opposite faces) are made by the fiber mesh embedded between two layers of mortar for a total thickness of about 10 mm. Shear tests also allow to determine the effective bond length, namely the length required to transmit the stress.

Shear tests shall be carried out with displacement control using screw-driven testing machines, generally at a speed of 0.5 mm/min. The specimen is placed inside the test machine through the specially designed device, described in Figure 3.7.

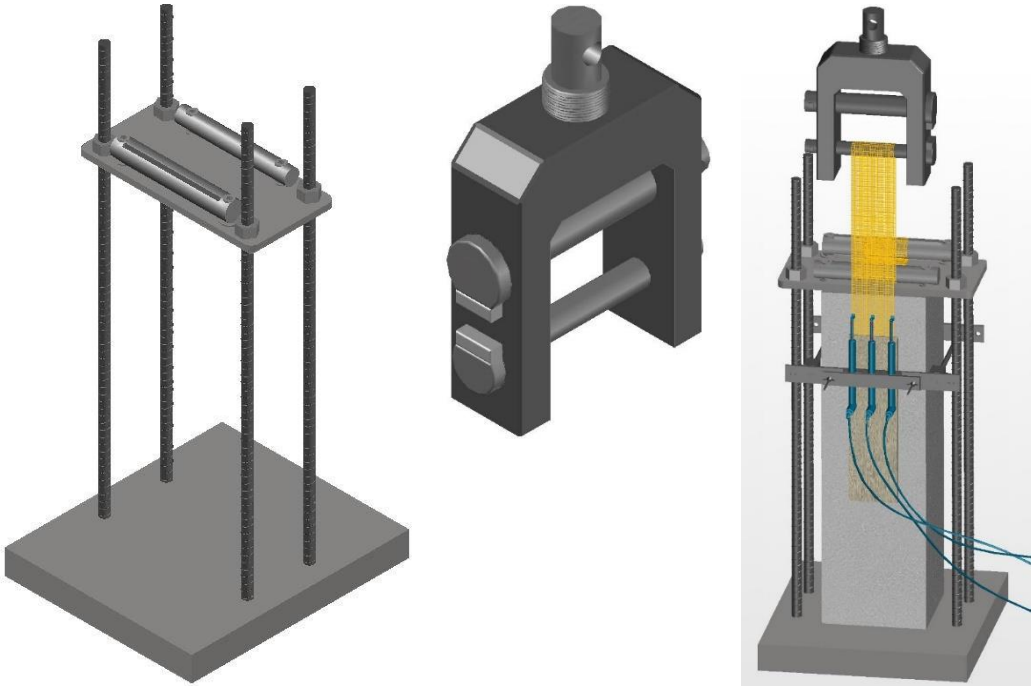

Figure 3.7 - Test set-up [Verre, 2014]

The testing machine shall be connected to a data acquisition system that processes information obtained through a software. The strains can be measured by electrical strain gauges placed on the fiber reinforcement. Based on the strains measured by the extensometers, ε_i, it is possible to calculate the maximum slippage of the reinforcement as follows:

$$\Delta = s_0 + \int_{x_0}^{L_b} \varepsilon(x) \cdot dx \tag{3.8}$$

Assuming that the slippage at the free end is zero and the stress between two gauges is constant, it is obtained:

$$\Delta = \sum_{i=1}^{n} \varepsilon_i \cdot \Delta x_i \tag{3.9}$$

Then, it is possible to plot *load - total slippage curves*.

Depending on substrate, the mortar matrix and the textile mechanical properties, and on the adherence developed at the interface *reinforcement-matrix*, different failure modes may occur. They herein listed and shown in Figure 3.8:

- Debonding with cohesive failure in the substrate (mode A);
- Debonding at the reinforcement to substrate interface (mode B);
- Debonding at the fabric to matrix interface (mode C);
- Sliding of the fabric within the reinforcement thickness (mode D);
- Fabric slippage within the matrix with cracking of the outer layer of mortar (mode E);
- Tensile rupture of the fabric out of the bonded area (mode F).

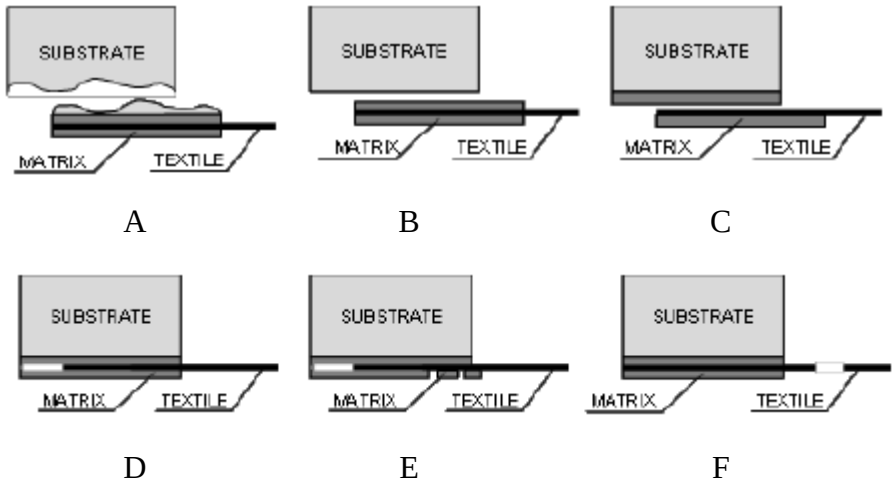

Figure 3.8 - Failure modes in shear bond tests on externally bonded FRCM strengthening systems [Ascione et al, 2015]

The first three failure modes (i.e., A, B, and C) generally give rise to a *force-slip* curve with a nearly flat branch, followed by a brittle failure. Failure mode D and E are generally related to a soft load decrease due to the progressive loss of friction of the textile sliding within the mortar. Differently, failure mode F is associated to instantaneous load reductions at the tensile failure of the bundles of the textile, that may occur before the flat branch of the curve is reached. In addition, the response curve related to mode F generally shows a sudden reduction and a further slight load decrease (Fig. 3.9). In this case, failure is activated by the telescopic rupture of the wire bundles and then followed by slippage of the first portion of the textile out of the mortar.

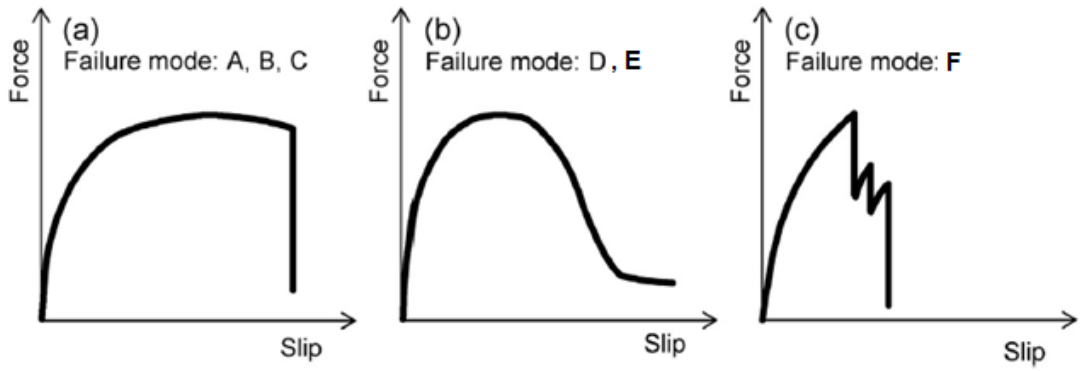

Figure 3.9 - Typical force-slip curves observed in shear bond tests on externally bonded FRCM strengthening systems related to failure modes A, B, and C (a), failure mode D and E (b), failure mode F (c) [Ascione et al, 2015]

Among all the failure modes, only slippage, case (D-E), and delamination, case (B-C), are expected to occur in FRCM. In particular, failure within the substrate (A) usually occurs in FRP composite bonded to concrete or masonry support. The reason is the great tensile capacity of the epoxy (about ten times greater than that of the concrete), while the tensile capacity of the cementitious matrix of FRCM system is similar to that of the support. However, failure mode A can be observed when the substrate is not well preserved and so its tensile capacity will be lower than that expected [69], [70]. Sometimes, low mechanical properties of the mortar or inadequate preparation of the support (the support must be cleaned of all debris and completely saturated to avoid the matrix drying during application), can lead to a debonding at the matrix to substrate interface (mode B).

3.3.5.2. Pull-off Test

The scope of test method is to determine one or more of the following:

1. The near-surface tensile strength of the substrate as an indicator of the adequacy of surface preparation before application of a repair or overlay material;
2. The bond strength of a repair or an overlay material to the substrate;
3. The tensile strength of a repair or overlay material, or an adhesive used in repairs, after the material has been applied to a surface.

For pull-off testing, an average of five FRCM or SRG specimens shall be prepared. The FRCM or SRG reinforcement shall be applied onto the substrate for a minimum of 63 mm (2.5 in) thick. After that, specimens shall be kept in standard laboratory conditions. Later 28 days of curing time, circular and hexagonal cuts, perpendicular to the substrate of the specimen, shall be performed in order to circumscribe the disk used for testing according to the general procedures of ASTM C1583.

The procedures of cut shall be carried out by drilling a shallow core, in the case of FRCM reinforcement, while by a hand grinder in the case of SRG mesh. The center-to-center distance of adjacent test specimens shall be at least of two disk diameters. The distance from the center of a test specimen and a free edge of the test object shall be at least of one disk diameter. After the drilling operations, any standing water shall be removed and the surface shall be cleaned by any debris and dried. Then, the steel disks are attached to the top of the test specimen using the epoxy adhesive. In this operation it is important to ensure that the disk is centered with the test specimen and that the axis of the disk is parallel to the axis of the test specimen. Besides, the adhesive must not to run down the side of the test specimen into the annular cut. Steel disks, nominally 50 mm (2.0 in) diameter and at least 25 mm (1.0 in) thick, shall be used. Tensile loading device shall be connected to the steel disk using a coupling fixture. This device is designed to withstand the tensile load capacity without yielding, and to transmit the tensile force parallel to and coincident with the axis of the cylindrical test specimen without imparting torsion or bending to the test specimen (Fig. 3.10).

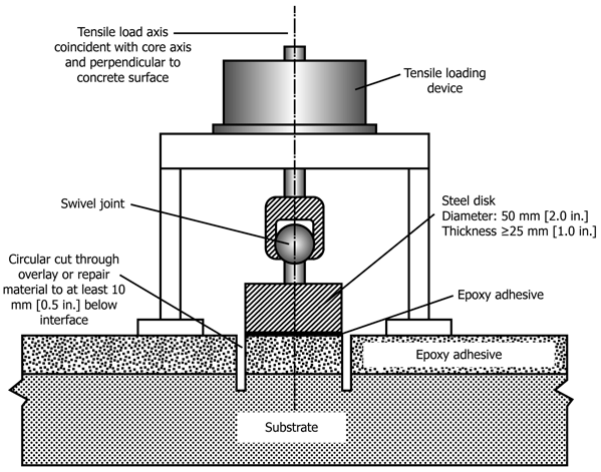

Figure 3.10 - Schematic of Setup to Test Material Applied to Substrate [ASTM C1583]

The tensile load shall be applied at a constant rate, so that the tensile stress increases at a rate of 35 ± 15 kPa/s [5 ± 2 psi/s]. It is applied to the steel disk until failure occurs. The failure load and the failure mode are recorded and the nominal tensile stress at failure is calculated as follows:

$$f_b = \frac{P_{max}}{A} \tag{3.10}$$

where

P_{max} is the tensile load at failure;

A is the area of the test specimen.

When the test is performed on the surface of a material applied to the substrate, the measured strength is controlled by the failure mechanism requiring the least stress. Thus, it is not possible to know beforehand which strength will be measured by the test. For this reason, the failure mode has to be reported for each individual test result, and tests results are averaged only if the same failure mode occurs. According to ASTM 1583, during a pull-off test, the failure modes can be occurred (a) in the substrate, (b) at the interface between the substrate and the repair or overlay material, (c) in the repair or overlay material, or (d) at the bond line between the repair or overlay material and the epoxy adhesive used to bond the steel disk, as shown in the Figure 3.11.

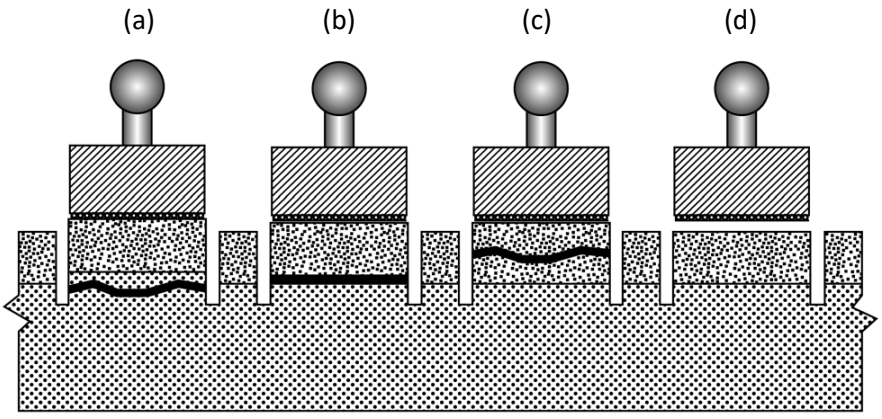

Figure 3.11 - Schematic of failure modes [ASTM C1583]

However, if failure occurs at the interface between the steel disk and the epoxy adhesive, the test result must be discarded and another test must be performed.

Chapter 4

Testing Procedures for the Uniaxial Tensile Characterization of Fabric-Reinforced Cementitious Matrix Composites

Given the increased interest in the utilization of FRCM composite systems for structural retrofitting applications, their specifications need to be available. System specifications include both material performance properties and installation instructions. While the manufacturer determines the installation instructions, research laboratories determine the material properties through experimental and analytical investigations. FRCM is a relatively new composite with unique and complex behavior, but it proved performance as a structural strengthening technique [Papanicolaou et al. 2008; D'Ambrisi et al. 2012; Ombres 2012; Babaeidarabad et al. 2014; Loreto et al. 2014]. The complexity of FRCM behavior has given rise to numerous research studies on the aspects that influence its mechanical properties.

4.1. Tensile Mechanical Behavior

TRC and FRCM showed a similar mechanical behavior under uniaxial loading. Three main states can be distinguished from the stress-strain diagram (Fig. 4.1):

- **State I** corresponds to the elastic region, where the composite behavior follows that of the mortar in tension. The stiffness of the composite is influenced by the presence of the fabric in this region. However, it has been proven to be negligible, thus the elastic modulus is usually controlled by that of the mortar [71].
- **State II** is equivalent to the first crack formation. It is represented by a transition point and determines the boundary between State II and the Elastic State. This state can be divided in two phases: in the first phase (***State IIa***) the stress is transferred to the reinforcement after the formation of the first crack. Multiple cracks form throughout the length of the specimen as tensile force

increases. The spacing of the cracks depends on the bond between the sleeve filaments and the concrete and it determines the transfer length. In the second phase of this state (***State IIb***) there is not further formation of cracks in the matrix; the minimum crack spacing is reached, thus the transfer length cannot be reached. In this state, the stress, caused by load increases, is carried by the filaments of the yarns, and the *stress-strain* curve proceeds parallel to the *stress-strain* curve of the textile used in the composite. The difference of the elastic modulus between FRCM and fabric can be observed in Figure 4.2 and it is the known as *tension stiffening effect*.

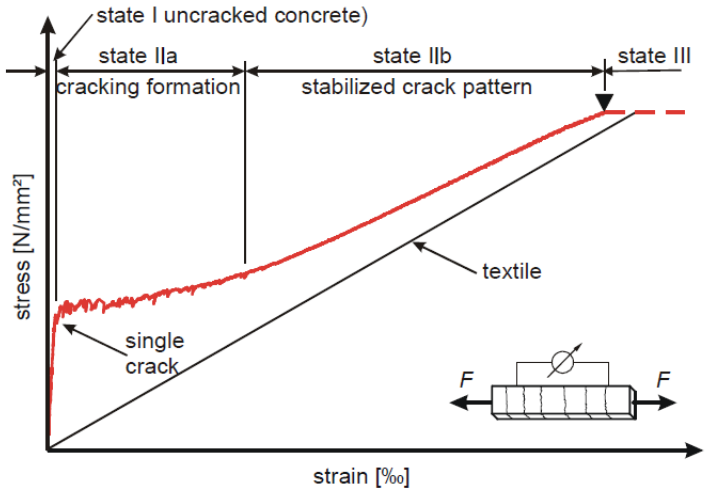

Figure 4.1 - Stress-strain diagram of textile reinforced concrete under uniaxial loading [Heg2004a, Jes2004a]

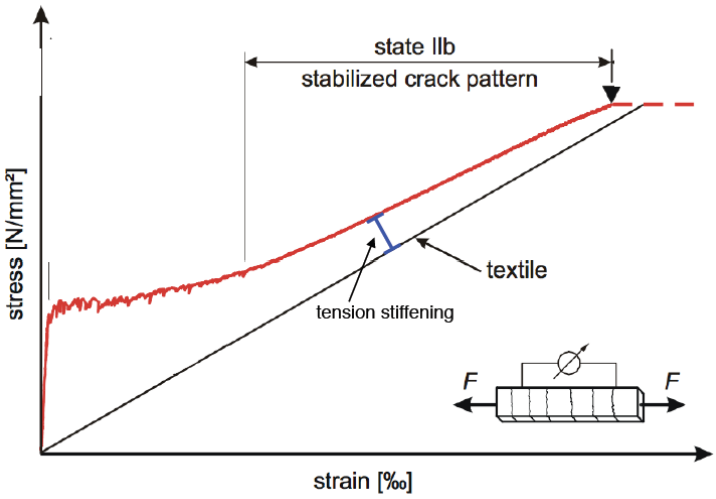

Figure 4.2 - Tension stiffening under uniaxial loading [Hegger et al. 2004]

❖ The study of **State III** is under debate due to the absence of a universally acknowledged test set-up. The academic world is divided between those who use the *clamping system* and those who use the *clevis system*. The former investigates the behavior of the fabric embedded in the mortar, preventing the slipping of the filaments. The failure of the specimen is due to tensile failure of the wires. Instead, the latter allows the mode known as *telescopic behavior*, where the core filaments are pulled out from the cementitious matrix. The filaments of the yarn are not fully engaged, thus the failure of the filaments is not reached. In this case, the failure of the specimen is due to slippage of the filaments. Therefore, the State III region does not defined [72] and an idealized bilinear tensile stress-strain curve is suggested in AC434 to tensile behavior of FRCM coupon specimen (Fig. 4.3).

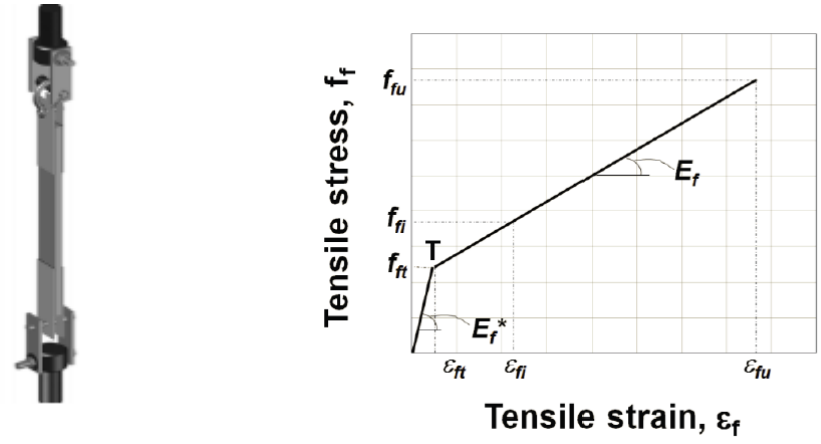

Figure 4.3 - Stress-strain bilinear curve of FRCM under uniaxial tension [AC434]

The bilinear curve has a transition point, T (f_{ft}, ε_{ft}), corresponding to the intersection point obtained by continuing the initial and secondary linear segments of the response curve. The initial linear segment of the curve corresponds to the FRCM un-cracked linear elastic behavior and it is characterized by the un-cracked tensile modulus of elasticity, E_f*. The second linear segment corresponds to the FRCM cracked linear elastic behavior and it is characterized by the cracked tensile modulus of elasticity, E_f.

4.2. Tensile Test Methods for FRCM

For structural reinforcement design, the values of the mechanical and bonding properties of the applied materials must be known. These values are determined through experimental tests. The apparent uniaxial tensile behavior of this type of composite is influenced by several factors, including the load transfer mechanism (grip method), specimen geometry and fabrication, and strain measurement technique.

Since none of these factors has yet been standardized, different set-ups for FRCM tensile tests with different gripping methods and specimen geometries have been developed [Contamine et al. 2011; Zhu et al. 2011; Hartig et al. 2012; Arboleda et al. 2012].

Figure 4.4 shows the main gripping methods used by different research groups.

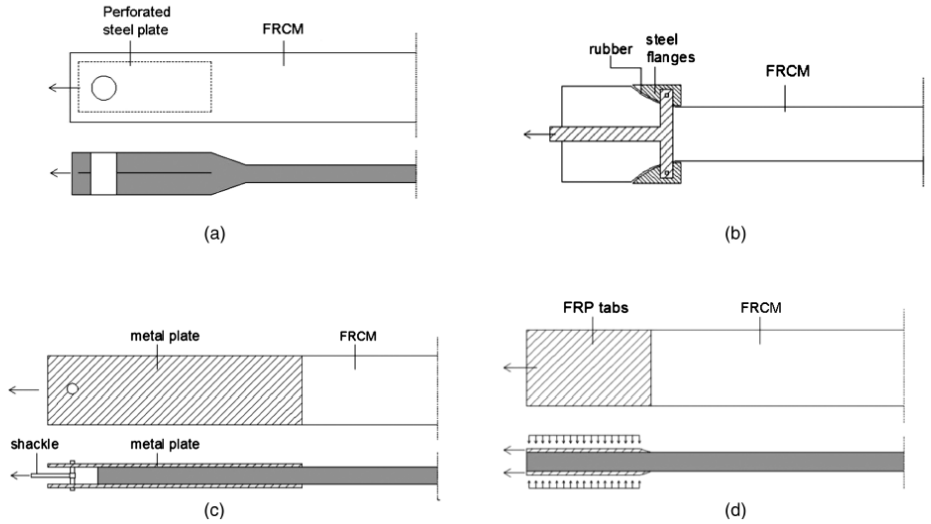

Figure 4.4 - Test setups: (a) Steel plate inside specimen; (b) Steel flanges; (c) Clevis (adhesive tension and shear) grip; (d) Clamping grips [Arboleda et al, 2016]

Hartig et al. (2010) identified two types of load application: rigid load application (Figs. 4.4a, 4.4c), in which the transfer mechanism between the specimen and the grip is by adhesive tension and shear realized through metal plates glued to the specimen ends (in this study realized with clevis grip); and soft clamping (Fig. 4.4d), which uses friction for load application realized by applying a compressive force normal to the plane of the specimen at its ends.

Molter (2005) proposed a waisted specimen in which the mortar is prevented from cracking within the supported range. Steel plates are glued or inserted inside the

specimen, causing the load transfer mechanism between specimen and clamping through adhesive tension and shear, and no slip can occur between clamping and specimen (Fig. 4.4a). The clamps adopted for bone-shaped specimens (Fig. 4.4b) are articulated steel flanges located in the curved part of the specimens over a rubber sheet [Orlowsky and Raupach 2008].

The ICC-Evaluation Service acceptance criteria [ICC-ES AC434 (2016)] recommends gripping the specimen through an adhesive tension and shear method such as a clevis grip (Fig. 4.4c). This includes two plates glued at each end of the specimen and connected with a transversal pin outside of the length of the specimen. This system is connected with a clevis joint to the testing frame. Gripping mechanism applies longitudinally the load by surface shear (through adhesive), and thus leave the ends free that are representative of repair applications where the material is not anchored at its ends (Fig. 4.5).

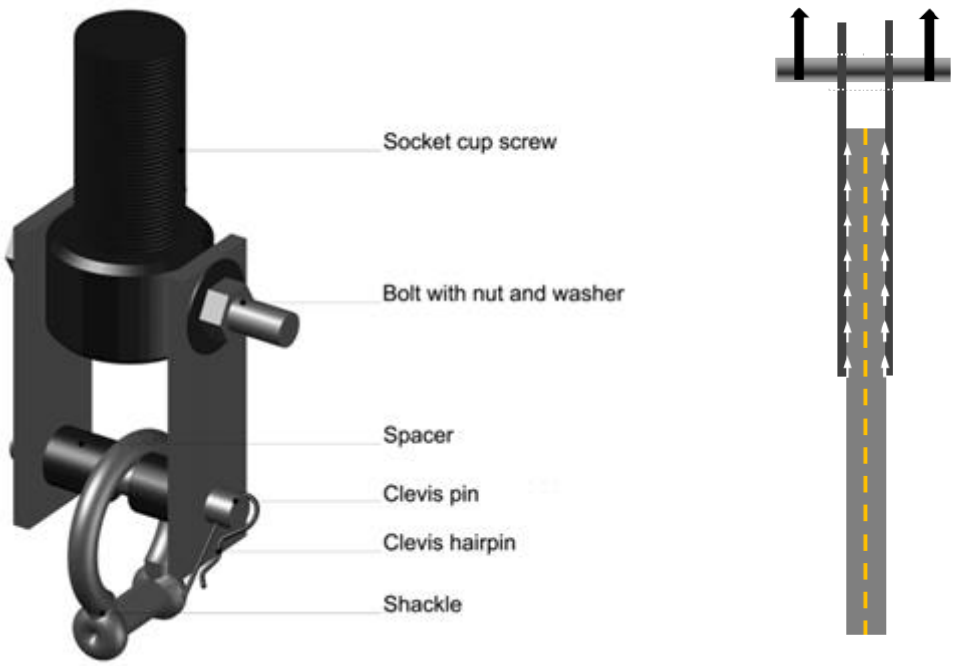

Figure 4.5 - Clevis grip [Arboleda, 2014]

Other research groups (Carozzi and Poggi 2015; De Santis and de Felice 2015) proposed an alternative system in which the two extremes of the specimens are fixed into the grips of a standard testing machine but the lower grip allows for torsional rotation. Gripping mechanism applies transversely the load (clamping) to

ensure the specimen does not slip. The specimens (and the fabric) are effectively anchoring at differing efficiency levels and producing results that are unrealistically high (Fig. 4.6). In this case, the clamps produce compressive stresses at the end of the specimens where fiber-reinforced tabs are applied using epoxy resin in order to facilitate a more homogeneous stress distribution and avoid local damage in the matrix.

Figure 4.6 - Clamp grip [Arboleda, 2014]

4.3. Idealized Trilinear Stress-Strain Curve

Typical stress-strain behavior of FRCM under a tensile test (Fig. 4.7b) is idealized as a trilinear curve (Jesse et al. 2008). The first linear phase represents the un-cracked state of the composite controlled by the matrix properties that are enhanced by the presence of fibers. The second phase corresponds to the formation and propagation of cracks. In this state, there is a significant decrease of the stiffness and relatively fine cracks form. The length and slope of this portion of the curve depend on the quality of the bond between fabric and matrix and on the volume proportion of the fibers activated for load transfer (Butler et al. 2010). The third phase is the crack-widening region, where the existing cracks become wider up to the final failure caused either by reaching the tensile strength of the fabric, or by slippage of the fabric from the matrix, or a combination of both. This phase is defined by a number of factors including end boundary conditions and fabric

properties such as volume percent, geometry, and whether the yarns are fully impregnated by resin or dry, meaning they are only partially impregnated by the cementitious matrix, or the yarns are partially coated by resin, thus having a dry-fiber core held in place only by frictional forces. In this phase, only the fabric resists the load and, therefore, the slope of the curve often reflects the elastic modulus of the dry fibers. In certain conditions, a tension stiffening effect is observed, where the modulus in this phase runs parallel, but at a slightly elevated stress compared to the fabric (Fig. 4.7b).

This is attributed to a contribution of the un-cracked matrix between the cracks. In conditions where the matrix strength is very low or the dry fibers slip, the modulus of the third phase can be indistinguishable from the second phase and a bilinear behavior is obtained instead (Fig. 4.7c).

The transition points T_1 and T_2 are defined at the change in slope of the stress-strain curve and are determined by the intersection of the linear portion representing the modulus of elasticity of each phase.

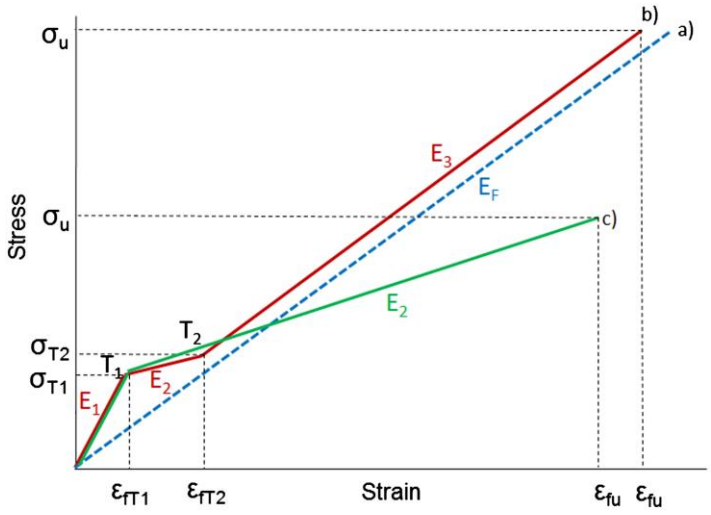

Figure 4.7 - Idealized stress-strain curves: (a) stand-alone fabric; (b) clamped FRCM; (c) pinned FRCM [Arboleda et al, 2016]

4.4. Fiber to Matrix Bonding

When yarns are fully impregnated with resin, they behave as internal FRP and increase the organic content of the composite. By definition, FRCM is composed of *dry-fiber fabric*, meaning that the yarns are not fully impregnated with resin.

When the fabric is completely dry, the mortar partially impregnates the outer fibers in the yarn bundle. When the fabric has a protective coating applied on the exterior of the yarn, the mortar does not impregnate the bundle. In either case, however, there is a core of dry fibers. Therefore, dry-fiber yarns can be modeled as having a sleeve and a core. It is important to investigate the adhesive bond between the external fibers of the yarn and the mortar and the frictional bond among the internal fibers within the yarn as well. Two types of slippage can occur: between fibers and mortar or within fibers in the dry core of the yarn. Slippage between fibers and mortar is attributable to incomplete impregnation of the fibers, debonding, or chemical incompatibility and it can be localized at the end of the specimen or in each crack region. Slippage appears among the fibers in the yarn attributable to a telescopic failure mode. It is known that a cement matrix is not ideal to impregnate fibers. The external fibers in a yarn are either in direct contact with the matrix or indirect contact with the matrix through the partial protective coating and they are thus tightly bonded, while the internal fibers in the core of the yarn are not and can slip more easily because of the low friction between the fibers.

Peled et al. (2008), Soranakom and Mobasher (2009), and Andic-Cakir et al. (2014) presented a model to simulate the yarn as a cylindrical structure comprised of concentric rings composed of several fibers (Fig. 4.8). The failure mode of the fibers in the sleeve is by fracture, while the internal fibers slip as a result of the pull-out force. The telescopic mode pull-out (Banholzer et al. 2006) is influenced by cement penetrability, the geometry of the reinforcement, the presence of a coating, and the level of friction among the fibers in each yarn.

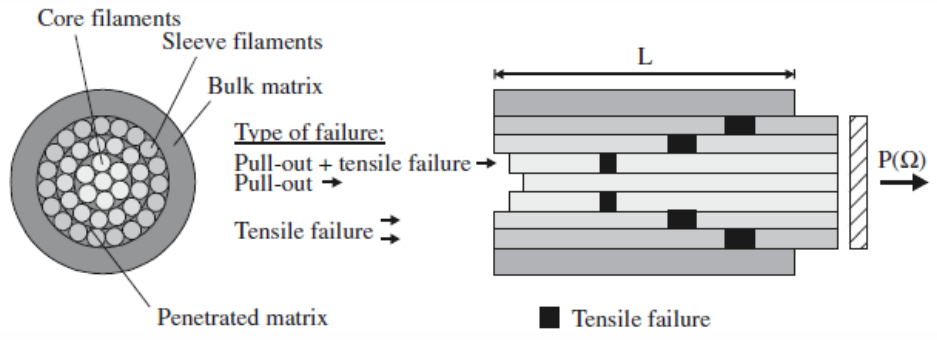

Figure 4.8 - Graphic representation of the fiber slip phenomena [Banholzer et al, 2006]

4.5. Experimental Program

Uniaxial tensile testing of composite material specimens was performed by Arboleda et al. [73] for the main purpose of determining the characteristic mechanical behavior of the material under controlled loading conditions. It is the most accepted method for obtaining material parameters needed for design calculations. The authors presented the influence of different test set-ups through the results of an extensive experimental investigation.

Rectangular coupons of various FRCM systems were tested using two different test set-ups. The main difference between the set-ups was the gripping method used to transfer the load. Clevis grip is the term used for load application through metal tabs glued on the specimen ends (Fig. 4.5) and clamping grip is the term used for load application through compressive stress normal to the specimen plane (Fig. 4.6).

The main difference between the two methods is the stress state generated by the grips. In the first case, only shear stresses are transferred. In this type of test, the full strength of the fabric is never reached because the failure mode is by slippage of the fabric. In the second case, the clamping grips generate compression and shear in the specimen to limit slippage between fabric and matrix at the grip.

The tests performed with clamping grips allow a complete mechanical behavior characterization of the composite with a tensile failure of each constituent material; however, in field applications of FRCM, the ends are not anchored and failure is often by slippage of the fibers. Thus, the tests performed with clevis grips intend to reproduce the as-installed FRCM behavior.

4.5.1. FRCM Composites Used during the Investigation

Five different FRCM systems were used during this study having these types of fabrics:

- Polyparaphenylene benzobisoxazole (PBO fiber), composed of dry fibers only (Fig. 4.9a);
- Two types of carbon (C fiber and cC fiber), one composed of dry fibers only (Fig. 4.9b) and the second one having a protective coating over the dry fibers;

- Two types of glass fabric (G fiber and cG fiber), the first one composed of dry fibers only, and the second one having a protective coating of styrene butadiene over the dry fibers.

Each type of fabric was matched with the mortar that is specifically designed for it by the FRCM system manufacturer. The corresponding systems are denominated x-FRCM, where x represents the name of the fabric (e.g., PBO-FRCM).

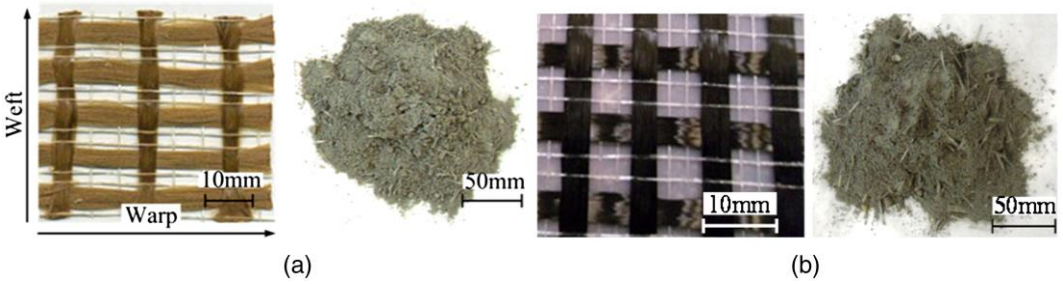

Figure 4.9 - (a) PBO-FRCM system; (b) C-FRCM system [Arboleda et al, 2016]

4.5.2. Fabric Reinforcement

Figure 4.10 shows the geometry of the different fabrics involved in the experimental study. Fabric parameters shown include spacing between yarns and yarn nominal width. For un-balanced fabrics (different fiber volume in each direction), the warp (main or load carrying) direction is shown up/down and the weft direction is shown left/right. Another important parameter is the equivalent thickness, which is used to determine the nominal cross-sectional area of the fabric when multiplied times its length.

The PBO fiber unbalanced fabric has equivalent thickness in the warp and weft directions of 0.046 mm and 0.011 mm, respectively. The carbon fiber (C fiber) is a balanced fabric with equivalent thickness is 0.047 mm in both directions. The coated carbon fiber (cC fiber) is an unbalanced fabric with equivalent thickness of the dry fibers in the warp direction of 0.175 mm. The glass fiber (G fiber) balanced fabric has an equivalent thickness of 0.036 mm per direction, and the coated glass fiber (cG fiber) unbalanced fabric has an equivalent thickness of 0.05 mm and a dry yarn net cross-sectional area of 0.9 mm^2.

Tensile tests of single yarns and of fabric strips of width 40 and 50 mm (containing 3 to 4 yarns as indicated in Table 4.1) in the warp direction were performed according to EN ISO 10618/2005 (BS EN 2005a).

Table 4.1 – Mechanical properties of the yarns

Fabric	n_{yarns}	A (mm^2)	n_{tests}	Average stress at failure (GPa)	CoV (%)	Elastic modulus (GPa)	CoV (%)
PBO fiber	1	0.41	6	3.9	3.2	216	20.8
	4	1.64	4	3.4	7.3	-	-
C fiber	1	0.42	3	1.9	14.9	203	9.8
	4	1.68	3	1.9	10.4	-	-
cC fiber	1	2.68	3	1.3	9.2	263	11.2
G fiber	1	0.24	4	1.4	11.4	49	-
cG fiber	1	0.90	5	1.2	2.7	56	30.5
	3	2.70	5	1.1	1.3	-	-

Tests were carried out using different testing machines with maximum load capacities of 2 and 100 kN and an extensometer with base length equal to 50 mm. In order to avoid local damage during the tensile tests, special tabs of glass-fiber-reinforced polymer (GFRP) were bonded using epoxy resin at the ends of the coupons. The tabs presented a width equal to the coupon and a length equal to 60 mm.

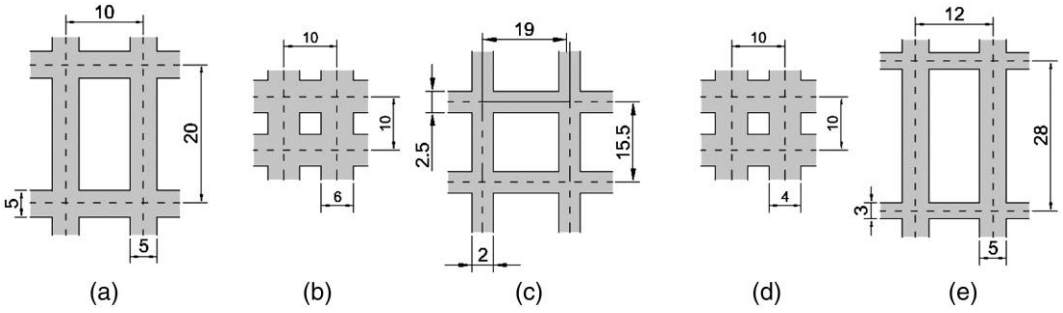

Figure 4.10 - Fabric geometry: (a) PBO; (b) glass; (c) coated glass; (d) carbon; (e) coated carbon (dimensions in millimeters) [Arboleda et al, 2016]

The failure mode shows a rupture of some fibers without a complete failure of the yarn for PBO and carbon fibers; in contrast, a complete cut is evident in glass fibers. The failures occurred on the length of the specimens, not close to the grips. Because of the difficulties of bonding all the internal filaments in the tabs, it is very difficult

to guarantee a homogeneous stress distribution in the filaments of the yarn. For this reason, not all filaments fail simultaneously. The experimental results are summarized in Table 4.1.

4.5.3. Inorganic Matrix

The inorganic matrix is specifically designed by each manufacturer of the FRCM composite system both to provide optimal fresh state and workability properties, and to form an optimal (chemical and mechanical) bond with the fabric and the substrate. The constitutive components of the mortar are not very different than those of traditional cement, but some of the dry additives are proprietary in nature and each fabric is used with its specific mortar. The matrices analyzed in this work are cementitious mortars enriched with short fibers in a percentage less than 5%. Only the mortar used with G fibers is lime based. Table 4.2 shows the main measurable mechanical properties and the corresponding experimental standards adopted.

Table 4.2 - Mechanical Properties of the Matrix

	Tensile EN 12390-6 (BS EN 2009)		**Compressive EN 1015-11 (BS EN 1999)**		**Flexural EN 1015-11 (BS EN 1999)**		**EN 14580 (BS EN 2005b)**
Matrix type	**Strength (MPa)**	**CoV (%)**	**Strength (MPa)**	**CoV (%)**	**Strength (MPa)**	**CoV (%)**	**Elastic modulus (GPa)**
Mortar used with **PBO fiber**	4.75 (7)[a]	4.05	33.90 (5)	10	> 2 (ds)	-	> 6 (ds)
Mortar used with **C fiber**	3.30 (5)	3.6	24.02 (5)	2.5	3.5 (ds)	-	> 7 (ds)
Mortar used with **cC fiber**	3-5 (ei)	-	> 45 (ds)	-	7 (ei)	-	7 (ei)
Mortar used with **G fiber**	2-4 (ei)	-	10 (ds)	-	3 (ei)	-	5 (ei)
Mortar used with **cG fiber**	3-5 (ei)	-	27.13 (7)	4.1	8.4 (14)	13.15	8 (ds)

[a]*Within brackets, number of tested coupons or source of data (ds = data sheet; ei = estimated interval)*

Some of the values were experimentally verified on mortar samples made and cured for 28 days in laboratory ambient conditions of 20°C and 60% relative humidity, while others were taken from the technical data sheets provided by the producers.

4.5.4. Specimen Geometry and Preparation

The test coupons were rectangular and manufactured using a manual impregnation technique in a flat rectangular mold by first applying a thin layer (5 mm) of the cementitious matrix, followed by pressing a layer of the fabric into the mortar. Then, the top layer of mortar matrix was applied as flat as possible with a finishing trowel. The c-Carbon fabric had retained some curvature from the roll it comes from and was placed in an oven at 60°C for 10 min the night before so the coating could soften and the fabric sheet could flatten out. All FRCM systems were made with one fabric layer, but additionally, coupons were made with overlap splice for PBO and carbon (PBO-FRCM and C-FRCM), and with two fabric layers for coated carbon (cC-FRCM).

The fabricated panels were cured at laboratory ambient conditions at temperature 20 °C and 60 % relative humidity for 28 days before cutting the individual coupons using a diamond-tipped wet saw. The coupons tested with the clevis grip had nominal dimensions equal to 410 × 50 × 10 mm and were cut from larger panels of 430 × 560 mm. The coupons tested with clamping grips were made in a similar way, but each coupon was prepared in a flat mold separately.

4.6. Test Set-up

4.6.1. Gripping

Adhesive tension and shear grips were implemented with a clevis. Metal tabs of 3 mm thickness with a bond length equal to 150 mm were fixed at the coupon ends with epoxy resin. The grip had multiple degrees of freedom providing a pinned end support. This configuration reduces bending moments and allows slippage of the fabric at the grip ends. For complete mechanical characterization of the system, clamping grips were selected. The two extremes of the coupon were fixed into the grips of a standard testing machine, with the lower grip allowing for torsional rotation, thus ensuring specimen alignment prior to test start. In this case, the clamps

can produce high compressive stresses (4 - 5 MPa) at the end of the coupons so GFRP tabs (dimensions 60 × 40 × 2 mm) were applied using epoxy resin in order to avoid damage in the matrix and guarantee a homogeneous stresses distribution.

4.6.2. Instrumentation

For the tests performed with clevis grip, a test frame with a maximum capacity of 130 kN was used with displacement control at a rate of 0.25 mm/min. Axial deformation was measured using a clip on extensometer with a 100 mm gauge length, placed mid-length of the coupon (Fig. 4.11a).

For the tests performed with clamping grip, a test frame with a load capacity of 100 kN was used with displacement control at a rate of 0.1 mm/min during the first phase (before matrix cracking), and 0.3 mm/min thereafter. Deformation was measured using an extensometer with a gauge length of 100 mm positioned in the central area of the coupon (Fig. 4.11b). Since the dimension of the coupon was 400 × 40 × 10 mm, the distance between the two grips of the testing machine was 280 mm. Therefore, the extensometer gauge length of 100 mm covered about 1/3 of the free surface of the coupon, giving an adequate measurement of the strain field.

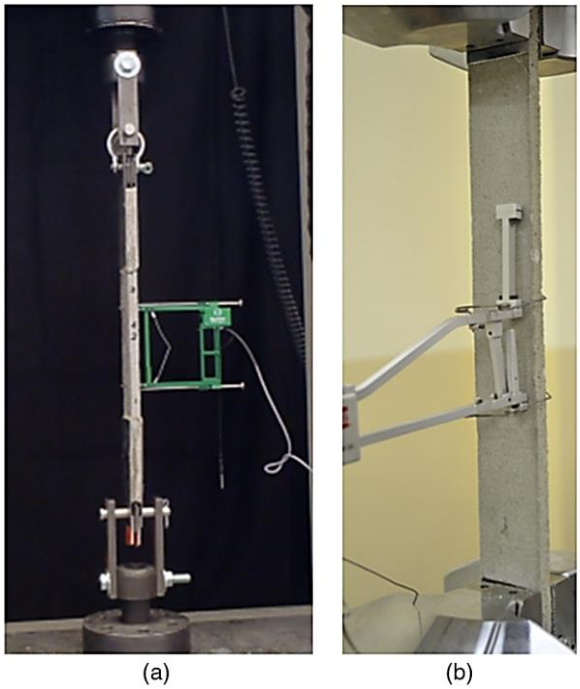

Figure 4.11 - Tensile test setup: (a) clevis grip; (b) clamping grip [Arboleda et al, 2016]

4.7. Experimental Results

Varieties of FRCM systems with one fabric layer were tested. Coupons with a layer splice overlap (PBO and C-FRCM) and with two fabric layers (cC-FRCM) were also tested. Their stress-strain behavior and failure modes were analyzed. A detailed description of the results obtained can be found in (Arboleda 2014; Carozzi and Poggi 2015). Results are summarized and critically analyzed to highlight the comparison of the two testing procedures.

All specimens demonstrated multiple cracking of the matrix, perpendicular to the direction of the load, throughout the length of the coupon. The point at which no more cracks develop is termed crack saturation.

For all specimens, the stress was determined by dividing the load by the nominal cross-section area of the fabric only, because after the specimen starts to crack, the load transfer occurs mainly through the fabric. Naturally, when the un-cracked portion of the response curve is determined using the actual cross section of the specimen, the resulting first crack stress and modulus of elasticity are comparable to that expected of the mortar only. Furthermore, since the specimen cross section has significantly more variability than the nominal fabric cross section, the high variability noticed in this first phase is reduced when the first crack is based on gross area.

4.7.1. Clevis Grip on One-Layer Specimens

The typical failure mode obtained with this test set-up was slippage of the fabric within the matrix after crack saturation. The fabric slippage is a combination of pull-out and tensile failure of the fibers.

The stress-strain behavior is bilinear with the first phase identified as the un-cracked specimen behavior; when the first cracks appear, the slope decreases and slippage between fibers and mortar is eventually observed. The modulus of the un-cracked specimen was calculated as the slope between the origin and the intersection of the linear trend of the first portion of the experimental curve and the linear trend of the second portion of the experimental curve. On the segment of the response curve corresponding to cracked behavior after the transition, two points are selected at a stress level equal to $0.90f_{fu}$ and $0.60f_{fu}$ [ACI 549 (2013)]. The slope of the line that

connects these two points represents the tensile modulus of elasticity at that region as summarized in Eq. 4.1:

$$E_f = \frac{\Delta f}{\Delta \varepsilon} = \frac{0.9 \cdot f_{fu} - 0.6 \cdot f_{fu}}{\varepsilon_{0.9 f_{fu}} - \varepsilon_{0.6 f_{fu}}} \tag{4.1}$$

The segment between $0.90f_{fu}$ and $0.60f$ was selected based on a statistical analysis of representative curves in order to ensure consistency of results. Tables 4.3 - 4.5 summarize average results with the coefficient of variation and Figure 4.12 shows the tensile response of the different FRCM materials. The G-FRCM and cG-FRCM were not tested with the clevis grip.

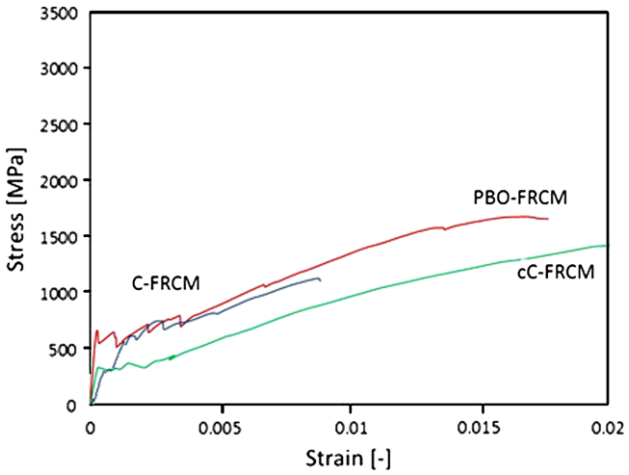

Figure 4.12 - Stress-strain curves with clevis grip of different FRCM materials [Arboleda et al, 2016]

4.7.2. Clamping Grip on One-Layer Specimens

With this gripping system, the typical failure mode is by damage to the fabric fibers close to the main cracks. In a few instances, fiber slippage is observed and is attributed to poor bond to the matrix.

The stress-strain behavior is predominantly trilinear with exceptions based on the type of FRCM material tested. Results show a large variability in the localization of transition points. This is caused by the variability in dimensions of the specimen section, the presence of cracks not visible to the naked eye, and the location of the first crack with respect to the extensometer (Bertolesi et al. 2014).

Tensile tests on C-FRCM and PBO-FRCM show a trilinear behavior; G-FRCM and cG-FRCM show a behavior where the second transition point is not evident because of the low elastic modulus of the glass fibers. When the slope of the third branch is lower than the elastic modulus of the dry fabric, a possible slippage phenomenon is occurring.

The modulus of all three phases is evaluated as the ratio between stress and strain of the first and last point of each phase. For the first phase only, in which the mortar is un-cracked, tensile stress (σ_{t1}^{*}) and elastic modulus (E_1^{*}) were also evaluated using the composite cross section in order to compare the cracking tensile stress and the elastic modulus with the mortar properties. The stress reached at the end of the first phase should be similar to the mortar tensile strength. As previously described, because of possible problems in sample preparation or in the curing phase (no planarity, different shrinkage, micro-cracking), this value could be lower than the mortar tensile strength.

Tables 4.3 - 4.5 summarize average results obtained by Arboleda et al. with the coefficient of variation and Figure 4.13 shows the tensile response of four different FRCM materials (cC-FRCM was not tested). The third phase shows most of the differentiation as a result of the different elastic moduli and tensile strengths of the fibers.

Table 4.3 - Results of Tensile Tests

Material	Grip type (number)[a]	Value type	E_1 (GPa)	E_2 (GPa)	E_3 (GPa)	E^{*}_1 (GPa)
PBO-FRCM 4 yarns	Clevis (10)	Average	1.805	128	-	-
		CoV (%)	25	12	-	-
C-FRCM 4 yarns	Clevis (5)	Average	512	80	-	-
		CoV (%)	25	23	-	-
cC-FRCM 3 yarns	Clevis (9)	Average	1.570	56	-	-
		CoV (%)	55	14	-	-
cC-FRCM 2 PLY	Clevis (5)	Average	465	52	-	8
		CoV (%)	24	17	-	15
PBO-FRCM 4 yarns	Clamp (34)	Average	1.181	76	216	5
		CoV (%)	20	33	9	20

C-FRCM 4 yarns	Clamp (10)	Average	1.102	68	186	5
		CoV (%)	18	28	22	18
G-FRCM 4 yarns	Clamp (8)	Average	1.029	41	56	2
		CoV (%)	31	59	36	31
cG-FRCM 3 yarns	Clamp (17)	Average	1.310	32	64	6
		CoV (%)	33	34	17	34

[a]*Within brackets, number of tested coupons*

Table 4.4 - Results of Tensile Tests

Material	**Grip type (number)[a]**	**Value type**	**σ_{t1} (MPa)**	**σ_{t2} (MPa)**	**σ_u (MPa)**	**σ^*_{t1} (MPa)**
PBO-FRCM 4 yarns	Clevis (10)	Average	375	-	1.664	-
		CoV (%)	22	-	5	-
C-FRCM 4 yarns	Clevis (5)	Average	458	-	1.031	-
		CoV (%)	10	-	5	-
cC-FRCM 3 yarns	Clevis (9)	Average	381	-	1.296	-
		CoV (%)	36	-	12	-
cC-FRCM 2 PLY	Clevis (5)	Average	149	-	1.133	3
		CoV (%)	24	-	10	22
PBO-FRCM 4 yarns	Clamp (34)	Average	890	-	3.316	4
		CoV (%)	15	-	14	15
C-FRCM 4 yarns	Clamp (10)	Average	482	-	1.492	2
		CoV (%)	21	-	19	21
G-FRCM 4 yarns	Clamp (8)	Average	545	-	1.292	2
		CoV (%)	25	-	8	2
cG-FRCM 3 yarns	Clamp (17)	Average	460	-	872	2
		CoV (%)	30	-	21	30

[a]*Within brackets, number of tested coupons*

Table 4.5 - Results of Tensile Tests

Material	**Grip type (number)[a]**	**Value type**	**ε_{t1} (%)**	**ε_{t2} (%)**	**ε_u (%)**
PBO-FRCM 4 yarns	Clevis (10)	Average	0.017	-	1.756
		CoV (%)	25	-	8

C-FRCM 4 yarns	Clevis (5)	Average CoV (%)	0.102 44	- -	0.996 14
cC-FRCM 3 yarns	Clevis (9)	Average CoV (%)	0.023 33	- -	1.641 14
cC-FRCM 2 PLY	Clevis (5)	Average CoV (%)	0.025 37	- -	1.79 25
PBO-FRCM 4 yarns	Clamp (34)	Average CoV (%)	0.082 31	0.5 34	1.69 18
C-FRCM 4 yarns	Clamp (10)	Average CoV (%)	0.06 13	0.24 20	0.74 21
G-FRCM 4 yarns	Clamp (8)	Average CoV (%)	0.064 25	0.44 28	1.82 47
cG-FRCM 3 yarns	Clamp (17)	Average CoV (%)	0.045 41	0.38 13	0.69 38

[a]*Within brackets, number of tested coupons*

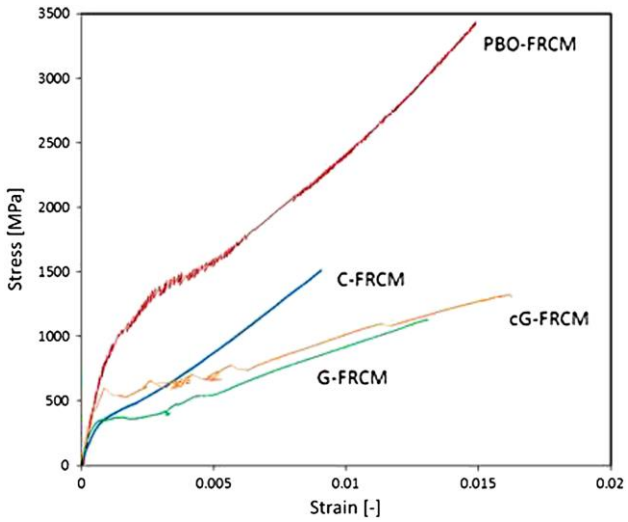

Figure 4.13 - Stress-strain curves with clamping grip of different FRCM materials [Arboleda et al, 2016]

Figures 4.14 and 4.15 show the comparison between the stress-strain curves obtained with the two gripping methods for PBO-FRCM and C-FRCM coupons. The characteristic behavior in the first phase is not expected to be very different for both gripping methods. However, since the stress is computed with respect to the textile cross-section area, the variable dimensions of the cross-section area of the matrix, as well as the location of the first crack with respect to the gauge length,

have a significant influence on the analyzed results. For tests performed with clevis grip, the second phase reached higher strain attributable to fiber slippage, and the third phase was not present.

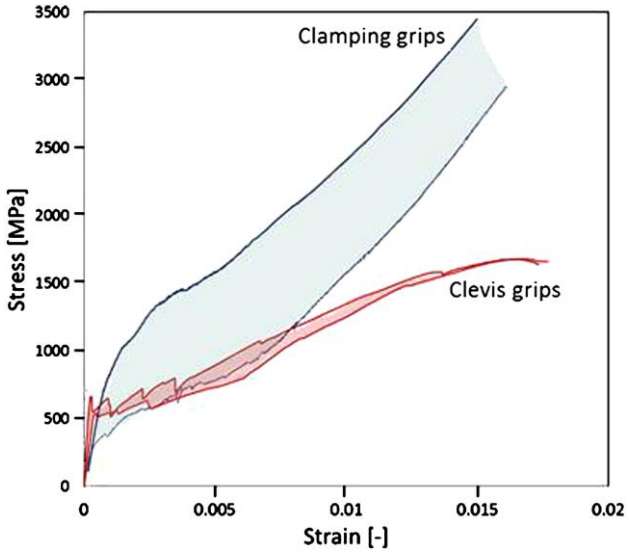

Figure 4.14 - PBO-FRCM single layer behavior with the different test setups [Arboleda et al, 2016]

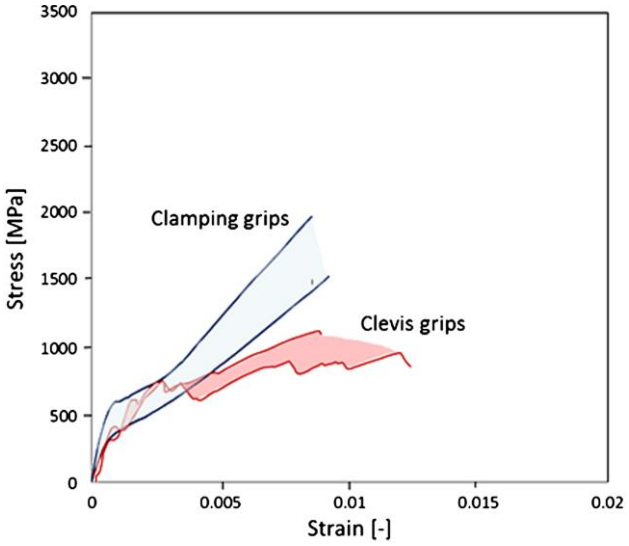

Figure 4.15 - C-FRCM single layer behavior with the different test setups [Arboleda et al, 2016]

4.7.3. Clevis Grips on Two-Layer Specimens

In order to analyze the efficiency of multiple layers, clevis grip tests were performed on coupons with two layers of coated carbon (cC) fabric. Six tests were performed. Figure 4.16 and Tables 4.3 - 4.5 show the stress-strain curves and the results

summary. The failure mode was by slippage of the fabric after crack saturation. The bilinear behavior was observed consistent with one-layer coupons. A post-failure phase showed increased *pseudo-ductility* attributable to the friction between the two fabric layers and the mortar.

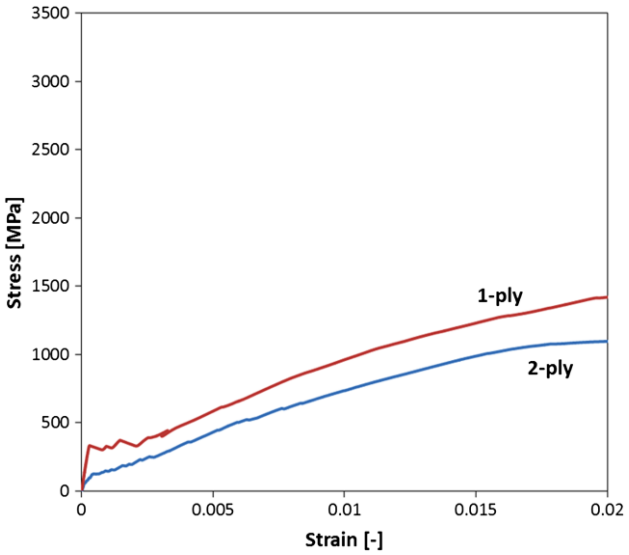

Figure 4.16 - cC-FRCM: two ply versus one ply [Arboleda et al, 2016]

4.7.4. Clevis Grips on Spliced Specimens

Investigation of fabric splicing with clevis grips showed that generally, the overlap length must be greater than or equal to the tab length used for load application, which itself is a function of the fabric development length within the matrix. Preliminary results demonstrate that an overlap of 100 mm is insufficient and must be increased to a minimum of 150 mm. In PBO-FRCM tests, the transition point occurs at a greater stress in the coupon with overlap as a result of the increase in matrix thickness; after the cracking phase, the slippage phenomena develops between fabric and mortar. Figure 4.17 compares the results for PBO-FRCM with the two gripping systems.

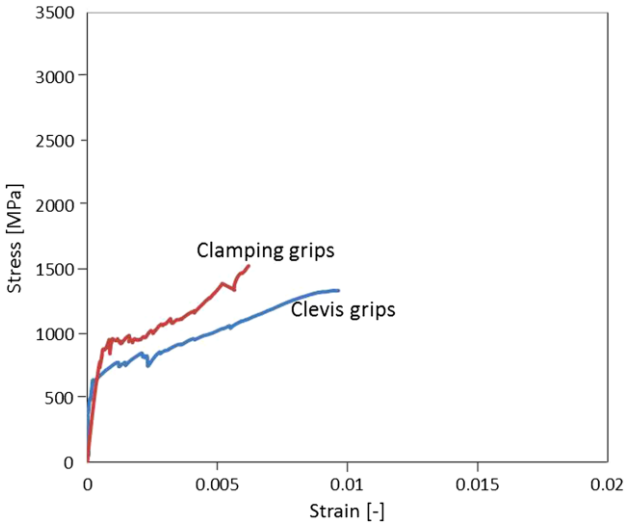

Figure 4.17 - PBO-FRCM lap splice behavior with the different test setups [Arboleda et al, 2016]

4.7.5. Clamping Grips on Spliced Specimens

Tensile tests were performed on coupons with a fabric overlap in the mid-section to determine the minimum overlap length. Two fabric layers were placed in the coupons, with a central splice overlap of 100 mm. Six tests were performed on PBO-FRCM coupons, and five tests were performed on C-FRCM. The fabric area was considered equal to one layer. The failure mode was slippage of the fabric between the two layers from the coupon center; for this reason the slope of the third phase and the maximum strength are lower than the one obtained with one-layer coupons. These results indicate that a length of overlap equal to 100 mm is not sufficient to guarantee a proper stress transfer for the systems tested.

4.8. Influence of Different Gripping Methods

As demonstrated by several studies (Contamine et al. 2011; Bianchi et al. 2013; Arboleda 2014; Carozzi et al. 2015), the resulting mechanical behavior for tensile tests is dependent on the gripping at the ends of the coupon, specifically, trilinear for clamping grip and bilinear for clevis grip. This consideration must be clearly understood when defining a procedure to be used for material characterization. Indeed, if the objective is the characterization of the FRCM system, the clamping grips that allow torsional rotation can provide a complete evaluation of the mechanical properties and all the parameters that characterize the trilinear stress-

strain curves can be determined. When the objective is the investigation of the maximum load bearing capacity of the system for the reinforcing application, the clevis-type grips are preferred because of failure by slippage.

It is possible, however, for an installation to take place with anchoring of the material at the ends in order to prevent the slippage phenomena in which case the maximum strength of the composite could be the sought after design parameter.

Chapter 5
Compressive Tests

5.1. Introduction

Cement is usually subjected to compressive stresses when used in the form of concrete or mortar. Mortar is a mixture of cement and sand in a specified ratio on which the strength of the mortar depends. If the mortar is weak, then also its compressive strength is very low, but if the mortar is a strong one then its compressive strength is also very high. The mixture of sand and cement in water is generally weak in tension and is strong in compression that is why when the concrete is subjected to tensile forces then it is provided with steel rods in area of tension that is why it is then called as reinforced concrete. Therefore, it is obvious the mortar will be strong in compression as compared to tension.

Mortar is generally used for brick masonry and plastering, but in the case of this research, mortar is used as matrix to embed the fibers. Hence, it is very much necessary to test the mortar for its compressive strength. For this purpose, required cement based matrix is prepared before its use and, after certain period of curing, it is tested. The strength of the mortar depends upon the fineness of cement, the gradation of sand and the water-cement ratio, which is the most important factor. If anyone of the above factors is not according to the ASTM-Standard, then the strength of mortar is badly effected. The standards of ASTM are provided for different ratios of mixture with which the test results are compared and then decided for its use. These values are taken when the mortar is just removed from curing.

5.2. Specimen Preparation and Test Set-Up

5.2.1. Specimen Geometry and Preparation

For conducting compressive tests, two types of mortar were chosen among those present on the market, specifically designed for structural reinforcement, namely cement based mortar (GLT) and hydraulic lime based mortar (GCF). Then, they were casted in cubical molds of 50 mm side length according to ASTM C109.

Mortar cube specimens were prepared by hand tamping the mortar in three layers through a rod, after mechanically mixing the mortar, as reflected in Figure 5.1. Upon hardening of the mortar, specimens were removed from the molds (Fig. 5.2) and placed in a humidity chamber for curing time. Upper surfaces, exposed to the moist air, were protected from dripping water. Finally, after a curing time of three, seven, fourteen and twenty-eight days, they were tested.

Figure 5.1 - Cube molding for compressive strength of mortar tests

Figure 5.2 - Cube de-molding for compressive strength of mortar tests

Five cubes were prepared for each type of mortar and each curing time, and tested with the help of a hydraulic type universal test frame. Finally, average of its strength was taken into account.

5.2.2. Test Set-Up

Uniaxial compression load was applied to the cube specimens using a hydraulic type universal test frame (Fig. 5.3). Load was applied to the cube faces that were in contact with the mold surfaces per standard requirements. The load was applied continuously and uniformly at a rate of 900 to 1800 N/s.

Figure 5.3 - Compressive test set-up

As the load is applied on the cube, it will develop cracks after certain load. Testing was continued until to the crushing of the specimen or development of a well-defined fracture pattern. Finally, the maximum load, carried by the sample during the test, was recorded and the type of fracture pattern was noted according to schema in Figure 5.4.

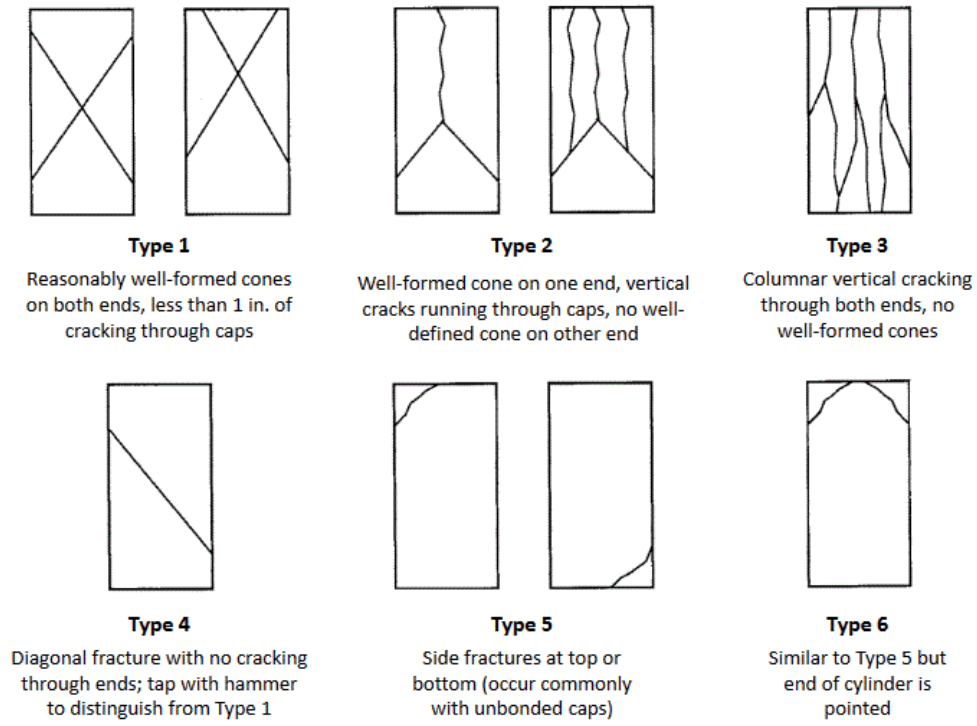

Figure 5.4 - Schematic of typical fracture patterns

5.3. Compressive Strength

The cube compressive strength (f'_c) was determined by dividing the maximum load applied, P_{max}, by the average area, A, of the cube face where the load was applied. Average area was obtained by the average of the length each side of the cube face measured at different locations as per ASTM C109 and reported in the following tables. Cubes were labelled according to the notation XXX-YY-N, in which XXX identifies the type of matrix, namely cement based mortar (GLT) and hydraulic lime based mortar (GCF), YY is the curing time, while N is the progressive number of each specimen.

5.4. Results

5.4.1. Hydralic Lime Based Mortar (GCF)

Tables 5.1-5.8 contain the tabulated summary results in terms of geometry, maximum load and compressive strength. Average, standard deviation and coefficient of variance values are also reported. The primary mode of failure was

compression of the cube, resulting to be a cone like structure as desired, represented in Figures 5.5-5.8.

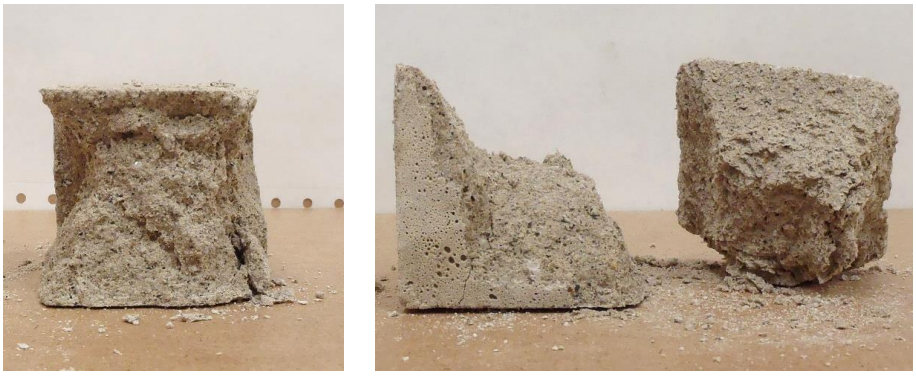

Figure 5.5 - Representative failure modes of cubes made of GCF at curing time of three days

Table 5.1 - Geometry of cubes made of GCF at curing time of three days

Cementitious Mortar	**$W_{1.1}$ (mm)**	**$W_{1.2}$ (mm)**	**$W_{1.average}$ (mm)**	**$W_{2.1}$ (mm)**	**$W_{2.2}$ (mm)**	**$W_{2.average}$ (mm)**	**Area (mm^2)**
GCF-3D-1	51.92	52.32	52.12	51.23	51.23	51.23	2670.24
GCF-3D-2	52.25	51.92	52.08	50.95	50.95	50.95	2653.74
GCF-3D-3	51.77	52.02	51.89	50.88	51.08	50.98	2645.35
GCF-3D-4	50.90	50.98	50.94	51.87	51.69	51.78	2637.55
GCF-3D-5	50.95	51.00	50.98	52.45	52.32	52.39	2670.60

Table 5.2 - Compressive test results of cubes made of GCF at curing time of three days

Cementitious Mortar	**Compressive Load (N)**	**Compressive Strength (MPa)**
GCF-3D-1	14233.60	5.33
GCF-3D-2	14500.48	5.46
GCF-3D-3	13922.24	5.26
GCF-3D-4	12632.32	4.79
GCF-3D-5	14989.76	5.61
Average	14055.68	5.29
St. Dev	886.82	0.31
CoV (%)	6.31	5.88

Figure 5.6 - Representative failure modes of cubes made of GCF at curing time of seven days

Table 5.3 - Geometry of cubes made of GCF at curing time of seven days

Cementitious Mortar	$W_{1.1}$ (mm)	$W_{1.2}$ (mm)	$W_{1.average}$ (mm)	$W_{2.1}$ (mm)	$W_{2.2}$ (mm)	$W_{2.average}$ (mm)	Area (mm^2)
GCF-7D-1	51.41	51.38	51.40	52.12	51.99	52.06	2675.58
GCF-7D-2	51.28	51.31	51.30	50.93	51.05	50.99	2615.57
GCF-7D-3	51.23	51.16	51.19	51.77	51.41	51.59	2640.95
GCF-7D-4	50.77	50.80	50.79	50.90	50.93	50.91	2585.80
GCF-7D-5	50.32	50.27	50.29	51.66	51.71	51.69	2599.54

Table 5.4 - Compressive test results of cubes made of GCF at curing time of seven days

Cementitious Mortar	Compressive Load (N)	Compressive Strength (MPa)
GCF-7D-1	28289.28	10.57
GCF-7D-2	22017.60	8.42
GCF-7D-3	29445.76	11.15
GCF-7D-4	27132.80	10.49
GCF-7D-5	27755.52	10.68
Average	26928.19	10.26
St. Dev	287363	1.06
CoV (%)	10.67	10.35

Figure 5.7 - Representative failure modes of cubes made of GCF at curing time of fourteen days

Table 5.5 - Geometry of cubes made of GCF at curing time of fourteen days

Cementitious Mortar	$W_{1.1}$ (mm)	$W_{1.2}$ (mm)	$W_{1.average}$ (mm)	$W_{2.1}$ (mm)	$W_{2.2}$ (mm)	$W_{2.average}$ (mm)	Area (mm^2)
GCF-14D-1	51.18	51.46	51.32	51.51	51.51	51.51	2643.59
GCF-14D-2	51.18	51.21	51.19	50.80	50.83	50.81	2601.29
GCF-14D-3	50.95	50.88	50.91	51.26	51.23	51.24	2609.08
GCF-14D-4	52.43	51.89	52.16	50.93	50.88	50.90	2654.97
GCF-14D-5	52.02	52.43	52.22	50.88	50.90	50.89	2657.54

Table 5.6 - Compressive test results of cubes made of GCF at curing time of fourteen days

Cementitious Mortar	Compressive Load (N)	Compressive Strength (MPa)
GCF-14D-1	24775.36	9.37
GCF-14D-2	28111.36	10.81
GCF-14D-3	26109.76	10.01
GCF-14D-4	25976.32	9.78
GCF-14D-5	25220.16	9.49
Average	26038.59	9.89
St. Dev	1281.69	0.57
CoV (%)	4.92	5.75

Figure 5.8 - Failure modes of cubes made of GCF at curing time of twenty-eight days

Table 5.7 - Geometry of cubes made of GCF at curing time of twenty-eight days

Cementitious Mortar	$W_{1.1}$ (mm)	$W_{1.2}$ (mm)	$W_{1.average}$ (mm)	$W_{2.1}$ (mm)	$W_{2.2}$ (mm)	$W_{2.average}$ (mm)	Area (mm^2)
GCF-28D-1	50.17	50.27	50.22	51.79	51.74	51.77	2599.43
GCF-28D-2	52.45	52.45	52.45	51.46	51.44	51.45	2698.48
GCF-28D-3	51.18	51.26	51.22	52.10	51.99	52.04	2665.68
GCF-28D-4	50.98	51.28	51.13	51.99	51.89	51.94	2655.86
GCF-28D-5	51.66	52.35	52.01	50.65	50.72	50.69	2635.99

Table 5.8 - Compressive test results of cubes made of GCF at curing time of twenty-eight days

Cementitious Mortar	Compressive Load (N)	Compressive Strength (MPa)
GCF-28D-1	26510.08	10.20
GCF-28D-2	31002.56	11.49
GCF-28D-3	24730.88	9.28
GCF-28D-4	32336.96	12.18
GCF-28D-5	29000.96	11.00
Average	28716.29	10.83
St. Dev	3129.22	1.13
CoV (%)	10.90	10.41

5.4.2. Cement Based Mortar (GLT)

Tables 5.9-5.16 contain the tabulated summary results in terms of geometry, maximum load and compressive strength. Average, standard deviation and coefficient of variance values are also reported. The primary mode of failure was compression of the cube, resulting to be a cone like structure as desired, represented in Figures 5.8-5.11.

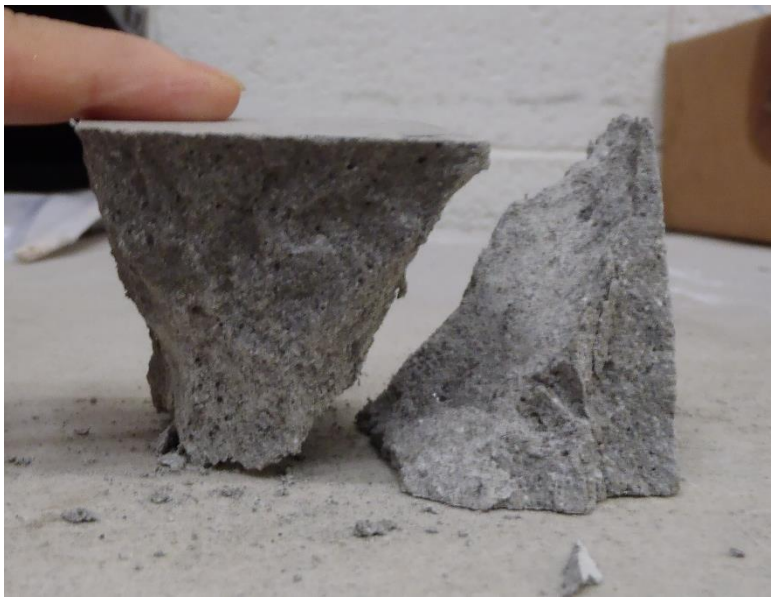

Figure 5.9 - Representative failure modes of cubes made of GLT at curing time of three days

Table 5.9 - Geometry of cubes made of GLT at curing time of three days

Cementitious Mortar	$W_{1.1}$ (mm)	$W_{1.2}$ (mm)	$W_{1.average}$ (mm)	$W_{2.1}$ (mm)	$W_{2.2}$ (mm)	$W_{2.average}$ (mm)	Area (mm^2)
GLT-3D-1	50.88	50.95	50.91	51.18	51.23	51.21	2607.14
GLT-3D-2	50.29	50.42	50.36	52.63	52.68	52.65	2651.43
GLT-3D-3	50.98	50.93	50.95	51.26	51.26	51.26	2611.68
GLT-3D-4	50.09	50.72	50.41	52.68	52.68	52.68	2655.38
GLT-3D-5	50.50	50.55	50.52	52.37	52.37	52.37	2646.01

Table 5.10 - Compressive test results of cubes made of GLT at curing time of three days

Cementitious Mortar	Compressive Load (N)	Compressive Strength (MPa)
GLT-3D-1	70945.60	27.21
GLT-3D-2	58224.32	21.96
GLT-3D-3	72546.88	27.78
GLT-3D-4	76372.16	28.76
GLT-3D-5	67920.96	25.67
Average	69201.98	26.28
St. Dev	6851.83	2.66
CoV (%)	9.90	10.12

Figure 5.10 - Representative failure modes of cubes made of GLT at curing time of seven days

Table 5.11 - Geometry of cubes made of GLT at curing time of seven days

Cementitious Mortar	$W_{1.1}$ (mm)	$W_{1.2}$ (mm)	$W_{1.average}$ (mm)	$W_{2.1}$ (mm)	$W_{2.2}$ (mm)	$W_{2.average}$ (mm)	Area (mm^2)
GLT-7D-1	50.42	50.70	50.56	52.10	52.12	52.11	2634.52
GLT-7D-2	51.41	51.66	51.54	51.66	51.66	51.66	2662.57
GLT-7D-3	51.23	51.16	51.19	51.92	51.89	51.90	2657.20
GLT-7D-4	52.45	52.53	52.49	51.64	51.33	51.49	2702.44
GLT-7D-5	51.61	51.64	51.63	52.22	52.17	52.20	2694.70

Table 5.12 - Compressive test results of cubes made of GLT at curing time of seven days

Cementitious Mortar	Compressive Load (N)	Compressive Strength (MPa)
GLT-7D-1	75260.16	28.57
GLT-7D-2	74726.40	28.07
GLT-7D-3	91673.28	34.50
GLT-7D-4	76683.52	28.38
GLT-7D-5	93986.24	34.88
Average	82465	30.88
St. Dev	9523.03	3.49
CoV (%)	11.55	11.29

Figure 5.11 - Failure modes of cubes made of GLT at curing time of fourteen days

Table 5.13 - Geometry of cubes made of GLT at curing time of fourteen days

Cementitious Mortar	$W_{1.1}$ (mm)	$W_{1.2}$ (mm)	$W_{1.average}$ (mm)	$W_{2.1}$ (mm)	$W_{2.2}$ (mm)	$W_{2.average}$ (mm)	Area (mm^2)
GLT-14D-1	51.69	51.31	51.50	52.40	52.15	52.27	2691.99
GLT-14D-2	52.02	52.63	52.32	51.05	51.10	51.08	2672.68
GLT-14D-3	50.65	50.77	50.71	52.17	52.88	52.53	2663.71
GLT-14D-4	52.10	52.07	52.08	51.66	52.02	51.84	2700.04
GLT-14D-5	51.97	51.89	51.93	51.33	51.74	51.54	2676.31

Table 5.14 - Compressive test results of cubes made of GLT at curing time of fourteen days

Cementitious Mortar	Compressive Load (N)	Compressive Strength (MPa)
GLT-14D-1	113201.60	42.05
GLT-14D-2	99323.84	37.16
GLT-14D-3	111111.04	41.71
GLT-14D-4	99635.20	36.90
GLT-14D-5	120362.88	44.97
Average	108726.91	40.56
St. Dev	9112.90	3.46
CoV (%)	8.38	8.54

Figure 5.12 - Representative failure modes of cubes made of GLT at curing time of twenty-eight days

Table 5.15 - Geometry of cubes made of GLT at curing time of twenty-eight days

Cementitious Mortar	$W_{1.1}$ (mm)	$W_{1.2}$ (mm)	$W_{1.average}$ (mm)	$W_{2.1}$ (mm)	$W_{2.2}$ (mm)	$W_{2.average}$ (mm)	Area (mm^2)
GLT-28D-1	50.83	50.98	50.90	51.49	51.44	51.46	2619.42
GLT-28D-2	51.03	51.03	51.03	51.03	51.05	51.04	2604.57
GLT-28D-3	51.82	51.79	51.80	51.64	51.54	51.59	2672.40
GLT-28D-4	52.68	52.27	52.48	51.79	51.74	51.77	2716.45
GLT-28D-5	52.07	51.82	51.94	52.68	52.27	52.48	2725.78

Table 5.16 - Compressive test results of cubes made of GLT at curing time of twenty-eight days

Cementitious Mortar	Compressive Load (N)	Compressive Strength (MPa)
GLT-28D-1	80775.68	30.84
GLT-28D-2	106307.20	40.82
GLT-28D-3	67209.28	25.15
GLT-28D-4	124721.92	45.91
GLT-28D-5	112445.44	41.25
Average	98291.90	36.79
St. Dev	23643.50	8.52
CoV (%)	24.05	23.15

Based on the experimental tests presented herein, the cement-based mortar, *GLT*, meets the requirements of AC434 Section 4.3, corresponding to 17 MPa at 7 days and 24 MPa at 28 days compressive strength. Regarding the hydraulic lime-based mortar, *GCF*, it also fulfills standard requirements, that is, the average compressive strength of at least three 50 mm cubes shall be not less than 1.7 N/mm^2 and no more than 10.3 N/mm^2 at the age of 28 days.

Chapter 6
Tensile Tests

6.1. Introduction

This thesis presents a laboratory investigation carried on SRG composites for the strengthening of masonry and concrete structures, which provides a mechanical characterization leading to the identification of design parameters. Aiming at reproducing the variability of available textiles and mortars, four SRG systems were tested, combining two unidirectional textiles of Ultra High Tensile Strength Steel with two matrices (a mineral mortar and a natural hydraulic lime mortar), as described below.

First, direct tensile tests were carried out on composite specimens to characterize the entire response under tension, from the un-cracked stage up to tensile rupture, and to derive information on crack pattern. Second, interlaminar shear tests were realized on short-beam specimens to determine the interlaminar properties that normally dominate specimen failure. Third, pull-off tests were performed on three types of substrate (clay bricks, concrete blocks and concrete masonry units) to investigate the SRG-to-substrate load transfer performance. The influence of the properties of textiles, matrices and substrates on bond strength and failure mode are analyzed as well.

6.2. Mechanical Behavior of SRG in Tension

A typical *stress–strain* behavior of SRG under tensile test is reported in Figure 6.1. The curve can be considered tri-linear: the linear branch represents the un-cracked state, where the slope of stress–strain curve reflects the elastic modulus of the matrix. The second phase corresponds to the formation of cracks. In this state, there is a significant decrease of the stiffness and relatively fine cracks grow with the tensile load. The length and slope of this portion of the curve depend on the quality of the bond between textile and matrix and on the volume proportion of the fibers activated for the load transfer. The third phase is the crack-widening region, where the existing cracks become wider up to the final failure that can be compared with

the tensile strength of the textile. In tests where the transition from second to third phase is not evident (point T_2), some extra cracks develop also in the third phase. In this phase, the only resistant part in the composite is the fabric and, therefore, the slope of the curve should reflect the elastic modulus of the dry fibers.

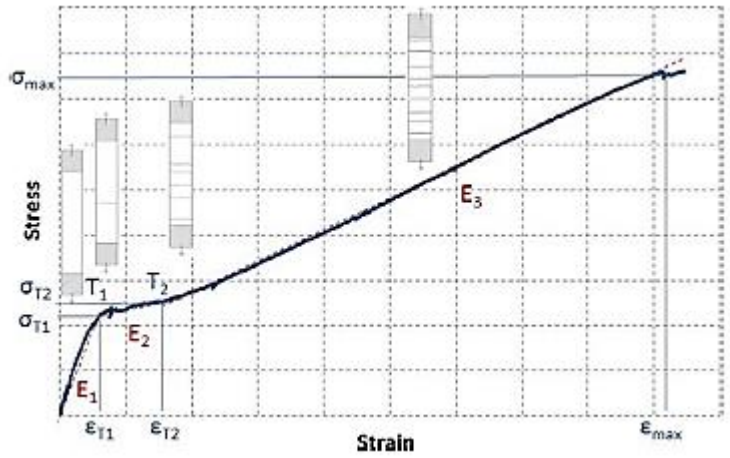

Figure 6.1 – Stress-strain behavior of FRCM composites subjected to tensile test [Carozzi et al, 2015]

The main significant parameters of direct tensile tests on SRG composites are the strength and the strain of transition points, the ultimate strength and the corresponding load per unit width and strain, Young's modulus, the maximum strain, and finally, the failure mode.

6.3. Materials

The studied SRG systems consist of two main elements, a cementitious mortar enriched with a low dosage of dry polymers and a fiber grid. In this study, two different steel textiles, *G6* and *G12*, were investigated. Each type of fiber was correlated with two different mortars, a cement-based mortar, *GLT*, and a hydraulic lime-based mortar, *GCF*. The corresponding combined systems are denominated *"GLT-G6"*, *"GCF-G6"*, *"GLT-G12"* and *"GCF-G12"*.

6.3.1. Textile Reinforcements

The *"G6"* fabric is characterized by a density of 1.57 cords/cm. Cords are equally spaced of about 6 mm to obtain a textile with 0.084 mm equivalent thickness and 670 g/m^2 mass density (Fig. 6.2a).

The *"G12"* net has a density of 3.19 cords/cm and, 0.169 mm equivalent thickness and 1200 g/m^2 mass density (Fig. 6.2b). Cords are placed adjacent to each other two by two such that the spacing between couples of cords is about 4 mm, in order to allow for the protrusion of the mortar during installation and to promote the matrix-to-textile interlocking. The main mechanical properties of steel fabric provided by manufacturer are reported in Table 6.1.

Table 6.1 - Mechanical properties of steel fabric provided by manufacturer

Steel Fabric	Cords/cm	Mass density (g/m2)	Equivalent thickness (mm)	Tensile Strength (MPa)	Elastic Modulus (GPa)	Deformation at rupture (%)
G12	3.19	1200	0.169	> 3000	> 190	> 2
G6	1.57	670	0.084	> 2800	> 190	> 1.5

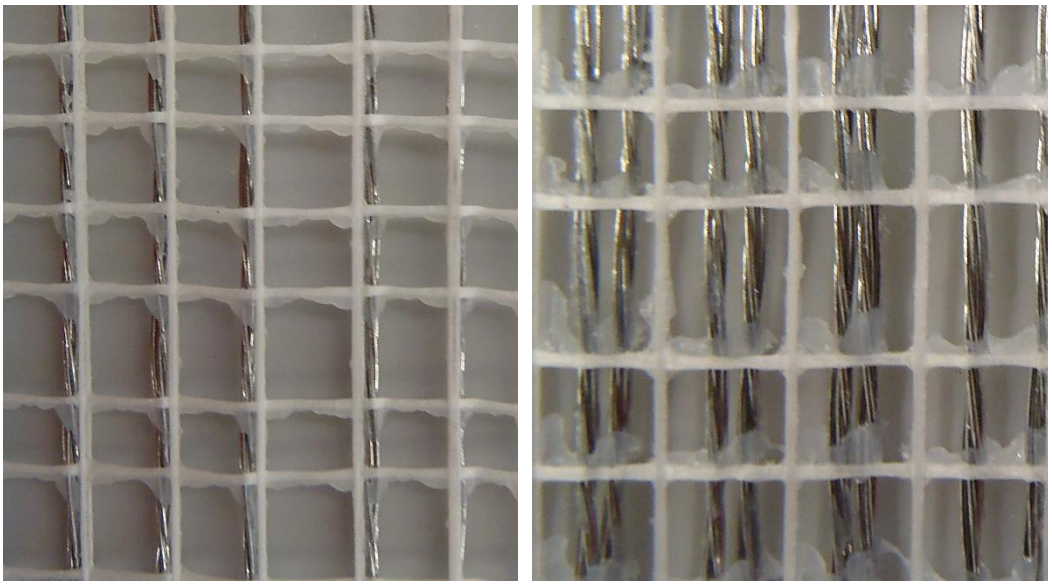

a) b)

Figure 6.2 - Galvanized UHTSS textile: a) Sheet G6; b) Sheet G12

6.3.2. Cementitious Matrix

Composite specimens were manufactured with two mortars, such as a mineral mortar (GLT) with a binder of natural kaolin and bauxite, and a natural hydraulic lime mortar (GCF), comprising mineral binders, aggregates of silica sand and dolomite limestone (Fig. 6.3).

Table 6.2 summarizes their values of compressive strength (f_{cm}), Young's modulus (E_{cm}), tensile strength (f_{tm}), and grain size range (D) provided by manufacturer in compliance EN 1504-3 standard.

Table 6.2 - Mechanical properties of mortar matrices provided by manufacturer

Matrix	f_{cm} (MPa)	E_{cm} (GPa)	f_{tm} (MPa)	D (mm)
Mineral Mortar	> 50 (28 gg)	22	> 8 (28 gg)	0 - 0.5
Natural Hydraulic Lime Mortar	> 15 (28 gg)	9	> 5 (28 gg)	0 - 1.4

a) b)

Figure 6.3 - Mortar matrices: a) Mineral Mortar (GLT); b) Natural Hydraulic Lime Mortar (GCF) [Kerakoll catalogue]

Extra-fine aggregates ensure a better workability and allow embedding the fabric reinforcement perfectly by achieving higher adhesion values (only comparable to organic matrices) to provide a monolithic reinforcement with high mechanical performance that enables the optimum transfer of the stress from the structural element to the reinforcement system.

6.4. Specimen Preparation and Test Set-Up

6.4.1. Specimen Geometry and Preparation

In order to investigate the mechanical behavior of SRG systems, tensile tests were carried out on several series of specimens. In the following part, the test set-up is described and the main results of the experimental program are reported.

Tensile coupons were made in a flat glass mold by applying a first layer of cementitious mortar (5 mm), the fiber mesh and a second layer of cementitious mortar (5 mm). The curing is lasted 28 days in humidity chamber. In the curing phase is important to pay attention to the possibility that some micro-cracks develop due to a non-homogeneous shrinkage.

The coupons (Fig. 6.4) were all rectangular (nominal size 510 x 51 x 10 mm). In order to avoid local damage in the specimens during the tensile tests, metal tabs were bonded using epoxy resin at the ends of the specimens. The tabs presented a width equal to the sample and a length equal to 254 mm. Tables 6.3-6.6 show the variability of the specimens transversal area due to the non-constant thickness (t_1, t_2, t_3) and width (w_1, w_2, w_3) measured in three points reported in the Figure 6.4.

Specimens are labelled according to the notation XXX-YYY-ZZ-N, in which XXX identifies the test type, YYY and ZZ are the matrix and the textile, respectively; while, N is the progressive number of each specimen.

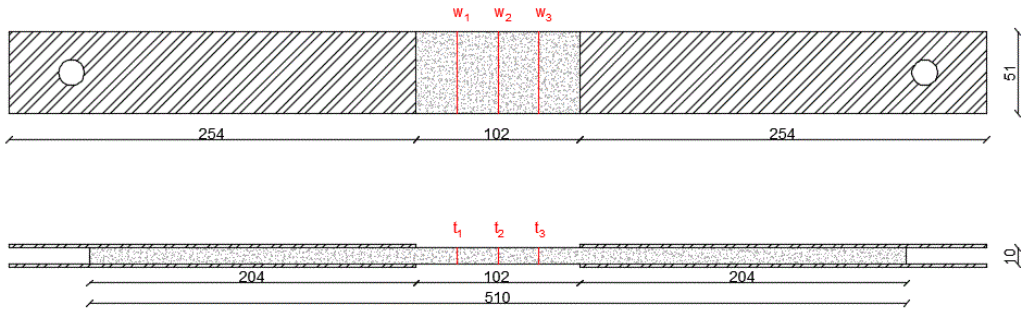

Figure 6.4 - Coupon size

Table 6.3 – Geometry of GLT-G6 Specimens

Specimens ID	Thickness			Width			Area		
	t_1	t_2	t_3	w_1	w_2	w_3	A_1	A_2	A_3
	(mm)	(mm)	(mm)	(mm)	(mm)	(mm)	(mm^2)	(mm^2)	(mm^2)
TNS-GLT-G6-1	10	10	11	53	54	53	544	552	588
TNS-GLT-G6-2	8	9	8	53	53	53	420	457	434
TNS-GLT-G6-3	8	8	9	53	53	53	434	438	453
TNS-GLT-G6-4	7	7	7	53	53	53	355	357	360
TNS-GLT-G6-5	10	10	10	52	52	52	504	501	502
TNS-GLT-G6-6	8	8	8	53	51	54	428	421	440
TNS-GLT-G6-7	8	8	8	53	53	53	440	419	434
TNS-GLT-G6-8	8	8	8	51	56	55	410	456	435
TNS-GLT-G6-9	9	9	9	51	51	50	457	435	430
TNS-GLT-G6-10	8	8	8	51	51	50	405	419	410
TNS-GLT-G6-11	7	7	7	51	52	52	373	386	382
TNS-GLT-G6-12	11	11	11	49	49	49	558	546	542
TNS-GLT-G6-13	8	8	8	51	51	50	424	406	422
TNS-GLT-G6-14	8	8	8	51	50	51	406	383	417
TNS-GLT-G6-15	8	8	8	51	51	51	396	402	395

Table 6.4 – Geometry of GCF-G6 Specimens

Specimens ID	Thickness			Width			Area		
	t_1	t_2	t_3	w_1	w_2	w_3	A_1	A_2	A_3
	(mm)	(mm)	(mm)	(mm)	(mm)	(mm)	(mm^2)	(mm^2)	(mm^2)
TNS-GCF-G6-1	11	11	11	52	52	52	563	576	576
TNS-GCF-G6-2	10	9	9	52	53	53	503	497	485
TNS-GCF-G6-3	10	10	11	51	51	51	532	529	545
TNS-GCF-G6-4	10	10	10	52	52	51	529	537	521
TNS-GCF-G6-5	9	9	9	51	51	51	469	482	482
TNS-GCF-G6-6	10	10	11	51	52	52	532	537	582
TNS-GCF-G6-7	10	9	10	52	52	53	524	487	521
TNS-GCF-G6-8	11	10	10	51	51	51	552	519	506
TNS-GCF-G6-9	11	10	11	51	52	52	560	524	555
TNS-GCF-G6-10	10	9	10	50	51	52	498	482	537

Table 6.5 – Geometry of GLT-G12 Specimens

Specimens ID	Thickness			Width			Area		
	t_1	t_2	t_3	w_1	w_2	w_3	A_1	A_2	A_3
	(mm)	(mm)	(mm)	(mm)	(mm)	(mm)	(mm^2)	(mm^2)	(mm^2)
TNS-GLT-G12-1	10	10	10	54	54	55	521	534	557
TNS-GLT-G12-2	11	11	11	50	51	51	560	553	561
TNS-GLT-G12-3	12	11	12	55	55	55	638	630	644
TNS-GLT-G12-4	10	7	9	55	54	54	543	381	476
TNS-GLT-G12-5	10	10	23	54	53	54	517	515	1231
TNS-GLT-G12-6	11	12	12	50	49	49	552	579	570
TNS-GLT-G12-7	11	11	11	49	49	49	542	536	533
TNS-GLT-G12-8	12	12	12	50	50	50	605	604	615
TNS-GLT-G12-9	13	13	12	50	50	50	630	630	617
TNS-GLT-G12-10	11	11	11	50	50	50	556	560	538
TNS-GLT-G12-11	11	12	12	50	50	50	557	601	585

Table 6.6 – Geometry of GCF-G12 Specimens

Specimens ID	Thickness			Width			Area		
	t_1	t_2	t_3	w_1	w_2	w_3	A_1	A_2	A_3
	(mm)	(mm)	(mm)	(mm)	(mm)	(mm)	(mm^2)	(mm^2)	(mm^2)
TNS-GCF-G12-1	12	12	11	53	53	53	610	619	607
TNS-GCF-G12-2	10	10	10	55	55	55	556	523	523
TNS-GCF-G12-3	10	10	10	56	56	56	532	533	535
TNS-GCF-G12-4	10	10	10	54	54	53	561	553	542
TNS-GCF-G12-5	10	10	10	53	52	52	527	537	537
TNS-GCF-G12-6	11	11	10	52	52	53	552	549	545
TNS-GCF-G12-7	10	10	11	53	53	53	515	522	569
TNS-GCF-G12-8	10	10	10	54	53	53	529	536	521
TNS-GCF-G12-9	10	10	10	55	55	55	531	547	536
TNS-GCF-G12-10	10	10	10	53	53	53	524	514	519

6.4.2. Clamping Method

Tensile tests were carried out according to *American Standard AC434-Annex A* that recommends gripping the specimen through an adhesive tension and shear method such as a clevis grip. This includes two plates glued at each end of the specimen

and connected with a transversal pin outside of the length of the specimen. This system is connected with a clevis joint to the testing frame. Gripping mechanism applies longitudinally the load by surface shear (through adhesive), and thus leave the ends free that are representative of repair applications where the material is not anchored at its ends. This configuration reduces bending and most importantly allows for slippage of the fabric at the grips, so that the bond between fiber-matrix can be investigated. The grip system of clevis type is illustrated in Figure 6.5.

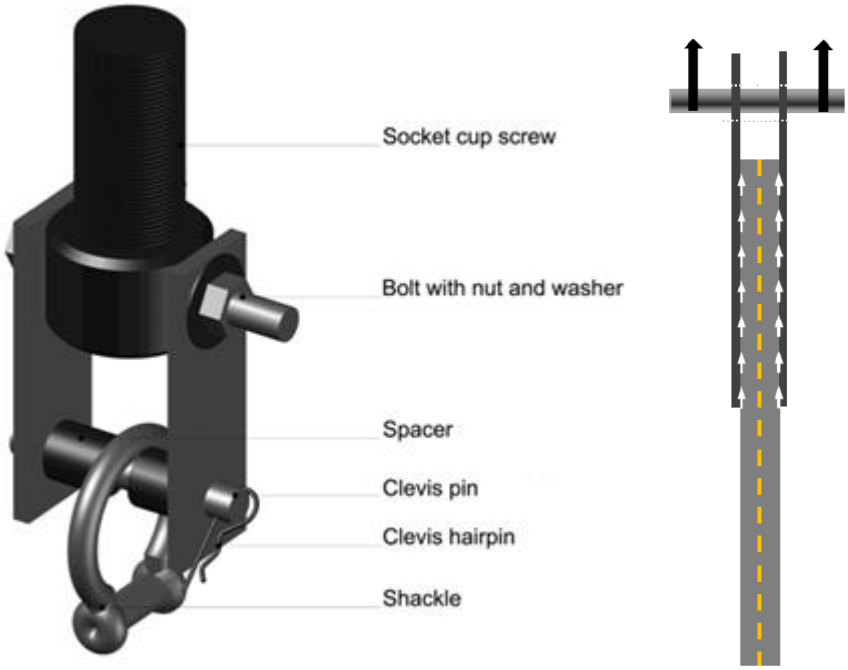

Figure 6.5 - Clevis-type grip [Arboleda, 2014]

6.4.3. Instrumentation

Uniaxial tensile load was applied to all specimens. Testing was performed using a screw driven universal test frame with a maximum capacity of 245 kN.

An initial minimal tension, less than 5 percent of ultimate capacity, was applied to engage the specimen and clevis grip setup.

Load was applied under displacement control at a rate of 0.25 mm/minute and recorded by the load cell integrated in the testing machine. Axial deformation was measured using two extensometers with a 100 mm and 50 mm gauge length, placed

mid-length of the specimen, that accommodate multiple cracks inside the monitored length (Fig. 6.6).

Figure 6.6 - Tensile test set-up

6.5. Results

In the following, the results of tests for each tested coupons are presented as tensile stress versus strain curves. For each type of composite system, tensile stress-strain curve of only one specimen is reported, because similar trends and considerations can be extended to all tested specimens of the same series. Then, based on experimental results, maximum force, ultimate strength and strain, and cracked elastic modulus have been calculated. Finally, failure mode has been described for each tested specimens.

6.5.1. Tensile Tests of GLT-G6-1 Specimen

The tensile *load-strain* curve of coupon GLT-G6-1 shows a linear trend up to the 2 kN load level (point T_1 in Figure 6.7). At this first stage, the specimen was un-cracked and the mortar matrix contributed both to load bearing capacity and stiffness.

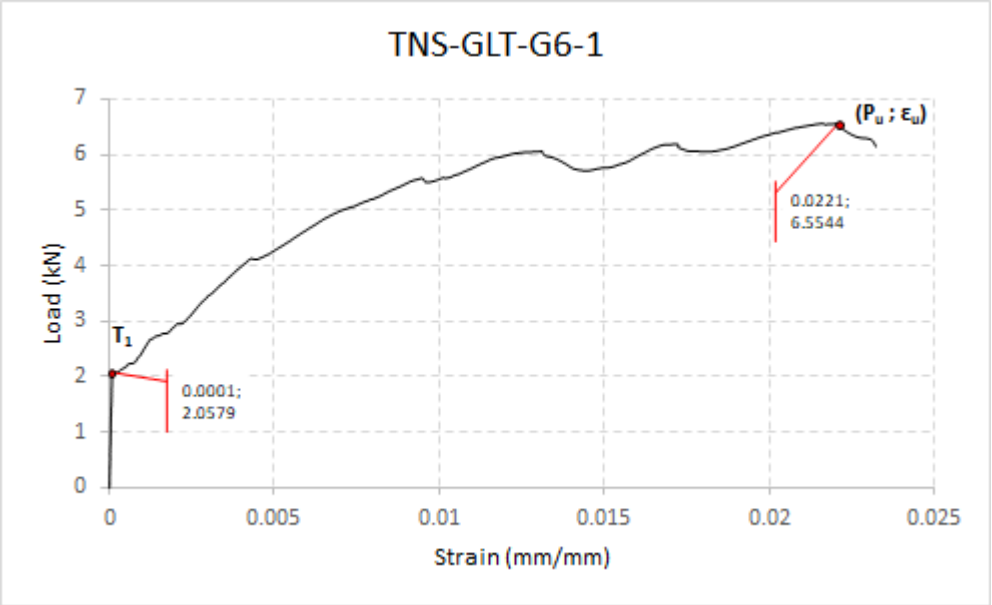

Figure 6.7 - Load-Strain Curve for coupon GLT-G6-1

After the point T_1, a first crack of the cementitious matrix occurred at the end of bonded length of metal tab (Figure 6.8a) and the *load-strain* curve changed slope. T_1 is the transition point and it corresponds to the intersection of initial and secondary segments of the response curve. At the second stage, it can be observed crack pattern developed progressively and new cracks occurred in the mid-length of coupon (Figure 6.8a). In the meantime, the width of the first crack increased with growing load and its development continued throughout bonded length of metal plate (Figure 6.8b). On the diagram, the second segment continues until the ultimate capacity (P_u, ε_u) is reached and therefore the crack pattern is completely developed (Figure 6.8c). Failure by rupture was due to the splitting of the matrix around the fiber cords. This because the mortar was not penetrated well in the fabric and was not engage effectively, making easy the slippage of fibers.

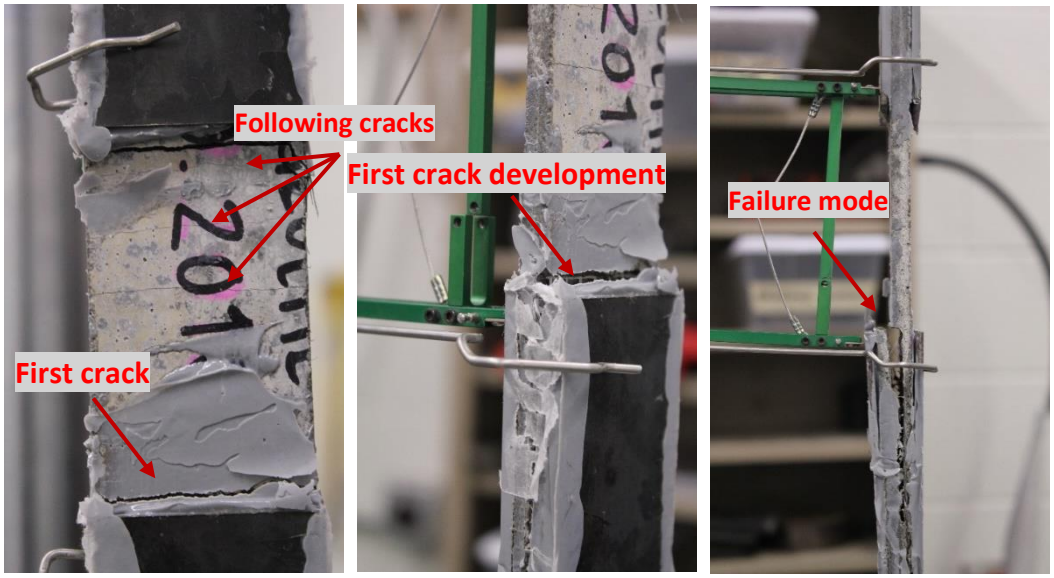

(a) (b) (c)

Figure 6.8 - Failure mode of coupon GLT-G6-1 subject to tensile test: (a) first and multiple cracks in the mortar; (b) enlargement of first crack; (c) ultimate failure.

Tensile strength at any time was calculated by the following equation:

$$f_f = \frac{P}{A_f \cdot n} \tag{6.1}$$

where P is the applied load (N), A_f is the area of grid reinforcement (mm^2) and n is the number of yarns.

The second segment is characterized by the cracked tensile modulus of elasticity, E_f. According to AC434, to calculate the tensile modulus of elasticity of the composite material, two points have to be selected on the experimental curve corresponding to cracked behavior after the transition. These two points are picked at a stress level equal to $0.90f_{fu}$ and $0.60f_{fu}$ (Fig. 6.9). The slope of the line that connects these two points represents the tensile modulus of elasticity of the cracked specimen:

$$E_f = \frac{\Delta f}{\Delta \varepsilon} = \frac{(0{,}90 \cdot f_{fu} - 0{,}60 \cdot f_{fu})}{\varepsilon_{f\_0.90f_{fu}} - \varepsilon_{f\_0.60f_{fu}}} \tag{6.2}$$

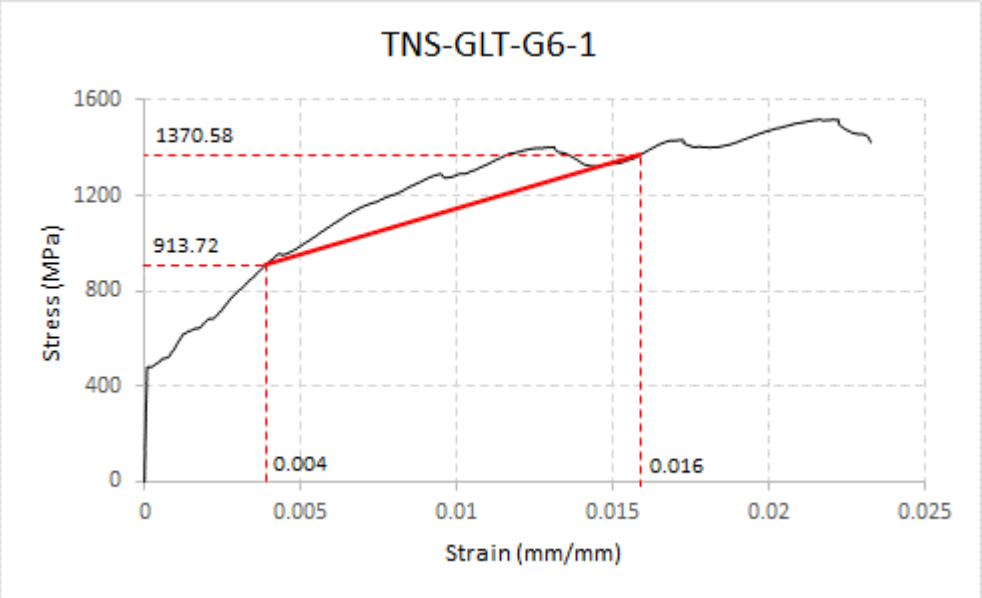

Figure 6.9 - Stress-Strain Curve for coupon GLT-G6-1

The results of the tensile test are reported in Table 6.7. The ultimate strength has been calculated dividing the maximum force by the total area of cords embedded in the coupon. It is equal to *1522.86 MPa* and it is lower than nominal maximum tensile strength of the fabric (> 2800 MPa). With reference to Figure 6.9, being the 90% and 60% of the ultimate strength equal to *913.72 MPa* and *1370.58 MPa*, respectively, and corresponding strains equal to *0.004 mm/mm* and *0.016 mm/mm*, the elastic modulus is *38.24 GPa*. So, it is very lower than elastic modulus of the dry steel textile (> 190 GPa). The ultimate strain is *2.206 %*; therefore, it is higher than the ultimate strain deformation of the fabric (> 1.5 %).

Table 6.7 - Tensile tests results on GLT-G6-1

Specimens ID	**Yarns**	**Max Force**	**Ultimate Strength**	**Cracked Elastic Modulus**	**Ultimate Strain**
	#	(kN)	(MPa)	(GPa)	(%)
TNS-GLT-G6-1	8	6.66	1522.86	38.24	2.206

6.5.2. GLT-G6 Series

A series of fifteen tensile tests were tested. Figure 6.10 shows the stress-strain behavior of a specimen of the series, which is described by a tri-linear diagram. Similar trend and consideration can be extended to all others tested specimens. The results of all coupons are reported in Table 6.8, while Table 6.9 lists the average values. In the assessment of average values, the results of GLT-G6-10 and GLT-G6-11 coupons have not been considered, because they were not acceptable.

The ultimate strength varies in a range between *862.43* and *2445.67 MPa*. The average value is *1445.63 MPa* and it is lower than nominal maximum tensile strength of the fabric (> 2800 MPa). The average elastic modulus (*74.06 GPa*) is lower than elastic modulus of the dry steel textile (> 190 GPa). The ultimate strain varies in a range between *0.799* and *4.381 %*. The average value is *2.133 %* and it is higher than the deformation at rupture of the fabric (> 1.5 %).

The experimental results show a quite large variability both for the elastic modulus and the deformations. This variability could be caused by several factors: the irregularities of the cross section of the specimens (Tables 6.3-6.6), the presence of micro-cracks invisible to the naked eye, the irregular position of the textile in the thickness and the localization of the first cracks with respect to the extensometer.

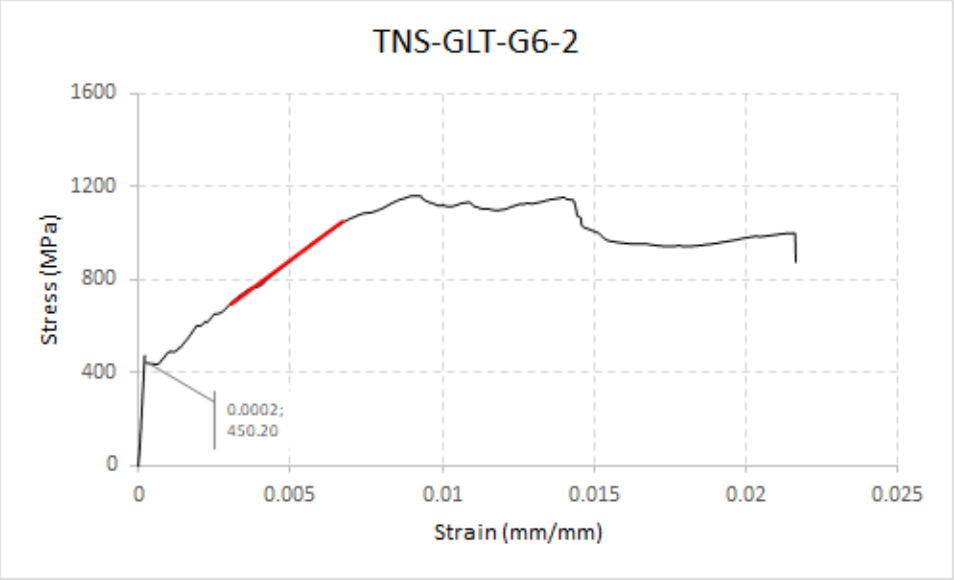

Figure 6.10 - Stress-Strain Curve for coupon GLT-G6-2

Table 6.8 - Tensile tests results on GLT-G6 series

Specimens ID	Yarns	Max Force	Ultimate Strength	Cracked Elastic Modulus	Ultimate Strain
	#	(kN)	(MPa)	(GPa)	(%)
TNS-GLT-G6-1	9	6.66	1522.86	38.24	2.207
TNS-GLT-G6-2	8	5.63	1162.49	94.72	0.909
TNS-GLT-G6-3	9	10.03	1912.69	38.69	4.180
TNS-GLT-G6-4	8	10.12	2445.67	42.12	3.982
TNS-GLT-G6-5	8	4.42	985.12	122.03	0.799
TNS-GLT-G6-6	8	4.93	1145.21	139.83	1.253
TNS-GLT-G6-7	8	5.83	646.19	1000.32	1.576
TNS-GLT-G6-8	5	6.07	2258	50.49	1.442
TNS-GLT-G6-9	9	5.94	1575.85	144.54	1.164
TNS-GLT-G6-10	7	6.09	1413.76	85.92	1.440
TNS-GLT-G6-11	8	6.64	1422.91	93.46	1.821
TNS-GLT-G6-12	7	6.22	1367.69	67.60	2.570
TNS-GLT-G6-13	8	5.75	862.43	33.72	4.381
TNS-GLT-G6-14	8	6.40	1363.71	25.92	2.207
TNS-GLT-G6-15	7	6.07	1612.76	36.04	0.909

Table 6.9 – Summary of tensile tests results on GLT-G6 series

	Thickness	Width	Area	Max Force	Ultimate Strength	Elastic Modulus	Ultimate Strain
	(mm)	(mm)	(mm^2)	(kN)	(MPa)	(GPa)	(%)
Average	8.51	51.78	440.53	6.53	1445.63	74.06	2.133
Sn-1	1.23	1.37	62.28	1.69	408.86	42.35	1.265
CoV((%)	14.5	2.6	14.1	25.9	28.3	57.2	59.335
Min	6.76	49.30	357.41	4.42	862.43	25.92	0.799
Max	11.14	53.66	565.88	10.12	2445.67	144.54	4.381

Table 6.9 also reports the coefficients of variation, *CoV*. It can be seen that the ultimate strength has a low scatter (*CoV = 28 %*), while modulus of elasticity and strain have a high scatter (*CoV = 57 %* and *CoV = 59%* respectively).

Regarding failure mode of all specimens of GLT-G6 series, they shown a collapse equal to the one reported in the Figure 6.8. It was characterized by the formation of a first crack in the end of bonded length of metal tab. From there, the development of crack continued throughout its length. Finally, the failure by rupture was due to the splitting of the matrix around the fiber cords. This because the mortar was not

penetrated well in the fabric and was not engage effectively, making easy the slippage of fibers.

6.5.3. GLT-G12 Series

A series of eleven tensile tests made with steel fabric *G12* and mortar *GLT* was tested. Figure 6.11 shows the stress-strain behavior of a specimen. Similar trend and consideration can be extended to all others tested specimens. The results of all coupons are reported in Table 6.10, while Table 6.11 lists the average values.

The ultimate strength was calculated dividing the maximum force by the section of the coupon. It varies in a range between *502.65* and *888.11 MPa*. The average value is *807.65 MPa* and it is lower than nominal maximum tensile strength of the fabric (> 3000 MPa). The average elastic modulus (*53.48 GPa*) is lower than elastic modulus of the dry steel textile (> 190 GPa). The ultimate strain varies in a range between *0.377* and *2.127 %*. The average value is *1.178 %* and it is lower than the deformation at rupture of the fabric (> 2 %).

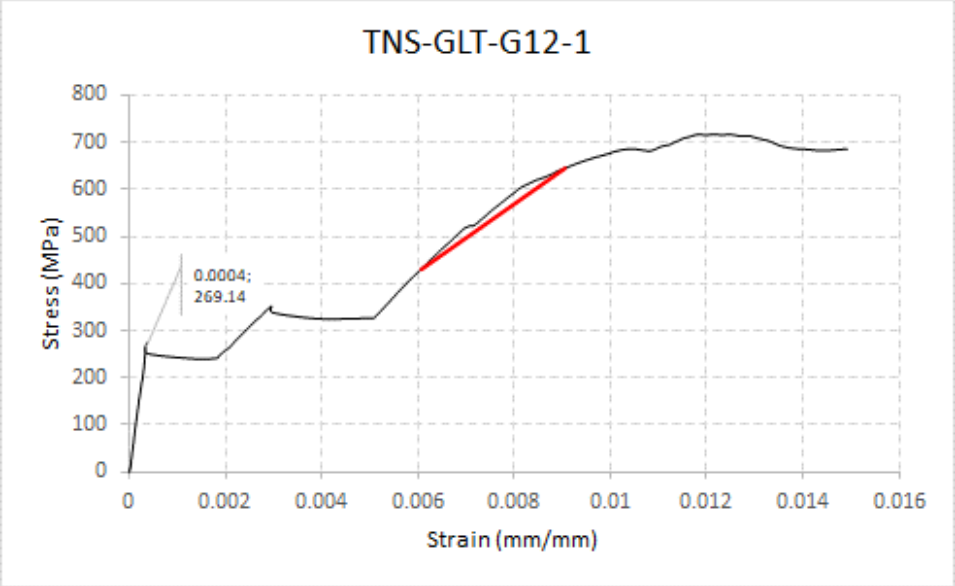

Figure 6.11 - Stress-Strain Curve for coupon GLT-G12-1

The experimental results show a quite large variability both for the elastic modulus and the deformations. This variability could be caused by several factors: the irregularities of the cross section of the specimens, the presence of micro-cracks

invisible to the naked eye, the irregular position of the textile in the thickness and the localization of the first cracks with respect to the extensometer.

Table 6.10 - Tensile tests results on GLT-G12 series

Specimens ID	Yarns	Max Force	Ultimate Strength	Cracked Elastic Modulus	Ultimate Strain
	#	(kN)	(MPa)	(GPa)	(%)
TNS-GLT-G12-1	16	6.59	715.12	71.58	1.215
TNS-GLT-G12-2	16	7.00	811.16	108.52	0.504
TNS-GLT-G12-3	14	7.24	826.02	57.35	1.004
TNS-GLT-G12-4	15	7.32	839.67	40.17	1.582
TNS-GLT-G12-5	15	7.25	836.21	70.82	1.436
TNS-GLT-G12-6	15	7.39	888.11	26.20	1.358
TNS-GLT-G12-7	15	6.76	502.65	49.03	0.377
TNS-GLT-G12-8	15	7.17	874.10	47.38	1.000
TNS-GLT-G12-9	15	7.10	859.16	47.57	1.108
TNS-GLT-G12-10	15	7.23	876.77	40.34	1.252
TNS-GLT-G12-11	15	7.09	855.21	29.29	2.127

Table 6.11 – Summary of tensile tests results on GLT-G12 series

	Thickness	Width	Area	Max Force	Ultimate Strength	Elastic Modulus	Ultimate Strain	Maximum Strain
	(mm)	(mm)	(mm^2)	(kN)	(MPa)	(GPa)	(%)	(%)
Average	11.4	51.4	584.1	7.10	807.65	53.48	1.18	1.178
Sn-1	2.1	2.3	105.2	0.24	111.52	23.33	0.48	0.483
CV((%)	18	4	18	3.41	13.81	43.63	40.97	40.974
Min	8.6	49.1	458.3	6.59	502.65	26.20	0.38	0.377
Max	16.0	55.0	833.1	7.39	888.11	108.52	2.13	2.127

Table 6.11 also reports the coefficients of variation, *CoV*. It can be seen that the ultimate strength has a low scatter (*CoV = 14 %*), while modulus of elasticity and strain have a high scatter (*CoV = 44 %* and *CoV = 41 %* respectively).

The Figures 6.12 show the cracking path developed by all specimens of GLT-G12 series throughout the tensile tests. A series of cracks occurred in the center area of the specimen that was monitored by the extensometer. Others take place in the end of bonded length of metal plate. From there, the development of crack continued

throughout its length. Finally, the failure by rupture was due to the splitting of the matrix around the fiber cords. The reason is that the mortar was not able to embed easily in the fabric, because the textile was characterized by high mass density (1200 g/m^2).

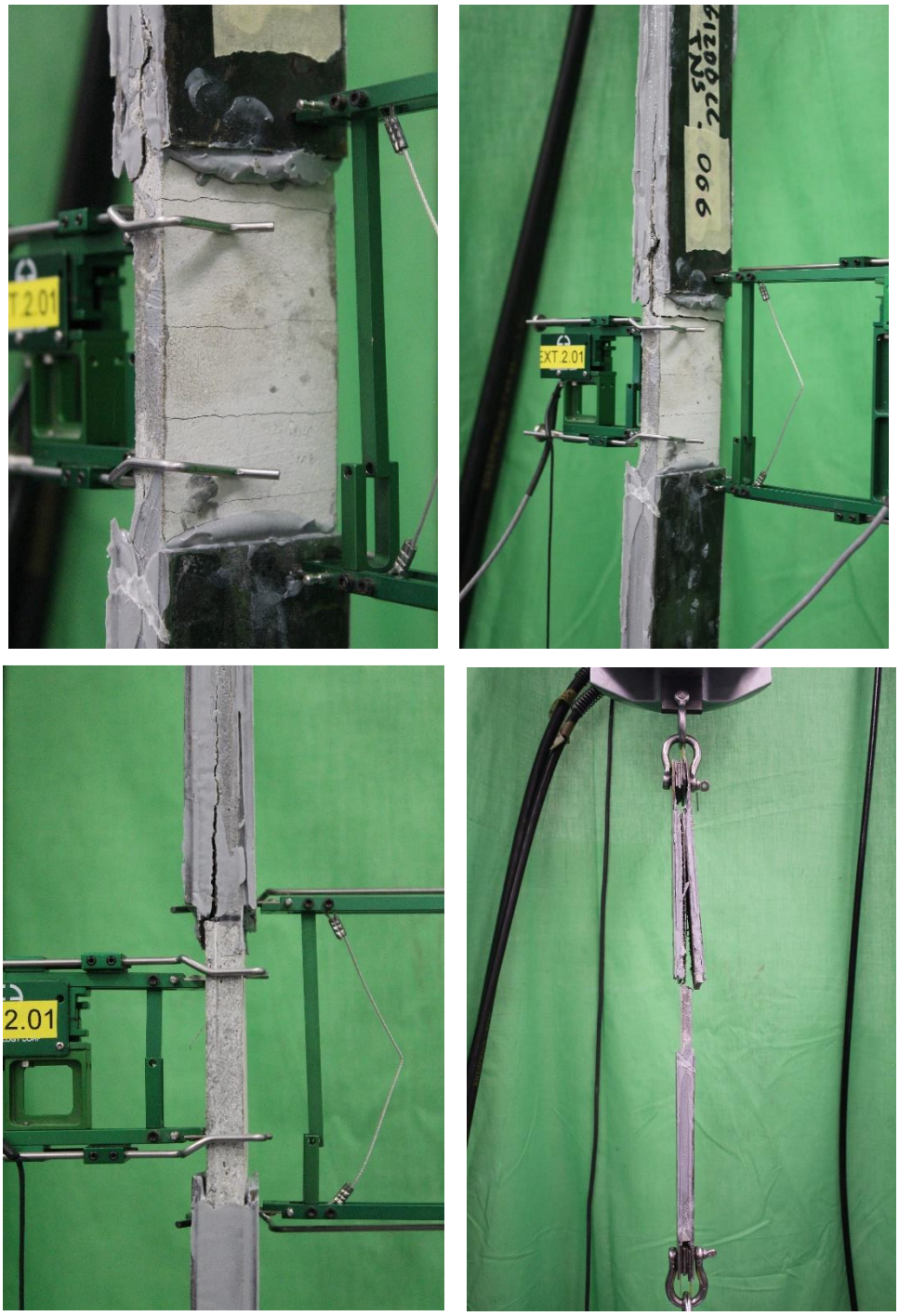

Figure 6.12 – Representative failure mode of coupons GLT-G12 subject to tensile test

6.5.4. GCF-G6 Series

A series of ten tensile tests made with steel fabric *G6* and mortar *GCF* was tested. Figure 6.13 shows the stress-strain behavior of a specimen. Similar trend and consideration can be extended to all others tested specimens. The results of all coupons are reported in Table 6.12, while Table 6.13 lists the average values. The ultimate strength was calculated dividing the maximum force by the section of the coupon. It varies in a range between *690.90* and *1328.62 MPa*. The average value is *934.72 MPa* and it is lower than nominal maximum tensile strength of the fabric (> 2800 MPa). The average elastic modulus (*54.65 GPa*) is lower than elastic modulus of the dry steel textile (> 190 GPa). The ultimate strain varies in a range between *0.762* and *2.302 %*. The average value is *1.575 %* and it is comparable to the deformation at rupture of the fabric (> 1.5 %).

The experimental results show a quite large variability both for the elastic modulus and the deformations. This variability could be caused by several factors: the irregularities of the cross section of the specimens, the presence of micro-cracks invisible to the naked eye, the irregular position of the textile in the thickness and the localization of the first cracks with respect to the extensometer.

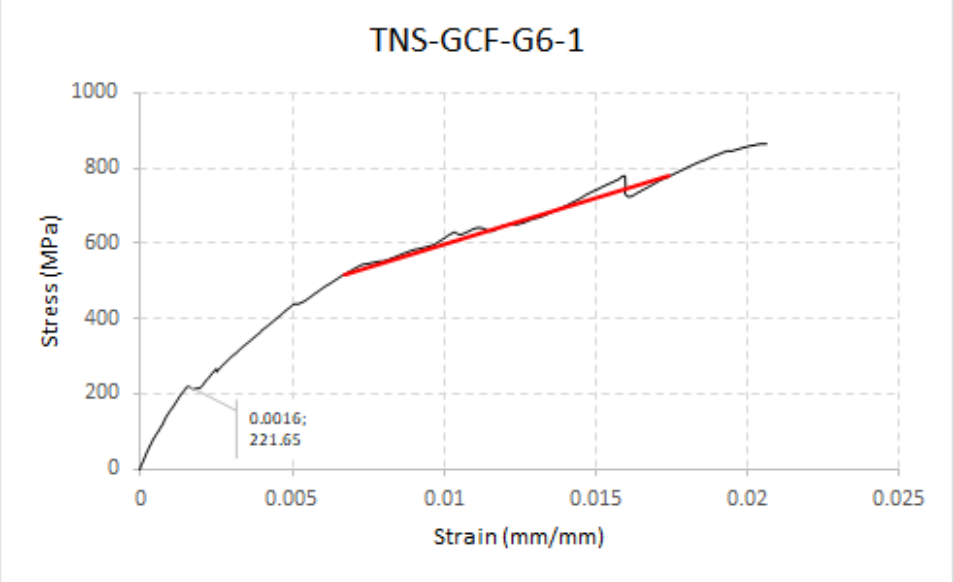

Figure 6.13 - Stress-Strain Curve for coupon GCF-G6-1

Table 6.12 - Tensile tests results on GCF-G6 series

Specimens ID	Yarns	Max Force	Ultimate Strength	Cracked Elastic Modulus	Ultimate Strain
	#	(kN)	(MPa)	(GPa)	(%)
TNS-GCF-G6-1	8	3.71	864.80	24.27	2.050
TNS-GCF-G6-2	8	3.46	767.10	37.37	1.506
TNS-GCF-G6-3	8	3.01	690.90	65.10	1.000
TNS-GCF-G6-4	8	3.12	724.86	38.82	1.521
TNS-GCF-G6-5	8	3.33	740.17	70.83	0.762
TNS-GCF-G6-6	8	4.45	1034.57	33.75	2.124
TNS-GCF-G6-7	8	5.79	1328.62	63.20	2.302
TNS-GCF-G6-8	8	4.46	1124.26	54.28	1.854
TNS-GCF-G6-9	8	3.91	870.91	66.70	1.386
TNS-GCF-G6-10	8	5.23	1201.06	92.21	1.246

Table 6.13 - Summary of tensile tests results on GCF-G6 series

	Thickness	Width	Area	Max Force	Ultimate Strength	Elastic Modulus	Ultimate Strain
	(mm)	(mm)	(mm^2)	(kN)	(MPa)	(GPa)	(%)
Average	10.19	51.53	524.74	4.05	934.72	54.65	1.575
Sn-1	0.63	0.60	31.48	0.92	223.70	20.84	0.503
CV((%)	6.2	1.2	6.0	22.8	23.9	38.1	31.934
Min	9.23	50.72	477.85	3.01	690.90	24.27	0.762
Max	11.09	52.66	573.78	5.79	1328.62	92.21	2.302

Table 6.13 also reports the coefficients of variation, *CoV*. It can be seen that the ultimate strength has a low scatter (*CoV = 24 %*) as well as the ultimate strain (*CoV = 32 %*), while modulus of elasticity has a high scatter (*CoV = 38 %*).

The Figures 6.14 show the cracking path developed by specimens of GCF-G6 series throughout the tensile tests. Two deep cracks occurred in the far ends of bonded length of metal tab. From there, the development of cracks continued throughout its length. The failure by rupture was not equal for all specimens. In fact, the collapse was due to the splitting of the matrix around the fiber cords in some cases. In other cases, it was achieved either for detachment of the tab from the coupon or the slippage of fibers.

Figure 6.14 - Representative failure mode of coupons GCF-G6 subject to tensile test

6.5.5. GCF-G12 Series

A series of ten tensile tests made with steel fabric *G12* and mortar *GCF* was tested. Figure 6.15 shows the stress-strain behavior of a specimen. Similar trend and consideration can be extended to all others tested specimens. The results of all coupons are reported in Table 6.14, while Table 6.15 lists the average values. The ultimate strength was calculated dividing the maximum force by the section of the coupon. It varies in a range between *472.15* and *710.90 MPa*. The average value is *582.78 MPa* and it is very lower than nominal maximum tensile strength of the fabric (> 3000 MPa). The average elastic modulus (*36.84 GPa*) is lower than elastic modulus of the dry steel textile (> 190 GPa). The ultimate strain varies in a range

between *0.843* and *1.551 %*. The average value is *1.197 %* and it is lower than the deformation at rupture of the fabric (> 2 %). The experimental results show a quite large variability both for the elastic modulus and the deformations. This variability could be caused by several factors: the irregularities of the cross section of the specimens, the presence of micro-cracks invisible to the naked eye, the irregular position of the textile in the thickness and the localization of the first cracks with respect to the extensometer.

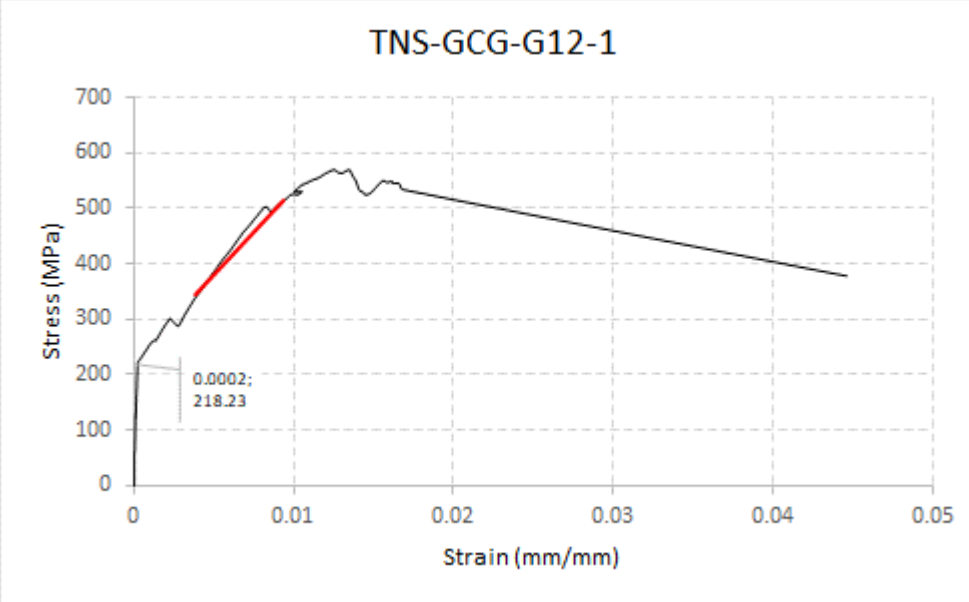

Figure 6.15 - Stress-Strain Curve for coupon GCF-G12-1

Table 6.14 - Tensile tests results on GCF-G12 series

Specimens ID	Yarns	Max Force	Ultimate Strength	Cracked Elastic Modulus	Ultimate Strain
	#	(kN)	(MPa)	(GPa)	(%)
TNS-GCF-G12-1	17	5.55	571.85	31.50	1.345
TNS-GCF-G12-2	17	4.51	472.15	28.55	1.040
TNS-GCF-G12-3	17	5.66	480.98	22.85	1.037
TNS-GCF-G12-4	17	5.66	594.28	36.38	1.398
TNS-GCF-G12-5	17	5.14	530.51	36.35	0.843
TNS-GCF-G12-6	16	6.01	710.90	45.62	1.296
TNS-GCF-G12-7	16	4.26	515.23	52.58	1.004
TNS-GCF-G12-8	16	5.31	616.76	33.83	1.085
TNS-GCF-G12-9	16	6.08	647.53	36.49	1.551
TNS-GCF-G12-10	12	4.44	687.61	44	1.371

Table 6.15 – Summary of tensile tests results on GCF-G12 series

	Thickness	Width	Area	Max Force	Ultimate Strength	Elastic Modulus	Ultimate Strain
	(mm)	(mm)	(mm^2)	(kN)	(MPa)	(GPa)	(%)
Average	10.1	53.6	543.5	5.26	582.78	36.84	1.197
Sn-1	0.6	1.2	27.9	0.66	83.60	8.71	0.224
CV((%)	6	2	5	12.50	14.34	23.63	18.747
Min	9.6	52.0	516.3	4.26	472.15	22.85	0.843
Max	11.5	55.9	612.1	6.08	710.90	52.58	1.551

Table 6.15 also reports the coefficients of variation, *CoV*. It can be seen that the ultimate strength has a low scatter (*CoV = 14 %*) as well as modulus of elasticity (*CoV = 24 %*) and ultimate strain (*CoV = 19%*).

The Figures 6.16 show the cracking path developed by the specimens of GCF-G12 series throughout the tensile tests. A series of cracks occurred in the center area of the specimen that was monitored by the extensometer. Others took place in the end of bonded length of metal plate. From there, the development of crack continued throughout its length. Finally, the failure by rupture was due to the splitting of the matrix around the fiber cords. The reason was that the mortar is not able to embed easily in the fabric, because the textile was characterized by high mass density (1200 g/m^2). The failure by rupture was not equal for all specimens. In fact, the collapse was due either to the splitting of the matrix around the fiber cords with consequent slippage of fibers or for enlargement of cracks that caused breakage of the specimen into several pieces.

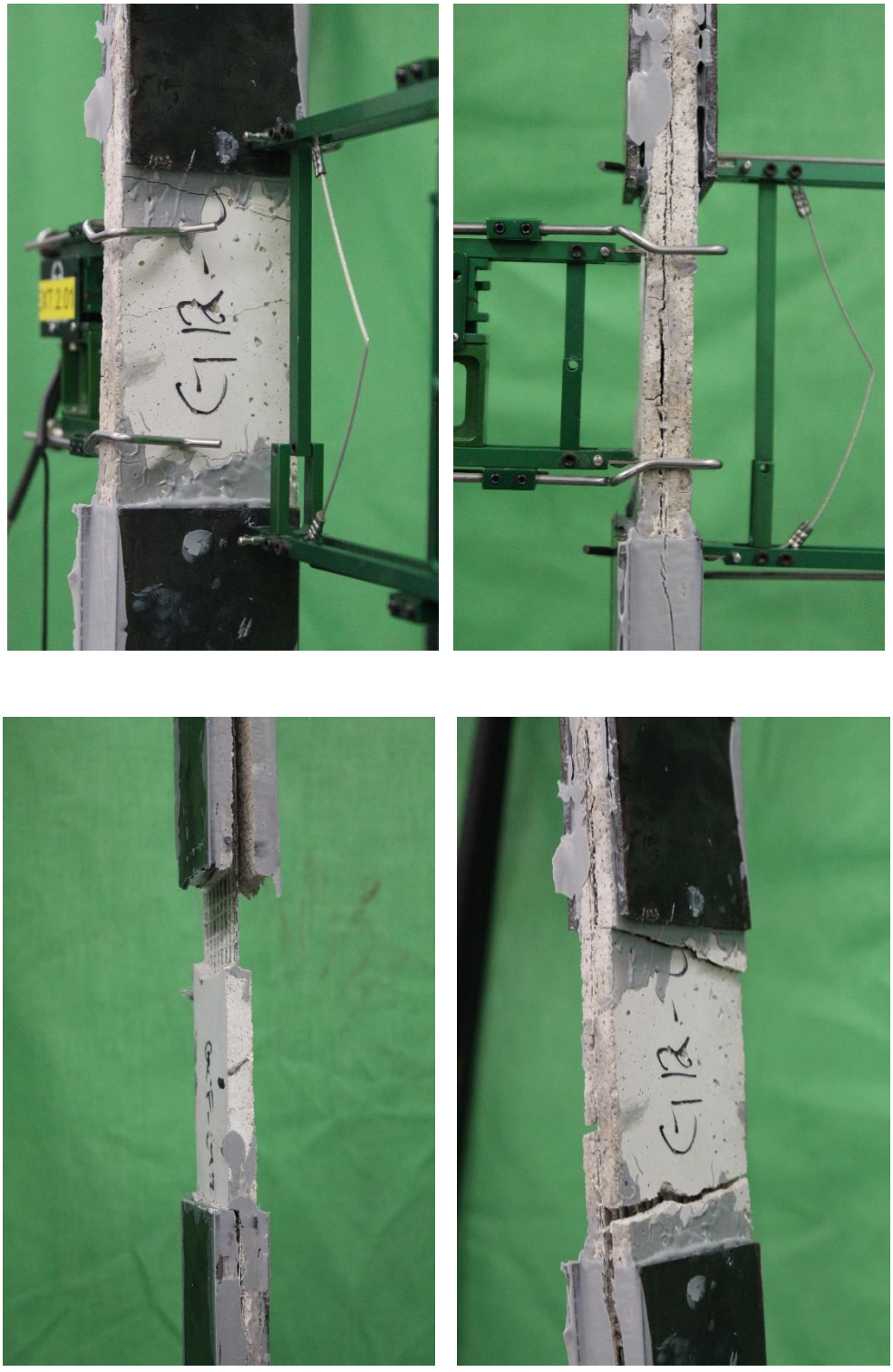

Figure 6.16 - Representative failure mode of coupons GCF-G12 subject to tensile test

Chapter 7
Interlaminar Shear Tests

7.1. Introduction

The search for a practicable test method by which interlaminar shear (ISS) strength can be reliably measured, has eluded the composites community for many years. Currently, the most widely practiced ISS strength standard is the three-point bend test ASTM D2344, also known as short beam shear (SBS). Many are the problems associated with such test method, such as the great deal of compressive stresses under the roller, the dependence of the "apparent" ISS strength on the support span to laminate thickness ratio (s/t), and the non-pure shear state of stress, which affect the true measurement of the desired mechanical property. On the other hand, the great advantage of this test method is its simplicity, and the ability of being performed rapidly and in much more reliable manner than other ISS strength test methods (such as Iosipescu and Double-notched tension), which involve complex fixtures or extensive machining.

Interlaminar properties of composites are important to be considered for a complete characterization of the material, because delamination is one of the major damage modes in laminated composite materials. In fact, interlaminar shear stresses are the source of failure, unique characteristic of composite structure. The presence of interlaminar shear stress in the laminated composite leads to delamination. Interlaminar shear stress arises due to various reasons. One is material property between layers. All layers may have different properties depending upon the selection of fibers in lamina as well as its orientation. Interlaminar shear stress is the out-of-plane stress σ_z, τ_{xz}, and τ_{yz} defined at the interface between layers in a laminated composite material. The interlaminar shear stresses are important because they have a marked effect on the failure strength of the composite laminate tending to shear apart the interface in the corresponding directions.

It should be noted that this test is related to the interlaminar shear strength characterization of FRP. FRCM interlaminar behavior cannot be compared to that of FRP, because of the presence of the inorganic matrix that cannot guarantee the

same bond properties at the interface between fabric and mortar. Few studies were performed on FRCM interlaminar properties, between these Arboleda et al. (2013) and Montesi (2015) [37, 38].
The short beam shear test (ASTM D2344) was recognized as the most suitable way to examine the interlaminar shear behavior of FRCM composites.

7.2. Specimen Preparation and Test Set-Up

7.2.1. Specimen Geometry and Preparation

In order to investigate the mechanical behavior of SRG systems, interlaminar shear tests were carried out for systems *"GCF-G6"*, *"GCF-G12"* and *"GLT-G12"*.
Specimens were machined from 330 x 508 mm panels with a diamond blade saw later a curing of 28 days in humidity chamber. Short beams of material, approximately 25 mm in width and 10 mm in thickness, were cut from the plate boundary in order to minimize the influence of manufacturing related defects on test results. Each specimens were characterized by two layers of fiber mesh embedded in two layers of 4 mm cementitious mortar. Another thin layer of mortar also divided the fibers.
Short beams were labelled according to the notation XXX-YYY-ZZ-N, in which XXX identifies the test type, YYY and ZZ are the matrix and the textile, respectively; finally, N is the progressive number of each specimen.

7.2.2. Test Set-Up

The test method required by AC434 to determine the interlaminar properties of FRCM/SRG refers to the ASTM Standard D2344 *"Standard Test Method for Short-Beam Strength of Polymer Matrix Composite Materials and Their Laminates"*. This test is a three-point bending test on short beam, where a transverse shear is induced in specimens with low support to specimen thickness ratios. This test method determines the apparent interlaminar shear strength of high-modulus fiber-reinforced composite materials, and it is commonly used to determine the short beam strength of FRP composites. The standard recommends the following geometries:

Specimen length = thickness × 6

Specimen width = thickness × 2.0

Test configuration according to the ASTM Standard is shown in Figures 7.1 and 7.2. The upper cylinder, through which the load is applied, is 6.00 mm in diameter, and the two supports cylinders on the bottom are 3.00 mm in diameter.

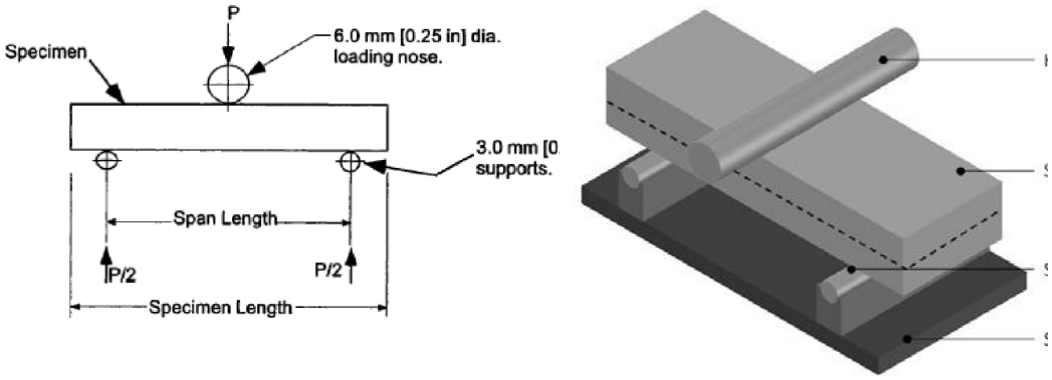

Figure 7.1 - Interlaminar test setup [ASTM D2344]

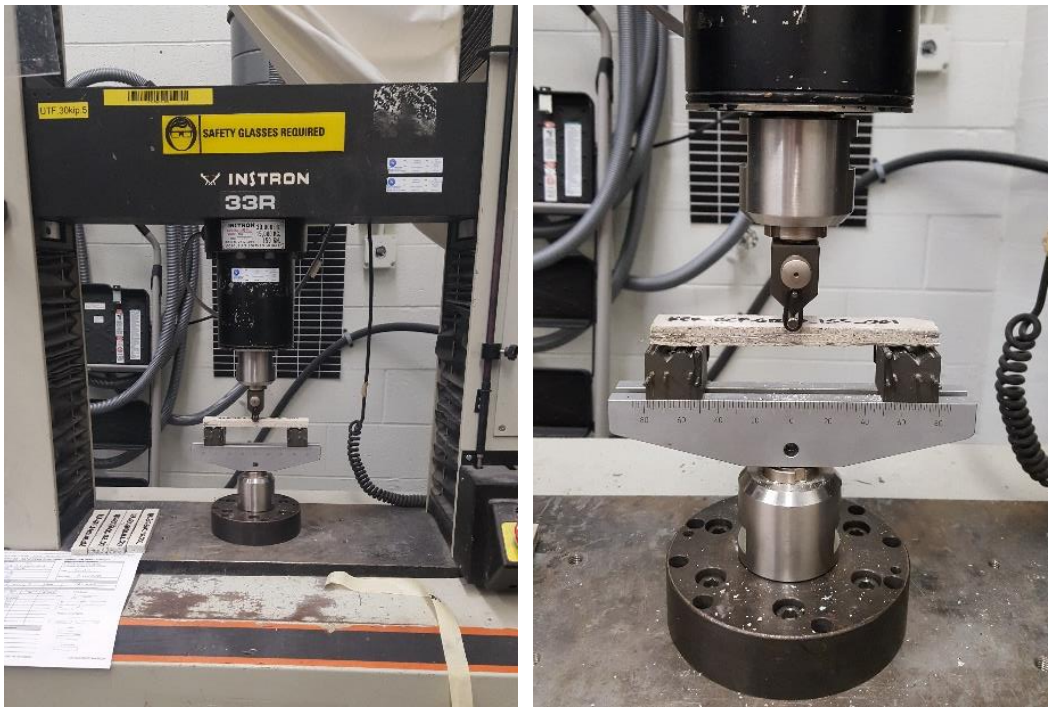

Figure 7.2 - Interlaminar test set-up

Tests were performed under load control at a constant rate of crosshead movement of 1.0 mm/min until either of the following occurred:

1. A load drop-off of 30 %;
2. Two-piece specimen failure;
3. The head travel exceeds the specimen nominal thickness.

Typical failure modes, that can be identified visually, are shown in Figure 7.3. However, these may be preceded by less obvious local damage modes such as transply cracking.

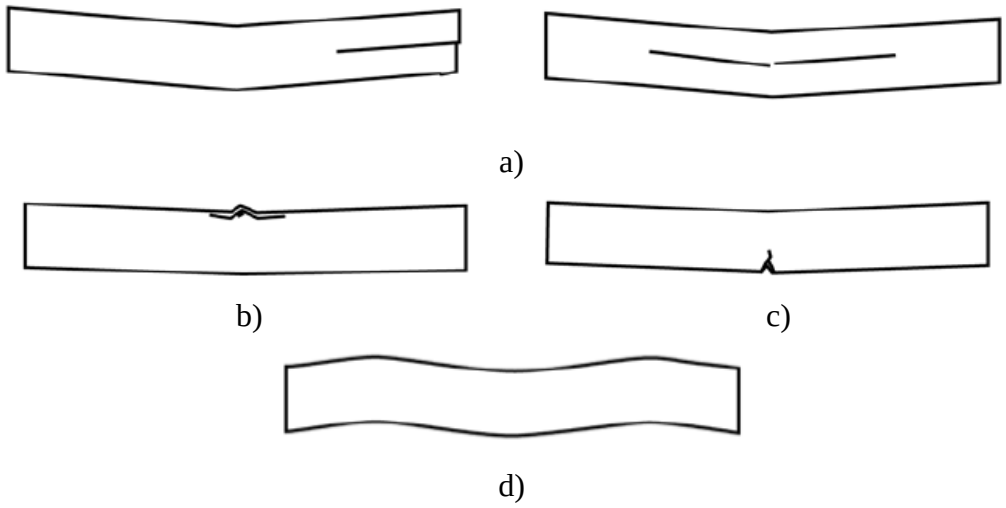

Figure 7.3 - Typical Failure Modes in the Short Beam Test: a) Interlaminar Shear, b) Flexure in compression, c) Flexure in tension, d) Inelastic Deformation [ASTM D2344]

7.3. Short-Beam Strength

In general, the strength of short beam is computed dividing the ultimate load registered by the testing machine by the area on which the load is applied multiplied by coefficient 0.75:

$$f_{sbs} = 0.75 \times \frac{P_{max}}{t \cdot w} \tag{7.1}$$

where:

f_{sbs} is short-beam strength, MPa;

P_{max} is maximum load observed during the test, N;

w is measured specimen width, mm;

t is measured specimen thickness, mm.

7.4. Results

A total of five tests per product under control ambient conditions are reported. Tables contain the tabulated summary for the products under evaluation, including the measured thickness (*t*) and width (*w*) of each specimen, the peak load recorded during test (P_{max}), the ultimate strength (f_{sbs}) computed as per ASTM D2344 (see Eq. 3). Average, standard deviation and coefficient of variance values are also reported, based on the complete set of specimens under evaluation for each product.

7.4.1. GCF-G6 series

Experimental results of the GCF-G6 specimens are summarized in Table 7.1. The primary mode of failure was by matrix cracking in the tension side. In fact, in all coupons, onset of damage was characterized by a single crack that propagated from the bottom of beam in the central region (Fig. 7.4). It can be observed that the specimens GCF-G6-2 and GCF-G6-3 also present a single crack in the top of beam, caused by the great deal of compressive stresses present underneath the loading roller. The specimens present similar results both in terms of load and strength, excepted the specimen GCF-G6-2. In this case, the load is lower of series, because the compressive stresses due to loading roller damaged the short beam deeply.

Table 7.1 - Results of the GCF-G6 specimens

Specimen ID	**t (mm)**	**w (mm)**	**P_{max} (N)**	**f_b (Mpa)**	**Failure Mode**
ISS-GCF-G6-1	11.02	25.54	234.87	0.63	Tension
ISS-GCF-G6-2	12.73	26.25	179.71	0.40	Tension
ISS-GCF-G6-3	11.07	23.98	212.18	0.60	Tension
ISS-GCF-G6-4	11.21	24.94	267.78	0.72	Tension
ISS-GCF-G6-5	11.02	23.95	234.87	0.67	Tension
Average			225.88	0.60	
S.D.			32.55	0.12	
CoV			14.41	19.92	

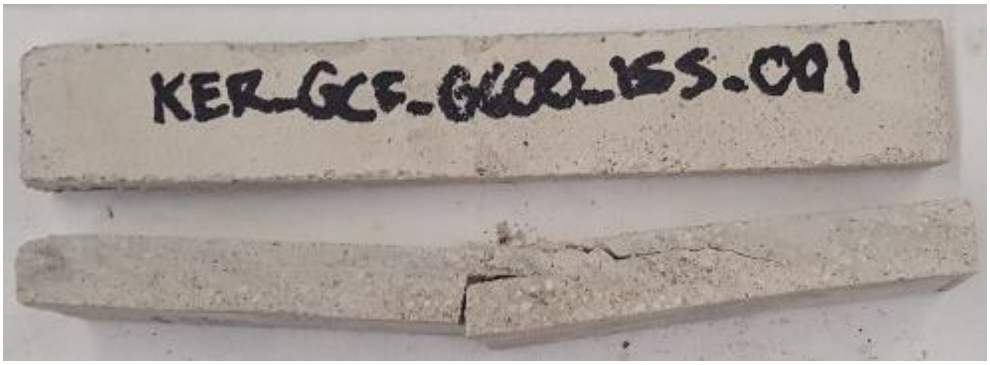

Figure 7.4 - Failure mode of the specimens GCF-G6-1

Figure 7.5 - Failure modes of the GCF-G6 specimens

7.4.2. GCF-G12 Series

Table 7.2 summarizes the experimental results of the GCF-G12 specimens. The primary mode of failure was interlaminar shear. In fact, Figure 7.6 shows

interlaminar shear failure of specimen GCF-G12-2. It can be observed the development of two cracks at fibes-matrix interface that propagate from the center of the specimen to the edge. The reason is because the G12 fabric has high mass density and does not permit the complete penetration in the matrix. In all coupons, a single crack with different width is presented in the top of beam. It is caused by the great deal of compressive stresses present underneath the loading roller. Indeed, this test methodology is not able to introduce a pure shear state of stress. The bending moment contributes in the deformation of the coupon, therefore introduces undesired stress components inhibiting the true measurement of the desired mechanical property. In regard to loads recorded during the tests, similar values are achieved (Table 7.2).

Table 7.2 - Results of the GCF-G12 specimens

Specimen ID	**t (mm)**	**w (mm)**	**P_{max} (N)**	**f_b (Mpa)**	**Failure Mode**
ISS-GCF-G12-1	11.95	25.57	350.08	0.86	Tension
ISS-GCF-G12-2	10.15	24.47	301.59	0.91	Interlaminar Shear
ISS-GCF-G12-3	10.68	24.37	342.96	0.99	Interlaminar Shear
ISS-GCF-G12-4	11.30	25.21	363.42	0.96	Interlaminar Shear
ISS-GCF-G12-5	10.63	24.07	321.16	0.94	Interlaminar Shear
Average			335.84	0.93	
S.D.			24.51	0.05	
CoV			7.30	5.25	

Figure 7.6 - Failure mode of the specimens GCF-G12-2

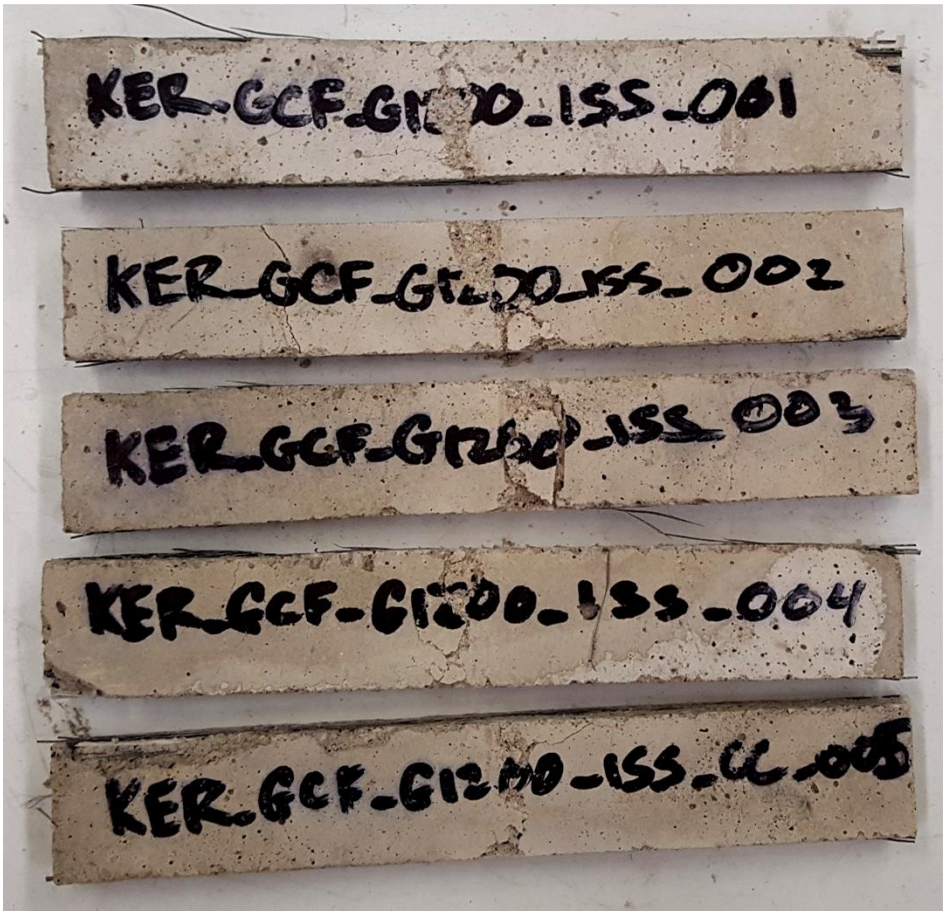

Figure 7.7 - Failure modes of the GCF-G12 specimens

7.4.3. GLT-G12 Series

Experimental results of the GLT-G12 specimens are summarized in Table 7.3. The primary mode of failure was by matrix cracking in the tension side. In fact, in all coupons, onset of damage was characterized by a single crack that propagated from the bottom of beam in the central region (Fig. 7.8). It can be observed that the specimens GLT-G12-1 and GLT-G12-3 also present a single crack in the top of beam, caused by the great deal of compressive stresses present underneath the loading roller (Fig. 7.9). In terms of resutls, loads achieve different values (Table 7.3). If on the one hand, the values of specimens GLT-G12-1, GLT-G12-2 and GLT-G12-5 are similar, on the other hand they are very different from the load results of specimens GLT-G12-3 and GLT-G12-4, so to be omited in the calculation of CoV. In the case of specimens GLT-G12-1, GLT-G12-2 and GLT-G12-5, the strengths are about half of values of GCF-G12 series. The reason is because the GLT mortar used as matrix has higher compressive strength than the GCF mortar.

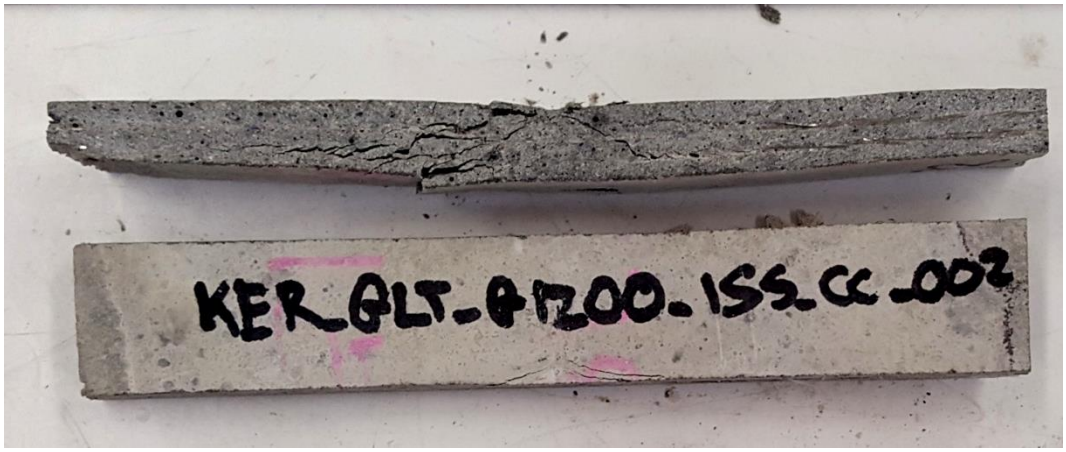

Figure 7.8 - Failure mode of the specimen GLT-G12-2

Figure 7.9 - Failure modes of the GLT-G12 specimens

Table 7.3 - Results of the GLT-G12 specimens

Specimen ID	**t (mm)**	**w (mm)**	**P_{max} (N)**	**f_b (Mpa)**	**Failure Mode**
ISS-GLT-G12-1	11.81	25.49	799.35	1.99	Tension
ISS-GLT-G12-2	11.47	25.46	663.23	1.70	Tension
ISS-GLT-G12-3	10.76	25.93	1001.74	2.69	Tension
ISS-GLT-G12-4	11.02	24.56	1349.59	3.74	Tension
ISS-GLT-G12-5	11.58	25.20	531.12	1.36	Tension
Average			664.56	1.69	
S.D.			134.12	0.31	
CoV			20.18	18.59	

Chapter 8
Pull-off Tests

8.1. Introduction

The scope of pull-off test is to determine one or more of the following:

1. The near-surface tensile strength of the substrate as an indicator of the adequacy of surface preparation before application of a repair or overlay material;
2. The bond strength of a repair or an overlay material to the substrate;
3. The tensile strength of a repair or overlay material, or an adhesive used in repairs, after the material has been applied to a surface.

8.2. Materials

The behavior of the SRG system applied on several substrates was investigated to analyze both the adherence between the reinforced system and the support and between the dry textile and the cementitious mortar. The experimental campaign was developed on different composite materials and substrates. The former were the same used in the tensile tests (see Chapter 6). The later were clay bricks (*"Y"*), concrete blocks (*"C"*) and cementitious masonry units (*"U"*).

The *"GCF-G6"* and *"GCF-G12"* systems were applied both on clay bricks and on cementitious masonry units; the *"GLT-G6"* and *"GLT-G12"* systems were applied on concrete blocks; while the *"GLT-G6"* system was also applied on cementitious masonry units.

Specimens were labelled according to the notation XXX-YYY-ZZ-N, in which XXX identifies the test type and the substrate, YYY and ZZ are the matrix and the textile, respectively; while, N is the progressive number of each specimen. Therefore, the corresponding systems were denominated *"BTY-GCF-G6", "BTY-GCF-G12", "BTU-GCF-G6", "BTU-GCF-G12", "BTC-GLT-G6", "BTC-GLT-G12"* and *"BTU-GLT-G6"*.

8.2.1. Textile Reinforcements

As previously said, the fabrics *"G6"* and *"G12"* as well as the matrices *"GCF" and "GLT"* have been described in the Chapter 6. The main mechanical properties of used steel fabrics (Fig. 8.1) and mortar matrices (Fig. 8.2) provided by manufacturer are reported in Tables 8.1 and 8.2.

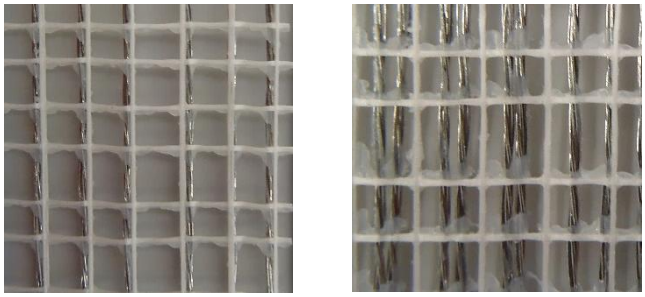

a) b)

Figure 8.1 - Textile reinforcements: a) Steel Sheet G6; b) Steel Sheet G12

Table 8.1 - Mechanical properties of steel fabrics provided by manufacturer

Steel Fabric	Cords/cm	Mass density (g/m2)	Equivalent thickness (mm)	Tensile Strength (MPa)	Elastic Modulus (GPa)	Deformation at rupture (%)
GeoSteel G1200	3.19	1200	0.169	> 3000	> 190	> 2
GeoSteel G600	1.57	670	0.084	> 2800	> 190	> 1.5

a) b)

Figure 8.2 - Mortar Matrices: a) Mineral Mortar (GeoLite);
b) Natural Hydraulic Lime Mortar (GeoCalce Fino) [Kerakoll catalogue]

Table 8.2 - Mechanical properties of mortar matrices provided by manufacturer

Matrix	f_{cm} (MPa)	E_{cm} (GPa)	f_{tm} (MPa)	D (mm)
Mineral Mortar	> 50 (28 gg)	22	> 8 (28 gg)	0 - 0.5
Natural Hydraulic Lime Mortar	> 15 (28 gg)	9	> 5 (28 gg)	0 - 1.4

8.3. Specimen Preparation and Test Set-Up

8.3.1. Specimen Geometry and Preparation

In order to investigate the mechanical behavior of SRG systems, twenty-eight pull-off tests were carried out on several series of specimens. The "GCF-G6" and "GCF-G12" systems were applied both on clay bricks and on cementitious masonry units; the "GLT-G6" and "GLT-G12" systems were applied on concrete block; while the "GLT-G6" system was also applied on cementitious masonry units. Geometry of the substrates is reported in Table 8.3.

Table 8.3 -Geometry of the substrates

Material	Label	B (mm)	H (mm)	L (mm)
Concrete block	C	102	102	356
Concrete masonry unit	U	191	89	394
Clay brick	Y	178	191	89

The SRG reinforcements were applied onto the substrate, previously cleaned, for a minimum of 63 mm thick (Fig. 8.3). After that, specimens were kept in standard laboratory conditions.

a)

b)

c) d)

Figure 8.3 - Specimens preparation: a) Cleaning of specimens by any debris, b) Reinforcement applied on clay bricks, c) Reinforced concrete blocks and d) Reinforced concrete masonry units

Later 28 days of curing time, hexagonal cuts, perpendicular to the substrate of the specimen, were performed in order to circumscribe the disk used for testing according to the general procedures of ASTM C1583/C1583M-13.

The procedures of cut were carried out by a hand grinder to a depth of 12 mm into the substrate. The center-to-center distance of adjacent test specimens were of two disk diameters. The distance from the center of a test specimen and a free edge of the test object were of one disk diameter. After the drilling operations, the surface were cleaned by any debris and dried. Then, the steel disks were attached by epoxy to the SRG surface as a means to pull off the circular area (Fig. 8.4). The adhesive was left to cure for 24 hours before performing the pull off test. Steel disks with 50 mm diameter and 25 mm thick were used.

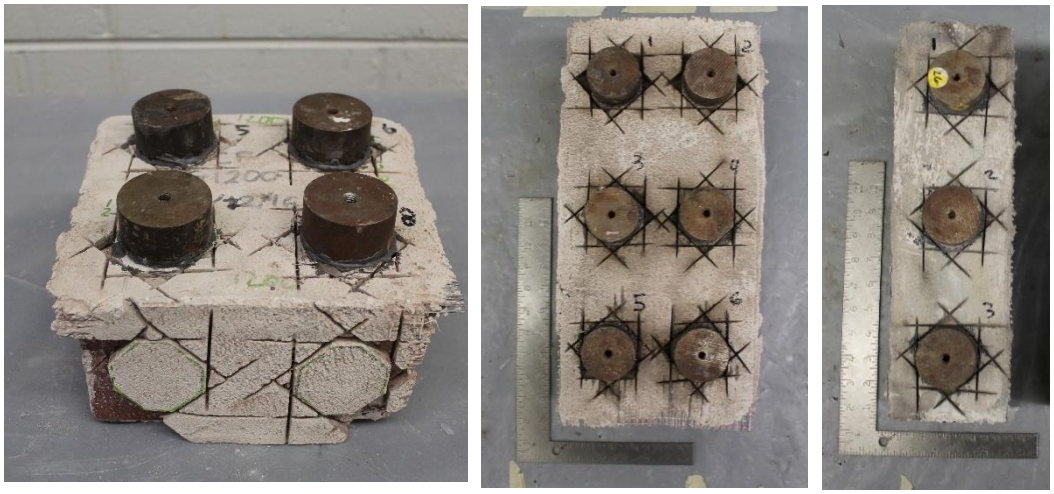

a) b) c)

Figure 8.4 - Steel disks attached on a) clay brick, b) concrete masonry unit and c) concrete block

8.3.2. Test Set-Up

Uniaxial tensile load was applied perpendicular to the test surface using a pull-off test machine. Tensile loading device was connected to the steel disk using a coupling fixture. This device is designed to bear the tensile load capacity without yielding, and to transmit the tensile force parallel to and coincident with the axis of the cylindrical test specimen without imparting torsion or bending to the test specimen. Figure 8.5 shows the test set-up.

Figure 8.5 - Pull-off test set-up

Tests were performed under load control at a constant rate so that the tensile stress increased at a rate of 35 ± 15 kPa/s. It is applied to the steel disk until failure occurs. The possible failure modes are reported in Figure 8.6. The failure mode can occur:

A) In the substrate;

B) At the FRCM-substrate interface;

C) At the interface between mortar and fabric;

D) At the interface between mortar and steel disk.

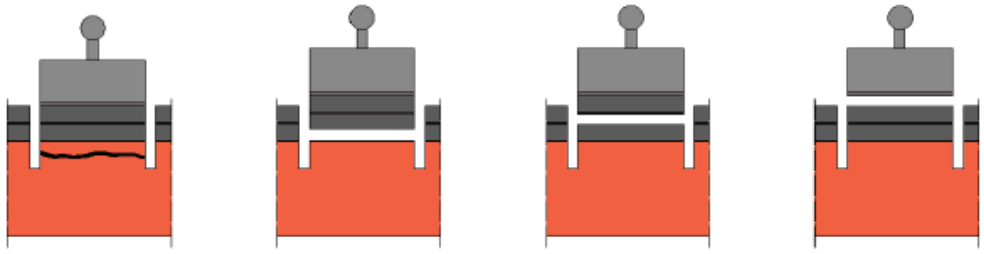

A) B) C) D)

Figure 8.6 - Possible failure modes of pull off test: A) Failure in the substrate, B) Bond failure at the FRCM-substrate interface, C) Failure at the mortar-fabric interface, D) Bond failure at the epoxy-FRCM [Donnini, 2016]

8.4. Bond Strength

In general, the ultimate bond strength is computed dividing the ultimate load registered by the testing machine by the area on which the load is applied:

$$f_b = \frac{P_{max}}{A} \tag{8.1}$$

However, this can be correct for a continuum system like the FRP, but in the case of FRCM or SRG, if the failure occurs at the fabric-mortar interface, this procedure is no longer correct. Therefore, when the failure occurs on the interface between the first and the second layer of mortar, where the fabric is embedded, the failure itself occurs because the mortar that connects the two layers of matrix (through the fabric) breaks. In this case, the loaded surface is not the entire area but only the net area, which is the entire area minus the area covered by the fabric. Therefore, the net area has to be used for the stress computation and so:

$$f_b = \frac{P_{max}}{A_n} \tag{8.2}$$

The last version of AC434 considers two different limits. When the mode of failure is cohesive (i.e., failure occurs in the substrate material) or adhesive (i.e., failure occurs at the interface FRCM/SRG reinforcement and substrate material), bond strength shall be at least 1.38 MPa. When failure is at the interface between the

structural reinforcement grid and matrix, strength shall be at least 2.76 MPa, because it is computed on the net matrix area.

8.5. Results

8.5.1. BTY-GCF-G6 Series

Figures 8.7 and Table 8.4 show the failure modes observed in the BTY-GCF-G6 series.

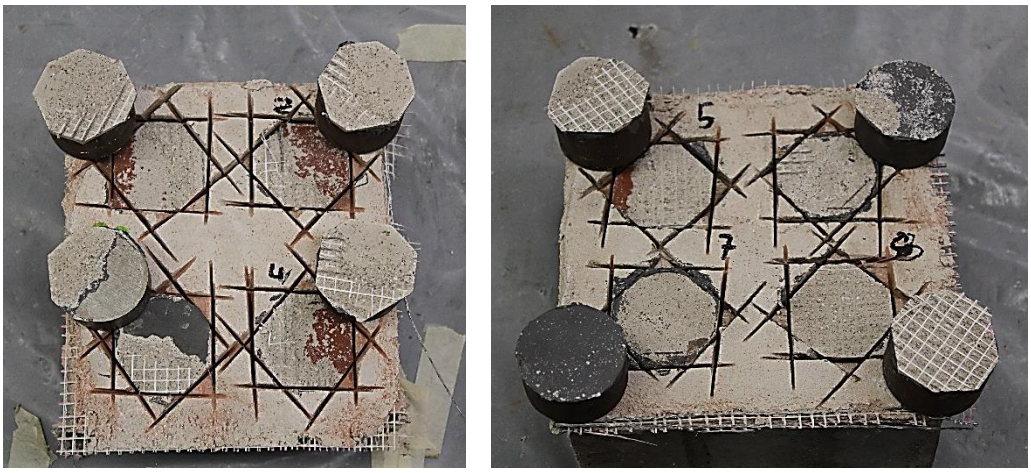

Figure 8.7 - Failure modes of the BTY-GCF-G6 series

Table 8.4 - Failure modes of the BTY-GCF-G6 series

Specimen ID	Failure Mode
BTY-GCF-G6-1	Failure at the mortar-fabric interface + FCRM-substrate interface
BTY-GCF-G6-2	Failure at the mortar-fabric interface + FCRM-substrate interface
BTY-GCF-G6-3	Failure at the mortar-fabric interface + mortar-steel disk interface
BTY-GCF-G6-4	Failure at the mortar-fabric interface + FCRM-substrate interface
BTY-GCF-G6-5	Failure at the mortar-fabric interface
BTY-GCF-G6-6	Failure at the interface between mortar and steel disk
BTY-GCF-G6-7	Failure at the interface between mortar and steel disk
BTY-GCF-G6-8	Failure at the mortar-fabric interface

As expected, the predominant failure mode was at the interface between fabric and mortar. The maximum strengths did not reach the minimum values established in AC434, due to the low mechanical properties of the mortar used as matrix (Table 8.5). However, this test proved not to be very representative of the real bond properties of the SRG/FRCM system when applied as external reinforcement, resulting more suitable to verify the bond between the mortar and the substrate rather than between fabric and mortar.

Table 8.5 - Pull-off tests results on BTY-GCF-G6 specimens

Specimen ID	**P_{max}**	**A**	**f_b**	**ext**	**Failure Mode**
	(N)	(mm^2)	(MPa)	mm	
BTY-GCF-G6-1	2146.75	1934.60	1.11	0.21	C + B
BTY-GCF-G6-2	2775.43	1934.60	1.43	0.30	C + B
BTY-GCF-G6-3	1816.12	1934.60	0.94	0.12	C + D
BTY-GCF-G6-4	1647.64	1934.60	0.85	0.16	C + B
BTY-GCF-G6-5	1897.61	1934.60	0.98	0.17	C
BTY-GCF-G6-6	2691.81	1962.50	1.37	0.26	D
BTY-GCF-G6-7	2032.40	1962.50	1.04	0.18	D
BTY-GCF-G6-8	2995.36	1934.60	1.55	0.30	C
Average	2250.39	1941.57	1.16	0.21	C
S.D.	501.44	12.92	0.26	0.07	
CoV	22.28	0.67	22.24	31.45	

8.5.2. BTY-GCF-G12 Series

Figures 8.8 and Table 8.6 show the failure modes observed in the BTY-GCF-G12 series.

Figure 8.8 -Failure modes of the BTY-GCF-G12 series

Table 8.6 - Failure modes of the BTY-GCF-G12 series

Specimen ID	Failure Mode
BTY-GCF-G12-1	Failure at the FRCM-substrate interface
BTY-GCF-G12-2	Failure at the mortar-fabric interface + FCRM-substrate interface
BTY-GCF-G12-3	Failure at the mortar-fabric interface +
BTY-GCF-G12-4	Failure at the FRCM-substrate interface
BTY-GCF-G12-5	Failure at the mortar-fabric interface
BTY-GCF-G12-6	Failure at the FRCM-substrate interface
BTY-GCF-G12-7	Failure at the mortar-fabric interface +

BTY-GCF-G12-8	Failure at the FRCM-substrate interface
BTY-GCF-G12-9	Failure at the mortar-fabric interface + FCRM-substrate interface
BTY-GCF-G12-10	Failure at the mortar-fabric interface + FCRM-substrate interface
BTY-GCF-G12-11	Failure at the mortar-fabric interface
BTY-GCF-G12-12	Failure at the FRCM-substrate interface

The predominant failure modes were at the interface between fabric and mortar and between reinforcement and substrate. The reason is due to both the low mechanical properties of the mortar used as matrix and the reduced area net. In fact, the steel fabric G12 has high mass density and so the matrix did not well embed between the cords. Consequently, the maximum strengths did not reach the minimum values established in AC434 (Table 8.7).

Table 8.7 - Pull-off tests results on BTY-GCF-G12 specimens

Specimen ID	**P_{max}**	**A**	**f_b**	**ext**	**Failure Mode**
	(N)	(mm^2)	(MPa)	mm	
BTY-GCF-G12-1	1714.70	1962.60	0.87	0.62	B
BTY-GCF-G12-2	2740.09	1878.64	1.46	1.21	C + B
BTY-GCF-G12-3	2738.42	1878.64	1.46	1.48	C + D
BTY-GCF-G12-4	489.92	1962.60	0.25	0.34	B
BTY-GCF-G12-5	1745.55	1878.64	0.93	0.78	C
BTY-GCF-G12-6	2428.77	1962.60	1.24	0.87	B
BTY-GCF-G12-7	2265.19	1878.64	1.21	2.61	C + D
BTY-GCF-G12-8	2569.03	1962.60	1.31	1.02	B
BTY-GCF-G12-9	2389.44	1878.64	1.27	0.85	C + B
BTY-GCF-G12-10	2221.13	1878.64	1.18	0.71	C + B
BTY-GCF-G12-11	2567.20	1878.64	1.37	1.65	C + B
BTY-GCF-G12-12	1276.78	1962.60	0.65	0.42	B
Average	2095.52	1913.58	1.10	1.05	C + B
S.D.	676.44	43.18	0.36	0.63	
CoV	32.28	2.26	32.95	59.95	

8.5.3. BTC-GLT-G6 Series

Figures 8.9 and Table 8.8 show the failure modes observed in the BTC-GLT-G6 series.

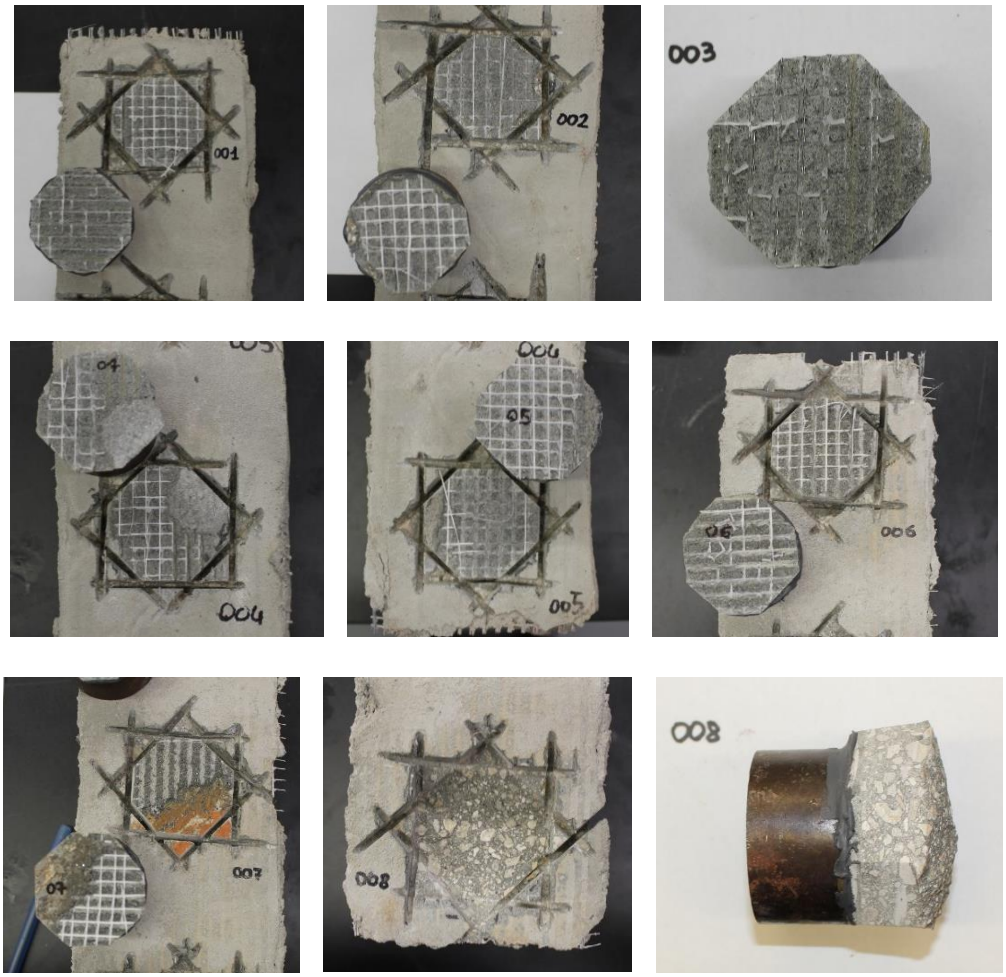

Figure 8.9 - Failure modes of the BTC-GLT-G6 series

Table 8.8 - Failure modes of the BTC-GLT-G6 series

Specimen ID	Failure Mode
BTC-GLT-G6-1	Failure at the mortar-fabric interface
BTC-GLT-G6-2	Failure at the mortar-fabric interface
BTC-GLT-G6-3	Failure at the mortar-fabric interface
BTC-GLT-G6-4	Failure at the mortar-fabric interface + FCRM-substrate interface

BTC-GLT-G6-5	Failure at the mortar-fabric interface
BTC-GLT-G6-6	Failure at the mortar-fabric interface
BTC-GLT-G6-7	Failure at the mortar-fabric interface + FCRM-substrate interface
BTC-GLT-G6-8	Failure in the substrate

As expected, the predominant failure mode was at the interface between fabric and mortar, even if the specimen BTC-GLT-G6-8 shown untypical failure in the substrate. A possible reason is that the adhesive ran down the side of the test specimen into the annular cut, creating a very integral grab. In almost all cases, the maximum strengths reach the limit values established in AC434 (Table 8.9). The reason is due to both the high mechanical properties of the mortar used as matrix and its ease to penetrate between the cords, because the space is 0.6 mm.

Table 8.9 – Pull-off tests results on BTC-GLT-G6 specimens

Specimen ID	**P_{max}**	**A**	**f_b**	**ext**	**Failure Mode**
	(N)	(mm^2)	(MPa)	(mm)	
BTC-GLT-G6-1	5832.00	1934.60	3.01	1.35	C
BTC-GLT-G6-2	5404.00	1934.60	2.79	1.13	C
BTC-GLT-G6-3	5423.00	1934.60	2.80	1.27	C
BTC-GLT-G6-4	4679.00	1934.60	2.42	1.03	C + B
BTC-GLT-G6-5	7975.00	1934.60	4.12	1.71	C
BTC-GLT-G6-6	8306.00	1934.60	4.29	1.69	C
BTC-GLT-G6-7	6772.00	1934.60	3.50	1.35	C + B
BTC-GLT-G6-8	6986.00	1934.60	3.61	2.27	A
Average	6422.13	1934.60	3.32	1.48	C
S.D.	1299.58	9.87	0.67	0.40	
CoV	20.24	0.51	20.19	27.06	

8.5.4. BTC-GLT-G12 Series

Figures 8.10 and Table 8.10 show the failure modes observed in the BTC-GLT-G12 series.

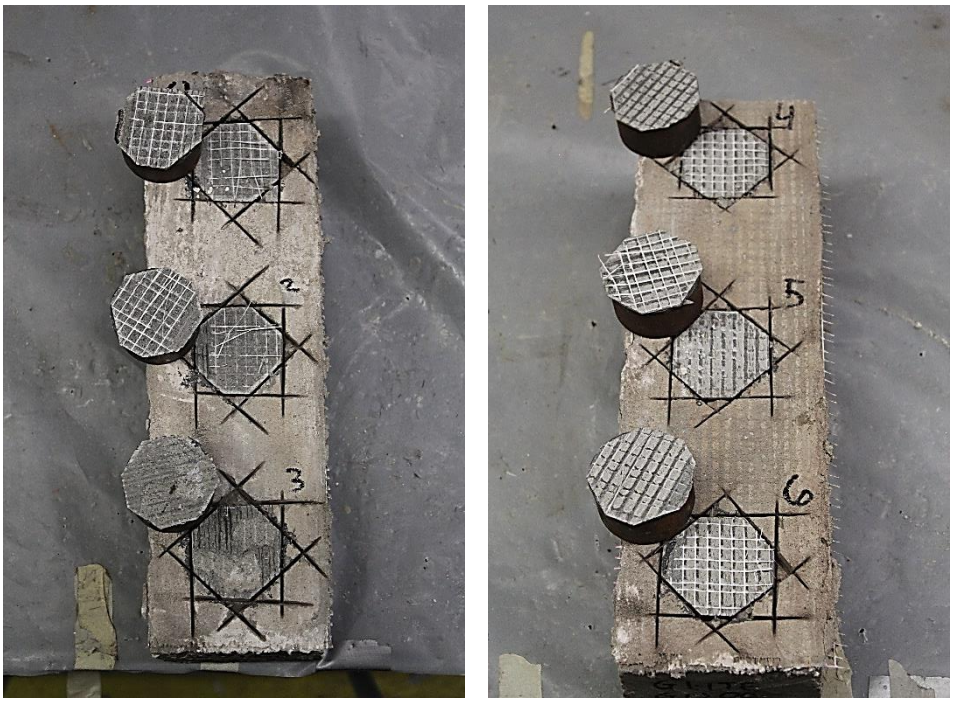

Figure 8.10 - Failure modes of the BTC-GLT-G12 series

Table 8.10 - Failure modes of the BTC-GLT-G12 series

Specimen ID	Failure Mode
BTC-GLT-G12-1	Failure at the mortar-fabric interface
BTC-GLT-G12-2	Failure at the mortar-fabric interface
BTC-GLT-G12-3	Failure at the mortar-fabric interface + FCRM-substrate interface
BTC-GLT-G12-4	Failure at the mortar-fabric interface
BTC-GLT-G12-5	Failure at the mortar-fabric interface
BTC-GLT-G12-6	Failure at the mortar-fabric interface

As expected, the predominant failure mode was at the interface between fabric and mortar. However, the maximum strengths did not reach the minimum values established in AC434 in every case as shown in Table 8.10. The reason is that the density of steel fabric G12 is higher than that of G6, so the mortar could not penetrate easily between the steel cords and consequently the bond at reinforcement-to-substrate interface decreased.

Table 8.11 -Pull-off tests results on BTC-GLT-G12 specimens

Specimen ID	P_{max}	A	f_b	ext	Failure Mode
	(N)	(mm^2)	(MPa)	(mm)	
BTC-GLT-G12-1	4595.68	1878.64	2.45	0.35	C
BTC-GLT-G12-2	5613.65	1878.64	2.99	0.44	C
BTC-GLT-G12-3	5159.63	1878.64	2.75	0.38	C + B
BTC-GLT-G12-4	3253.77	1878.64	1.73	0.25	C
BTC-GLT-G12-5	3487.70	1878.64	1.86	0.27	C
BTC-GLT-G12-6	3209.07	1878.64	1.71	0.29	C
Average	4219.92	1878.64	2.25	0.33	C
S.D.	1044.81	0.00	0.56	0.07	
CoV	24.76	0.00	24.76	22.32	

8.5.5. BTU-GCF-G6 Series

Figures 8.11 and Table 8.12 show the failure modes observed in the BTU-GCF-G6 series.

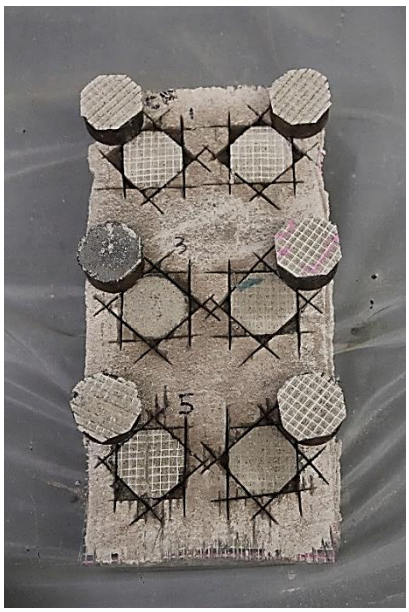

Figure 8.11 - Failure modes of the BTU-GCF-G6 series

Table 8.12 - Failure modes of the BTU-GCF-G6 series

Specimen ID	Failure Mode
BTC-GCF-G6-1	Failure at the mortar-fabric interface
BTC-GCF-G6-2	Failure at the mortar-fabric interface
BTC-GCF-G6-3	Failure at the interface between mortar and steel disk
BTC-GCF-G6-4	Failure at the mortar-fabric interface
BTC-GCF-G6-5	Failure at the mortar-fabric interface
BTC-GCF-G6-6	Failure at the mortar-fabric interface

As expected, the predominant failure mode was at the interface between fabric and mortar. However, the maximum strengths did not reach the minimum values established in AC434, due to the low mechanical properties of the mortar used as matrix (Table 8.13).

Table 8.13 - Pull-off tests results on BTU-GCF-G6 specimens

Specimen ID	**P_{max}**	**A**	**f_b**	**ext**	**Failure Mode**
	(N)	(mm^2)	(MPa)	mm	
BTU-GCF-G6-1	1640.46	1934.60	0.85	0.18	C
BTU-GCF-G6-2	1401.86	1934.60	0.72	0.17	C
BTU-GCF-G6-3	891.19	1962.50	0.45	0.16	D
BTU-GCF-G6-4	2257.84	1934.60	1.17	0.22	C
BTU-GCF-G6-5	1550.35	1934.60	0.80	0.26	C
BTU-GCF-G6-6	2076.55	1934.60	1.07	0.19	C
Average	1636.38	1939.25	0.84	0.20	C
S.D.	489.42	11.39	0.25	0.04	
CoV	29.91	0.59	30.18	19.10	

8.5.6. BTU-GCF-G12 Series

Table 8.14 shows pull-off tests results and the failure modes observed in the BTU-GCF-G12 series. As expected, the predominant failure mode was at the interface between fabric and mortar. However, the maximum strengths did not reach the

minimum values established in AC434. The reason is that the density of steel fabric G12 is higher than that of G6, so the mortar could not penetrate easily between the steel cords and consequently the bond at reinforcement-to-substrate interface decreased.

Table 8.14 - Pull-off tests results on BTU-GCF-G12 specimens

Specimen ID	**P_{max}**	**A**	**f_b**	**ext**	**Failure Mode**
	(N)	(mm^2)	(MPa)	(mm)	
BTU-GCF-G12-7	2238.02	1878.64	1.19	0.19	C
BTU-GCF-G12-8	1122.04	1878.64	0.60	0.43	C
BTU-GCF-G12-11	1771.52	1878.64	0.94	0.42	C
BTU-GCF-G12-12	1187.72	1878.64	0.63	0.11	C
BTU-GCF-G12-13	1916.49	1878.64	1.02	0.12	C
BTU-GCF-G12-14	1921.56	1878.64	1.02	0.37	C
BTU-GCF-G12-15	1813.14	1878.64	0.97	0.15	C
BTU-GCF-G12-16	2294.74	1878.64	1.22	0.19	C
BTU-GCF-G12-17	1960.81	1878.64	1.04	0.18	C
BTU-GCF-G12-18	1485.29	1878.64	0.79	0.37	C
Average	1771.13	1878.64	0.94	0.25	C
S.D.	396.80	0.00	0.21	0.13	
CoV	22.40	0.00	22.40	50.14	

8.5.7. BTU-GLT-G6 Series

Table 8.15 shows pull-off tests results and the failure modes observed in the BTU-GCF-G12 series. As expected, the predominant failure mode was at the interface between fabric and mortar. However, the maximum strengths did not reach the minimum values established in AC434. The reason is due to both the high mechanical properties of the mortar used as matrix and its ease to penetrate between the cords, because the space is 0.6 mm.

Table 8.15 -Pull-off tests results on BTU-GLT-G6 specimens

Specimen ID	P_{max}	A	f_b	ext	Failure Mode
	(N)	(mm^2)	(MPa)	mm	
BTU-GLT-G6-1	3931.41	1934.60	2.03	0.55	C
BTU-GLT-G6-2	3062.21	1934.60	1.58	0.18	C
BTU-GLT-G6-3	3639.63	1934.60	1.88	0.52	C
BTU-GLT-G6-4	3221.97	1934.60	1.67	0.37	C
BTU-GLT-G6-5	3964.84	1934.60	2.05	0.29	C
BTU-GLT-G6-6	3483.59	1934.60	1.80	0.50	C
BTU-GLT-G6-7	3704.05	1934.60	1.91	0.24	C
BTU-GLT-G6-8	3630.81	1934.60	1.88	0.26	C
BTU-GLT-G6-9	4908.41	1934.60	2.54	0.62	C
BTU-GLT-G6-10	4494.34	1934.60	2.32	0.57	C
BTU-GLT-G611	4675.44	1934.60	2.42	0.33	C
BTU-GLT-G6-12	3057.96	1934.60	1.58	0.26	C
Average	3814.56	1934.60	1.97	0.39	C
S.D.	611.39	0.00	0.32	0.15	
CoV	16.03	0.00	16.03	38.58	

Table 8.16 summarizes the average results of pull-off tests. As expect, the specimens packed with the cement-based matrix (GLT) have reached the maximum levels of load as well as strength, regardless of the calculation of the area (net or total area) or substrate. In particular, the specimen BTC-GLT-G6 has achieved the highest level of load and strength. The reason is that tensile strength of mortar GLT is higher than that of mortar GCF (hydraulic lime based mortar). In addition, the density of steel fabric G6 is lower than that of G12, so the mortar could penetrate more easily between the steel cords. For this explanation, the peak average tensile strength of system BTC-GLT-G6 is higher than that of BTC-GLT-G12 (Table 8.16).

Main collapse mode of SRG composite is failure at reinforcement-matrix interface, so the density of fabric is an important parameter. In fact, the lower is the mass density and the higher is the bond strength. For this reason, the specimen BTC-GLT-G6 achieves a high strength value, because the matrix could penetrate more easily between the bundles and to increase the bond. However, no series reaches the strength limit imposed by the standard AC434, except for the specimen BTC-GLT-G6.

Table 8.16 - Average results of pull-off tests

Specimen ID	**P_{max}**	**A**	**f_b**	**ext**	**Failure Mode**
	(N)	(mm^2)	(MPa)	(mm)	
BTY-GCF-G6	2250.39	1941.57	1.16	0.21	C
BTY-GCF-G12	2095.52	1913.58	1.10	1.05	C + B
BTC-GLT-G6	6422,13	1934.60	3.32	1.48	C
BTC-GLT-G12	4219.92	1878.64	2.25	0.33	C
BTU-GCF-G6	1636.38	1939.25	0.84	0.20	C
BTU-GLT-G6	3814.56	2025.80	1.88	0.39	C
BTU-GCF-G12	1771.13	2025.80	0.87	0.24	C

Chapter 9
Qualification parameters

9.1. Introduction

Fiber Reinforced Cementitious Matrix composites are now widely used for repair and retrofitting existing structures. Guidelines for product qualification are needed to characterize the strengthening systems before they are made available in the market and installed. Two procedures could be followed: US standard *AC434*, and European procedure. The former determines the FRCM/SRG material properties by tensile tests performed on a significant number of specimens (at least five specimens for each test condition according to AC434-13) to be used for designing; the latter combines the results of direct tensile and shear bond tests to provide engineering design parameters for externally bonded FRCM reinforcements.
Therefore, a brief overview of both methods is reported in the following.

9.2. European qualification procedure

9.2.1. Direct tensile tests

Direct tensile tests are performed monotonically under displacement control on prismatic composite specimens. Specimens are clamped in the wedges of a testing machine, such that the applied normal stress avoids sliding in the griping areas, making it possible to derive the whole response curve of the composite up to the tensile rupture of the textile. In order to ensure a homogeneous stress distribution and prevent mortar crushing, either FRP reinforcements or tabs can be applied. This method differs from the clevis-type gripping mechanism recommended by Annex A of US standard AC434, in which the load is transferred from the testing machine to the mortar by adhesion, and failure is expected to occur by textile slipping within the matrix. Test results are expressed in the form of a mean stress - mean strain relationship. The stress is referred to the cross section area of the textile, which is evaluated as the product of equivalent design thickness and width (the latter being the number of fiber bundles/cords multiplied by their spacing). By doing so, the

possible variations of mortar cross section, which are unavoidable, especially in field applications, do not affect the results. The strain can be evaluated:

1. As the global displacement measured between the clamping wedges of the testing machine, because no sliding occurs in the gripping areas;
2. Recorded locally by means of extensometers or displacement transducers applied on the mortar matrix, if the gage length of the device is large enough with respect to the crack spacing. In this way, the measurements are not affected by the location of cracks, which may randomly vary from test to test.

Three stages characterize the response of FRCM composites under tensile loading, namely un-cracked (I), crack development (II) and cracked (III) (Fig. 9.1). In stage I, the specimen is undamaged and the response is linear. The occurrence of the first crack conventionally identifies the transition to stage II, during which a decrease of stiffness may be recognized and crack pattern develops progressively. The behavior in the first two stages depends on the mechanical properties of both the mortar and the textile, as well as on the textile-to-matrix stress transfer.

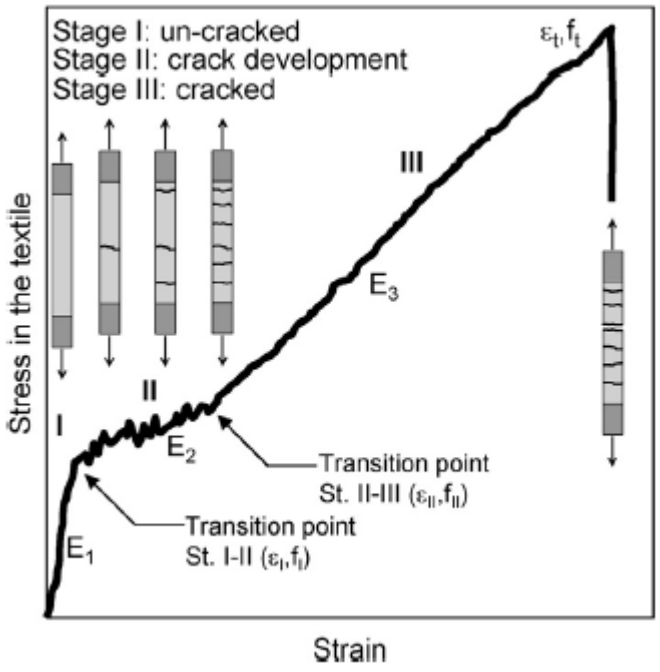

Figure 9.1 - Typical stress-strain response curve of FRCM systems under tensile loading [Ascione et al., 2015]

These parameters affect crack width and distribution, which, in their turn, may influence the durability of the reinforcement system as the textile is exposed to external aggression (e.g., salt attack). As soon as the number of cracks stabilizes, a stiffness increase normally occurs, defining the transition to stage III, in which additional imposed strain results in widening of existing cracks, and both load bearing capacity and tensile modulus of elasticity mainly depend on the textile. In stage III, the matrix, although cracked, may still provide transversal load redistribution. Failure usually occurs by tensile rupture of the textile, taking place in one roving/cord and suddenly propagating to the other ones.

9.2.2. Shear bond tests

Shear bond tests are carried out on specimens manufactured by applying a reinforcement strip to a substrate (brick, stone unit, concrete block, etc.), following the installation recommendations of the supplier. Either a single-lap or a double-lap scheme can be used. The former allows for an unmistakable identification of the load but requires particular attention in specimen alignment, to ensure that a pure shear stress is applied to the reinforcement and prevent the result from being affected by parasitic normal stresses on the substrate-to-matrix interface. In the latter, the reinforcement is applied to the two sides of the specimen, such that the geometry of the system is symmetric. However, this does not guarantee that the load distribution on the two surfaces is equal, and the force actually applied on each side needs to be carefully evaluated [74]. As in direct tensile tests, load is applied monotonically under displacement control up to failure, even if shear bond tests are normally run at a lower rate than tensile tests. In addition to the force, the relative displacement between reinforcement and substrate at the loaded end of the bonded area and the strain of the un-bonded textile are also recorded. Depending on the properties of the substrate, the shear strength of the mortar matrix, the tensile strength of the textile and the textile-to-matrix bond/interlocking, different failure modes may occur (Fig. 9.2), such as: debonding with cohesive failure in the substrate (mode A), debonding at the reinforcement-to-substrate interface (B) or at the textile-to-matrix interface (C), sliding of the textile within the reinforcement

thickness (D), and, finally, tensile rupture of the textile either in the un-bonded portion (E) or within the mortar matrix (F).

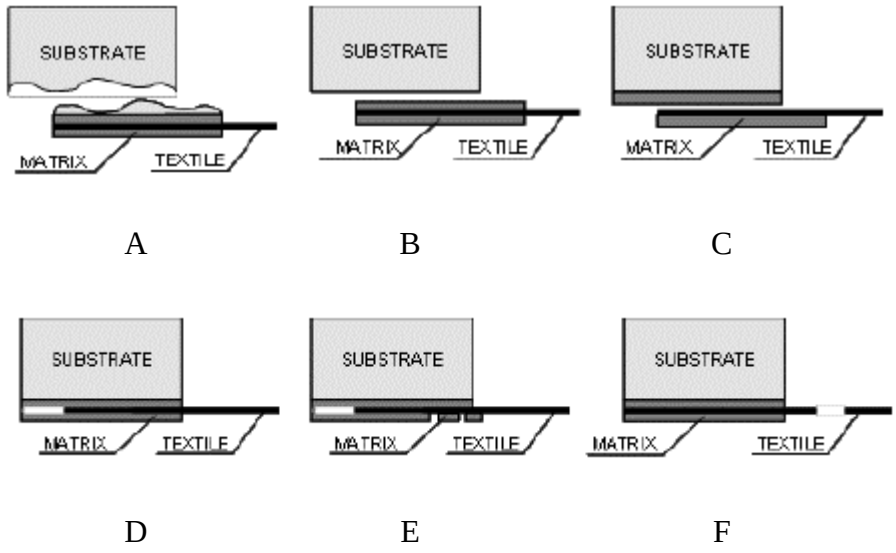

Figure 9.2 - Failure modes in shear bond tests on externally bonded FRCM strengthening systems [Ascione et al., 2015]

9.3. Combination of the results and identification of qualification parameters

A standard procedure for both product qualification and material assurance purposes should provide the fundamental mechanical parameters for the structural design and, at the same time, combine simplicity and reliability. As for externally bonded reinforcements with FRCM composites, safety requirements under ultimate limit state conditions are met (i.e., the system is able to carry the applied design loads) as long as the stress in the textile is lower than its tensile strength. Moreover, for the applications in which the load is transferred by shear from the structural element to the strengthening system, the stress in the textile needs to be lower than that inducing the detachment of the reinforcement from the substrate (Fig. 9.2).

In order to satisfy both these requirements, the proposed procedure is based on the combination of the results of direct tensile and shear bond tests, and provides the maximum stress, the corresponding strain and the tensile modulus of elasticity for design purposes. The qualification procedure is composed of the following steps:

1. Displacement controlled monotonic shear bond tests are performed and both the applied load and the relative displacement (slip) between reinforcement and substrate are recorded. Force values are divided by the cross section area of the textile, and stress-slip curves are built (Fig. 9.3a). The parameters directly provided by shear bond tests are both the ultimate stress (σ_u) and the prevalent failure mode (Fig. 9.2).
2. Monotonic direct tensile tests are carried out under displacement control up to failure, and stress-strain response curves are derived.
3. The ultimate stress (σ_u) from shear bond tests is identified on the stress-strain response curve under tensile loading together with the corresponding strain (ε_u) (Fig. 9.3b). The point having coordinates (ε_u, σ_u) conventionally qualifies the system on the considered substrate. Finally, the secant elastic modulus is derived as:

$$E_3 = \frac{\sigma_u}{\varepsilon_u} \tag{9.1}$$

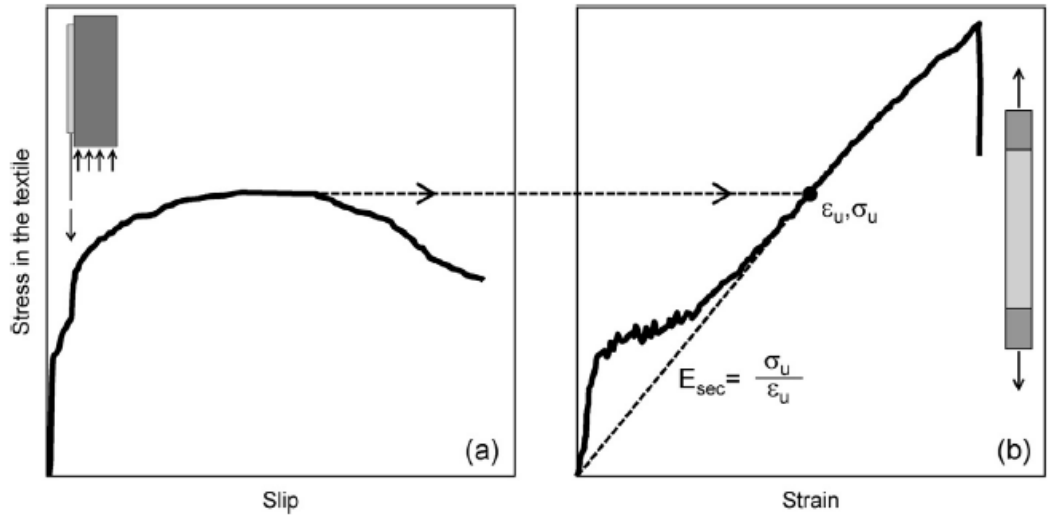

Figure 9.3 - Combination of the results of shear bond tests (a) and direct tensile tests (b) for the identification of qualification parameters [Ascione et al., 2015]

9.4. Differences between US standard AC434 and European procedure

Physical, mechanical, and durability properties have to be determined to

characterize the composite systems. Regarding testing in the control condition, AC434 recommends directly tensile tests to determine the mechanical behavior and bond and interlaminar shear tests to assess the possible modes of failure. They are three:

a) Cohesive, when failure occurs in the substrate material;
b) Adhesive, when failure occurs at the interface FRCM and substrate material;
c) Adhesive, when failure is at the interface between the reinforcement mesh and matrix within the FRCM.

On the other side, the European procedure suggests to combine the results of direct tensile and shear bond tests to provide engineering design parameters for externally bonded FRCM reinforcements. Furthermore, (single - double) lap shear tests are carried out to assess the possible modes of failure. In this case, in addition to the three modes mentioned above, the sliding of the fabric within the reinforcement thickness and the tensile rupture of the fabric out of the bonded area have to be considered.

As defined in AC434, the idealized tensile stress-strain curve of an FRCM coupon specimen is initially linear until cracking of the cementitious matrix occurs, deviates from linearity, and becomes linear again until failure by slippage. The plot can be reduced to a simple bilinear curve with a bend-over point (transition point) corresponding to the intersection point obtained by continuing the initial and secondary linear segments of the response curve. The initial linear segment of the curve corresponds to the FRCM un-cracked linear behavior and it is characterized by the un-cracked tensile modulus of elasticity E_f^*. The second linear segment, which corresponds to the FRCM cracked linear behavior, is characterized by the cracked tensile modulus of elasticity E_f. Instead, per European procedure, the expected tensile stress-strain curve is maded up of three consecutive branches corresponding to the un-cracked sample stage, to the cracking one and to the cracked one. Therefore, the further phase of cracking is considered. Then, the tensile modulus of elasticity of the cracked specimen is simply calculated as:

$$E_3 = \frac{\sigma_u}{\varepsilon_u} \tag{9.2}$$

The ultimate tensile stress is calculated using the results of lap shear tests, according to the following equations:

$$\sigma_u = \frac{F_{max}}{A_{dry\ reinf}} \tag{9.3}$$

where

F_{max} is maximum force of lap shear test before failure;

$A_{dry\ reinf}$ is the area of the cross section of the dry reinforcement into the specimen, regardless of the presence of the matrix, mm^2.

While the ultimate tensile strain ε_u is the x-coordinate corresponding to the ultimate tensile stress on the stress-strain curve of the tensile test.

According to AC434, to calculate the tensile modulus of elasticity of the cracked specimen, two points have to be selected on the segment of the response curve corresponding to cracked behavior after the transition. These two points are selected at a stress level equal to $0.90f_{fu}$ and $0.60f_{fu}$. The slope of the line that connects these two points represents the tensile modulus of elasticity of the cracked specimen:

$$E_f = \frac{\Delta f}{\Delta \varepsilon} = \frac{(0{,}90 \cdot f_{fu} - 0{,}60 \cdot f_{fu})}{\varepsilon_{f\_0.90f_{fu}} - \varepsilon_{f\_0.60f_{fu}}} \tag{9.4}$$

The ultimate tensile strength is calculated by the following equations:

$$f_{fu} = \frac{P_{max}}{A'_f \cdot w} \tag{9.5}$$

where

P_{max} is maximum load of tensile test before failure;

$A'_f \cdot w$ is obtained as the product of the area of each strand A_{fi} and n, where n is the number of strands effectively present in the width of the coupon.

Ultimate tensile strain is the y-intercept of the line used to compute E_f (that is,

$y_{intercept} = 0.60 f_{fu} - E_f \cdot \varepsilon_{f\_0.60 f_{fu}}$) and the following equation:

$$\varepsilon_{fu} = \frac{(f_{fu} - y_{intercept})}{E_f} \tag{9.6}$$

9.5. The merge of US standard AC434 in the Design Code ACI 549

Although the constituent material properties of FRCM systems are disclosed by manufacturers, they cannot be directly used to infer the values of the parameters to be used in design, nor to assess the durability of an FRCM system. A qualification test plan should be undertaken following the requirements of AC434 with the intent of verifying the design properties to be used in FRCM systems. This testing would provide data on material properties, force, and deformation limit states, including failure modes of FRCM to support a rational analysis, and design procedure. Specimens should be constructed under conditions specified by AC434 and be prepared to verify the range of FRCM configurations, including layers, thickness, components, and bonding agents recommended by the manufacturer. Tests should simulate the anticipated range of loading conditions, load levels, deflections, and ductility. Based on the provisions of AC434, the values of strength and strain (f_{fe}, ε_{fe}), used in the design equations, reported in the chapters 10-13 of ACI 549, are defined. Therefore, effective tensile stress and strain level in the FRCM reinforcement attained at failure (f_{fe}, ε_{fe}), is limited to the design tensile stress and strain of the FRCM composite material (f_{fd}, ε_{fd}), provided by qualification test plan according to AC434.

9.6. Qualification parameters of tests results

Results of tests, previously described and discussed, can be used for the determination of the design parameters for the considered systems. As reported in the AC434 (AC434, 2013), FRCM/SRG material properties determined by tests performed on a significant number of specimens (at least five specimens for each test condition) to be used for designing.

The values of strength and strain to be used in the design equations are defined as the average value of the test results minus one standard deviation, while the elastic modulus is simply the average value of test results.

The qualification parameters (f_{fk}, ε_{fk}, E_{fk} and bond strength f_{bk}) for the four SRG systems investigated in this study, are listed in Table 9.1. The bond stress value is reported only for the GLT-G6 system that, as above mentioned, satisfies the conditions of acceptance of the AC434 standard.

Table 9.1 - Qualification parameters

SRG system	$\mathbf{f_{fk}}$ **(MPa)**	$\boldsymbol{\varepsilon_{fk}}$ **(%)**	$\mathbf{E_{fk}}$ **(GPa)**	$\mathbf{f_{bk}^{*}}$ **(MPa)**
GCF-G6	711.02	1.07	54.65	-
GCF-G12	499.18	0.97	36.84	-
GLT-G6	1036.77	0.87	74.06	2.65
GLT-G12	696.14	0.70	53.48	-

The comparison of results obtained for the SRG systems examined, evidences that only the GLT-G6 system satisfies the requirements of the AC434 and, then it can be considered as strengthening material. The remaining SRG systems, as previously evidenced, do not satisfy the condition of acceptance on the bond stress value; in addition, in comparison with the GLT-G6 system, their mechanical parameters are less significant for a structural point of view.

Conclusions

The purpose of this experimentation was to study and characterize from a physical and mechanical point of view, a new emerging technique for structural reinforcement of masonry and concrete structures, referred to as SRG (Steel Reinforced Grout). The mechanical characterization of materials is a necessary process that aims at the standardization of testing methodology, to determine the materials properties needed for design and to evaluate their performance.

SRG is the latest development on repair techniques. It is another tool among the concrete and masonry strengthening methods that complements existing FRCM (Fiber Reinforced Cementitious Matrix) and FRP (Fiber Reinforced Polymer). SRG has emerged as promising and cost-effective technology for the external strengthening of RC structures. It consists of a reinforcement fabric made of Ultra-High-Strength Steel cords embedded in a cementitious grout and externally bonded to the surface of the structural elements and, thanks to their high strength-to-weight ratio, provide a significant improvement of the structural capacity with minimum mass increase. In fact, use of Ultra-High Strength Steel fibers increases the ductility of the reinforced elements. It is higher than that of conventional reinforcements in composite, thus favoring the applications in the case of seismic problems. Another important feature is shear strength of steel that simplifies the connection and anchoring issues. Low and medium density fabrics also allow employing cement based mortars. This implicates benefit in cost, fire resistance and operational simplicity, which are typical limit of the use of traditional composite materials.

The achievement of high resistance classes (between 2400 and 4000 MPa) with very small diameters (between 0.20 - 0.48 mm), suitable for use in composite materials, leads to a loss of ductility of the yarn. It implicates, consequently, the risk of brittle failure by delamination and a lesser elongation at break if compared with larger diameter wires.

Given the current level of knowledge, it has emerged that greater knowledge of SRG is required. Therefore, two different steel fabric meshes impregnated by means of two several matrices were selected for this research. The fabric meshes are steel textiles constituted by cords of Ultra High Tensile Strength Steel (UHTSS) micro-wires with different mass density, namely *G6* (600 g/m^2) and *G12* (1200 g/m^2). The

"G6" fabric is characterized by a density of 1.57 cords/cm. Cords are equally spaced of about 6 mm to obtain a textile with 0.084 mm equivalent thickness. Instead, the *"G12"* net has a density of 3.19 cords/cm and 0.169 mm equivalent thickness. Cords are placed adjacent to each other two by two such that the spacing between couples of cords is about 4 mm, in order to allow for the protrusion of the mortar during installation and to promote the matrix-to-textile interlocking. The matrices are a cement-based mortar, *GLT*, and a hydraulic lime-based mortar, *GCF*. Steel fabrics, *G6* and *G12*, and mortars, *GLT* and *GCF*, have been used to produce a total of four SRG systems, called *GLT-G6, GLT-G12, GCF-G6* and *GCF-G12*. Tensile, interlaminar shear, bond and compressive tests were performed on specimens in environmental condition in order to evaluate the performance of SRGs and so to understand their effectiveness and compatibility with concrete and masonry substrates. Therefore, the preliminary considerations obtained from this thesis can be considered as first step toward the characterization of mechanical behavior of SRG systems and they are shown below:

1. *Compressive tests*. Maximum load carried by the samples during the test was recorded and the type of fracture pattern was noted. The primary mode of failure was compression of the cube resulting to be a cone like structure as desired. Based on the experimental tests presented herein, the cement-based mortar, *GLT*, meets the requirements of AC434 Section 4.3, corresponding to 17 MPa at 7 days and 24 MPa at 28 days compressive strength. Regarding the hydraulic lime-based mortar, *GCF*, it also fulfills standard requirements, that is, the average compressive strength of at least three 50 mm cubes shall be not less than 1.7 N/mm^2 and no more than 10.3 N/mm^2 at the age of 28 days.
2. *Tensile tests.* The results of tests on coupons are presented as tensile strength versus strain curves. Based on experimental results, maximum force and ultimate strain have been obtained. Then, ultimate strength and cracked elastic modulus have been calculated by means of the equations reported in AC434. Finally, failure mode has been described for each tested specimens. Regarding collapse of all specimens of *GLT-G6* series, they shown a failure mode characterized by the formation of a first crack in the end of bonded length of metal tab. From there, the development of crack continued throughout its

length. Finally, the failure by rupture was due to the splitting of the matrix around the fiber cords. This because the mortar was not penetrated well in the fabric and was not engage effectively, making easy the slippage of fibers.

In the case of *GLT-G12* series, a series of cracks occurred in the center area of the specimen, which was monitored by the extensometer. Others took place in the end of bonded length of metal plate. From there, the development of crack continued throughout its length. Finally, the failure by rupture was due to the splitting of the matrix around the fiber cords. The reason is that the mortar was not able to embed easily in the fabric, because the textile is characterized by high mass density (1200 g/m^2).

Specimens of *GCF-G6* series developed two deep cracks in the far ends of bonded length of metal tab. From there, the development of cracks continued throughout its length. The failure by rupture was not equal for all specimens. In fact, the collapse was due to the splitting of the matrix around the fiber cords in some cases. In other cases, it was achieved either for detachment of the tab from the coupon or the slippage of fibers.

In the case of *GCF-G12* series, several cracks occurred in the center area of the specimen that was monitored by the extensometer. Others took place in the end of bonded length of metal plate. From there, the development of crack continued throughout its length. Finally, the failure by rupture was due to the splitting of the matrix around the fiber cords. The reason is that the mortar was not able to embed easily in the fabric, because the textile is characterized by high mass density (1200 g/m2). The failure by rupture was not equal for all specimens. In fact, the collapse was due either to the splitting of the matrix around the fiber cords with consequent slippage of fibers or for enlargement of cracks that caused breakage of the specimen into several pieces.

3. *Interlaminar shear tests*. This test method determines the apparent interlaminar shear strength of high-modulus fiber-reinforced composite materials. In fact, known the peak load recorded during test, the ultimate strength has been computed by means of the equation reported in ASTM-D2344. Failure modes were reported as well. The systems packaged with *G6* steel fabrics presented a collapse due to the matrix cracking in the tension side. In fact, in all coupons,

onset of damage was characterized by a single crack that propagated from the bottom of beam in the central region. In the case of the systems packaged with *G12* steel fabrics, the primary mode of failure was interlaminar shear. Indeed, it is been observed the development of two cracks at fiber-matrix interface that propagated from the center of the specimen to the edge. The reason is because the *G12* fabric has mass density higher than *G6* textile and did not permit the complete penetration in the matrix. Therefore, the bond at fiber-matrix interface was not efficient.

4. *Pull-off tests.* Given the ultimate load recorded during test, the ultimate strength have been calculated by means of the equation reported in ASTM-C1583 and the failure modes were reported. As expect, the specimens packed with the cement-based matrix (GLT) have reached the maximum levels of load as well as strength, regardless of the calculation of the area (net or total area) or substrate. In particular, the specimen BTC-GLT-G6 has achieved the highest level of load and strength. The reason is that tensile strength of mortar GLT is higher than that of mortar GCF (hydraulic lime based mortar). In addition, the density of steel fabric G6 is lower than that of G12, so the mortar could penetrate more easily between the steel cords. For this explanation, the peak average tensile strength of system BTC-GLT-G6 was higher than that of BTC-GLT-G6. Main collapse mode of SRG composite is failure at reinforcement-matrix interface, so the density of fabric is an important parameter. In fact, the lower is the mass density and the higher is the bond strength. For this reason, the specimen BTC-GLT-G6 achieves a high strength value, because the matrix could penetrate more easily between the bundles and to increase the bond. However, no series reaches the strength limit imposed by the standard AC434, except for the specimen BTC-GLT-G6.

Based on the assumption that SRG composites have desirable long-term performance, they can be considered as a solution for strengthening or rehabilitation of existing masonry and concrete structures. The preliminary considerations obtained from this study represent a first step toward the development of proper design formulae for characterization of SRG systems and of standardization of test method. Clevis grips are more suitable than clamps grips for the tensile test. Reason

is that only shear stresses are transferred in the first case. The full strength of the fabric is never reached because the failure mode is by slippage of the fabric, namely the most typical damage of FRCM composite systems. Instead, the clamping grips generate compression and shear in the specimen to limit slippage between fabric and matrix at the grip. However, the European procedure provides results on the base of the weakest mechanism of failure that takes place, due to the possible occurrence of different failure modes during the lap shear tests. In fact, shear bond tests provide the effectiveness of the substrate-to-reinforcement load transfer, allowing the weakest failure mechanism to activate. Differently, the application of a normal tensile stress to the substrate-to-reinforcement interface, as in pull-off tests does not allow for the detection of some failure modes, namely the textile sliding or the tensile. Therefore, thanks to its simplicity, the European method could be also suitable for standard product qualification and material assurance purposes, even if the tests performed with clevis grips reproduce the as-installed FRCM behavior. However, further experimental investigations are necessary both to strengthen the suitability of the clevis grips and to understand the mechanical behavior of steel fibers under different conditions. An experimental investigation on bond between thermally conditioned FRCM-masonry joints should be undertaken. Single lap shear tests should be conducted on clay brick specimens strengthened with different FRCM systems (basalt, steel, PBO-FRCM systems etc.) or with steel fabric of different mass density. Before testing, specimens should be kept in oven and exposed to constant temperature over a period of some hours. The values of temperature could be different, as 20 °C, 100 °C, 150 °C and 200 °C. Then, they should be removed and cooled down freely at ambient temperature and finally tested. Experimental results would allow evaluating the influence of the thermal conditioning on the local bond-slip response of strengthened specimens.

The use of externally bonded steel reinforced grout (SRG) is a promising and cost-effective new technology for increasing flexural, compressive, and shear capacities of reinforced concrete (RC) members. The presence of the external strengthening significantly increases the flexural strength of slabs, with percentage increases over the control (un-strengthened) member ranging from a minimum value of 27%,

when using a single layer of low-density tape, to higher values in the case of system with one layer of high-density sheet.

The SRGs are an effectiveness alternative technique of shear reinforcement. In fact, they provide a significant increase in shear strength and stiffness. Furthermore, the non-application of epoxy resins contribute to solve important problems in terms of high temperature and long-term behavior, compatibility and reversibility of reinforcement. Therefore, another interesting experimental investigation could be carried out on masonry columns strengthened with SRG systems in order to understand the increase of the compressive strength depending on the corner radius ratio or the fiber density. Research topic still not sufficiently debated in the literature.

Appendix: Stress vs Strain Curves of Tensile Tests

1. GLT-G6 Series

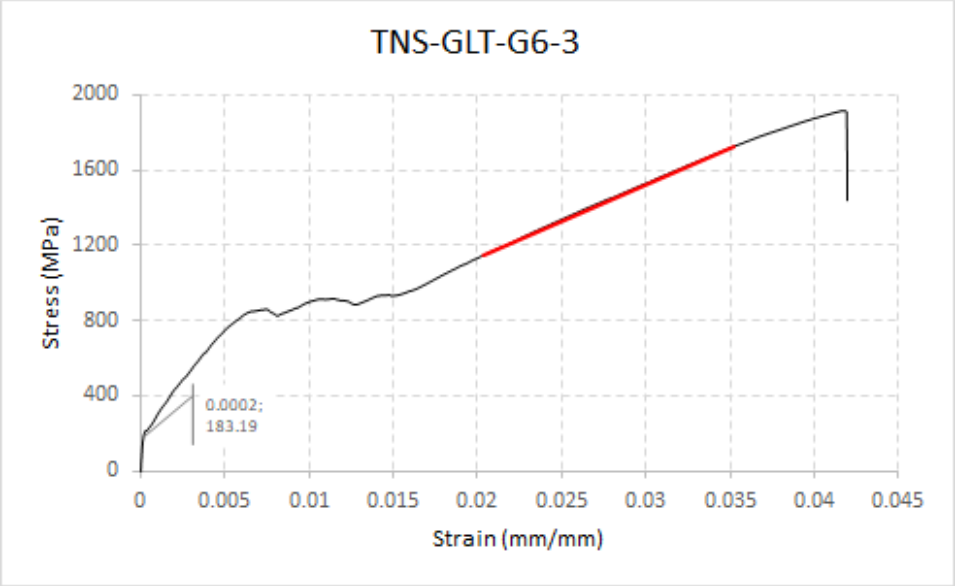

Figure Appendix.1 -Stress-Strain Curve for coupon GLT-G6-3

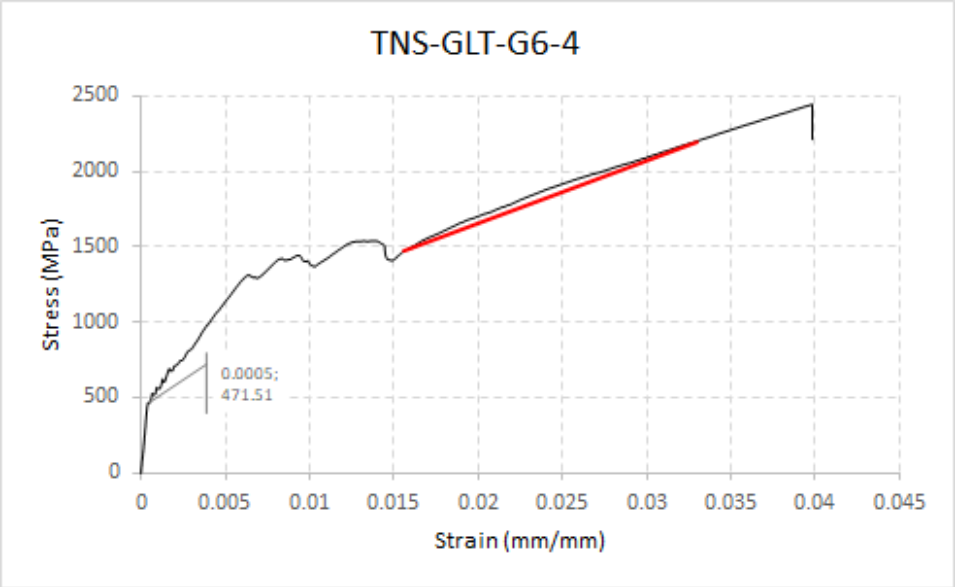

Figure Appendix.2 -Stress-Strain Curve for coupon GLT-G6-4

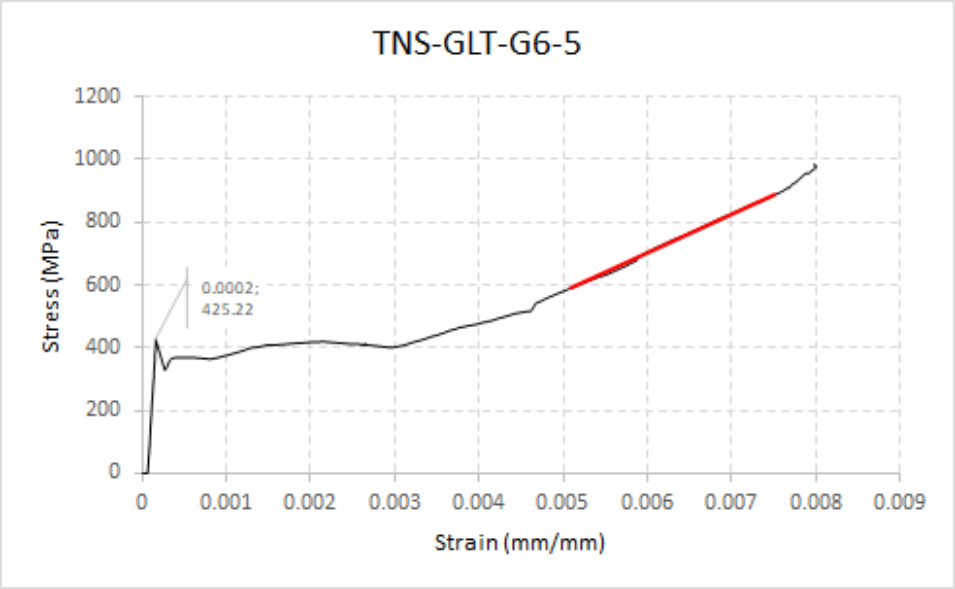

Figure Appendix.3 - Stress-Strain Curve for coupon GLT-G6-5

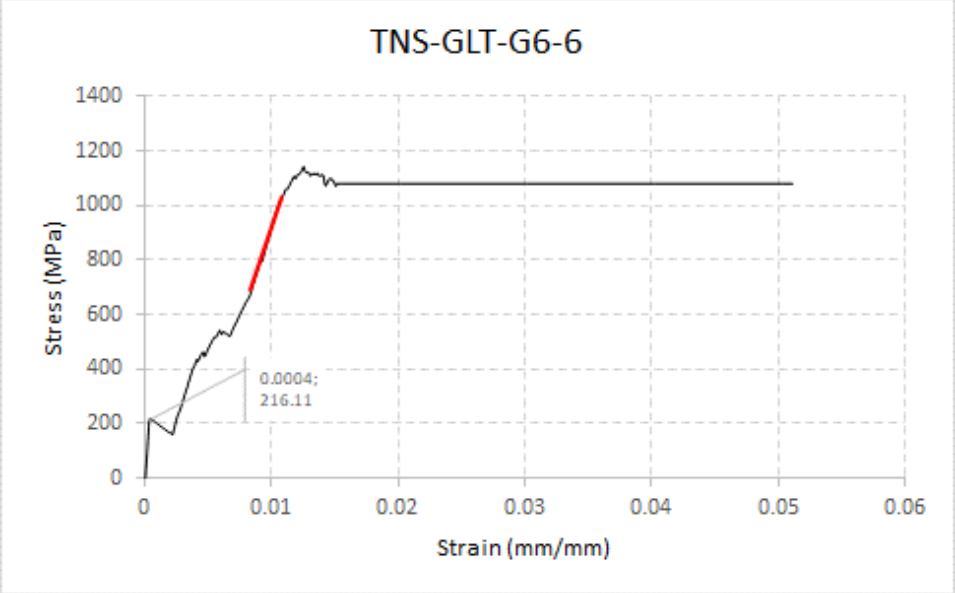

Figure Appendix.4 - Stress-Strain Curve for coupon GLT-G6-6

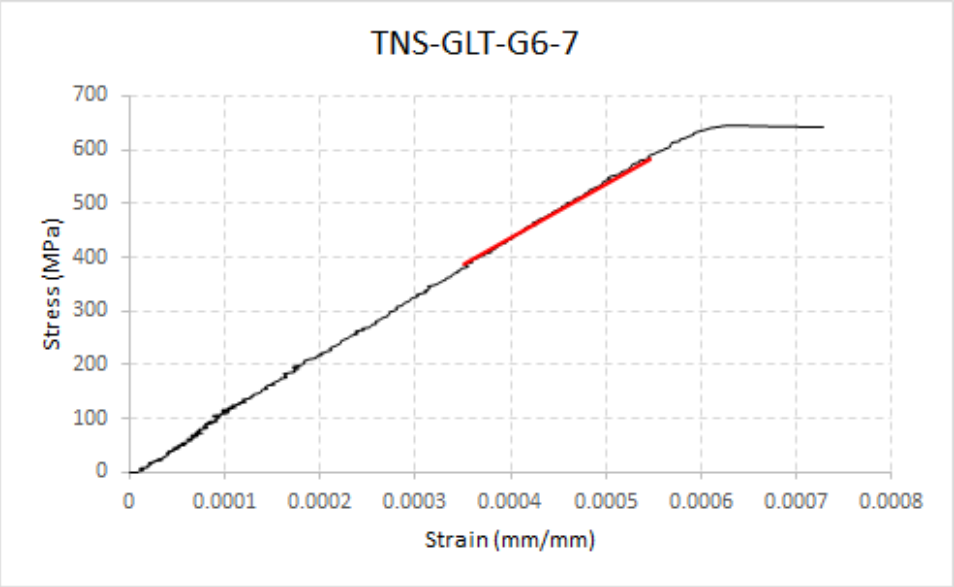

Figure Appendix.5 - Stress-Strain Curve for coupon GLT-G6-7

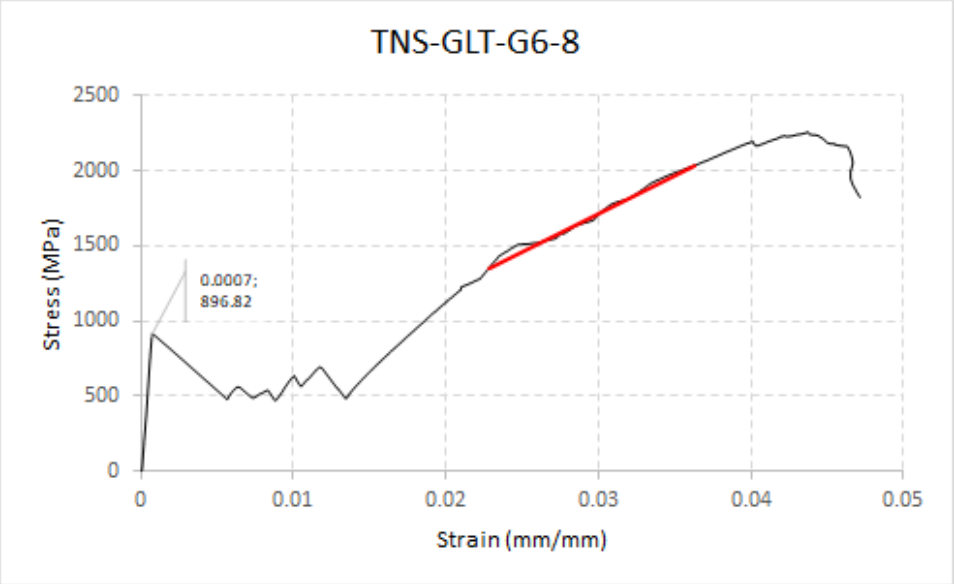

Figure Appendix.6 - Stress-Strain Curve for coupon GLT-G6-8

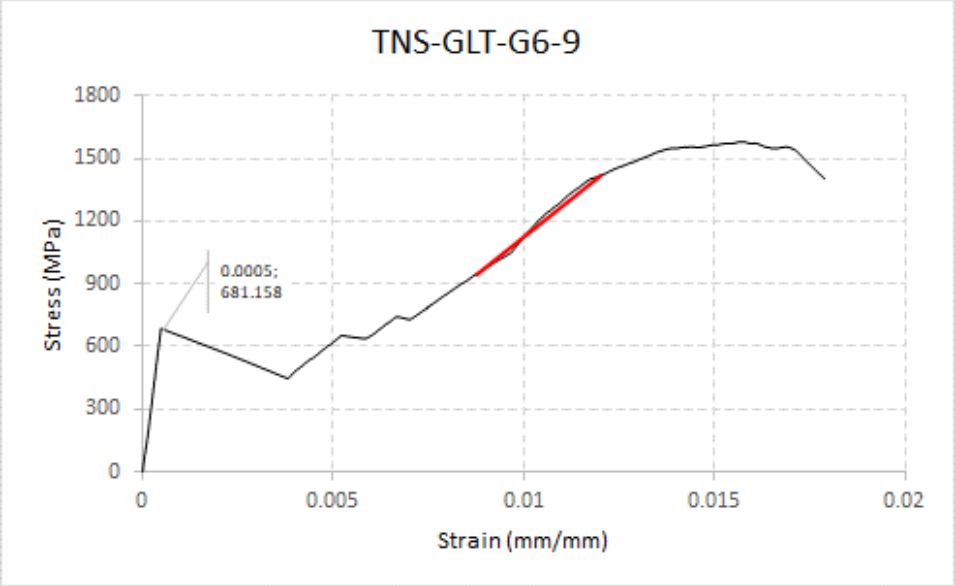

Figure Appendix.7 - Stress-Strain Curve for coupon GLT-G6-9

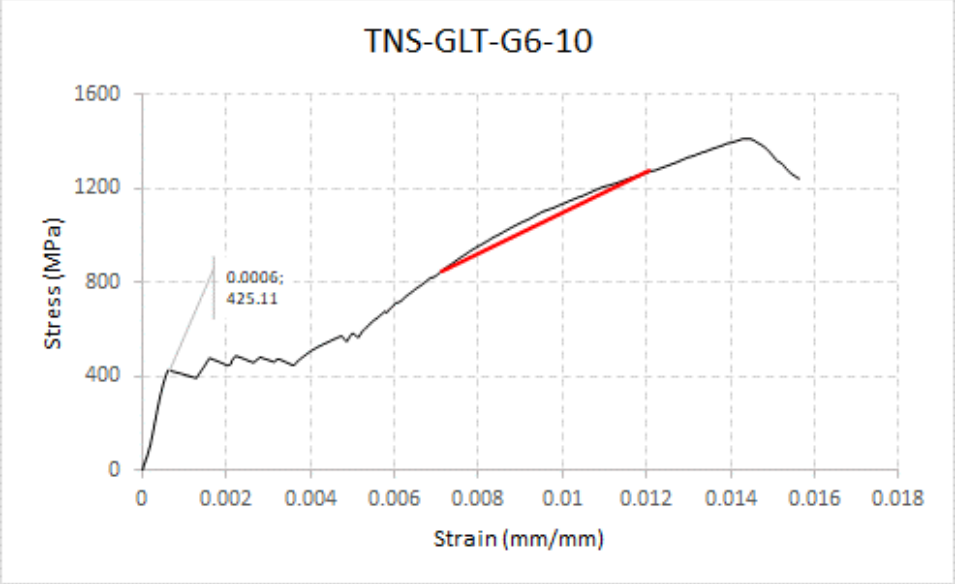

Figure Appendix.8 - Stress-Strain Curve for coupon GLT-G6-10

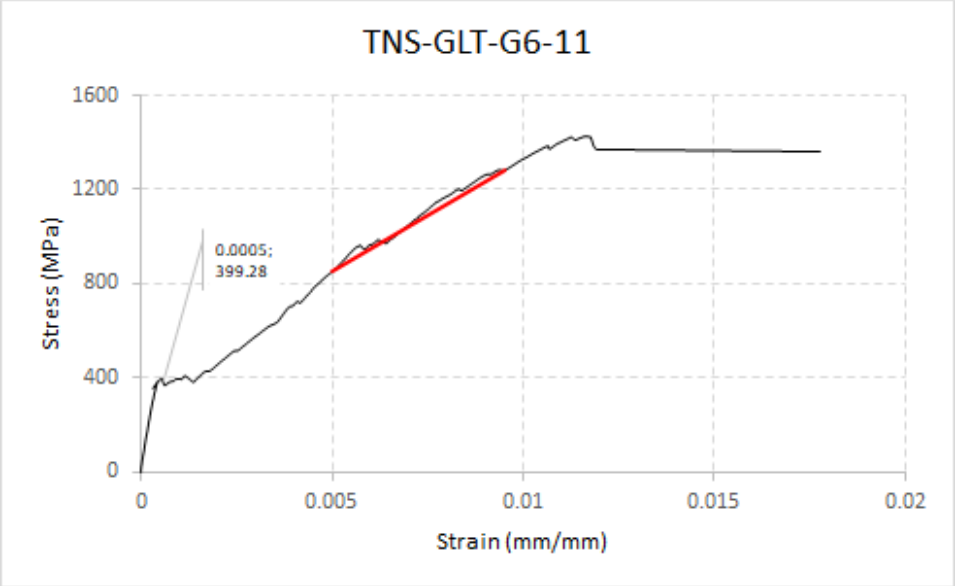

Figure Appendix.9 - Stress-Strain Curve for coupon GLT-G6-11

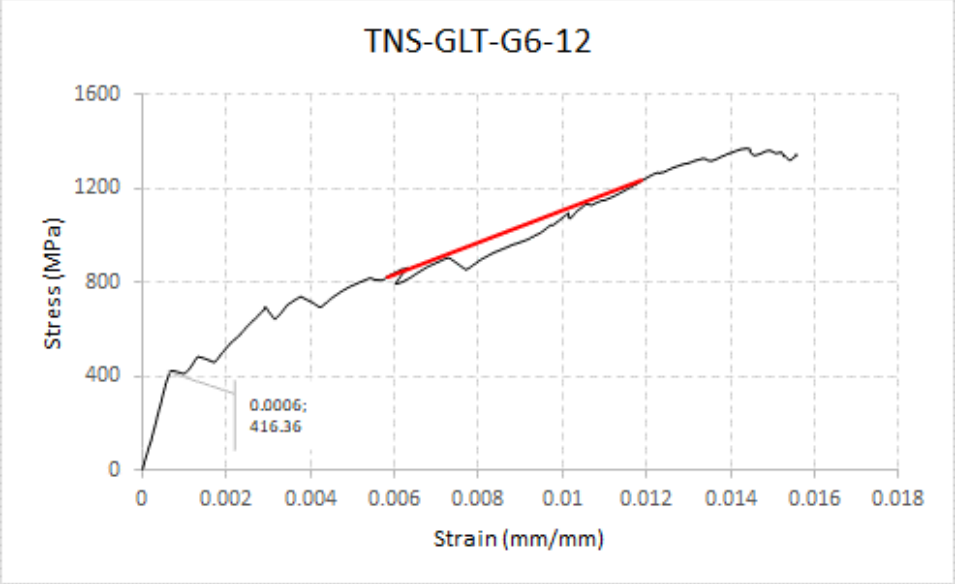

Figure Appendix.10 - Stress-Strain Curve for coupon GLT-G6-12

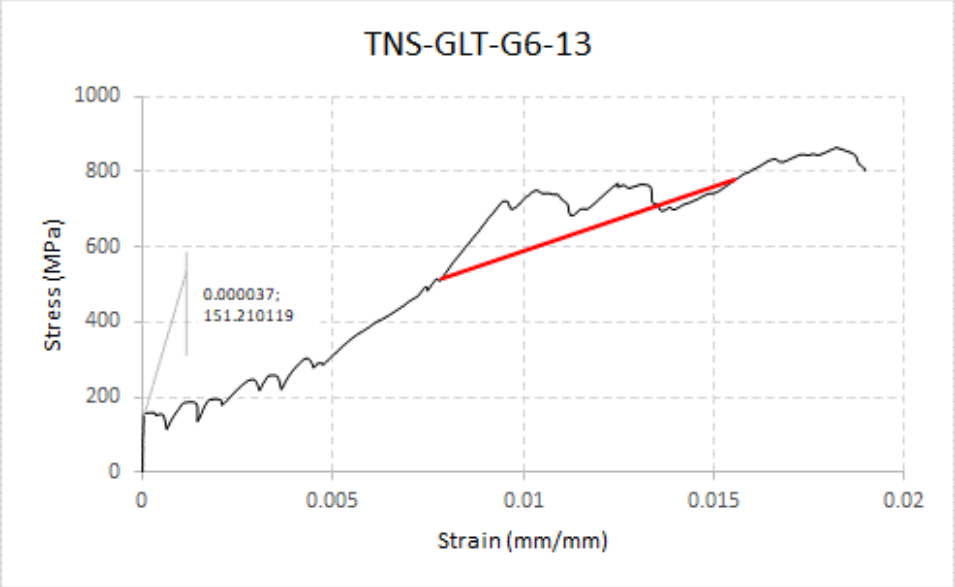

Figure Appendix.11 - Stress-Strain Curve for coupon GLT-G6-13

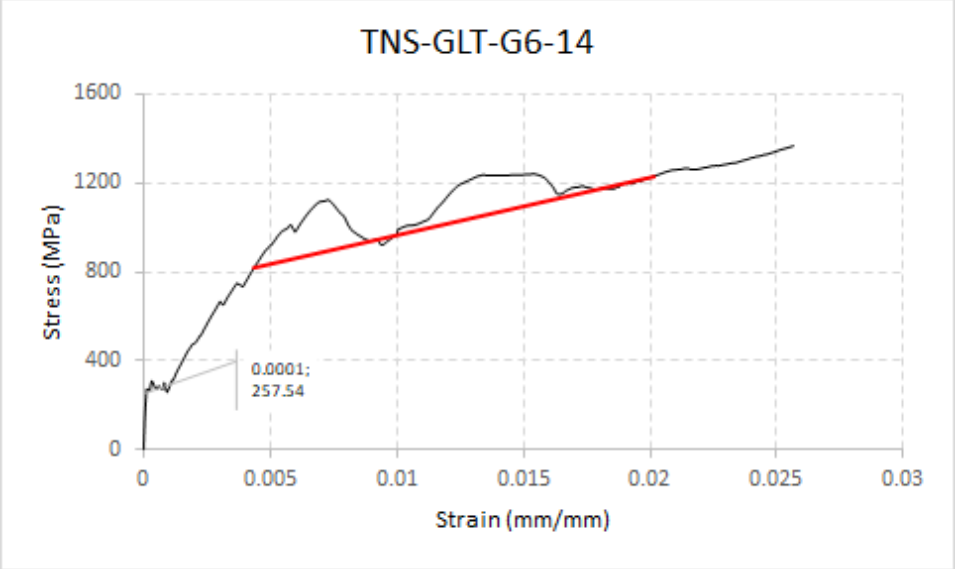

Figure Appendix.12 - Stress-Strain Curve for coupon GLT-G6-14

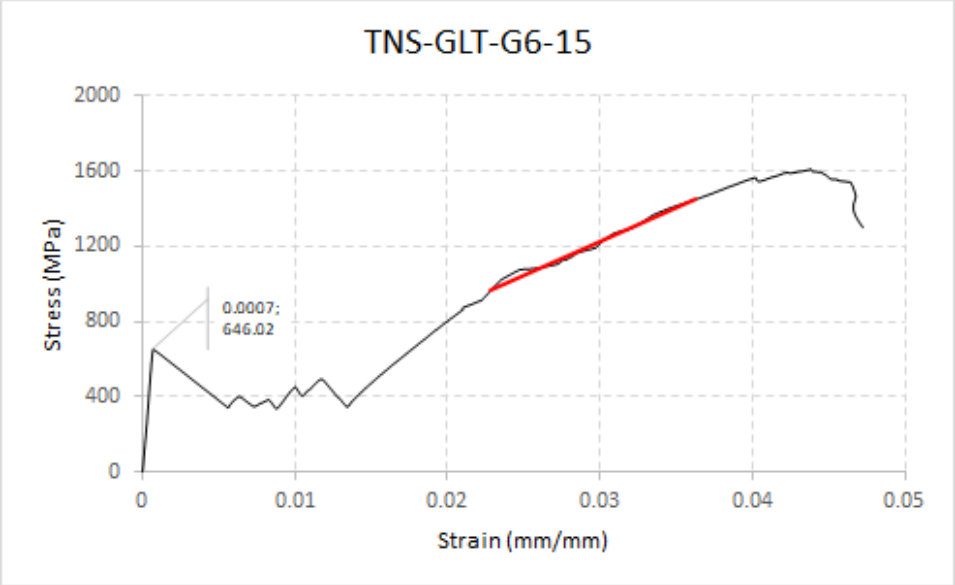

Figure Appendix.13 - Stress-Strain Curve for coupon GLT-G6-15

2. GLT-G12 Series

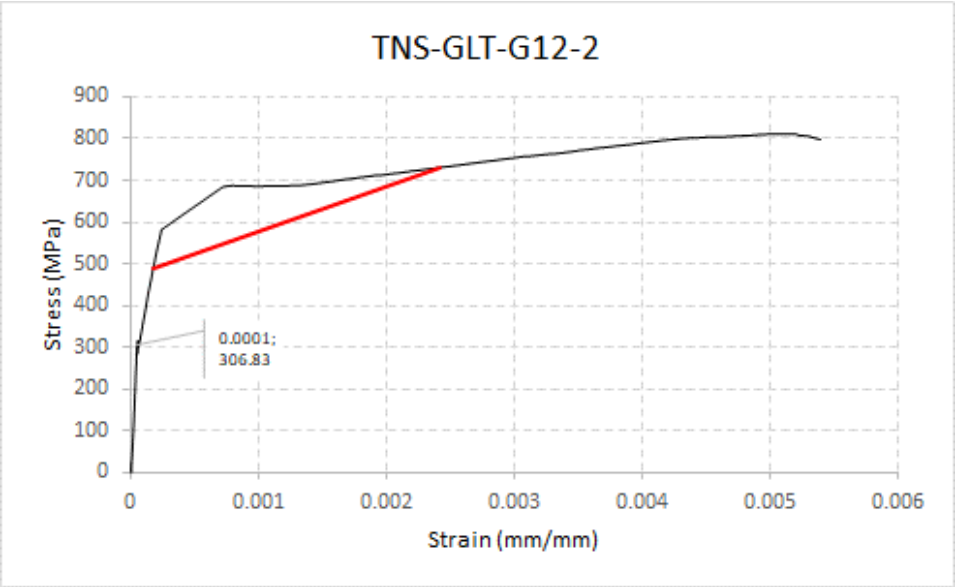

Figure Appendix.14 - Stress-Strain Curve for coupon GLT-G12-2

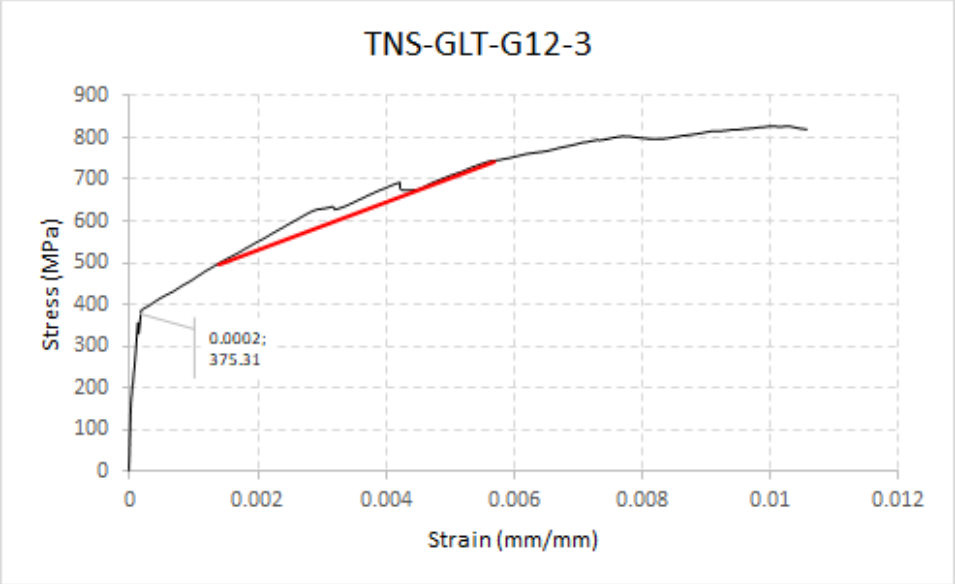

Figure Appendix.15 - Stress-Strain Curve for coupon GLT-G12-3

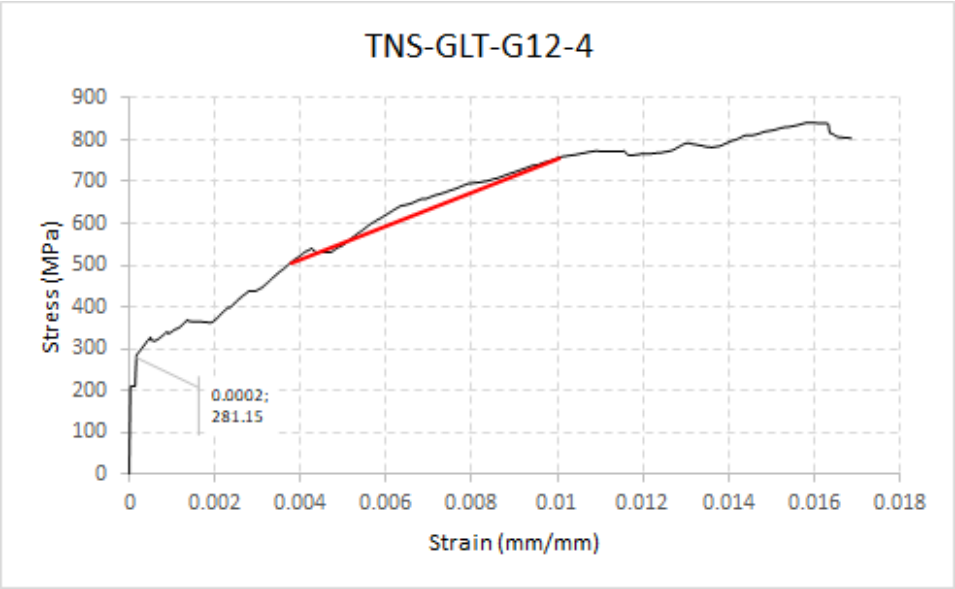

Figure Appendix.16 -Stress-Strain Curve for coupon GLT-G12-4

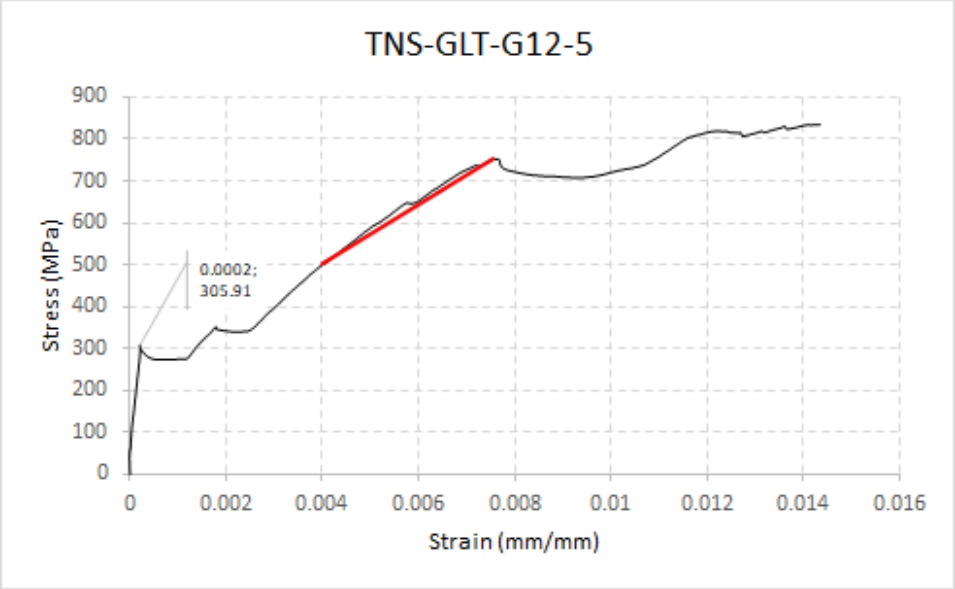

Figure Appendix.17 - Stress-Strain Curve for coupon GLT-G12-5

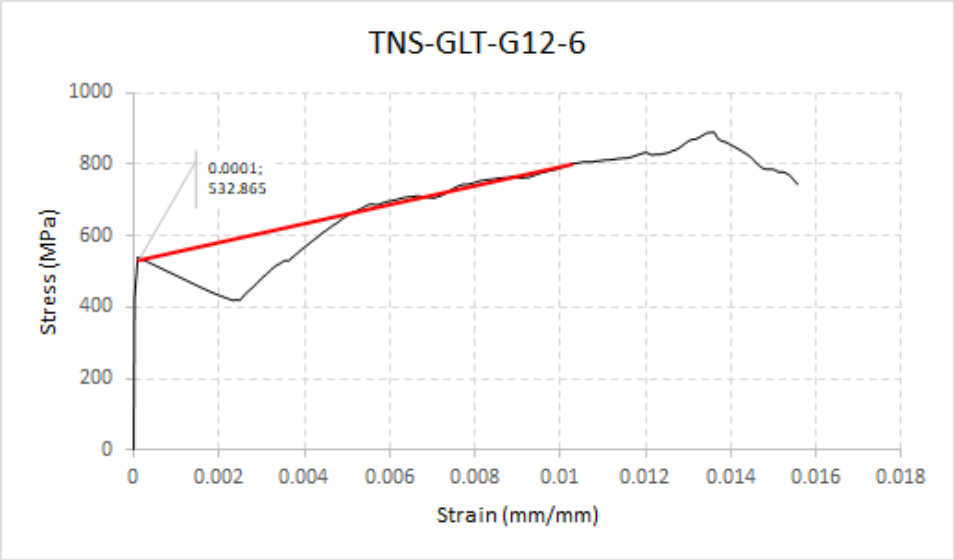

Figure Appendix.18 - Stress-Strain Curve for coupon GLT-G12-6

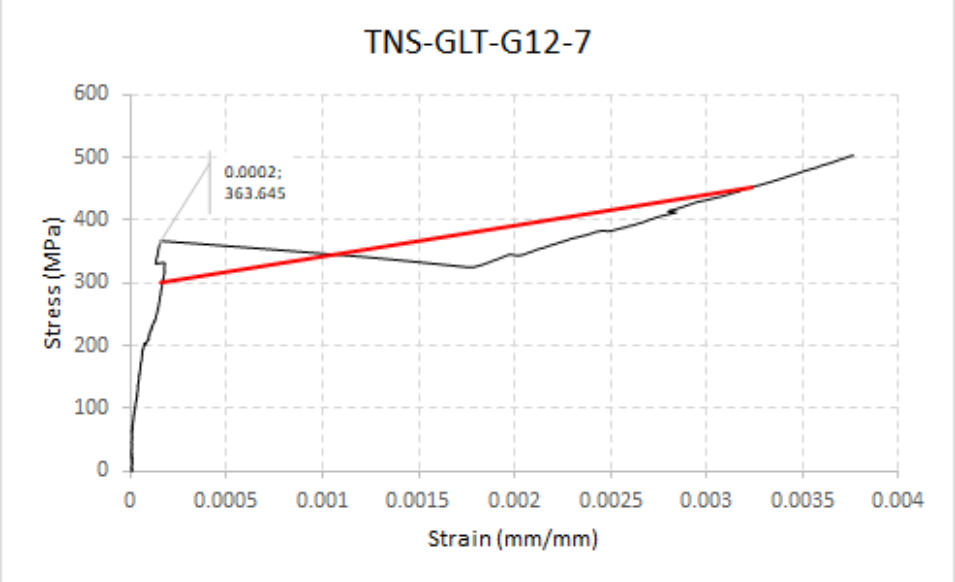

Figure Appendix.19 - Stress-Strain Curve for coupon GLT-G12-7

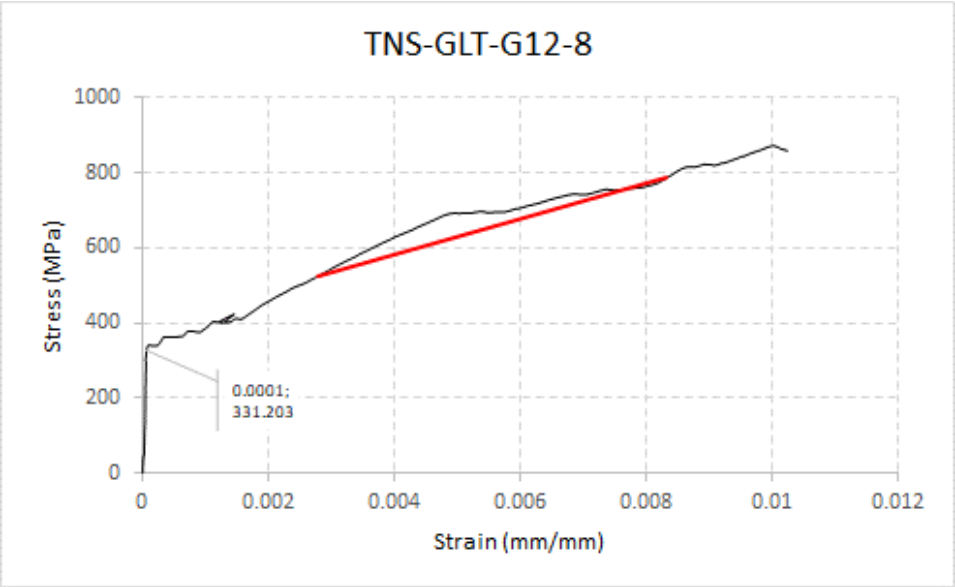

Figure Appendix.20 - Stress-Strain Curve for coupon GLT-G12-8

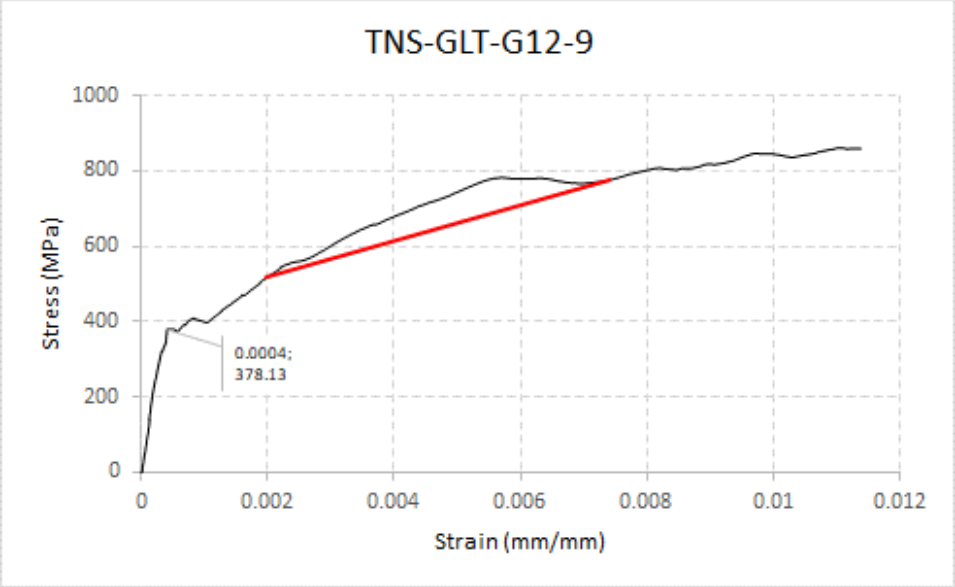

Figure Appendix.21 - Stress-Strain Curve for coupon GLT-G12-9

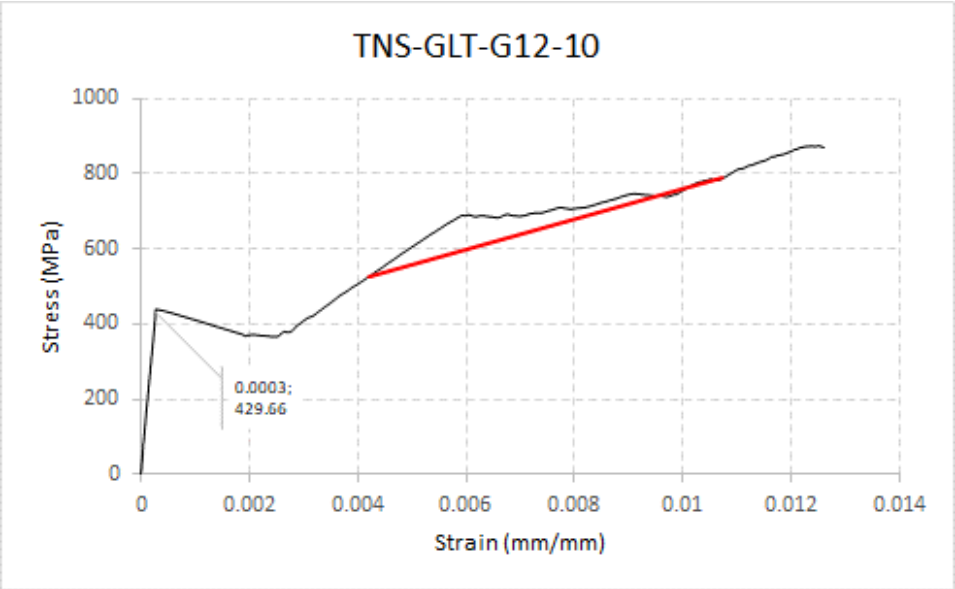

Figure Appendix.22 - Stress-Strain Curve for coupon GLT-G12-10

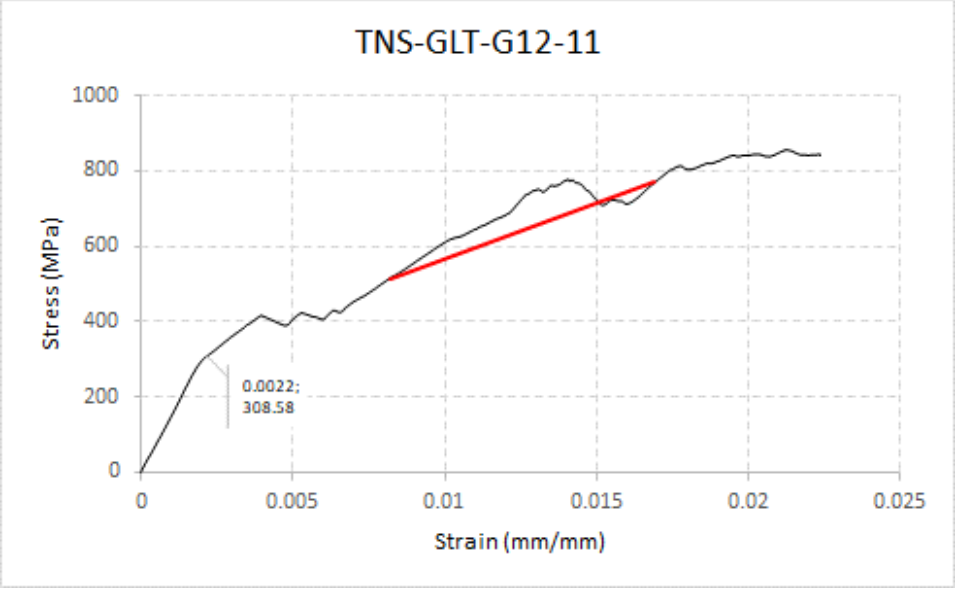

Figure Appendix.23 - Stress-Strain Curve for coupon GLT-G12-11

3. GCF-G6 Series

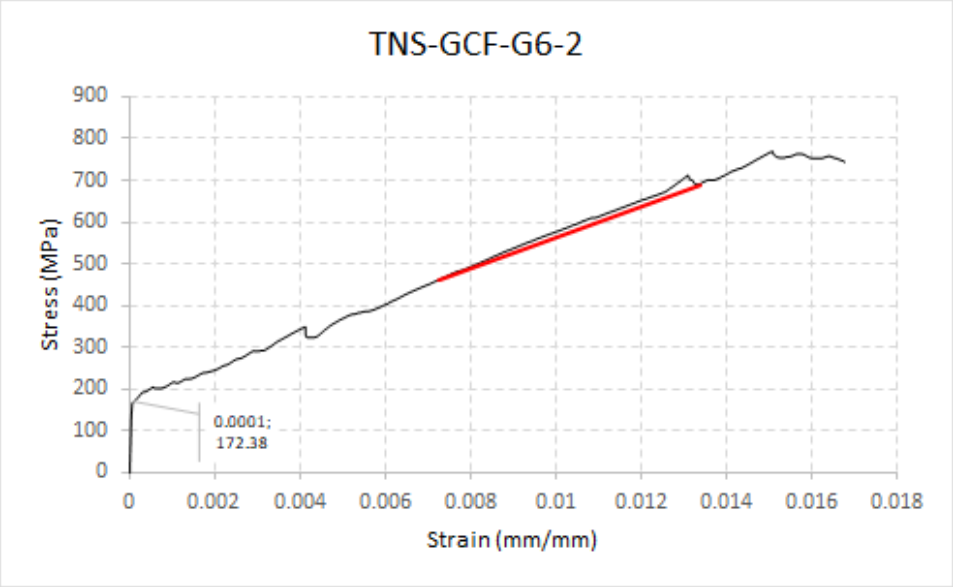

Figure Appendix.24 - Stress-Strain Curve for coupon GCF-G6-2

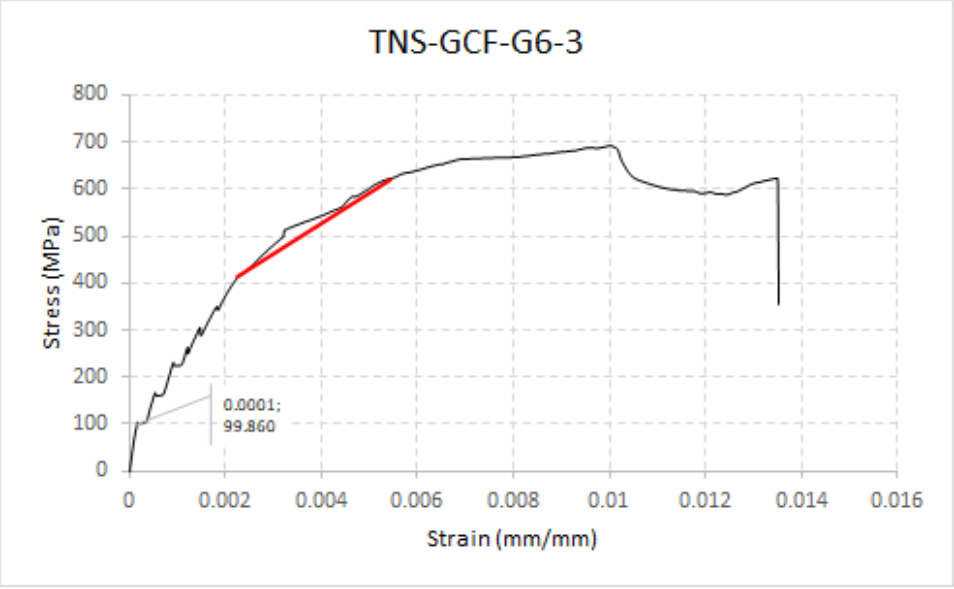

Figure Appendix.25 - Stress-Strain Curve for coupon GCF-G6-3

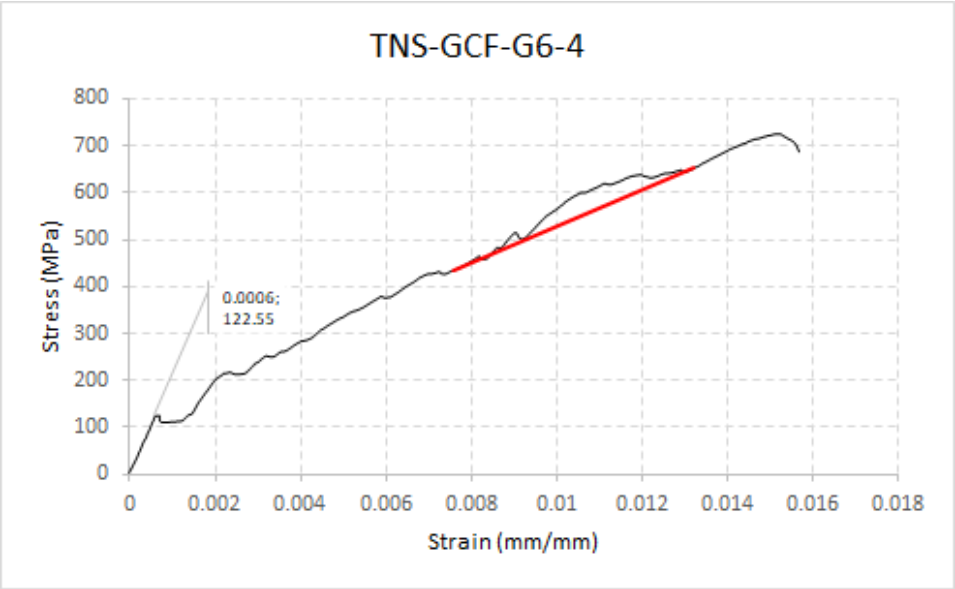

Figure Appendix.26 - Stress-Strain Curve for coupon GCF-G6-4

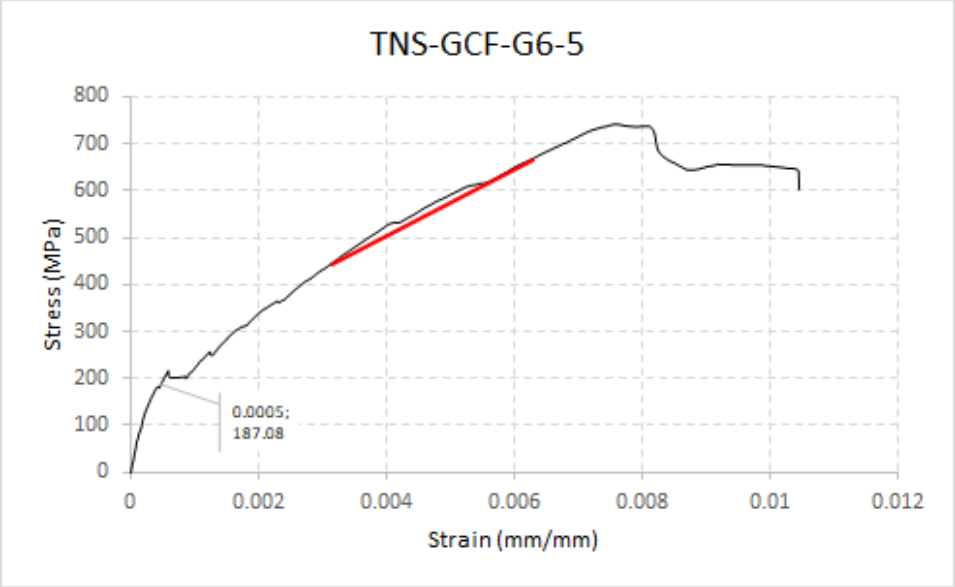

Figure Appendix.27 - Stress-Strain Curve for coupon GCF-G6-5

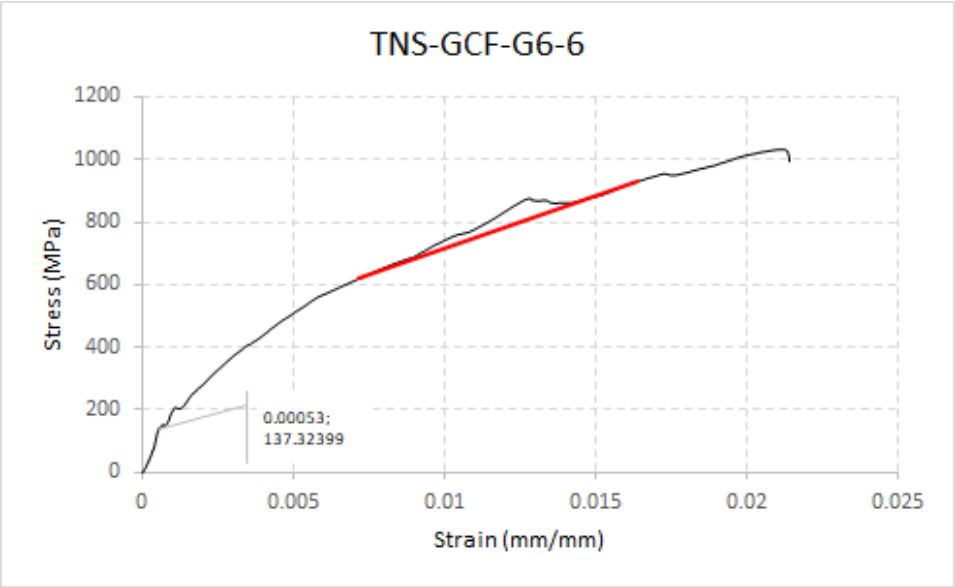

Figure Appendix.28 - Stress-Strain Curve for coupon GCF-G6-6

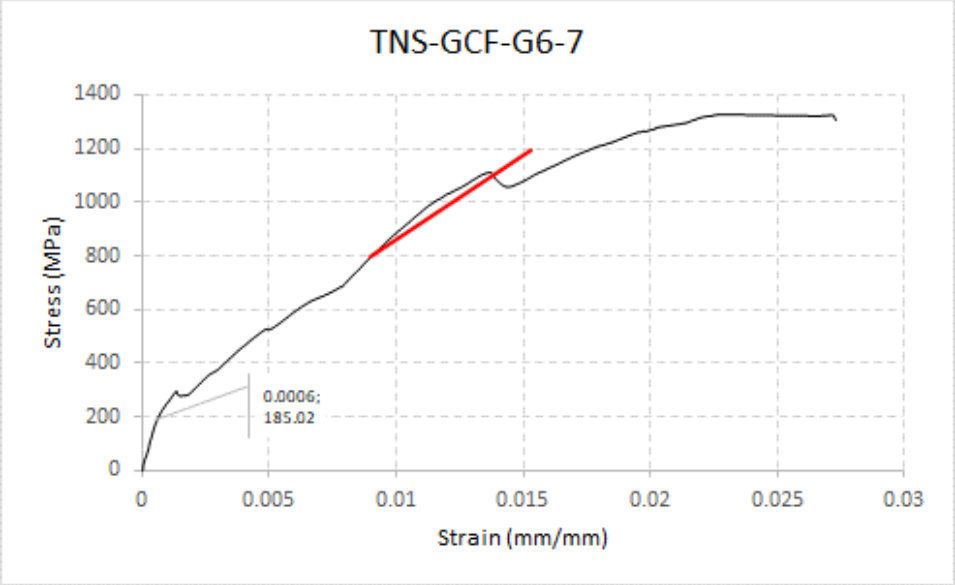

Figure Appendix.29 - Stress-Strain Curve for coupon GCF-G6-7

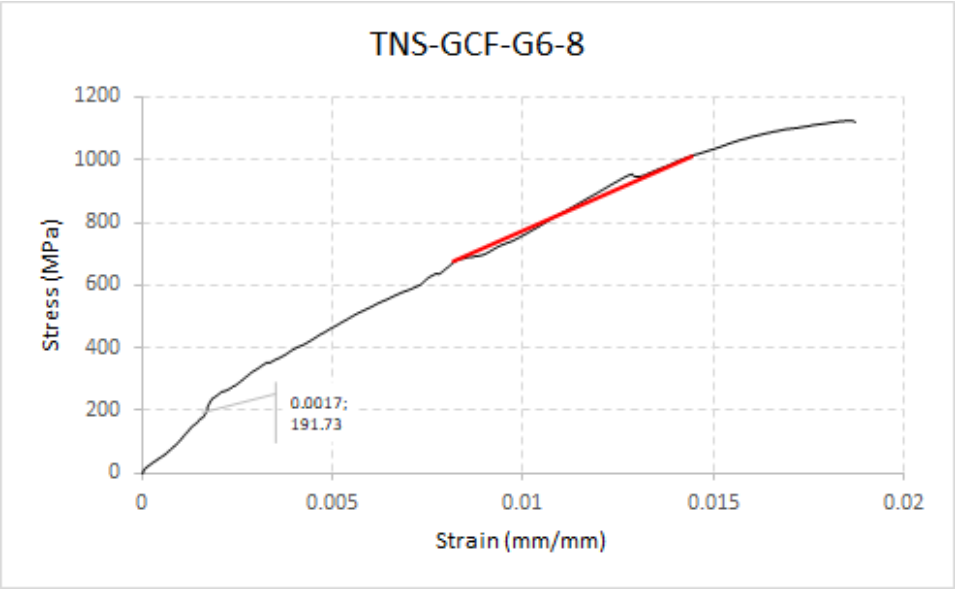

Figure Appendix.30 - Stress-Strain Curve for coupon GCF-G6-8

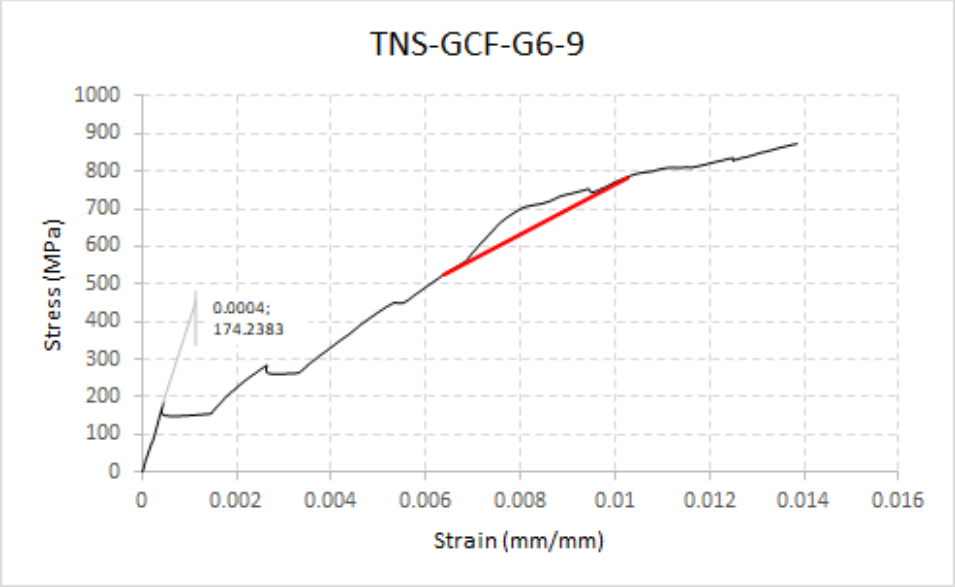

Figure Appendix.31 - Stress-Strain Curve for coupon GCF-G6-9

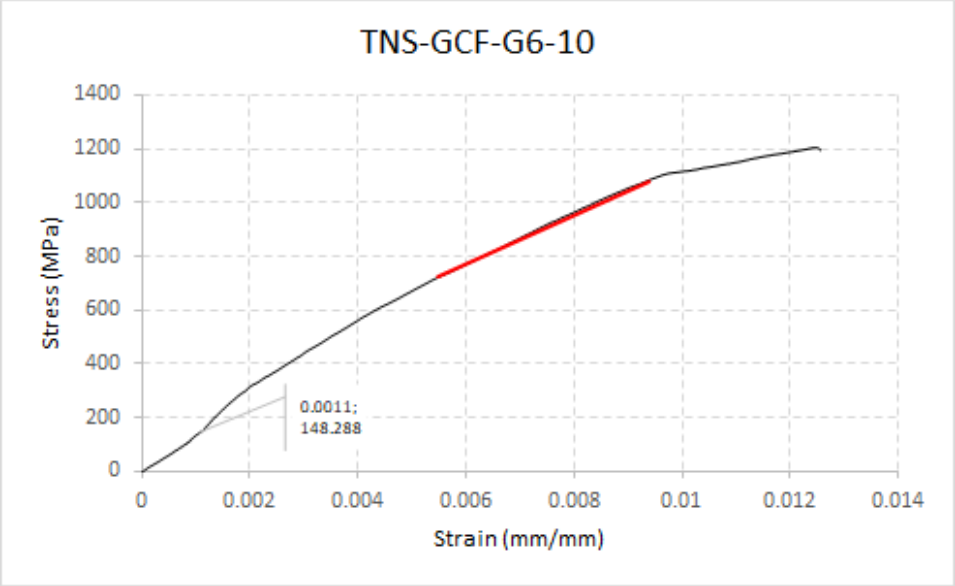

Figure Appendix.32 - Stress-Strain Curve for coupon GCF-G6-10

4. GCF-G12 Series

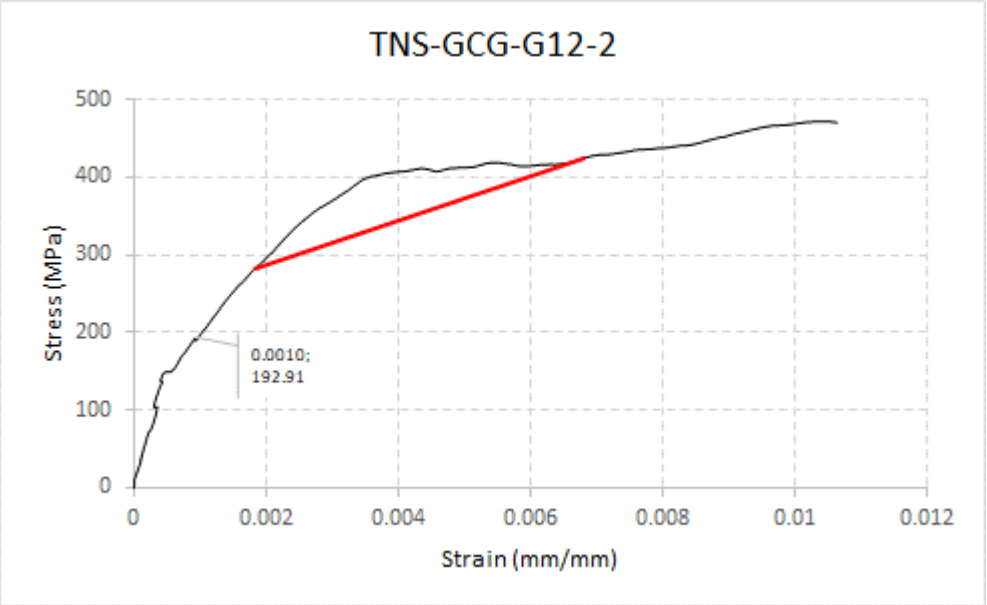

Figure Appendix.33 - Stress-Strain Curve for coupon GCF-G12-2

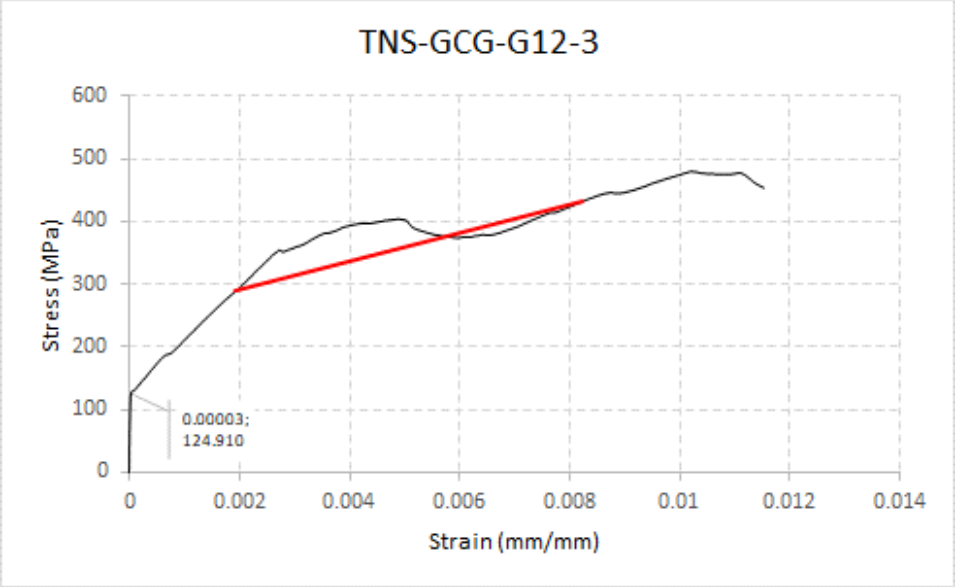

Figure Appendix.34 - Stress-Strain Curve for coupon GCF-G12-3

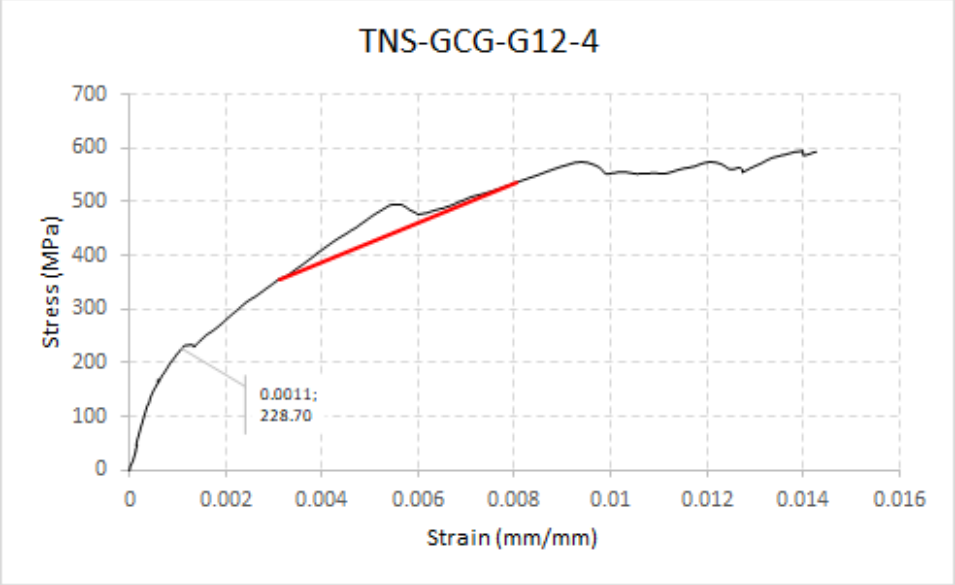

Figure Appendix.35 - Stress-Strain Curve for coupon GCF-G12-4

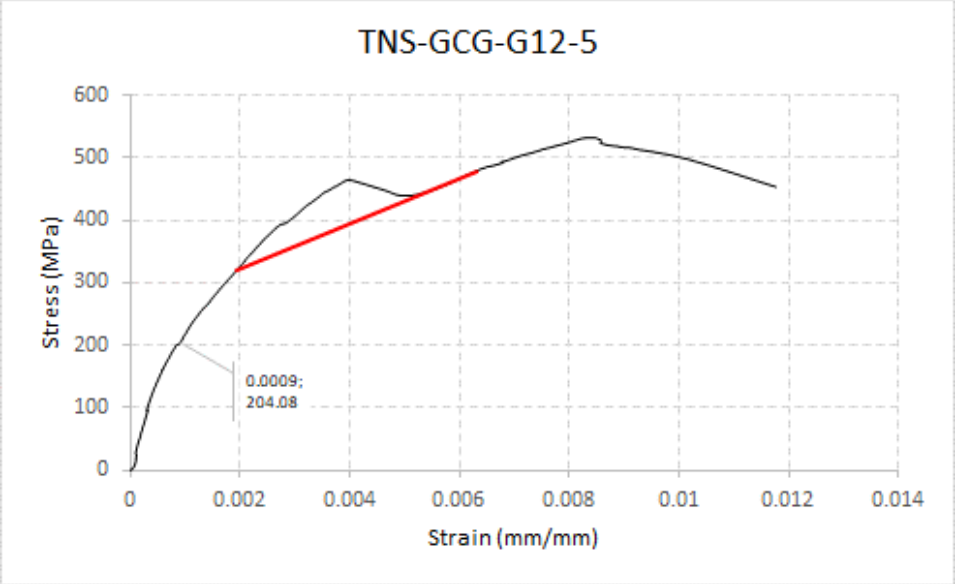

Figure Appendix.36 - Stress-Strain Curve for coupon GCF-G12-5

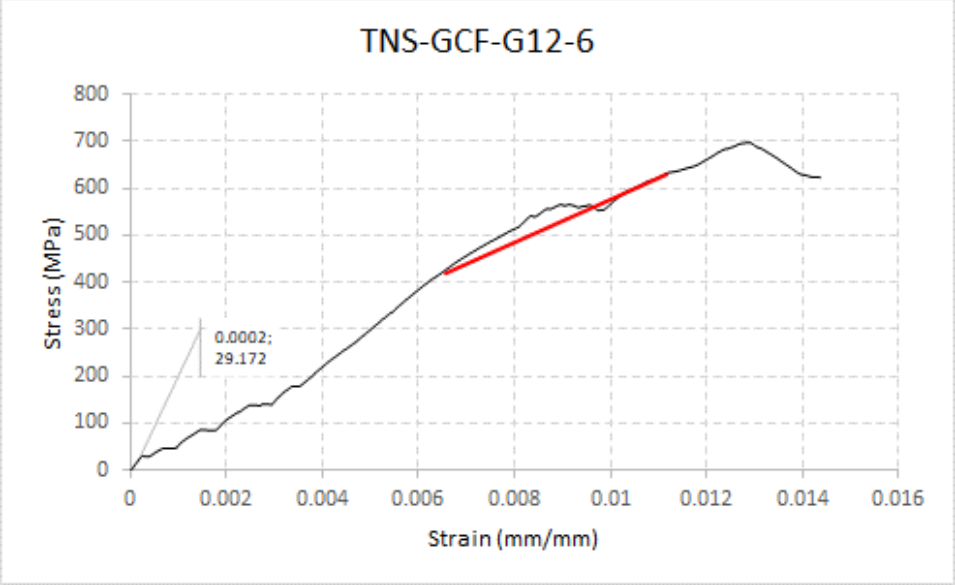

Figure Appendix.37 - Stress-Strain Curve for coupon GCF-G12-6

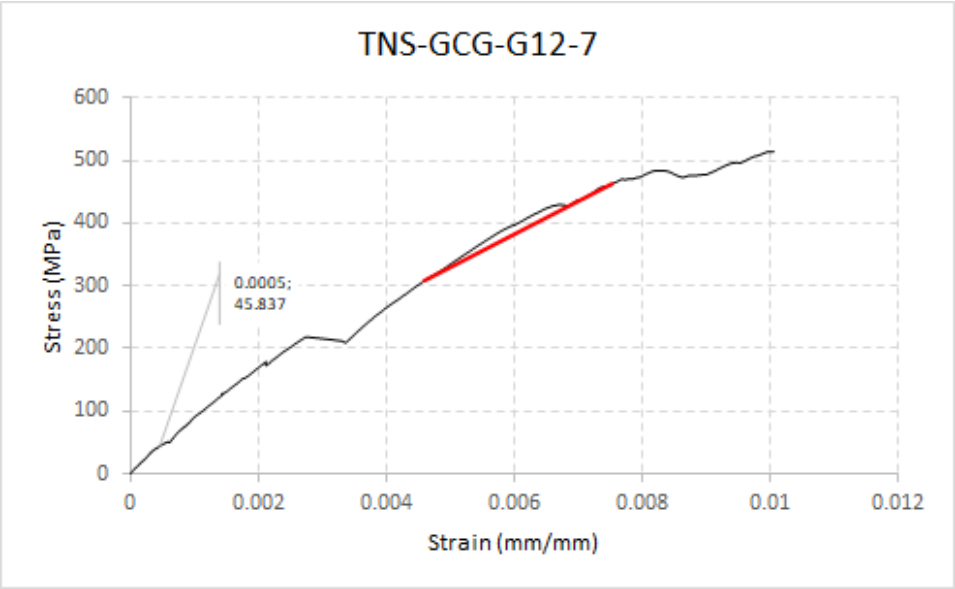

Figure Appendix.38 - Stress-Strain Curve for coupon GCF-G12-7

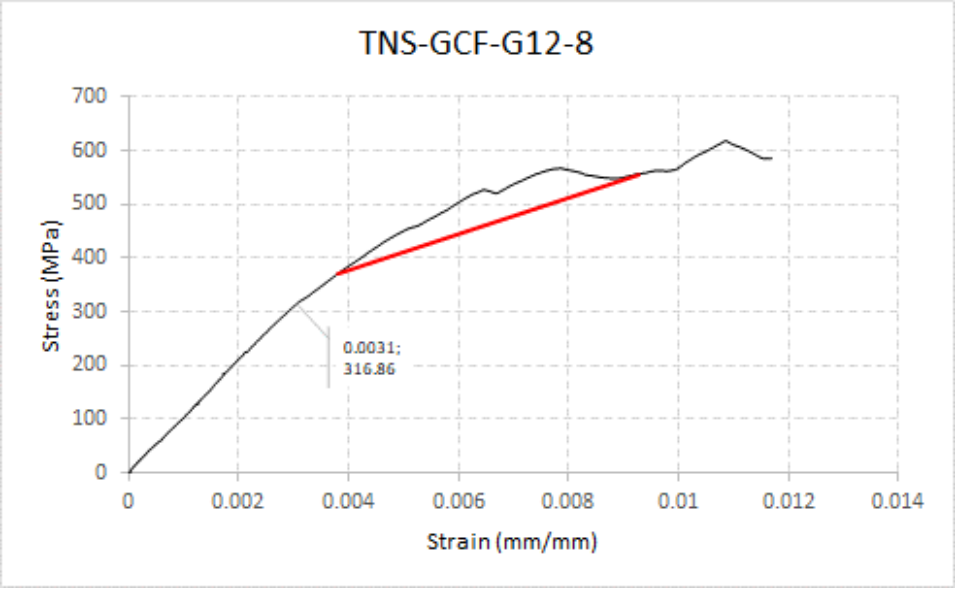

Figure Appendix.39 - Stress-Strain Curve for coupon GCF-G12-8

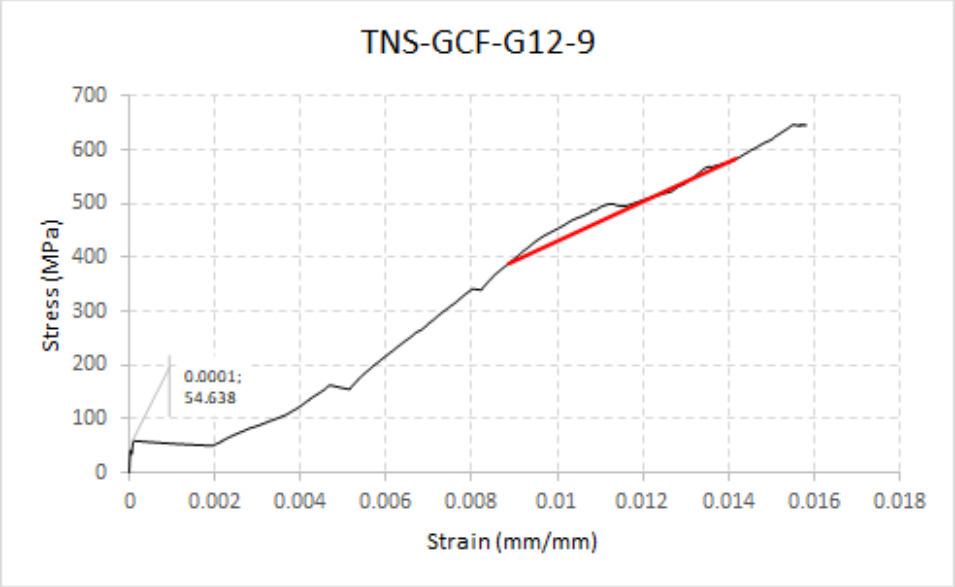

Figure Appendix.40 - Stress-Strain Curve for coupon GCF-G12-9

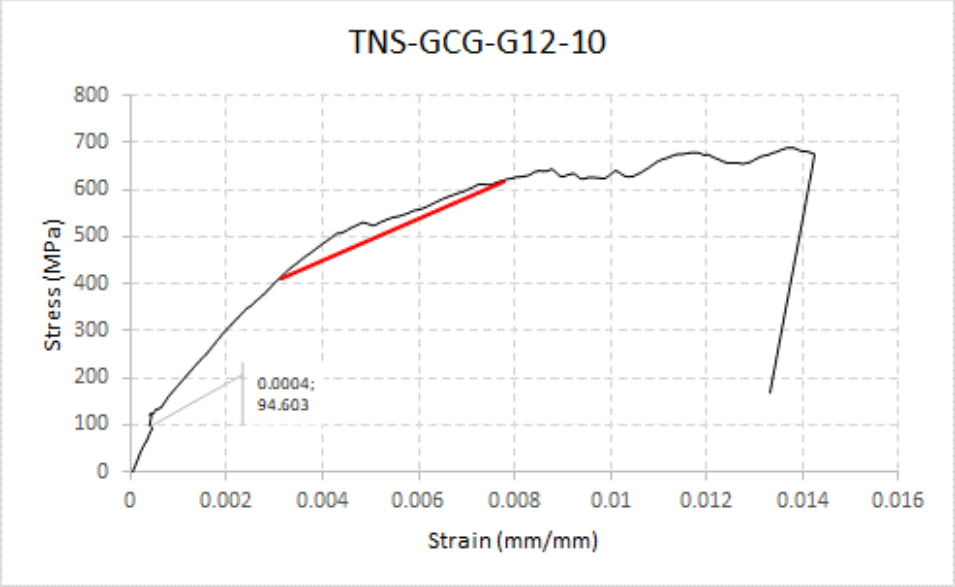

Figure Appendix.41 - Stress-Strain Curve for coupon GCF-G12-10

Bibliography

[1] A. E. Naaman, «Textile reinforced cement composites: competitive status and research directions.,» *International RILEM Conference on Material Science,* vol. 1, pp. 3-22, 2010.

[2] A. Peled , A. Bentur e D. Yankelevsky , «Flexural performance of cementitious composites reinforced with woven fabrics,» *Journal of Materials in Civil Engineering, ASCE,* pp. 325-330, 1999.

[3] B. Banholzer, «Bond behaviour of a multi-filament yarn embedded in a cementious matrix,» *PhD Thesis, In: Schriftenreihe Aachener Beitra¨ge zur Bauforschung, Institut fur Bauforschung der RWTH Aachen,* n. 12, 2004.

[4] A. Wiberg, «Strengthening of Concrete Beams using Cementitious Carbon Fibre Composites,» *Doctoral Thesis, Royal Institute of Technology, Stockholm, Sweden,* n. TRITA-BKN Bulletin 72, 2003.

[5] A. Peled , Z. Cohen , Y. Pasder , A. Roye e T. Gries , «Influences of textile characteristics on the tensile properties of warp knitted cement based composites,» *Cement and Concrete Composites,* vol. 30, n. 3, pp. 174-183, 2008.

[6] A. Peled , D. Yankelevsky e A. Bentur , «Microstructural Characteristic of Cementitious Composites Reinforced With woven Fabrics,» *Advances in Cement Research Journal,* vol. 9, n. 36, pp. 149-155, 1997.

[7] A. Peled e A. Bentur , «Reinforcement of Cementitious Matrices by Warp Knitted Fabrics,» *Materials and Structures,* vol. 31, pp. 543-550, 1998.

[8] A. Peled , A. Bentur e D. Yankelevsky , «The Nature of Bonding Between Monofilament Polyethylene Yarns and Cement Matrices,» *Cement & Concrete Composites Journal,* vol. 20, n. 4, pp. 319-328, 1998.

[9] A. Peled , S. Sueki e B. Mobasher , «Bonding in fabric-cement systems: Effects of fabrication methods,» *Cement and concrete research,* vol. 36, n. 9, pp. 1661-1671, 2006.

[10] A. Peled , E. Zaguri e G. Marom , «Bonding characteristics of multifilament polymer yarns and cement matrices,» *Composites Part A: Applied Science and Manufacturing,* vol. 39, n. 6, pp. 930-939, 2008.

[11] A. Bentur , A. Peled e D. Yankelevsky, «Enhanced Bonding of Low Modulus Polymer Fibers-Cement Matrix by Means of Crimped Geometry,» *Cement Concrete Research Journal,* vol. 27, n. 7, pp. 1099-1111, 1997.

[12] J. Hartig , U. Häußler-Combe e K. Schicktanz , «Influence of bond properties on the tensile behaviour of Textile Reinforced Concrete,» *Cement and Concrete Composites,* vol. 30, n. 10, pp. 898-906, 2008.

[13] C. Soranakom e B. Mobasher , «Geometrical and mechanical aspects of fabric bonding and pullout in cement composites,» *Materials and structures,* vol. 42, n. 6, pp. 765-777, 2009.

[14] S. Sueki , C. Soranakom , B. Mobasher e A. Peled , «Pullout-slip response of fabrics embedded in a cement paste matrix,» *Journal of Materials in Civil Engineering,* vol. 19, n. 9, pp. 718-727, 2007.

[15] Z. Cohen e A. Peled , «Effect of nanofillers and production methods to control the interfacial characteristics of glass bundles in textile fabric cement-based composites,» *Composites Part A: Applied Science and Manufacturing,* vol. 43, n. 6, pp. 962-972, 2012.

[16] R. Ortlepp , A. Bruckner e M. Curbach , «Textile reinforced concrete for strengthening in bending and shear,» *Materials and Structures,* vol. 39, n. 292, pp. 741-748, 2006.

[17] B. Mobasher, «Mechanics of fiber and textile reinforced cement composites,» *CRC Press,* 2011.

[18] Z. Cohen , A. Peled, Y. Pasder , A. Roye e T. Gries , «Effects of warp knitted fabrics made from multifilament in cement-based composites,» *1st International Conference Textile Reinforced Concrete (ICTRC),* pp. 23-32, 2006.

[19] M. Richter, «Entwicklung mechanischer Modelle zur analytischen Beschreibung der Materialeigenschaften von textilbewehrtem Feinbeton. (Development of mechanical models for analytical description of material properties on textile reinforced fine concrete.)",» *PhD Thesis, Berichte des Instituts fur Mechanik und Flachentragwerke, Technische Universitat Dresden,* n. 2, 2005.

[20] A. Borri , G. Castori , M. Corradi e E. Speranzini, «Shear behavior of unreinforced and reinforced masonry panels subjected to in situ diagonal compression tests,» *Constr Build Mater,* vol. 25, n. 12, pp. 4403-14, 2011.

[21] M. R. Valluzzi , C. Modena e G. de Felice , «Current practice and open issues in strengthening historical buildings with composites,» *Mater Struct,* vol. 47, n. 12, pp. 1971-85, 2014.

[22] X. Huang , V. Birman , A. Nanni e G. Tunis , «Properties and potential for application of steel reinforced polymer and steel reinforced grout composites,» *Compos Part B– Eng,* vol. 36, pp. 73-82, 2005.

[23] A. Kwiecien, G. de Felice , D. Oliveira , B. Zajac, A. Bellini, S. De Santis e et al., «Repair of composite-to-masonry bond using flexible matrix,» *Mater Struct,* vol. 49, n. 7, pp. 2563-80, 2016.

[24] V. Karbhari, «Fabrication, Quality and Service Life Issues for Composites in Civil Engineering,» *Durability of Composites for Civil Structural Applications, Woodhead Publishing,* pp. 13-29, 2007.

[25] D. Mela, «Shear Bond Strength of Carbon FRP Laminates to Concrete,» *MS Thesis, Polytechnic of Milan, Italy.,* 2013.

[26] A. Prota, K. Tan , A. Nanni, M. Pecce e G. Manfredi, «Performance of shallow R/C beams with externally bonded steel-reinforced polymer,» *ACI Struct J,* vol. 103, n. 2, pp. 163-70, 2006.

[27] J. Kim , A. Fam , A. Kong e R. El-Hacha, «Flexural strengthening of RC beams using steel reinforced polymer (SRP) composites,» *In: Proc. of the 7th int. symp. FRP reinforcement for concrete structures, ACI SP-230,* vol. 93, pp. 1647-64, 2005.

[28] A. Lopez , N. Galati , T. Alkhrdaji e A. Nanni , «Strengthening of a reinforced concrete bridge with externally bonded steel reinforced polymer (SRP),» *Composites Part B,* vol. 38, pp. 429-36, 2007.

[29] N. Gallo, «Durabilità di Materiali Compositi Applicati su Murature in Ambiente Aggressivo: Influenza sulla Cristallizzazione Salina sul Fenomeno di Aderenza,» *MS Thesis, University of Padua, Italy.,* 2014.

[30] V. Karbhari, «Introduction: the Use of Composites in Civil Structural Applications,» *Durability of Composites for Civil Structural Applications, Woodhead Publishing,* pp. 1-10, 2007.

[31] R. Atadero e V. Karbhari, «Sources of Uncertainty and Design Values for Field Manifacturered FRP,» *Composite Structures,* vol. 89, pp. 83-93, 2009.

[32] C. G. Papanicolaou , T. C. Triantafillou , K. Karlos e M. Papathanasiou, «Textile reinforced mortar (TRM) versus FRP as strengthening material of URM walls: in-plane cyclic loading,» *Mater Struct,* vol. 40, n. 10, p. 1081–97, 2007.

[33] E. Agneloni e P. Casadei , «Case studies on advanced composite materials for civil engineering and architectural applications,» *Struct Eng Int J Int Assoc Bridge Struct Eng (IABSE) ,* vol. 21, n. 3, pp. 271-8, 2011.

[34] S. De Santis , F. Carozzi , G. de Felice e C. Poggi , «Test methods for textile reinforced mortar systems,» *Compos Part B-Eng,* n. http://dx.doi.org/10.1016/j.compositesb.2017.03.016., 2017.

[35] A. D'Ambrisi , L. Feo e F. Focacci, «Experimental and analytical investigation on bond between Carbon-FRCM materials and masonry,» *Compos Part B – Eng,* vol. 46, pp. 15-20, 2013.

[36] F. Carozzi , P. Colombi e C. Poggi , «Calibration of end-debonding strength model for FRP-reinforced masonry,» *Compos Struct,* vol. 120, pp. 366-77, 2015.

[37] F. Carozzi, G. Milani e C. Poggi, «Mechanical properties and numerical modeling of Fabric Reinforced Cementitious Matrix (FRCM) systems for strengthening of masonry structures,» *Compos Struct,* vol. 107, pp. 711-25, 2014.

[38] M. Gams , M. Tomazevic e A. Kwiecien , «Strengthening brick masonry by repointing – an experimental study,» *Key Eng Mater,* vol. 624, pp. 444-52, 2015.

[39] R. Capozucca, «Experimental FRP/SRP–historic masonry delamination,» *Compos Struct,* vol. 92, n. 4, pp. 891-903, 2010.

[40] G. de Felice, S. De Santis, L. Garmendia, B. Ghiassi, P. Larrinaga, P. B. Lourenço e e. al, «Mortar-based systems for externally bonded strengthening of masonry,» *Mater Struct,* vol. 47, n. 12, pp. 2021-37, 2014.

[41] M. Malena e G. de Felice , «Debonding of composites on a curved masonry substrate: experimental results and analytical formulation,» *Compos Struct,* vol. 112, n. 1, pp. 194-206, 2014.

[42] A. Balsamo, M. Di Ludovico, A. Prota e G. Manfredi, «Masonry walls strengthened with innovative composites,» *Am Concr Inst ACI Spec Publ,* vol. 2, n. 275, pp. 769-86, 2011.

[43] A. D'Ambrisi , F. Focacci e A. Caporale , «Strengthening of masonry–unreinforced concrete railway bridges with PBO-FRCM materials,» *Compos Struct,* vol. 102, p. 193–204, 2013.

[44] T. D'Antino , C. Carloni , L. H. Sneed e C. Pellegrino, «Matrix-fiber bond behavior in PBO FRCM composites: a fracture mechanics approach,» *Eng Fract Mech,* vol. 117, pp. 94-111, 2014.

[45] F. Carozzi e C. Poggi , «Mechanical properties and debonding strength of Fabric Reinforced Cementitious Matrix (FRCM) systems for masonry strengthening,» *Compos Part B – Eng,* vol. 70, pp. 215-30, 2015.

[46] F. Pacheco-Torgal e S. Jalali , «Cementitious building materials reinforced with vegetable fibres: a review,» *Constr Build Mater,* vol. 25, n. 2, pp. 575-81, 2011.

[47] R. Codispoti , D. Oliveira , R. S. Olivito e P. B. Lourenço , «Mechanical performance of natural fiber-reinforced composites for the strengthening of masonry,» *Compos Part B – Eng,* vol. 77, pp. 74-83, 2015.

[48] A. Razavizadeh , B. Ghiassi e D. V. Oliveira, «Bond behavior of SRG-strengthened masonry units: testing and numerical modeling,» *Constr Build Mater,* vol. 64, pp. 387-97, 2014.

[49] S. De Santis e G. de Felice, «Tensile behaviour of mortar-based composites for externally bonded reinforcement systems,» *Compos Part B – Eng,* vol. 68, pp. 401-13, 2015.

[50] X. Huang , V. Birman , A. Nanni e G. Tunis , «Properties and potential for application of steel reinforced polymer and steel reinforced grout composites,» *Compos Part B– Eng,* vol. 36, pp. 73-82, 2005.

[51] A. Prota , G. Manfredi, A. Nanni, E. Cosenza e M. Pecce , «Flexural strengthening of R/C beams using emerging materials: ultimate behavior,» *In: Proc. of cice. Adelaide, Australia,* pp. 163-70, 2004.

[52] «Characterization of reinforced concrete beams strengthened by steel reinforced polymer and grout (SRP and SRG) composites,» *Mater Sci Eng A,* vol. 412, n. 1-2, pp. 129-36, 2005.

[53] F. Da Porto , E. Stievanin , E. Gabin e M. R. Valluzzi, «SRG application for structural strengthening of RC beams,» *ACI Spec Pub,* vol. 286, pp. 119-32, 2012.

[54] A. Balsamo, F. Nardone, I. Iovinella, F. Ceroni e M. Pecce, «Flexural strengthening of concrete beams with EB- FRP, SRP and SRCM: experimental investigation,» *Compos Part B-Eng* , vol. 46, pp. 91-101, 2013.

[55] A. Napoli e R. Realfonzo, «Reinforced concrete beams strengthened with SRP/SRG systems: experimental investigation,» *Constr Build Mater*, vol. 93, pp. 654-77, 2015.

[56] E. Wobbe , P. Silva , B. Barton , L. Dharani , V. Birman , A. Nanni , T. Alkhrdaji , J. Thomas e T. Tunis , «Flexural capacity of R/C beams externally bonded with SRP and SRG,» *In: Proc. of society for the advancement of material and process engineering symp. Long Beach, CA, USA,* pp. 20-7, 2004.

[57] R. Hawileh , J. Abdalla , W. Nawaz , A. Alzeer e R. Muwafi , «Strengthening reinforced concrete beams in flexure using hardwire steel fiber sheets,» *In: Proc. of cice. Vancouver, Canada, August 20–22,* p. 22, 2014.

[58] A. Borri , P. Casadei , G. Castori e J. Hammond, «Strengthening of brick masonry arches with externally bonded steel reinforced composites,» *J Compos Constr,* vol. 13, n. 6, pp. 468-75, 2009.

[59] V. Giamundo, G. Lignola, G. Maddaloni, A. Balsamo, A. Prota e G. Manfredi, «Experimental investigation of the seismic performances of IMG reinforcement on curved masonry elements,» *Compos Part B-Eng,* vol. 70, pp. 53-63, 2015.

[60] A. Borri , G. Castori e M. Corradi, «Shear behavior of masonry panels strengthened by high strength steel cords,» *Constr Build Mater,* vol. 25, n. 2, pp. 494-503, 2011.

[61] S. De Santis , G. De Canio , G. de Felice , M. Malena e M. Mongelli, «Seismic performance of masonry walls retrofitted with steel reinforced grout,» *Earth Eng Struct Dyn,* 2015.

[62] A. Borri , G. Castori , M. Corradi e E. Speranzini , «Shear behavior of unreinforced and reinforced masonry panels subjected to in situ diagonal compression tests,» *Constr Build Mater,* vol. 25, n. 12, pp. 4403-14, 2011.

[63] G. De Canio , G. de Felice , S. De Santis, A. Giocoli , M. Mongelli, F. Paolacci e et al., «Passive 3D motion optical data in shaking table tests of a SRG-reinforced masonry wall,» *Earthq Struct,* vol. 10, n. 1, pp. 53-71, 2016.

[64] S. De Santis , P. Casadei , G. De Canio , G. de Felice , M. Malena , M. Mongelli e et al., «Seismic performance of masonry walls retrofitted with steel reinforced grout,» *Earthq Eng Struct D,* vol. 45, n. 2, pp. 229-51, 2016.

[65] M. R. Valluzzi , C. Modena e G. de Felice , «Current practice and open issues in strengthening historical buildings with composites,» *Mater Struct,* vol. 47, n. 12, pp. 1971-85, 2014.

[66] G. Ramaglia , G. Lignola, A. Balsamo , A. Prota e G. Manfredi, «Seismic strengthening of masonry vaults with abutments using textile reinforced mortar,» *J Compos Constr,* n. 04016079, 2016.

[67] L. Ascione, G. de Felice e S. De Santis, «A qualification method for externally bonded Fibre Reinforced,» *Composites: Part B Engineering 2015; 78: 497-506.*, vol. 78, pp. 497-506, 2015.

[68] A. D'Ambrisi , L. Feo e F. Focacci , «Bond-slip relations for PBO-FRCM materials externally bonded to concrete,» *Composites Part B: Engineering,* vol. 43, n. 8, pp. 2938-2949, 2012.

[69] R. Ortlepp , U. Hampel e M. Curbach , «A new approach for evaluating bond capacity of TRC strengthening,» *Cement and Concrete Composites,* vol. 28, n. 7, pp. 589-597, 2006.

[70] D. Arboleda, «Fabric Reinforced Cementitious Matrix (FRCM) Composites for Infrastructure Strengthening and Rehabilitation: Characterization Methods,» *Doctoral dissertation, University of Miami,* n. 22, 2014.

[71] F. Jesse , N. Will , M. Curbach e J. Hegger , «Load bearing behaviour of textile reinforced concrete,» *Dubey, A. (Ed.): Textile Reinforced Concrete. ACI Special Publication,* 2006.

[72] J. Hegger , N. Will , A. Bentur , M. Curabach , F. Jesse , B. Mobasher, A. Peled e J. Wastiels, «Textile Reinforced Concrete - State-of-the-Art Report,» *RILEM TC 201-TRC,* 2006.

[73] D. Arboleda, F. Carozzi, A. Nanni e C. Poggi, «Testing Procedures for the Uniaxial Tensile Characterization of Fabric-Reinforced Cementitious Matrix Composites,» *Journal of Composites for Construction ,* vol. 20, n. 3, 2016.

[74] G. de Felice , S. De Santis , L. Garmendia , B. Ghiassi, P. Larrinaga , P. Lourenço e et al., «Mortar-based systems for externally bonded strengthening of masonry,» *Mater Struct ,* vol. 47, n. 12, pp. 2021-37, 2014.

[75] G. de Felice e S. De Santis, «Tensile behaviour of mortar-based composites for externally bonded reinforcement systems,» *Compos Part B – Eng,* vol. 68, pp. 401-13, 2015.

[76] A. Razavizadeh , B. Ghiassi e D. V. Oliveira , «Bond behavior of SRG-strengthened masonry units: testing and numerical modeling,» *Constr Build Mater,* vol. 64, pp. 387-97, 2014.

[77] S. De Santis, F. Ceroni, G. de Felice, M. Fagone, B. Ghiassi, A. Kwiecien, G. Lignola, M. Morganti, M. Santandrea, M. Valluzzi e A. Viskovic, «Round Robin Test on tensile and bond behaviour of Steel Reinforced,» *Composites Part B ,* vol. 127, pp. 100-120, 2017.

[78] F. Carozzi e C. Poggi, «Mechanical properties and debonding strength of Fabric Reinforced,» *Composites Part B ,* vol. 70, pp. 215-230, 2015.

[79] J. Donnini, "Study of enhanced Fiber Reinforced Cementitious Matrix (FRCM) systems for structural rehabilitation", Doctoral dissertation, Università Politecnica delle Marche, 2016.

[80] A. Borri, P. Casadei, G. Castori e J. Hammod, «Strengthening of brick masonry arches with externally bonded steel reinforced composites,» *J Compos Constr,* vol. 13, pp. 468-75, 2009.

[81] «Flexural strengthening of RC beams using steel reinforced polymer (SRP) composites,» *In: Proc. of the 7th int. symp. FRP reinforcement for concrete structures, ACI SP-230,* vol. 93, pp. 1647-64, 2005.

Acknowledgements

Although this page is devoid of scientific content, it is the one with more personal character, because it is full of gratitude towards those who have supported and endured me during these years. More than 3 years have passed since I embarked upon this path, during which I have matured as a professional, in what I discovered to be my passion, but also and above all as a person. There is so much knowledge that I have acquired, friendships I have cultivated, and relationships I have made. Therefore, please allow me to express a few words of gratitude to some of these people.

The first thanks is to Prof. Ombres, supervisor of this doctoral thesis. I would like to thank him for his availability and accuracy shown during the whole writing period, as well as the great knowledge he has given to me in all these years. He gave me all the tools I needed to take the right path and complete my thesis. Without him, this work would not have come to life!

To Prof. Nanni, my supervisor during my research period at the University of Miami and of this thesis. There are no words to thank him for the incredible opportunity he gave me to conduct the experimental tests, topic of this thesis, at the Materials Laboratory of the Department of Civil Engineering of the University of Miami. He taught me the importance of passion and dedication in scientific research.

To the colleagues that I met during my period abroad. Thanks for the happy hours spent in the laboratory and for the fantastic collaboration. You have always been ready to help me and support me. I will keep some beautiful memories and I hope that ours was not a goodbye but rather an *arrivederci*.

To the colleagues of the SIACE doctorate, it was a pleasure to share concerns and hopes during these years. Although we have embarked upon different paths, I wish you to continue to give the best of yourselves, aim high and never give up.

To my family who allowed me to get here with their sweet and tireless support, contributing to my personal education and training. In particular, to my mother who

has always accepted my choices, and while she may not have always shared them, she has never imposed limits on me.

Thanks also to my one time English teacher, now friend, *Kirsten Lawson* who has supported me tirelessly during my linguistic adventure. Not only did she accompany me on my English language journey, but she did so offering me lots of tea and shortbread despite me having mispronounced her name for more than a decade.

Thanks to *Luca* for giving me love and patience. Even during the long months of separation, he has always stood close by helping me through difficult moments. If I have reached the end of this journey, I owe it also to him.

To all the friends (and with all, I mean all of them!) who have had a decisive weight in the attainment of this result, point of arrival and at the same time of departure of my life. Thank you for listening to me, advising me and encouraging me to continue and believe in my abilities.

Finally to myself, be proud of the goal you have reached, but now go, *"throw off the bowlines, sail away from the safe harbor and catch the trade winds in your sails. Explore. Dream. Discover (H. Jackson Brown Jr., P.S. I Love You)".*

Ringraziamenti

Sebbene la pagina che mi accingo a scrivere sia priva di contenuti scientifici, è quella con più carattere personale, in quanto piena di gratitudine verso coloro i quali mi hanno supportato e sopportato durante questi anni. Più di 3 anni sono passati da quando ho intrapreso questo percorso, durante il quale sono maturata come professionista in quello che ho scoperto essere la mia passione, ma anche e soprattutto come persona. Sono tante le conoscenze che ho acquisito, le amicizie che ho coltivato, i rapporti che ho stretto. Permettetemi, dunque, di esprimere qualche parola di ringraziamento nei confronti di alcune di queste persone.

Il primo ringraziamento è per il *Prof. Ombres*, relatore di questa tesi di dottorato. Grazie per la disponibilità e precisione dimostratemi durante tutto il periodo di stesura, oltre che la grande conoscenza donatami in tutti questi anni. Mi ha fornito tutti gli strumenti di cui avevo bisogno per intraprendere la strada giusta e portare a compimento la mia tesi. Senza di lui questo lavoro non avrebbe preso vita!

Al *Prof. Nanni*, mio supervisore durante il periodo di ricerca presso l'Università di Miami e relatore di questa tesi. Non ci sono parole per ringraziarla dell'incredibile opportunità di condurre l'attività sperimentale, oggetto di questa tesi, presso il Laboratorio di Materiali del Dipartimento di Ingegneria Civile dell'Università di Miami. Mi ha insegnato l'importanza della passione e della dedizione nella ricerca scientifica.

Ai *colleghi* che ho incontrato durante il mio periodo all'estero. Grazie per le ore liete trascorse in laboratorio e per la fantastica collaborazione. Siete sempre stati pronti ad aiutarmi e sostenermi. Conserverò dei bellissimi ricordi e spero che il nostro sia stato solo un arrivederci.

Ai *colleghi* del dottorato SIACE. È stato piacevole condividere preoccupazioni e speranze durante questi anni. Seppur abbiamo intrapreso strade diverse, vi auguro di continuare a dare il meglio di voi stessi, puntare in alto e non arrendervi mai.

Alla *mia famiglia* che, con il loro dolce e instancabile sostegno, mi ha permesso di arrivare fin qui, contribuendo alla mia educazione e formazione personale. In

particolare *mia madre*, che ha sempre accettato le mie scelte, non sempre condivise, non imponendomi mai limiti.

Grazie anche alla mia unica insegnante di inglese, ora amica, *Kirsten Lawson*, che mi ha sostenuto instancabilmente durante la mia avventura linguistica. Non solo mi ha accompagnato nel mio cammino nella lingua inglese, ma mi ha offerto un sacco di tè e *shortbread* nonostante avessi pronunciato male il suo nome per più di un decennio.

Grazie a *Luca* per avermi donato amore e pazienza. Mi è sempre stato vicino anche nei lunghi mesi di lontananza, aiutandomi a superare i momenti di sconforto. Se sono arrivata alla fine di questo percorso, lo devo anche a lui.

A tutti gli *amici* (e con tutti, intendo proprio tutti!) che hanno avuto un peso determinante nel conseguimento di questo risultato, punto di arrivo e contemporaneamente di partenza della mia vita. Grazie per avermi ascoltata, consigliata, incoraggiata a proseguire e credere di più nelle mie capacità.

Infine a me stessa, sii orgogliosa del traguardo raggiunto, ma ora va, *"molla gli ormeggi, esci dal porto sicuro e lascia che il vento gonfi le tue vele. Esplora. Sogna. Scopri (H. Jackson Brown Jr., P.S. I Love You)"*.